UNCLASSIFIED

AD NUMBER

AD825618

NEW LIMITATION CHANGE

TO

Approved for public release, distribution unlimited

FROM

Distribution authorized to U.S. Gov't. agencies and their contractors; Critical Technology; MAY 1967. Other requests shall be referred to Air Force Cambridge Research Labs., Hanscom Field, MA.

AUTHORITY

AFCRL ltr, 22 Dec 1971

THIS PAGE IS UNCLASSIFIED

APCRL-68-0[illegible] (II)
MAY 1968
SPECIAL REPORTS, NO. [illegible]
[illegible]

Qualified requesters may obtain copies of this report from the Defense Documentation Center. Orders will be expedited if placed through the sponsoring agency or the Clearinghouse for Federal Scientific and Technical Information (CFSTI), Sills Building, 5285 Port Royal Road, Springfield, Virginia 22151.

AIR FORCE CAMBRIDGE RESEARCH LABORATORIES
L. G. HANSCOM FIELD, BEDFORD, MASSACHUSETTS

AFCRL-68-0[illegible]

Proceedings of the Third Symposium on the Plasma Sheath – Plasma Electromagnetics of Hypersonic Flight

Volume II. Reentry Plasmas: Simulation, Diagnostics, and Alleviation Techniques

W. ROTMAN
R. MOORE
A. PAPA
J. LENNON
Editors

OFFICE OF AEROSPACE RESEARCH
United States Air Force

DDC
RECEIVED
AUG 3 1967
B

82561/8

AFCRL-67-0280 (Volume III)
MAY 1967
SPECIAL REPORTS, NO. 64 (III)

PROCEEDINGS OF THE THIRD SYMPOSIUM ON THE PLASMA SHEATH – PLASMA ELECTROMAGNETICS OF HYPERSONIC FLIGHT
Volume III, Reentry Plasmas: Simulation, Diagnostics, and Alleviation Techniques

W. Rotman, H. Moore, R. Papa, J. Lennon, Editors

ERRATA

Page 193, the first sentence of the abstract should read:

A discussion is conducted of the electromagnetic and dynamic requirements which dictate the geometry of the cavity and the mode of interaction of the magnetic field with the flow itself.

AIR FORCE CAMBRIDGE RESEARCH LABORATORIES
OFFICE OF AEROSPACE RESEARCH
UNITED STATES AIR FORCE
BEDFORD, MASSACHUSETTS

Best
Available
Copy

AFCRL-67-0280 (Volume III)
MAY 1967
SPECIAL REPORTS, NO. 64 (III)



MICROWAVE PHYSICS LABORATORY PROJECT 4642

AIR FORCE CAMBRIDGE RESEARCH LABORATORIES

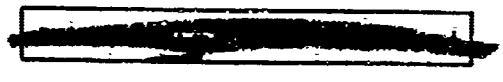
L. G. HANSCOM FIELD, BEDFORD, MASSACHUSETTS

Proceedings of the Third Symposium on the Plasma Sheath - Plasma Electromagnetics of Hypersonic Flight

Volume III. Reentry Plasmas: Simulation, Diagnostics, and Alleviation Techniques

W. ROTMAN
H. MOORE *
R. PAPA
J. LENNON
Editors

*Lowell Technological Institute Research Foundation, Lowell, Mass.



OFFICE OF AEROSPACE RESEARCH
United States Air Force



Abstract

This volume is a collection of the unclassified papers presented at the Third Symposium on the Plasma Sheath – Plasma Electromagnetics of Hypersonic Flight. This symposium consisted of the review of progress in reentry communication studies during the three year period since the prior meeting. The program of this symposium on plasma electromagnetics of hypersonic flight involves a wide range of scientific disciplines, including electromagnetics, aerodynamics, aerothermochemistry, plasma dynamics, electronics, and high-temperature phenomena. The papers were selected to explore as many of these facets of research, including the results of laboratory, flight, and system tests, as time permitted.

Contents

The Papers in this volume are from the sessions directed by Dr. Warren McBee, Sperry Rand Research Center, Sudbury, Mass., and Dr. Tetsu Marita, Stanford Research Institute, Menlo Park, California

I. ANALYSIS OF PLASMA GENERATORS FOR TESTING REENTRY COMMUNICATIONS SYSTEMS; by Joerger and Glatt 1

II. SIMULATION OF REENTRY PLASMAS BY ELECTRODELESS DISCHARGES; by Eckert 35

III. SHOCK TUBE SIMULATION OF RE-ENTRY PLASMA FLOWS AND THEIR MICROWAVE NOISE EMISSION; by Hartsel and Caldecott 69

IV. AN EXPERIMENTAL STUDY OF PLASMA-COVERED SLOTTED-CYLINDER ANTENNAS; by Karas and Antonucci 107

V. INTERACTION OF ELECTROMAGNETIC WAVES WITH THE EXHAUST FLAME OF LAUNCH VEHICLES; by Hasserjian and Clark 131

VI. INFORMATION LOSS CAUSED BY REENTRY PLASMA DISPERSION; by Fox and McPherron 167

VII. DEVELOPMENT OF A PROBE FOR THE MEASUREMENT OF POINT VALUES OF ELECTRON DENSITIES IN SUPERSONIC FLOWS; by Abele and Medecki 193

VIII. MEASUREMENT OF PLASMA PARAMETERS USING A RADIAL TRANSMISSION LINE; by Mullen and Medgyesi-Mitschang 231

IX. REFLECTOMETER MEASUREMENT OF THE PLASMA SHEATH ENCOUNTERED DURING THE PROJECT ASSET FLIGHTS by Plugge 259

X. PLASMA SHEATH REDUCTION BY ELECTRON ATTACHMENT PROCESSES by Carswell and Richard 281

XI. THE EFFECT OF CHEMICAL ADDITIVES ON MICROWAVE TRANSMISSION IN AN AIR PLASMA by Atallah and Sanborn 319

XII. REDUCTION OF FREE ELECTRON CONCENTRATION IN A REENTRY PLASMA BY INJECTION OF LIQUIDS by Evans 343

I. ANALYSIS OF PLASMA GENERATORS FOR TESTING REENTRY COMMUNICATION SYSTEMS

C.D. Joerger and M.A. Glatt

Space and Missile Engineering Division
McDonnell Aircraft Corporation
St. Louis, Missouri

ABSTRACT

This paper surveys existing plasma generators to determine their usefulness in providing realistic environments simulating re-entry plasmas for testing communications systems. From typical re-entry plasmas, simulation requirements are derived. Ten plasma generators are then described relating their characteristics to simulation requirements. It is shown that no one facility can meet all simulation requirements, but for any specific type of test a facility is available.

INTRODUCTION

The plasma sheath surrounding a re-entry vehicle is generated by an immense conversion of vehicle kinetic energy to random kinetic energy. Because it is difficult both to obtain a comparable level of energy in the laboratory and to produce the release of this energy as it occurs during re-entry, plasma simulation facilities are limited in their ability to reproduce precise re-entry conditions. The purpose of this paper is to enumerate the characteristics of various plasma generators in simulating re-entry plasmas and to indicate their usefulness for the testing of communication systems or components.

This paper is chiefly drawn from work supported by USAF, WPAFB, RTD Contract No. AF33(615)-11464.

The selection of a plasma generator for performing a specific test should not be made without knowledge of the operation and limitations of these devices. The facilities normally considered for electromagnetic transmission tests include: radio frequency (R.F.) plasmas, glow discharge tubes, low pressure flames, alkali plasmas, free flight ranges, diaphragm shock tubes, electromagnetic shock tubes, shock tunnels, hypervelocity impulse tunnels, arc jets, and arc heated tunnels. Because many of these facilities were developed for completely different purposes, modification or abnormal operation is required for accomplishing communication tests.

RE-ENTRY PLASMAS

The plasma sheath around a re-entry vehicle is characterized by four flow regions - stagnation, intermediate, aft body, and wake[1]. (Fig. 1)

The stagnation region consists of highly compressed, high temperature gases separated from the body of the vehicle by a thin boundary layer and enclosed by a near-normal shock. Gas temperatures and pressures in the boundary layer are lowered by convection to the vehicle skin and by ablation products. For orbital re-entry velocities (24,000 ft/sec.), the maximum deceleration for a blunt vehicle occurs at an altitude of about 200,000 feet. For these conditions the plasma frequency that is reached in the stagnation region is approximately 5×10^{10} cps with a corresponding collision frequency of 10^{10} encounters per second. The maximum deceleration for a pointed vehicle occurs at an altitude of about 100,000 feet. For this shape of vehicle the stagnation region is much smaller, with a peak plasma frequency of about 10^{12} cps and a corresponding frequency of 10^{11} encounters per second. These plasma frequencies do not include the ionization introduced

by low ionization potential ablation materials, that usually exist in the boundary layer. The plasma frequency is a function of both velocity and altitude; the collision frequency is primarily a function of altitude. The depth of the plasma at high velocities can be as much as 30 percent of the vehicle diameter.

The intermediate region is characterized by rapid extension of the stagnation gases as these flow toward the aft body. Here the composition and the ionization depart appreciably from equilibrium conditions. This intermediate region contains the most severe plasma conditions aft of the stagnation region, and is most often the principal cause of re-entry communication blackout. If the vehicle maintains an angle of attack, this flow may pass over the top of the vehicle, not affecting rear-mounted antennas. Values of plasma frequency in this region can be estimated by assuming the same percentage of ionized gas as existing in the stagnation region but at the local gas density. For the Gemini re-entry conditions, a peak plasma frequency of 10^{10} cps was calculated in this manner and was qualitatively verified by flight data.

The aft body ionization is created by gases which pass across an oblique shock. For pointed vehicles at low angles of attack, the maximum ionization occurs in the thin boundary layer next to the skin of the vehicle. At surface deflection angles greater than thirty degrees, the ionization in the inviscid flow region approaches the concentration in the boundary layer. The plasma frequency distributions as a function of position from the vehicle, for wedges and cones both blunt and sharp, are shown in Figures 2 and 3. The computation of the plasma profile becomes extremely complex for other than simple body shapes.

The wake region trails behind the vehicle. It consists of a cool outer layer and a warmer inner region. The peak local pressures correspond to isentropic compression, and the peak enthalpy is rarely greater than one third to one half of the stagnation enthalpy. The cool outer layer causes ionization to decay at a relatively rapid rate. Frequencies of C-band or higher are usually not affected by the wake ionization unless excessive contaminants are present.

SIMULATION REQUIREMENTS

Antennas are not usually mounted at the stagnation region because of the high plasma frequencies and severe material problems. The antennas are normally located near the rear of the vehicle, taking advantage of the lower temperatures in this region. Plasma simulation for re-entry communication studies therefore requires duplication of only the conditions for aft antenna locations.

The following is a list of desirable conditions for simulated re-entry communication tests.

(a) The facility should be able to simulate a wide range of plasma parameters with good repeatability. A maximum electron concentration of 5×10^{12} electrons per cc ($f_p = 2 \times 10^{10}$ cps) and a maximum electron collision frequency of 10^{10} encounters per second would include all normal orbital re-entry conditions at aft antenna locations.

(b) The size of the plasma and the distribution of the plasma parameters of a re-entry vehicle flow field at the antenna location should be duplicated, avoiding any scaling of wavelength. The area must be sufficiently large so that refractions and stray radiations do not appear as traveling through the plasma.

(c) The plasma should be in thermal equilibrium having equal ambient temperatures of electrons, ions, and neutral particles, or in realistic non-equilibrium. A maximum temperature of about 4,000°K is sufficient for temperature studies. A cool plasma may be used for most propagation experiments, since only electron concentration, collision frequency, and profile simulation are important.

(d) A facility capable of continuous operation is most desirable; however, useful measurements can be made in brief periods with proper instrumentation.

(e) The facility should allow plasma conditions to be determined easily efficiently, and accurately.

(f) If the chemistry of the flow is important for the test, the plasma should be free from facility-induced contamination. For most tests, however, plasma parameters alone will be important.

(g) The cost of using a specific plasma generator should be commensurate to the value of a test.

(h) It is desirable that the facility have been in use for several years so that its characteristics are well understood and documented.

PLASMA GENERATORS

RADIO FREQUENCY GENERATED PLASMA

The radio frequency plasma generator produces a plasma by induction heating of the test gas. A field is impressed on a test gas by passing it through a coiled wire. The ambient electrons contained within the coils gain energy from the RF field, collide with gas atoms, and produce additional

electrons through inelastic collisions. The electron concentration builds up in this manner until breakdown occurs. A gas flow moves the plasma away from the coils and into the test area.

A radio frequency generator is presently being operated at McDonnell (Figure 4). The generator consists of an 8000 volt full-wave rectifier, and a high-power 24 kw oscillator, resonant at 1 mc when driving a load coil. The load coil is several turns of water-cooled copper tubing carrying a maximum of 288 amperes. The plasma is contained in a one inch water-cooled quartz tube. By narrowing or widening the gas outlet, the mass flow rate may be increased or decreased. Testing is done downstream of the heating coils. Other RF generators are discussed in the literature.[2,3,4,5]

For small diameter gas columns, the plasma nearly fills the entire tube. For large diameter gas columns, the RF energy penetrates only the surface of the gas column, leaving the inner core unaffected and un-ionized. Lowering the excitation frequency increases the depth of RF energy penetration. Efficient coupling of energy is obtained when the inner core is evenly heated.

For a low pressure RF plasma source (pressures less than 75 mm of Hg), the plasma usually exists under extreme nonequilibrium conditions, having electron temperatures hundreds of times higher than the gas temperature, because very little momentum is transferred to the atoms or molecules by the electrons. At McDonnell, a high temperature gas has been measured at low pressures when a good match between the exciting coils and the plasma was obtained. This heating can be explained by inelastic collision between the electrons and the neutrals followed by a rapid relaxation which gives off kinetic energy to the gas. At the McDonnell facility, electron concentrations of 10^{13} per cc and gas temperatures near 10,000°K were measured in the test

section, four inches below the coil region. The gas pressure was less than 1 mm of Hg. For a generator operated near one atmosphere, the plasma is always a high density thermal type with high Joule heating.

The RF generator has been used for diffusion and seeding experiments. These experiments are important as they provide basic physical data at conditions near those experienced during re-entry.

The RF generator has the advantages of a simple, well-understood design, continuous contaminate-free operation over a wide range of conditions, and at times high neutral gas temperatures. Its major disadvantages are small test volumes and high RF noise levels.

GLOW DISCHARGE

The glow discharge is a well known phenomena of gaseous electronics which appears at a low pressure (typically 10 mm of Hg or less) with current densities between .001 and .5 amperes per cm^2. The appearance of the discharge is quite complicated, with a number of light and dark regions occurring along the axis. The ionization near the cathode is caused by positive ion bombardment of the cathode; the ionization in the positive column is caused by electron bombardment of the neutral gas. The positive column is a long luminous region extending almost to the anode, and is the most important region for plasma tests.

Basically a glow discharge facility is made from some convenient dielectric material such as Pyrex tubing, capped at each end by an electrode, and sealed to insure a good vacuum. To obtain a high current density without the glow discharge breaking down into an arc discharge, cathode designs

such as a hollow cathode are required.[6,7,8] The cost of a given discharge tube is relatively inexpensive; the major expense is the power supply. The plasma shape is determined by the container geometry; therefore, a wide range of plasma shapes are possible. McDonnell facilities include a rectangular glow discharge tube designed to simulate the plasma distribution in the boundary layer of a re-entry vehicle. This facility (Figure 5) measures 18" long, 12" high, and 1" thick, and, among many applications, has been used to investigate pulse degradation over varied plasma conditions.[9,10]

Many authors discuss the characteristics of the positive column of the glow discharge[11,12,13]. In the range of pressures from 0.1 to 10 mm of Hg, the loss of electrons and ions from the positive column to the walls is primarily due to ambipolar diffusion. The distribution of electrons across a cylindrical tube is a Bessel function, and the distribution across a rectangular tube is a sine function. The electron concentration along the axis is proportional to the current density and inversely proportional to the electron drift velocity. With a hollow cathode, electron concentrations of 10^{12} electrons per cc can be generated before the glow discharge degenerates to an arc discharge. Since the glow discharge operates at low pressures, thermodynamic equilibrium between the gas components does not exist. The electron temperature is on the order of 30,000°K, while the gas and ion temperatures are slightly higher than room temperature.

A high power glow discharge is capable of generating plasmas of various shapes and of relatively large volumes, is continuous in operation, and is controllable over a wide range of conditions. The plasma conditions are well established, and the facility is inexpensive to build and operate. The test gas does not provide real gas temperatures and contains a small DC electric

field. Striations at some conditions introduce some rapid fluctuations in the plasma, and a small amount of sputtering at the cathode introduces contamination; nevertheless, this facility provides probably the best plasma environment for static electromagnetic studies.

LOW PRESSURE FLAMES

The ionization induced by the high temperatures in various flames both at atmospheric and reduced pressures has been used to simulate re-entry plasma conditions. Since the ionization potentials are very high for all the ordinary equilibrium flame gases, O_2, N_2, H_2, H_2O, CO, CO_2, OH, O, and H, the amount of ionization from these ingredients is quite small. Only NO, whose equilibrium concentration is usually below one percent, has a low ionization potential which leads to ionization levels of about 3×10^{10} electrons per cc at flame temperatures. The addition of one part in 10^6 of Ca., or one part in 10^8 of K. or Na. gives higher ionizations than that due to NO. In organic flames, high values of ionization are generated through a chemi-ionization process. Here the energy of an elementary exothermic chemical reaction leaves one of the products in an ionized state.

Huber and Gooderum[14] produced a potassium-seeded cyanogen oxygen flame. Vaporized potassium was introduced into the flame whose gases were then expaned through a 3 inch diameter subsonic free jet. The temperature of the flame was about 4,200°K. The resulting plasma was probed with transmitted frequencies up to 20 Kmc. At SRI,[15,16] a low pressure ethylene-oxygen flame was used to study the effect of plasma in the near-zone field of an antenna and on antenna breakdown. An Langley[17], rocket exhausts were

blown across models in an altitude chamber to simulate a re-entry plasma sheath. The rockets produced a thrust of about 100 pounds for 10 to 20 seconds and a gas Mach number near ten. Signal attenuations of the order of 40 db at 244.3 Mc were recorded.

The low pressure flame gives a continuous high temperature plasma when seeded with alkali metals. The gradients of plasma conditions are severe and not very controllable. Some of the constituents of the flame may also be toxic. This facility, however, provides a good environment for antenna breakdown tests.

ALKALI PLASMAS

The vapors of the alkali metals are particularly attractive as the test gas for plasma generators because of their low ionization potentials. Both photon and contact ionization are used to excite the neutral molecules. Photon-ionization is supplied by ultraviolet radiation in the wavelength range from 2000 to 3180 angstroms; the lower limit is determined by the availability of window material. Contact, or resonant, ionization is obtained at the hot surface of an emitter. The condition for ionization is that the work function of the emitter at the emitter temperature exceeds the ionization potential of the gas. This condition is met in a cesium vapor on refractory metal emitters (W, Mo, Ta) at high temperatures (greater than 2000°K). The test chamber must be heated to a high temperature in order to have an appreciable vapor pressure of the metal. At low test chamber pressures, a magnetic field is applied to reduce recombination at the walls.

A typical ultraviolet generator of this type is about three feet long, four inches in diameter, and constructed of materials such as quartz[18] or

stainless steel[19], carefully bonded and sealed to resist the highly corrosive nature of the alkali metals. By controlling the temperature of the container walls, the pressure in the tube is controlled. The ultraviolet radiation is generated by any one of a number of commercial sources such as a B-H6 high pressure capillary tube. The radiated power enters the tube through quartz windows. The use of a heated refractory metal as the ionizing source is very similar, as demonstrated in the construction of microwave plasma amplifiers, thermionic converters, and ion engines.

Preliminary data at McDonnell has indicated that in a magnetic field of 600 gauss a concentration of 10^{12} electrons per cc can be obtained with 160 watts of ultraviolet radiation. This represents an ionization of about 1.0 percent. Wade and Knechtli[20], using a contact ionizing source, have reported similar concentration with a 90 percent ionization at magnetic field strengths of 1500 gauss. For this case, the electron temperature was about the same as the emitter temperature, about 2100°K.

The alkali plasmas have been used as an ion source for space engines[21], as the plasma for microwave amplifiers, in thermionic converters[22], and in plasma wave studies.[18]

The advantages of the alkali metal plasma are its high percentage of ionization, freedom from extraneous electric fields, and its continuous operation. Its disadvantages are the usual presence of a magnetic field, low electron collision frequencies, and the limitations of a test gas to only alkali metals, which are very difficult to handle because of their highly corrosive nature. With generators of the present designs, re-entry communication testing cannot be practically performed in alkali metal plasmas.

DIAPHRAGM SHOCK TUBE

The shock tube, in its simplest form, is a tube divided by a thin diaphragm into two chambers, the driver (high pressure) section and the driven (low pressure) section. Upon bursting of the diaphragm, a family of compression waves originates at the pressure interface, and travels into the low pressure section, rapidly forming into a shock wave. Behind the shock there is a region of steady flow, which is the normal region for testing. Testing is also accomplished in the gases that are stagnated by the shock wave reflecting off the end of the tube.[23]

The details of operation may be characterized by the shock Mach number relative to the unshocked gas. The Mach number and the initial conditions are sufficient to calculate the gas conditions immediately behind the shock. The optimum conditions for producing strong shocks are a low molecular weight and a low ratio of specific heats for the driver gas; and a high molecular weight for the driven gas. With helium at room temperature driving air, the maximum theoretical Mach number is only 10.6; with hydrogen into argon, the theoretical maximum is 26.8.

The simplest method to create a plasma is to increase the strengths of shocks by heating the driver gas. One of the most common procedures is to use a multi-diaphragm shock tube. The first diaphragm is burst, creating a shock which heats the gas in a second compartment, which in turn is used as the driver gas for generating the test shock. A combustible mixture, such as oxygen and and hydrogen, may also be used to heat the driver gas. A third method to obtain strong shock velocities is to reduce the cross-section of the flow. The strongest shocks have been achieved by combining several of these methods.

Diaphragm shock tubes have diameters generally greater than one inch in order to avoid undue attenuation of the shock from boundary layer drag on the walls. The test section is located at least 8 to 10 tube diameters from the diaphragm in order for a plane, well-defined shock to have a sufficient distance to form. The driver section must be sufficiently long to allow the experiment to be completed before the rarefaction wave is reflected from the back of the driver section.

The shock tube at AVCO[24] consists of a 50 foot long, 24 inch diameter, low pressure section, and a 6 foot long, 5 inch diameter high pressure section, connected by a 4 foot long transition section. The driver gas consists of the combustion products of a hydrogen, oxygen, and nitrogen ignited by four exploding wires. Normally copper diaphragms are used; these burst open after the pressure builds up to 140 atmospheres. For a high performance shock tube as used at AVCO, the maximum shock Mach number reported in air is 23. At an initial pressure in the test section of 20 microns of Hg, this Mach number would generate a density rise of 17 and a temperature of 5500°K, which is an electron concentration of 4×10^{12} per cc and an electron collision frequency of 10^{10} encounters per second. These conditions will remain relatively constant for the duration of the test period, approximately 30 microseconds for this example.

The diaphragm shock tube produces a flow that is well understood, that is relatively free of foreign material, and that is in thermal equilibrium between electrons, ions, and neutral species. The disadvantages are related to its short test time.

ELECTROMAGNETIC SHOCK TUBE

The electromagnetic shock tube was originally developed to surmount the limits of the conventional diaphragm-type shock tubes. The basic principle of the EM shock tube is the rapid discharge of capacitor stored energy through low pressure gas in a chamber. The discharge heats, ionizes, and accelerates the gas out of the discharge region into the regions of cold gas. The acceleration takes place by the combination of pressure of thermal origin and magnetic currents. In some cases the hot gases are preceded by a shock in the cool gases downstream of the discharge region. In practice only rough calculations of the gas conditions can be made, as the processes involved are not understood.

An excellent review article on electromagnetic shock tubes has been written by Thornton.[25] The construction of an electromagnetic shock tube is similar to that of the diaphragm types, except that strong shocks may be produced without the mechanical problems associated with the high pressure driver section and diaphragm. Typical tubes are 2 to 6 inches in diameter and many feet long. Figure 6 shows such a tube at McDonnell. A typical system might consist of a low inductance 5μ fd, 20,000 volt capacitor; a 20,000 volt supply; and a triggered spark gap switch for discharging the capacitor through the electrode system. When used with a tube of the general type described above, such a capacitor will produce peak discharge currents of 10^5 amperes, ringing at frequencies greater than 100 KC.

Many of the characteristics of the electromagnetic shock tube are logical extensions of those of the diaphragm-type tube. Maximum reported velocities

are on the order of 200 km/sec for air and 1000 km/sec for hydrogen, both at pressures below 100 microns Hg. The gas conditions behind the shock cannot be determined from the shock velocity alone, since the theory of operation of electromagnetic tubes is not as well understood as the diaphragm type. Measurements of electron concentrations behind shocks traveling at 10 km/sec indicate greater than 10^{13} electrons per cc for a period of 100 to 200 microseconds.

Electromagnetic tubes are being used in magneto-aerodynamic[26] and reaction kinetic studies[27], for injection of hot plasma into fusion type machines[28,29] and for plasma communication studies.

The electromagnetic shock tube is in a relatively early stage of development. It can produce high electron concentrations and high gas temperatures with moderate power levels. The flow is quite complicated, with ionization existing in more than the shock-processed air. The flow is as yet not theoretically understood; therefore, the conditions must be measured experimentally, and, if adequate instrumentation is employed, it provides the most easily obtainable high electron concentration in the laboratory for very low cost.

SHOCK TUNNEL

The shock tunnel, in its early development, involved the addition of a diverging nozzle to the end of a conventional shock tube. By expanding these hot gases through a nozzle, the gas temperature would drop, and the gas velocity would rise, resulting in a high Mach number simulation for models suspended in the flow. Accurate simulations of re-entry Mach and Reynolds numbers are the primary object of this facility.

The shock tube portion of this facility consists of a driver section, diaphragm and throat. Connected to the throat is the nozzle section. This consists of a two-stage bilateral expansion, first in the horizontal plane, and then in the vertical plane. The opening of the second nozzle may be utilized as the test section, or expanded and joined with a constant diameter test section.

A large hypersonic shock tunnel is operated by Cornell Aeronautical Laboratory[31]. The tunnel has a driver tube 40 feet long, 20 feet of which can be heated, and a driven section 50 feet long. The test section utilizes a 24 inch diameter, 10.5 degree half angle conical nozzle.

This facility has been complemented by a wave superheater hypersonic tunnel.[32] This tunnel operates as a Gatling gun, with a large number of shock tubes firing in sequence and timed to give a continuous flow of high temperature gas. Test times have been increased to 15 seconds in this facility.

The test section electron density varies only slightly for a wide range of tunnel operating regimes and stagnation conditions.[33] From the attenuation of electromagnetic signals, a typical value for electron concentration in unseeded flows is 10^{10} electrons/cm^3. Care must be taken in cleaning the walls of the facility to eliminate seeding the flow with contaminates, which usually increase the ionization in the plasma sheath around the model. A survey of shock tunnel performance has been made by Vicente and Foy[34], and Hertzberg[31]. Stagnation temperatures of about 6000°K, at Mach numbers of about 25, are the typical maximum conditions obtained. For these conditions, electron concentrations and collision frequencies of 10^{12} electrons per cc and 10^{10} encounters per second can be expected. The test sections range

from 3 inches to 100 inches in diameter with test times up to 14 milliseconds. Since the original purpose of the shock tunnel was to simulate re-entry conditions for hypersonic vehicles, most experimentation performed to date has been directed towards that end. Past experiments have included a large number of flow diagnostic and instrumentation tests, antenna window tests and some electromagnetic plasma interaction studies.

The prinicpal advantage of the shock tunnel is its realistic simulation of shock shape and flow conditions around models of moderate size in a contaminate free flow. Electron concentrations are thermally generated and are of accurate levels in the stagnation region. However, aft body conditions cannot be obtained except by seeding the flow. The shock tunnel, nevertheless, is excellent for electromagnetic testing because it is the only facility in which realistic plasma sheaths are generated with a non-contaminate high velocity air flow. The wave superheater is particularly attractive because of its long test periods

HYPERVELOCITY IMPULSE TUNNEL

The Hypervelocity Impulse Tunnel, or "Hot Shot" tunnel as it is often called, gives accurate simulation of Mach and Reynolds number by expanding high pressure and temperature gases through a nozzle in the same manner as the shock tunnel. The difference is that the high pressure and temperature gases are obtained by an arc discharge in a pressurized chamber rather than a shock wave.

A typical Hypervelocity Impulse Tunnel (HIT) is comprised of an arc chamber, diaphragm, throat, conical expansion nozzle, and reservoir. The test section is any portion of the nozzle. The arc chamber is pressured by a mass of driving gas necessary to give the desired flow characteristics for the amount of electrical energy released and for the test section pressure. The expansion chamber is usually evacuated to about one micron of Hg. The facility at McDonnell has a nozzle 25 feet long culminating in a 50 inch diameter test section. A capacitor bank stores, at 12,000 volts, 7×10^6 joules of energy which is released into the arc chamber within three milliseconds at a peak discharge current of 3,600,000 amperes. A survey of "Hot Shot" tunnels has been made by Vicente and Foy.[34]

The plasma conditions in the stagnation region of the model can reach electron concentrations of greater than 10^{12} electrons per cc and collision frequencies of 10^{11} encounters per second, for arc chamber temperatures of 5000°K and pressures of 4000 atmospheres. The seeding of the flow by metallic properties, melted during the discharge, increases the electron concentration above those experienced by a re-entry vehicle similar conditions. At high temperatures and rapid nozzle expansions, as are required for these plasma conditions, the flow remains partially ionized even before interacting with the test model. This does not influence the stagnation region simulation but introduces errors into the other flow region simulation around the body. At extremely high arc chamber conditions (10,000°K), the entire flow contains ionization concentrations above 10^{12} electrons per cc for periods of up to 10 milliseconds.[35] Normal test periods are from 30 to 100 milliseconds.

This type of facility has been devoted to hypervelocity aerodynamic and thermodynamic simulation experiments of heat transfer rates, force and balance measurements, and pressure distributions along a test model.

The hypervelocity impulse tunnel is able to provide a large scale simulation over a wide range of re-entry conditions. Realistic shock structures can be generated. Flow velocities, temperatures, electron concentrations, and collision frequencies typical of re-entry conditions can also be obtained. A major disadvantage of the HIT for plasma communication experiments is the contamination in the flow stream which increases the ionization concentration and complicates diagnostics. The cost of utilizing such a large facility at the required high temperature is high, with recycle time relatively long.

ARC JET AND ARC HEATED TUNNELS

The arc jet and arc heated tunnels are continuous operating, high enthalpy facilities which heat the test gas by an electric arc, and then expand the high temperature gases through a nozzle. The arc jet is used for propulsion devices and high enthalpy generation; the arc tunnel is used to generate high velocity gas flows for re-entry simulation. The arc heated tunnel consists of the arc jet exhausting into a large vacuum chamber

A typical arc heater has a tungsten rod cathode and a copper anode in the shape of a converging-diverging nozzle. The arc is stabilized by vortexing or by using a moderate magnetic field. This causes the point of attachment to rotate on the anode and to produce more uniform heating with longer anode life. All parts which are subject to high heating rates are water cooled. The heating in the arc chamber is not uniform over the chamber area,

and therefore, the gases are trapped in a plenum chamber, where they come to a uniform temperature before they are expanded into the test chamber. Typical operating conditions are a centerline stagnation temperature of 5000°K, a static pressure of 425 microns of Hg, a flow rate of 1.16 grams per second, and a power input of 11.4 kilowatts.

Electron concentration measurements have been given by Talbot and Brundin.[36] They report 10^{10} to 10^{12} electrons per cm^3, measured both with Langmuir probes and microwave interferometry. Van Camp et al[37] measured 10^8 to 10^{10} electrons per cm^3 using single and double Langmuir probes in a hydrogen arc jet. Gas enthalpy calculations indicated concentrations of 10^8 BTU/lb should be obtained. Mach number ranges from 3 to 12.7[38]. The core, which contains these gases, is variable in size, and is greatly affected by the gas used and cone angle; for example, with a 6 inch diameter nozzle and with argon, a 1.5 inch diameter core was observed at Mach 9.

The experiments conducted thus far have been mainly of the diagnostic type, and have been aimed at obtaining a better understanding of the facility itself.[39] Some investigations of deep-space propulsion engines have been conducted in such a facility, and, where arc jet conditions were well known, ablation material studies were also performed.

Arc jets and arc heated wind tunnels have the distinct advantage of providing long duration, high enthalpy flow. Running times of thirty minutes have been reported. The facilities can be operated on air or other gases, but with air, contamination is introduced. The small size of the ionized core makes communication testing difficult.

FREE FLIGHT RANGE

The free flight range is a facility which propels small models at hypersonic velocities through a stationary environment. This high velocity flight has been accomplished through the use of light-gas type launchers.

The light-gas type of launcher may consist of one, two, or three stages of acceleration.[40] Typical single-stage launchers use a chemical combustion or an electrical discharge to heat a light gas (hydrogen or helium) which in turn drives the model. A two stage launcher uses the combustion of a propellant or a hydrogen-oxygen-helium mixture to accelerate a piston which in turn heats the light gas that accelerates the projectile. A three stage launcher just adds a second piston and a second combustible mixture. Single stage launchers have accelerated masses from 0.1 to 900 grams in the velocity range of 3.0 to 6.0 km/sec.[41] A large two stage launcher has accelerated a 1000 gram model to 6 km/sec.[42] In addition to the launcher, the free flight range includes a dump tank, to absorb the driver gas and to separate the protective sabot from the model, and an evacuated range with its associated instrumentation and pumping equipment. Free flight ranges are presently being operated at Arnold Air Development Center[43], General Motors Flight Physics Laboratory[44], NRL, Ballistic Research Laboratories[40], CARDE[45], and M.I.T.[46]

Since the plasma is created by a hypervelocity projectile, its characteristics closely approximate those of a full scale re-entry vehicle. However, where non-equilibrium effects are important, the small body sizes invalidate the simulation. The free flight range has been used for drag and stability studies, for ablation and wake studies[47,48], and for hypervelocity impact effects. This facility produces plasmas by the same mechanism and of the same shape as actual re-entry vehicles.

Free flight range experiments performed in the model wake should give good correlation to actual vehicle characteristics. As the only contamination in the test is produced by the vehicle itself, the facility is used to study the effects of ablative materials. The primary disadvantage of the facility is that only small model sizes can be used, and therefore, the plasma flow is highly restricted. The high g levels experienced in the launch phase require sturdy on-board equipment. All the diagnostic techniques are complicated by small model size, high velocity, and short test time. At present, tests are confined to propagation experiments in the wake plasma.

SUMMARY

The characteristics of the plasma generators are complied in Table 1. In this table the generators are typed as static, where the ionized gas is directly formed, and as dynamic, where the ionized gas either is contained in a high velocity flow or generated by a high velocity flow impacting on a test model. The plasma parameters are maximum values known to be available for the particular generator in reentry communication studies. All these values are not necessarily available concurrently or in the same facility. The test area is the usable cross-section of the plasma or the cross-section of the high velocity gases flowing across a test model.

Ionization equilibrium refers to the gas temperature. For facilities with test models, equilibrium is of course only in the stagnation region, with varying degrees of non-equilibrium ionization existing along the aft body as a function of model length and gas flow velocity, as is the case for the reentry vehicle. The difficulty of plasma parameter measurements is primarily a function of time available for measurement, the physical difficulties in making the measurements, and the lack of previous measurements. The desirable

test gas is air; however, most facilities' performance is improved by working with an inert gas. Detrimental contamination usually consists of metallic particles or gases which change the normal concentration from that which would be experienced in a pure air environment, thus hindering the accuracy of plasma sheath simulation and plasma condition measurement.

The cost of a facility, a most influential factor when selecting a plasma generator, can vary widely. The estimates given in the table are purely qualitative and consider both initial and operating costs. The stage of development reflects the amount of effort and the success in using such a facility for reentry simulation.

CONCLUSION

Most effects of plasma sheaths on electromagnetic signals can be experimentally studied without a flow velocity and a real gas temperature simulation. The reentry communication problem thus can be studied in considerable detail in static plasma facilities, provided a good description of the reentry plasma environment is available. Also techniques may be studied for alleviating the reentry communication blackout when the chemistry or when the modifications of the flow field are not involved. On the other hand, antenna breakdown, flow field seeding, shock effects with realistic gradients, and reentry communication studies with unknown plasma conditions, all require dynamic plasma simulation.

It is evident from an examination of the facilities discussed in this paper that most of them were not developed specifically for studying communication/plasma relationships. Nevertheless facilities are available for testing communication components or new techniques. In conclusion it is strongly recommended that these kinds of facilities be utilized to stretch communication technology.

ACKNOWLEDGMENT

The writers would like to acknowledge the support by the USAF Contract AF33(615)-1198, project monitor L.R. Nawman and the technical inputs of D. Hesser, project engineer, P. Krause, J. Fivel, and A. Kuhlman.

REFERENCES

1. Hesser, D.R., "Analysis of Plasma Generators", RTD-TDR-63-4222, 16 Jan. 1964

2. Reed, T.B., "Induction-Coupled Plasma Torch", Journal of Applied Physics, Vol. 32, No. 5, May 1961

3. Chuan, R.L., et al. "Plasma Heating of a Supersonic Gas Stream", ASME Paper 61-WA-245, 31 Aug. 1961

4. Eckert, H.U., "A Cool Mercury Plasma Tunnel", Journal of the Aerospace Sciences Vol. 26, No. 8, pg. 515, Aug. 1959

5. Mironer, A. and Hushfor, F., "Radio Frequency Heating of a Dense, Moving Plasma", AIAA Paper 63045-63, March 1963

6. Little, P.F. and von Engel, A., "The Hollow-Cathode Effects and the Theory of Glow Discharges", Proc. Roy. Soc. A 224, 209, 1954

7. Lidsky, L.M., Rothleder, S.C., Rose, D.J., and Yashikawa, S., Michelson, C., and Mackin, Jr., R.J., "Highly Ionized Hollow Cathode Discharge," Journal of Applied Physcis, Vol. 33, No. 8, Aug. 1962

8. White, A.D., "New Hollow Cathode Glow Discharge", Journal Applied Physics No. 5, 771, May 1959

9. Anderson, P.J., "A Rectangular Glow Discharge for Microwave-Plasma Interaction Studies" (to be published)

10. McPherron, T.R., "Study and Experimentation on Modulation Degradation by Ionized Flow Fields", Technical Documentary Report No. AFAL-TR-65-10 Feb. 1965

11. Cobine, J.D., "Gaseous Conductors", Dover Publication Inc. N.Y., 1941

12. Brown, S.C., "Basic Data of Plasma Physics", John Wiley & Sons, New York 1959

13. Penning, F.M., "Electrical Discharges in Gases", Philips Technical Library, Netherlands, 1957

14. Huber, P.W. and Goodcrum, P.B., "Experiments with Plasma Produced by Potassium-Seeded Cyanogen Oxygen Flames", NASA TN D-627, Jan. 1961

15. Chown, J.B., "Study of Plasma-Induced Voltage Breakdown at Low Pressure", SRI Rpt.3369F, July 1961

16. Taylor, W.C. and Weissman, D.E., "The Effects of a Plasma in the Near-Zone Field of an Antenna", Final Rpt. SRI Project 4555, July 1964

17. Cuddehy, W.F. and Hughes, J.K., "Simulated Reentry Tests of a Method for Reducing Radio Blackout by Material Addition to Ionized Flow Field", NASA TMX-988, Aug. 1964

18. Murphy, R.E. and Bruce, M.H., "The Hydromagnetic Wave Tube", AFCRL report Instrumentation for Geophysics and Astrophysics, No. 30, Nov. 1963

19. Walker, J.L., "An Ultraviolet Plasma Generator", McDonnell Aircraft Corporation (to be published)

20. Wada, J.Y., and Knechtli, R.C., "Generation and Application of Highly Ionized Quiescent Cesium Plasma in Steady State", Proceedings of the IRE, Vol. 49, No. 12, pg. 1926, Dec. 1961

21. Brewer, G.R., Currie, M.R., and Knechtli, R.C., "Ionic and Plasma Propulsion for Space Vehicles", Proceedings of the IRE, Vol. 49, No. 12, pg. 1789, Dec. 1961

22. Block, F.G., et al. "Construction of a Thermionic Energy Converter" Proceedings of the IRE, Vol. 48, No. 11, pg. 1846, Nov. 1961

23. Kantrowitz, A., "Shock Tubes for High Temperature Gas Kinetics", AVCO Research Report 141, Oct. 1962

24. Lin, S.C., Neal, R.A., and Fyfe, W.I., "Rate of Ionization Behind Shock Waves in Air", The Physics of Fluids, Vol. 5., No. 12, Dec. 1962

25. Thornton, J.A., "Electric and Electromagnetic Shock Tubes" AIAA Paper 63-368, Aug. 1963

26. Ziemer, R.W., American Rocket Society Journal, Vol. 29, pg. 642, 1959

27. Griem, H.R., and Kolb, A.C., Journal of Quantum Spectroscopy and Radiation Transfer Vol. 29, pg. 503, 1963

28. Scott, F.R. and Wenzel, R.F., Physical Review Vol. 119, pg. 1187, 1960

29. Tuckfield, R.G., Jr., Scott, F.R., and Drall, N.A., Bulletin of American Physical Society Vol. 8, pg. 162, 1963

30. DeLash, R.G., "Antenna Window a Technique for Propagating through a Plasma Sheath", Bendix Corp. Rpt. 8420-3, March, 1962

31. Hertzberg, A., Wittliff, C.E., and Hall, J.G., "Development of the Shock Tunnel and Its Application to Hypersonic Flight", Hypersonic Flow Research, F.R. Riddell editor, Academic Press, 1962

32. "Wave Superheater Hypersonic Tunnel", Cornell Aeronautical Laboratory, Description and Capabilities, Oct. 1963

33. "Ionization Non-Equilibrium in Expanding Airflows," RADC-TN-60-231, Sept. 1960

34. Vicenti, F.A. and Foy, A., Aerospace Corporation Report TOR-169(3305)-1, "Hypersonic Wind Tunnel Facilities in the United States," March 1963

35. Joerger, C.D., "Investigation of Magnetohydrodynamic Waves", AFCRL-63-782, Nov. 1963

36. University of California Engineering Project Report HE-150-186, "A Comparison Between Langmuir Probes and Microwaves Electron Density Measurements in an Arc Heated Low Density Supersonic Wind Tunnel", January 1961

37. McDonnell Aircraft Corporation Report 9621, "Hydrogen Arc Jet Diagnostics", Aug. 1963

38. Sherman, F.S., and Talbot, I.L., "Diagnostic Studies of a Low Density, Arc Heated Wind Tunnel Stream", In Hypersonic Flow Research, F.R. Ridell editor, Academic Press, 1962

39. Potter, J.L. et al, "Gasdynamic Diagnosis of High Speed Flows Expanded from Plasma States", IEEE Transactions on Nuclear Sciences, Vol. NS11, pg. 145, Jan. 1964

40. Aberdeen Proving Ground Memo Report 1516, "A Survey of Light Gas on Development in the United States", Oct. 1963

41. Swift, H.F., "Hypervelocity Ballistic Accelerometers", Proceedings 5th Symposium Hypervelocity Impact, April 1962

42. Swift, H.F., et al. "NRL Accelerator Development", Proceedings 6th Symposium Hypervelocity Impact, Cleveland, Ohio, April 1963

43. AEDC-TDR-62-97, "Design of Light Gas Model Launchers for Hypervelocity Research", May 1962

44. Charters, A.C. "The Flight Range - A Tool of Research in the Physics of High Speed Flight", ARS Paper 1984-61, Aug. 1961

45. Hill, G.V., "Reentry Studies in Free Flight Ranges", Proceedings of the Seventh Anglo-American Aeronautical Conference, New York, N.Y. Oct. 1959

46. Loecker, B., "An Investigation of the Performance of a Compression Heater for Use with Gun Tunnels or Hypervelocity Launchers", Proceedings 6th Symposium Hypervelocity Impact, Cleveland, Ohio, April 1963

47. Eckerman, J. and Stern, R.G., "Electron-Ion Recombination in High Temperature Air", AIAA 63-445, Aug. 1963

48. M.I.T. Technical Report 266, "Electromagnetic Studies of Ionized Wakes", 20 April 1962

TABLE 1

SUMMARY OF PLASMA GENERATORS

FACILITY	R F GENERATOR	GLOW DISCHARGE	LOW PRESS FLAME	ALKALI PLASMAS	DIAPHRAGM SHOCK TUBE	ELECTROMAG-NETIC SHOCK TUBE	SHOCK TUNNEL	HIT	ARC HEATED TUNNELS & ARC JETS	FREE FLIGHT RANGE
TYPE	STATIC	STATIC	STATIC & DYNAMIC (IONIZED FLOW)	STATIC	DYNAMIC (IONIZED FLOW)	DYNAMIC (IONIZED FLOW)	DYNAMIC (MODEL)	DYNAMIC (MODEL)	DYNAMIC (IONIZED FLOW)	DYNAMIC (MODEL)
MAX ELECTRON CONCENTRATION (CM^{-3})	10^{13}	10^{12}	10^{12}	10^{12}	10^{13}	10^{14}	10^{12}	10^{12}	10^{12}	10^{12}
MAX COLLISION FREQUENCY (SEC^{-1})	10^{12}	10^{10}	10^{10}	10^{6}	10^{10}	10^{9}	10^{10}	10^{11}	10^{10}	10^{10}
TEST AREA	3 IN DIA	12 IN ^{2}	3 IN DIA	5 IN DIA	24 IN DIA	6 IN DIA	100 IN. DIA	50 IN. DIA.	1.5 IN DIA.	3 IN DIA WAKES
GAS TEMPERATURE ($^{\circ}K$)	100 TO 10,000	300	4200	500	5000	HIGH	6000	5000	5000	5000
IONIZATION EQUILIBRIUM	EQUILIBRIUM TO NON-EQUILIBRIUM	NON-EQUILIBRIUM	NON EQUILIBRIUM	NON-EQUILIBRIUM	EQUILIBRIUM	NON-EQUILIBRIUM	EQUILIBRIUM	EQUILIBRIUM	EQUILIBRIUM	EQUILIBRIUM
TEST TIMES	CONTINUOUS	CONTINUOUS	CONTINUOUS	CONTINUOUS	30 μ SEC	100 μ SEC.	55 MILLISECONDS OR 15 SEC.	100 MILLISECONDS	CONTINUOUS	MILLISECOND
PLASMA PARAMETER MEASUREMENT	AVERAGE	EASY	AVERAGE	DIFFICULT	AVERAGE	DIFFICULT	DIFFICULT TO AVERAGE	DIFFICULT	AVERAGE	DIFFICULT
COMPOSITION	AIR, INERT GASES	AIR, INERT GASES	COMBUSTIBLE MIXTURES WITH ALKALI SEEDANT	ALKALI METALS	AIR	AIR	AIR	AIR	AIR, INERT GASES	AIR
CONTAMINATION	SMALL	SMALL	NA	NA	SMALL	SMALL	SMALL	SIGNIFICANT	SIGNIFICANT	NONE
COST	MODERATE	INEXPENSIVE	INEXPENSIVE	MODERATE	MODERATE	INEXPENSIVE	EXPENSIVE	EXPENSIVE	MODERATE	EXPENSIVE
STAGE OF DEVELOPMENT	MODERATE	MODERATE	MODERATE	INITIAL	ADVANCED	INITIAL	MODERATE	MODERATE	MODERATE	MODERATE

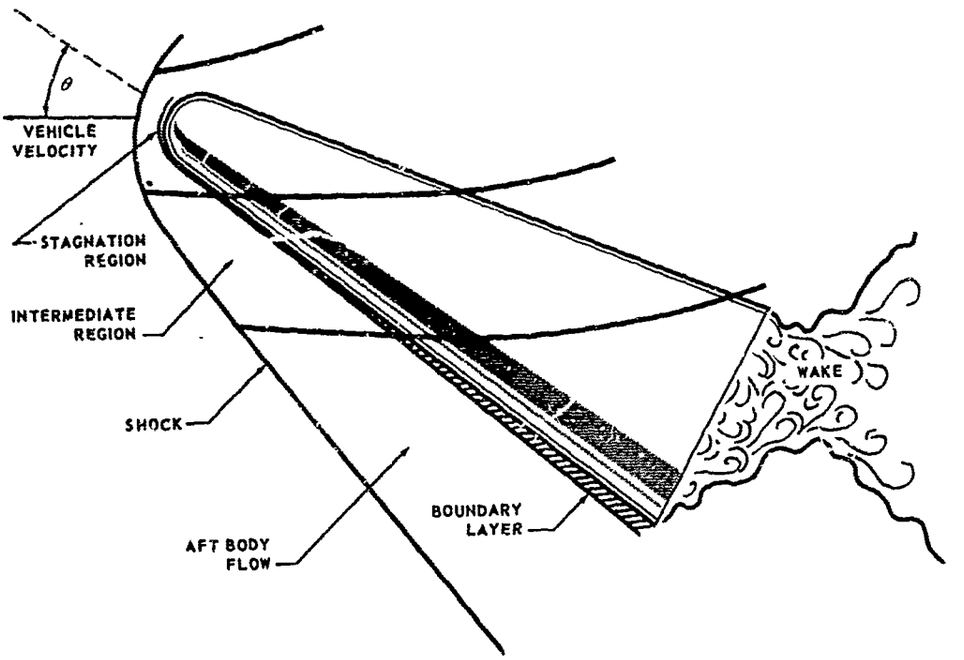


Figure 1. Flow regions about a conic shaped vehicle

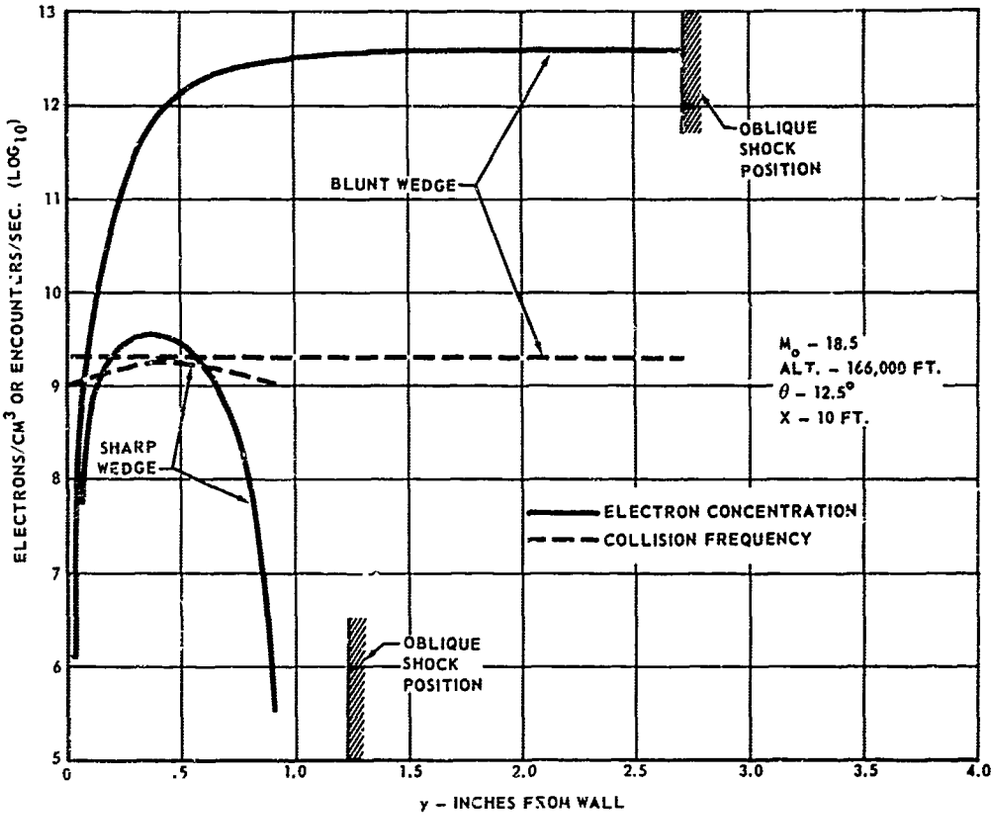


Figure 2. Boundary layer electron concentration and collision frequency (wedge configuration)

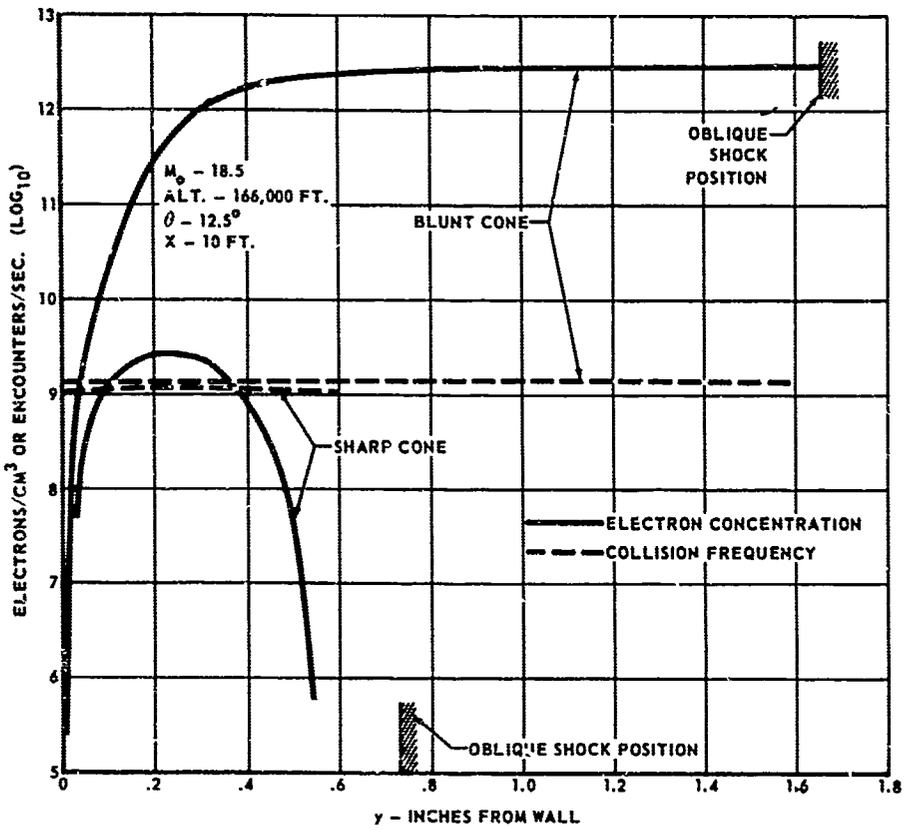
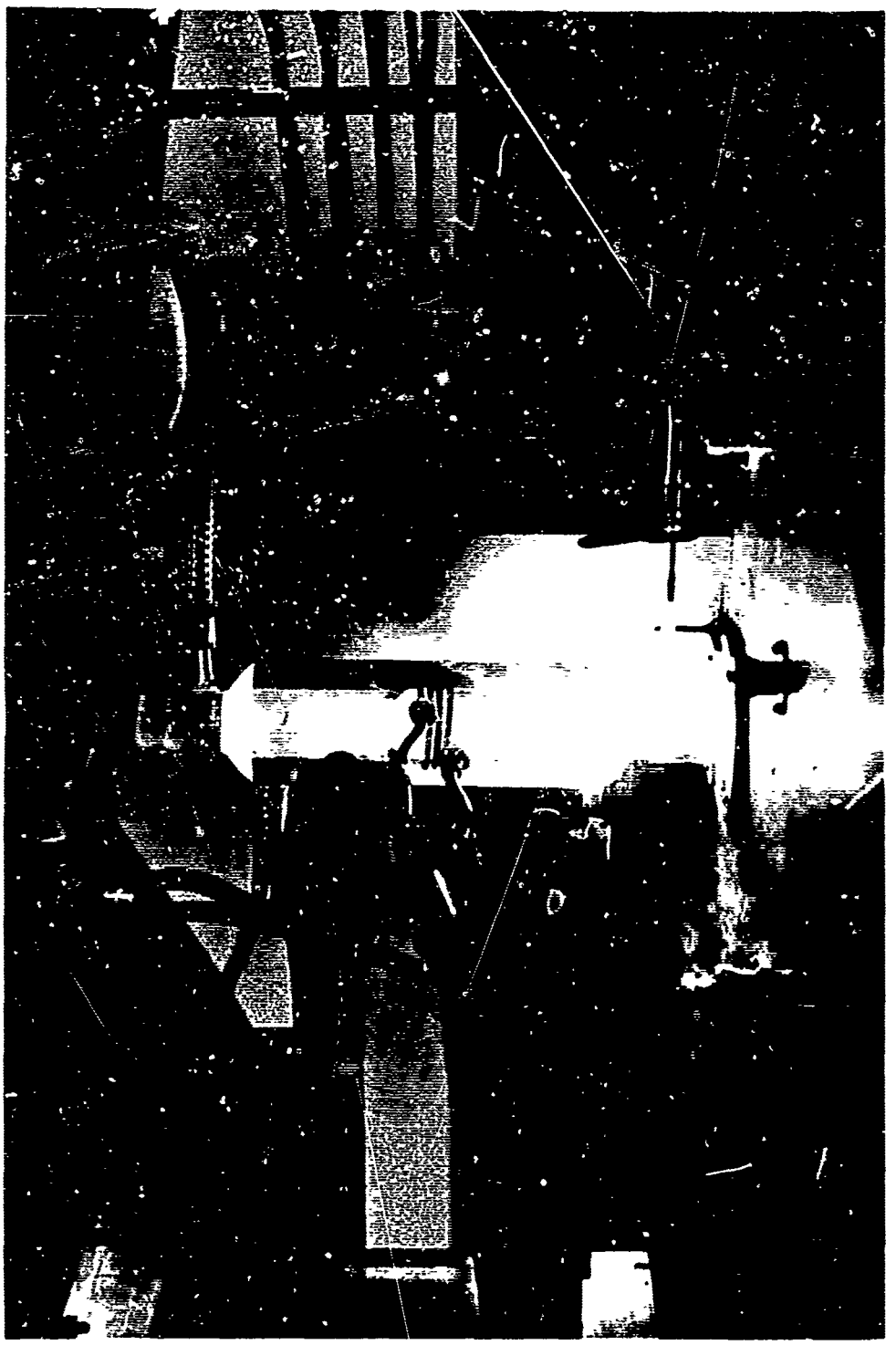


Figure 3. Boundary layer electron concentration and collision frequency profile (cone configuration)



RF PLASMA GENERATOR

FIGURE 4

RECTANGULAR GLOW DISCHARGE FACILITY SHOWING TEST SETUP FOR C-BAND TRANSMISSION

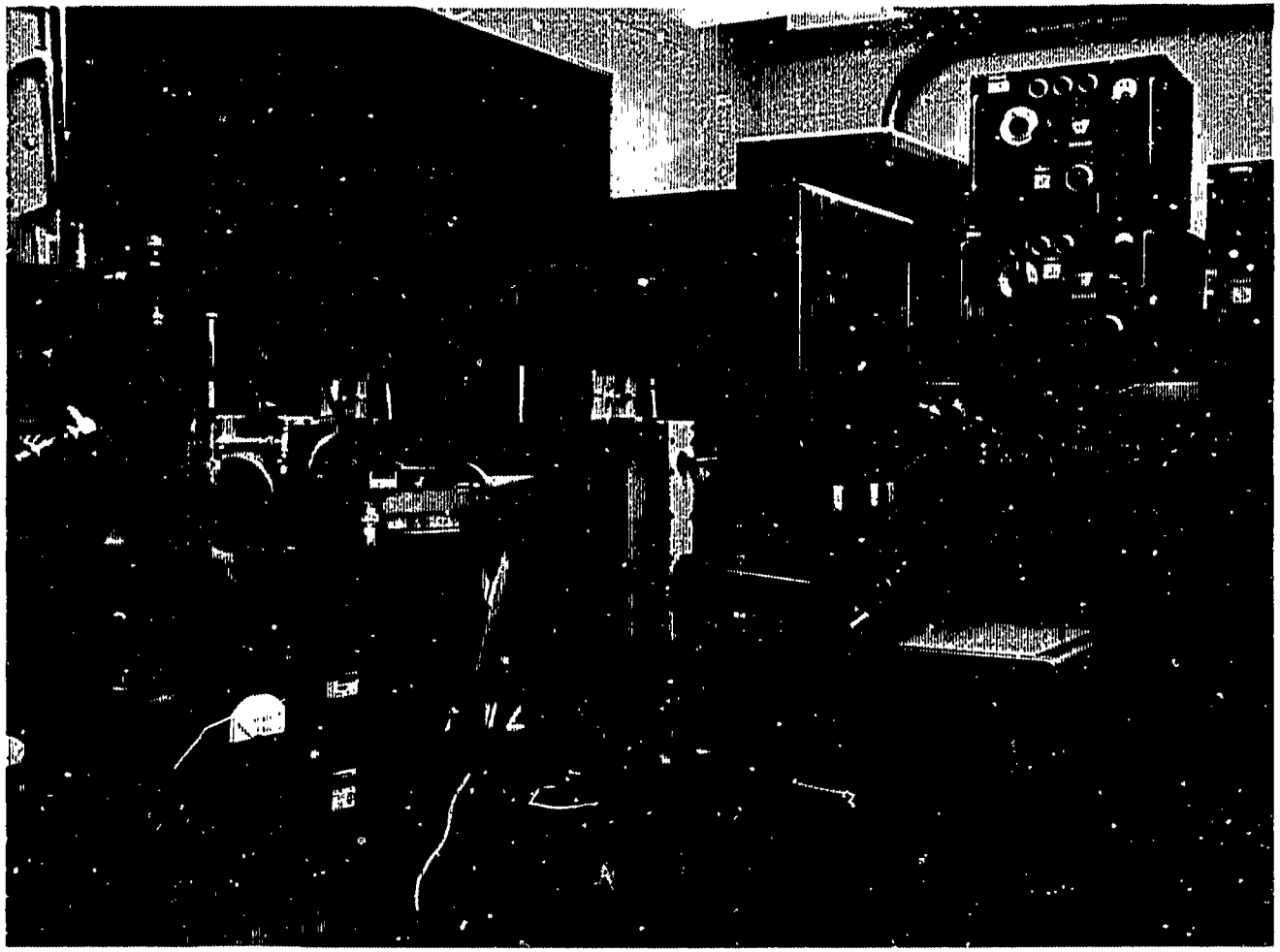


FIGURE 5

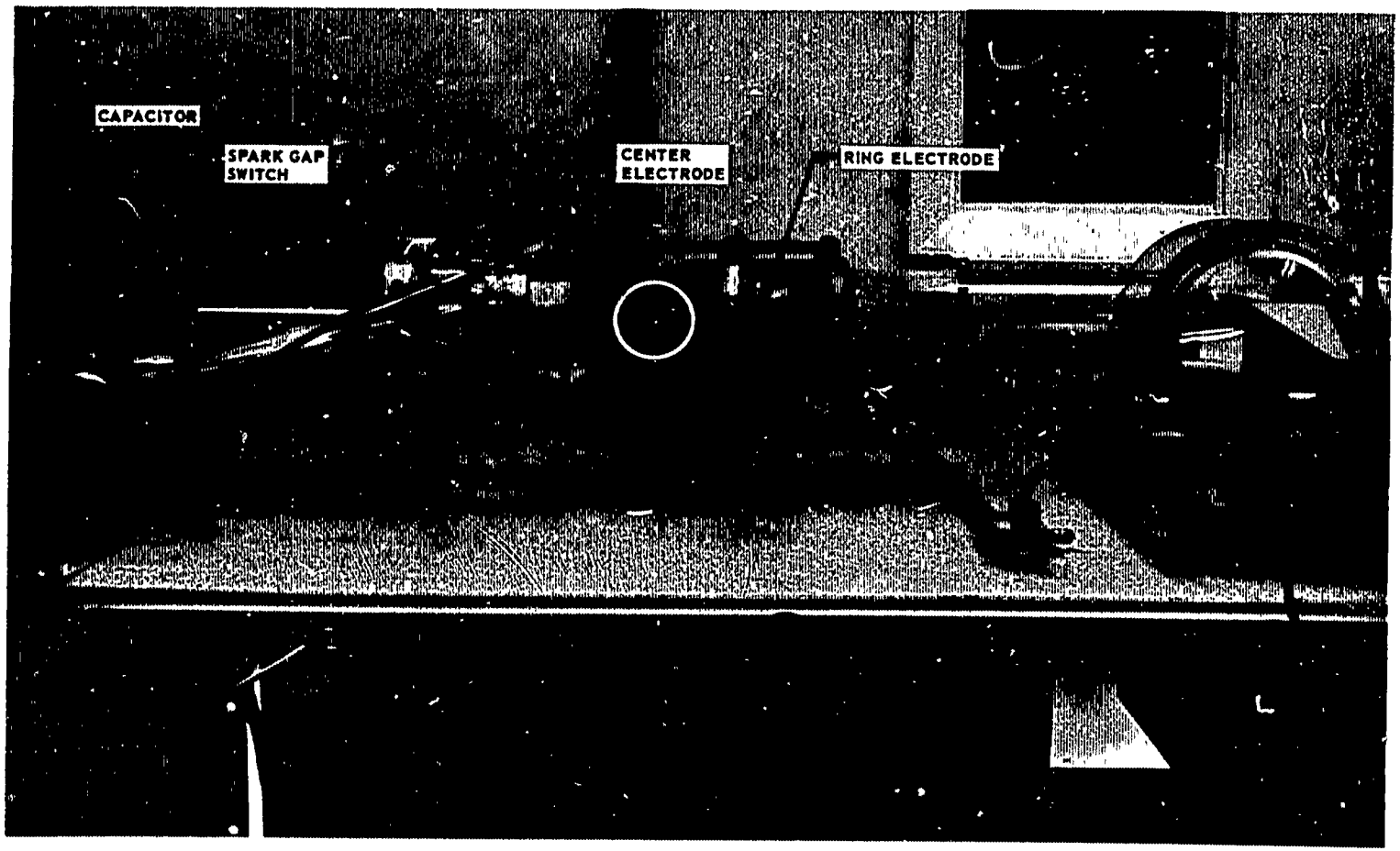


Figure 6. Electromagnetic shock tube showing driver section. The tube is 6 ft. long and 3 inches in diameter

II. SIMULATION OF REENTRY PLASMAS BY ELECTRODELESS DISCHARGES

H. U. Eckert

Plasma Physics Laboratory
Physical and Life Sciences Laboratory
Lockheed-California Company
Burbank, California

ABSTRACT

The absence of contamination by electrode material makes the electrodeless discharge a promising device for all reentry simulation studies where plasma purity is essential. In an analytical study the electron balance equation is evaluated for a steady, diffusion controlled discharge using microwave breakdown data and other empirical information for the ionization characteristics of air. Volume recombination is approximately taken into account in the calculation of electron density distributions across the discharge tube and is shown to cause appreciable electron depletion near the axis at rather low density levels. Effective absolute electron densities are calculated for particular tube radii and maintenance fields from the change in discharge characteristics with skin depth. These densities duplicate those encountered in light to medium severe reentry conditions.

In a practical application of the electrodeless discharge, the effect of typical ablating materials upon electron density has been measured by microwave techniques downstream of the discharge zone in a flowing system. The observed changes in electron density were found to correlate approximately with the changes in static pressure due to the addition of material. At fifty percent overpressure, cork produced an increase in electron density from $10^{10}/cm^3$ to $10^{11}/cm^3$ while teflon lowered it to $4 \times 10^{9}/cm^3$.

Section 1

INTRODUCTION

The electrodeless discharge has been known for more than fifty years as a light and ion source. More recently it has been shown by Babat[1] and Reed[2] that this discharge, when operated at high pressure, can also be a source of high temperature plasmas at a range previously believed obtainable only with direct current arcs. This latter feature is undoubtedly the main reason for the upsurge in interest. Compared to the arc, the electrodeless discharge has the advantage that the danger of plasma contamination by electrode material is eliminated. Since even traces of contaminants can considerably affect the radiative characteristics and electron density of a plasma, this advantage counts heavily in applications involving diagnostic and especially communication tests. Only if a clean plasma is used in a reentry model experiment can one expect that the results will hold for the free flight situation. Plasma purity is, however, not the only requirement for model experiments. The extent and reliability of information one can obtain from such experiments depend greatly on how well the processes of plasma generation in the discharge itself are understood. Since the inductive discharge represents a case of strong interaction between an ionized medium and an electromagnetic wave, its study has also a direct bearing upon the reentry communication problem. To start with an analysis of the induction torch, where thermal ionization and the superimposed flow field cause a highly complex situation, does not seem promising, however. The best chance

for success exists with a stationary medium pressure discharge at medium power level where ionization is primarily due to electron impact with gas molecules and deionization to ambipolar diffusion with subsequent recombination at the container walls. In this glow discharge regime the electron component is, of course, strongly out of equilibrium, and gas temperatures are not representative of reentry conditions. But electron concentrations are as we will see, and these may be of primary interest in a meeting concerned with electromagnetic aspects of reentry. In communication experiments it is, moreover, often desirable to eliminate the need for high temperature materials and techniques.

In several previous publications[3,4] we had developed a theory for the glow regime of the inductive discharge and applied the results to hydrogen. In this paper we want to briefly review this theory, point out the additional difficulties when applying it to discharges in air, and show what results can be obtained with a limited analytical effort.

Finally, we will report on some practical applications of an electrodeless discharge plasma.

Section 2

ANALYSIS: THE ELECTRON BALANCE EQUATION FOR INDUCTIVE DISCHARGES

2.1 RADIAL DISTRIBUTION OF ELECTRON DENSITY

It represents a significant step towards understanding an electric discharge if one is able to predict the electron concentration without recourse to diagnostic means. For an inductive rf discharge at medium pressure, the electron density depends on ionization characteristics of the gas and geometry of the discharge vessel as well as upon intensity and frequency of the induced electric field. We consider the vessel to be a long cylindrical tube positioned coaxially with the excitation coil, which is also long compared to its diameter, so that the problem is one of cylindrical symmetry and the radial coordinate r is the only space variable. The arrangement is illustrated in Fig. 1.

In a steady state discharge the electron density is constant with time and determined by the balance between ionization and deionization processes. Besides by diffusion the deionization of air takes place by electron attachment and volume recombination. Under these conditions the electron balance equation has the form:

$$\nu_i n = \nu_a n + \alpha n^2 - \frac{d^2(nD)}{dr^2} - \frac{1}{r}\frac{d(nD)}{dr} \qquad (1)$$

where ν_i and ν_a are the ionization and attachment frequencies, respectively, n is the electron density, α is the recombination coefficient, and D is the ambipolar diffusion coefficient, considered as variable with r. ν_i, ν_a, α, n, and D represent time averaged values.

We see that volume recombination introduces a nonlinearity into Eq. (1) which makes it difficult to solve. There have been published a few analyses of discharges with simultaneous diffusion and recombination losses in uniform electric fields[5,6] but none for nonuniform fields of which the inductive discharge is a case. We will show in the following how this problem can be attacked for small recombination rates.

Defining an effective ionization frequency

$$\nu = \nu_i - \nu_a ,$$

we rewrite Eq. (1)

$$\frac{d^2(nD)}{dr^2} + \frac{1}{r}\frac{d(nD)}{dr} + \left[\frac{\nu}{D}(r) - \frac{\alpha(nD)}{D^2}\right] nD = 0 . \qquad (2)$$

The local value of the expression ν/D is assumed to be determined by the effective induced electric field E, defined by $E = E_{rms}\,\frac{\nu_c}{(\nu_c^2 + \omega^2)^{1/2}}$ (ν_c = electron collision frequency; ω = driving frequency). E in turn is a function of r. The bracketed term in Eq. (2) thus represents the difference between two functions of r. Since E vanishes at the axis ν/D can be

expected to be zero there or slightly negative (due to attachment). At the wall, on the other hand, where $r = R$, E has maximum value E_R, and consequently ν/D will also be a maximum there. The electron density, however, is assumed to vanish at the wall so that $\alpha n/D$ will also vanish there. At the axis nD will be different from zero unless α becomes infinitely large.

It appears, therefore, that the range covered by Eq. (2) can be divided into three zones: A zone near the wall where electron production dominates and $\nu >> \alpha n$; a central zone around the axis where volume recombination dominates, so that $\alpha n >> \nu$; and a third zone between these two where both processes are of the same order and approximately cancel out.

A solution of Eq. (2) for the wall zone can be obtained if $\alpha n/D$ is set equal to zero and ν/D is represented by the power law

$$\frac{\nu}{D} = \left(\frac{\nu}{D}\right)_R \left(\frac{r}{R}\right)^q \qquad (3)$$

where the subscript R refers to conditions at the tube wall $r = R$.

When use is made of the boundary condition

$$nD = 0, \quad \text{at } r = R, \qquad (4)$$

the solution of Eq. (2) in the wall zone can be written

$$nD = C\left[Y_o(\xi) - \frac{Y_o(\xi_R)}{J_o(\xi_R)}\ J_o(\xi)\right] \tag{5}$$

where J_o and Y_o are the Bessel functions of zero order and

$$\xi = \frac{2}{q+2}\left(\frac{\nu}{D}\right)_R^{1/2} R\left(\frac{r}{R}\right)^{\frac{q+2}{2}} \tag{6}$$

is the transformed radial coordinate. ξ_R corresponds to the position $r = R$.

In the intermediate zone where $\nu/D \approx \alpha n/D$, the solution of Eq. (2) is simply

$$nD = C'\left(\ln \frac{r}{R} + C''\right). \tag{7}$$

In the vicinity of the axis, Eq. (2) reduces with $\nu/D = 0$ to

$$\frac{d^2y}{dx^2} + \frac{1}{x}\frac{dy}{dx} - ay^2 = 0 \tag{8}$$

where for briefness has been set

$$\frac{r}{R} = x, \quad nD = y, \quad \text{and } \alpha n \frac{R^2}{D} = a.$$

With the boundary conditions

$$y = y_o \quad \text{and} \quad \frac{dy}{dx} = 0 \quad \text{at} \quad x = 0\,, \tag{9}$$

the solution of Eq. (8) is given by the series*

$$\frac{y}{y_o} = 1 + a\frac{x^2}{4} + a^2\frac{x^4}{32} + a^3\frac{x^6}{256} + \frac{3a^4}{2192}\,x^8 + \ldots \tag{10}$$

Comparing the series (10) with that of the modified Bessel function

$$I_o(\beta x) = 1 + \beta^2\frac{x^2}{4} + \beta^4\frac{x^4}{64} + \beta^6\frac{x^6}{2304} + \ldots \tag{11}$$

We see that with $a = \beta^2$ the first two terms are identical while the third term in Eq. (10) is larger by the factor two. For values of a and x small enough to make the series converge, Eq. (11) may therefore be used in place of Eq. (10). Series (11) had been obtained in some recent work[7] as solution of the balance equation in the axial region for the case of a purely diffusion controlled discharge in a tube of finite length L where β represents the term $\pi R/L$. The rather tedious procedure of matching the regional solutions had already been carried out in that work. Now for $\beta = a^{1/2} = R(\alpha n/D)^{1/2}$ and within the above limits these matched solutions apparently also represent the effect of volume recombination upon the product nD. Since near the axis $n \approx n_o$ and $D \approx D_o$ the parameter β can be written

$$\beta = R\left(\frac{\alpha n_o}{D_o}\right)^{1/2} \tag{12}$$

---

* For this solution the author is indebted to D. P. Hamm of the Oceanography Department, Lockheed-California Company.

It represents the ratio of recombination to diffusion losses at the axis and is identical with that arrived at in References 5 and 6.

Typical nD distributions for the case $q = 8$ and various values of β are shown in Fig. 2. The case $\beta = 0$ is distinguished by a flat maximum at $x = 0$ while the other curves have a minimum there which deepens as β increases. An estimate indicates that for $\beta = 1$ the error made by using Eq. (11) instead of Eq. (10) is about 2 percent; for $\beta = 2$ it is around 8 percent. In the limiting case $\beta \to \infty$, n follows the power law distribution of Eq. (3). Electrons then have no time to diffuse and their distribution is identical to that at birth.

For a practical example, we take $\alpha = 10^{-8}\text{sec}^{-1}\text{cm}^3$, $R = \sqrt{10}$ cm, and $D_0 = 10^3\text{cm}^2\text{sec}^{-1}$. To obtain $\beta = 1$, requires $n_0 = 10^{10}$ electrons/cm^3. In view of the fact that electron densities of 10^{12}/cm^3 can be obtained without difficulty for electrodeless discharges in air, this is a rather low value which indicates a strong effect of volume recombination upon the shape of the density profile.

Some explanation has to be given about the role of the quantity q in Eq. (3) which enters as a parameter in all the results presented here. It accounts for the field nonuniformity across the discharge tube and is defined by[4]

$$q = R\left(\frac{d \ln \nu/D}{dE}\right)_R \left(\frac{dE}{dr}\right)_R . \qquad (13)$$

The first bracketed term is entirely determined by the properties of the air. The second one can be influenced by the strength of induction, that is, ampere turn density and frequency of current in the coil. It has been estimated[3] that q cannot be less than about 2 but may assume values of 20 and higher.

2.2 THE CHARACTERISTIC EQUATION

In order to obtain the absolute distribution of n from the nD/n_oD_o profiles in Fig. 2, additional information is needed in two respects. First, the distribution of D/D_o has to be known which, strictly speaking, must come from solution of the electron energy equation. This distribution is not critical however. As shown in Reference 4 it can approximately be derived from the distribution of E and a crude first approximation for the distribution of n/n_o can in fact be obtained by setting $D/D_o = 1$. The essential information needed is the value of n_o which determines the level of electron density.

It has also been shown in Reference 4 that for a diffusion controlled inductive discharge an effective value of the electron density $\bar{n}$ can be calculated for the higher density levels where the penetration depth of the rf field becomes less than the tube radius. Restriction of electron production to an increasingly more narrow wall zone will increase diffusion losses and require a higher field at the wall for maintaining the discharge. $\bar{n}$ can therefore be correlated with E_R for a tube of particular radius R. In the following we will indicate how this procedure must be generalized when the

electron density profile is represented by zonewise solutions.

The condition that in the wall zone nD vanish at ξ_R, and only there, determines ξ_R as a characteristic value

$$\xi_R = \lambda_1 , \tag{14}$$

where λ_1 is the first root of Eq. (5). It has the familiar value 2.405 in case the matching point is located at $\xi = 0$, that is, Eq. (5) holds over the entire tube radius. This is the limiting case $\alpha n_o \to 0$. In the other limiting case when the wall zone becomes infinitely narrow and $\xi \to \xi_R$, λ_1 approaches infinity. Values of λ_1 for intermediate cases are given in Reference 8.

Combining Eqs. (14) and (6) yields

$$\frac{2}{q+2} \left(\frac{\nu}{D}\right)_R^{1/2} R = \lambda_1 \tag{15}$$

As is well known[9], the term $(\nu/D)^{-1/2}$ represents a length which in a uniform field discharge ($q = 0$) equals the diffusion length Λ of the container. Thus, for the infinite cylinder

$$\Lambda_\infty = \frac{R}{\lambda_1} = \left(\frac{\nu}{D}\right)^{-1/2} . \tag{16}$$

For a finite cylinder of length L

$$\Lambda = R(\lambda_1^2 + \beta^2)^{-1/2} \tag{17}$$

where $\lambda_1 = 2.405$ and $\beta = \pi R/L$.

For the inductive discharge one can define from the coordinate transformation Eq. (6) or Eq. (15) an equivalent uniform field radius R' which is related to the geometrical radius by

$$R' = \frac{2R}{q+2} \tag{18}$$

This leads to the following expression for the diffusion length of the inductive discharge

$$\Lambda = R\left[\left(\frac{q+2}{2}\right)^2 \lambda_1^2 + \beta^2\right]^{-1/2} \tag{19}$$

where λ_1 is now dependent on β.

The similarity in the Eqs. (10) and (11) suggests that the recombination losses for the infinite cylinder be treated like axial diffusion losses in a finite cylinder and to set in Eq. (19)

$$\beta^2 = \frac{\alpha n_o}{D_o} R^2 . \tag{12}$$

Combining then Eqs. (12), (13), (16), and (19), we obtain the desired relationship between R and E_R, called characteristic equation of the inductive

discharge.

$$R\left[\frac{\nu}{D}(E_R)\right]^{1/2} = \left\{\left[1 + \frac{E_R}{2}\left(\frac{d \ln \nu/D}{dE}\right)_R f(\rho_R)\right]^2 \lambda_1^2 + \frac{\alpha n_o R^2}{D_o}\right\}^{1/2} \quad (20)$$

Here the function $f(\rho_R)$ stands for

$$f(\rho_R) \equiv \left(\frac{dE}{dr}\right)_R \frac{R}{E_R} \quad (21)$$

It represents the gradient of E at the wall related to the average gradient of E across the tube radius and is equal to one if no skin effect is present. The argument ρ_R in Eq. (21) is defined by

$$\rho_R = \sqrt{\frac{4\pi\bar{\sigma}\omega\mu}{c^2}}\, R \quad (22)$$

where $\bar{\sigma}$ is an effective plasma conductivity. The magnetic permeability μ in Eq. (22) has been assumed equal to one. ρ_R is related to the skin depth δ by

$$\rho_R = \sqrt{2}\,\frac{R}{\delta}\,. \quad (23)$$

In the regime where the discharge is sensitive to skin effect, we can therefore obtain a value for the plasma conductivity on the basis of Eqs. (20) to (22) if we know the relationship between R and E_R either from calculation or from experiment. From the conductivity we can proceed with a plausible assumption about the electron collision frequency to an estimate of the electron

density in the discharge. It is seen from Eq. (20), however, that the recombination term requires us to assume a value for n_o so that the electron density level can be obtained only through an iteration procedure. It is also not simple to determine the proper characteristic value λ_1 since this makes it necessary to establish the location of the matching point ξ between the wall and intermediate region.

An estimate has indicated that the first term on the right side of Eq. (20) is generally of the order 10^3. To bring the second term to the same order would require with the values for α, D, and R of the previous example $n_o = 10^{13} cm^{-3}$.

Although such densities are not unusual for inductive discharges, it did not seem warranted to include volume recombination in the evaluation of Eq. (20) at this time because of the still considerable uncertainties in the basic data and the large amount of additional labor involved. Rather, it was decided to calculate $\bar{n}$-values on the basis of diffusion losses alone.

With $\alpha n_o R^2/D_o = 0$ and $\lambda_1 = 2.405$, Eq. (20) reduces to Eq. (23) of Reference 4.

$$R = \frac{2.405\left[1 + \frac{E_R}{2} f'\rho_R)\left(\frac{d \ln \nu/D}{dE}\right)_R\right]}{\frac{\nu}{D}(E_R)^{1/2}}. \qquad (24)$$

2.3 CALCULATION OF EFFECTIVE ELECTRON DENSITIES FOR DISCHARGES IN AIR

To evaluate the relationship between R and E_R from Eq. (24) we have to know the variation of the function ν/D with E, or rather, in the general form with gas pressure as parameter, $\frac{1}{p^2}\frac{\nu}{D}$ as a function of E/p. Measurements of maintenance fields in air discharges from which this information could be extracted most conveniently are not available in sufficient quantity and quality. However, several authors have measured electric breakdown fields in microwave cavities, and these data yield $\frac{1}{p^2}\frac{\nu}{D_-}$ as a function of E/p, where D_- is the free electron diffusion coefficient. One can therefore obtain the desired information by substituting D for D_-. In Fig. 3 are shown the results of Herlin and Brown[10] and the more recent measurements of MacDonald, Gaskell and Gitterman[12]. The latter data, which represent averages from a greater number of tests, were used for the present calculations. Values of $\frac{1}{p^2}\frac{\nu}{D}$ were obtained from the relationship

$$\frac{D}{D_-} = \frac{\mu_+}{\mu_-} \tag{25}$$

where μ_+ and μ_- are the positive ion and electron mobilities, respectively.

In air, positive ions are believed to be mostly NO^+ ions. No information on the mobility of this ion could be found in the literature. According to the compilation of data given by McDaniel[13], mobilities of the N^+, N_2^+, N_3^+ and O_2^+ ions vary between 1.8 and 3.5 $cm^2/sec\ V$ at 760 Torr. A probable value of 2.5 $cm^2/sec\ V$ was therefore assumed. The value is not critical

since only the square root of the mobilities enters into the calculations. For μ_- a value of 400 $cm^2/sec\ V$ at 760 Torr was derived from the recent measurements by Schlumbohm[14] of drift velocities of electrons in nitrogen. With the above value for μ_+, this yields $\mu_+/\mu_- = 6.25 \times 10^{-3}$.

Since the driving frequency for inductive discharges is several orders of magnitude below microwave frequencies, the effect which electron cooling between driving cycles has upon the time averaged ionization frequency must be taken into account. This effect has been calculated by Gould and Roberts[11] for E/p values up to 50, and their results are reproduced in Fig. 4. The bottom curve represents the case $p\lambda = 0$, where λ is the wavelength of the driving field. In the regime of electrodeless discharges which we consider, $p\lambda$ would vary from about 10^3 to 10^5 which is best represented by the top curve labeled $p\lambda = 5 \times 10^4 \approx p\lambda = \infty$. Extrapolation of this curve to higher E/p values has been carried out as shown in the figure. It is facilitated by the measurements of Scharfman and Morita[15] and several other authors quoted in Reference 15 whose data are also shown in Fig. 4. Fortunately, the "modulation factor" represented by the ratio of curves $p\lambda = \infty$ to $p\lambda = 0$ becomes less significant for high E/p values and approaches one. The values for $\frac{1}{p^2}\frac{\nu}{D}$ obtained before were multiplied by this factor and the resulting function was found to be representable within $\pm$ 5% by the expression

$$\frac{1}{p^2}\frac{\nu}{D} = A \exp\left(-\frac{Bn}{E}\right) \qquad (26)$$

with A = 25000 and B = 240.

Combination of Eq. (26) with Eq. (24) then yields

$$pR = \frac{2.405}{A}\left[1 + \frac{B}{2}\frac{p}{E_R} f(\rho_R) \exp \frac{B}{2}\frac{p}{E_R}\right]. \qquad (27)$$

The evaluation of the system of Eqs. (21), (22), and (27), followed closely that described in Reference 4. It may be remarked that Eq. (22) yields $\bar{\sigma}/p^2$ as similarity parameter if pR instead of R is used as variable.

In order to obtain an effective electron density $\bar{n}$ from the conductivity data, the relationship

$$\frac{\bar{n}}{p^2} = \frac{\bar{\sigma}}{p^2}\frac{m}{e^2}\nu_c \qquad (28)$$

has been used which applies if $\nu_c >> \omega$. For convenience ν_c has been assumed to depend on p only, and the relation

$$\nu_c = 5.3 \times 10^9 p \qquad (29)$$

has been used[12,15]. Combination of Eqs. (28) and (29) yields with the numerical values for e and m

$$\frac{\bar{n}}{p^3} = 1.9 \times 10^{13}\frac{\bar{\sigma}}{p^2} \qquad (30)$$

where $\bar{\sigma}$ is in Mhos/cm.

The results of these calculations are shown in Fig. 5 where $\bar{n}/p^3$ is plotted vs. E/p with pR as parameter. A driving frequency of 8 Mc/sec corresponding to $\omega = 5 \times 10^7 \text{ sec}^{-1}$ has been assumed. The curves show the following:

1. The electron density level increases with increasing maintenance field.
2. For each pR exists a minimum value of E_R/p below which the discharge cannot exist.
3. For E_R/p values sufficiently above the minimum value for a particular pR, the effect of pR vanishes.

The first two results are plausible. The third one can be understood from the consideration that with increasing electron density the skin depth becomes so small that the effect of curvature of the tube wall becomes insignificant.

The selection of pressure if of course, not arbitrary if we want to stay in the diffusion controlled glow discharge regime. We estimate that at the upper limit of the graph p cannot be higher than about .1 Torr and for the bottom of the graph not higher than about 3 Torr. These pressures roughly correspond to altitudes between 100,000 and 200,000 feet and are within the range of interest for reentry experiments. The predicted electron densities then vary between about 10^9 and $10^{13}/\text{cm}^3$ which according to the calculations of Sicko and Fiskin[16] correspond to those encountered from light to medium severe reentry conditions.

While, as mentioned, volume recombination losses are not considered in these calculations, for the sake of simplicity some effects which would tend to raise the electron density have also been left out, most significantly the lowering of the attachment frequency at elevated gas temperatures and the reduction in diffusion losses by the pressure of the rf magnetic field. It is likely, however, that electrical insulation or cooling problems set a practical limit to operation at the high field side.

The final answer, as to what extent the calculated data are realistic and where the limits are has, therefore, to come from experiments. Diagnostic experiments for checking the calculated data are under way but coul not be finished in time and will be presented in a later paper.* Instead we are reporting some seeding experiments which are related to reentry phenomena.

*Note added February 1967: Limited experimental data obtained since presentation of this paper indicate fair agreement between calculated and measured $\bar{n}$-values when referred to the same pR. The measured values of E_R are however, lower by about 50 percent.

Section 3

EXPERIMENTS: PLASMA CONTAMINATION BY ABLATING MATERIALS

The purpose of these experiments was to explore the behavior of some typical ablating materials which are expected to influence the electron density in the shock envelope and the wake of a reentry body. The tests were made with an arrangement which is shown in Fig. 6. The discharge vessel is here an open 2-inch diameter quartz tube through which dry air is flowing at a velocity of a few feet per second and at a pressure of 0.8 Torr. At the exit section, the tube is traversed twice by an x-band microwave beam. The beam is modulated by spinning the reflecting microwave horn so that a better signal to noise ratio is obtained. To eliminate reflections from the tube walls, quartz segments are placed at a quarter wavelength on both sides of the tube. Since attenuation is very slight, the electron density is derived from phase shift alone, assuming a plausible value for the collision frequency. A sample of the seeding material weighing approximately 100 milligrams is placed near the front end of the tube at a suitable position where it is neither vaporized too fast by the plasma to affect the discharge noticeably nor too slow to cause an immeasurable effect. This position varies for materials with different heats of vaporization and has to be found by trial and error. Usually it took eight to ten minutes to completely vaporize the sample.

With solid seeding materials a problem exists in determining the ratio of seeding rate to air flow rate. Dividing the weight loss during a test by the

test time yields only a crude average of vaporization rates since these rates vary considerably during a test. They start with zero, go through a maximum and taper off to zero again at the end of a test run. Attempts to continually weigh the sample by suspending it on a tiny beam balance did not succeed. It was therefore decided to simply correlate the changes in electron density with the observed changes in static pressure of the plasma. Since the cross section of the flow is considerably restricted downstream of the discharge zone, one can expect that the mass addition essentially causes a rise in pressure rather than acceleration of the flow. According to Dalton's law, the pressure rise is proportional to the relative increase in the number of molecules, provided they are at the same temperature. This appears to be a fair assumption. It also seems justified to disregard the electron contribution to the pressure. Although the electron temperature may exceed that of the gas by an order of magnitude, the relative concentration of the electrons is only of the order of one hundreth of a percent. The number of molecules may be changed considerably, however, by chemical reactions between the seedant and air components. This would require a special investigation in each case and was beyond the scope of the present tests.

The measurements resulting from two materials having opposite effects on the electron density are shown in Fig. 7. Before seeding, the electron density is approximately $1.5 \times 10^{13}/cm^3$. Adding the combustion products of cork causes the electron density to rise, and at an overpressure of 55 percent the electron density has increased by an order of magnitude.

When the sample is burned out, pressure and electron density return to their original values. The effect of cork may be due partly to its content of alkali metals and partly to thermal electron emission from soot particles.

Sublimation of teflon, on the other hand, lowers the electron concentration as the second curve shows. This is known to be due to the liberation of fluorine which has a large cross section for electron attachment. That the curves for rising and descending pressure do not coincide indicates that time has not been completely eliminated as a parameter. Still, one can conclude from these data that the gross effects of seeding can be represented as a function of pressure.

In view of the pressure changes of up to fifty percent which represent high seeding ratios, the observed variations in electron density may appear rather small. One must consider, however, that the measurements were made downstream of the discharge where the plasma is decaying and the effects are reduced. There is also the possibility that mixing with the air stream was incomplete although the strong thermal agitation in the discharge zone does not make this very likely.

Evidence for chemical reactions in these tests was obtained from spectral observations of the plasma.[17] Cork produced strong CN bands at 3883 Å and 3590 Å as is shown in Fig. 8. With teflon, weak Si lines appeared, indicating that the quartz tube had been attacked by fluorine.

Although these tests were of an exploratory nature, they demonstrate the suitability of electrodeless discharges for investigating the effects of seeding materials.

Section 4

REFERENCES

1. G. Babat, "Electrodeless Discharges and Some Allied Problems," Journ. Inst. Elect. Eng. (London) Ser III, Vol. 94, pp. 27-37 (1947)

2. T. B. Reed, "Induction Coupled Plasma Torch," Journ. Appl. Phys. Vol. 32, p. 2534 (1961)

3. H. U. Eckert, "Equations of the Electrodeless Ring Discharge and Their Solution for the Breakdown Criterion," Proc. IVth Internatl. Conf. Ioniz. Phen. Gases I, p. 320-4, North Holland, Amsterdam, (1960)

4. H. U. Eckert, "Diffusion Theory of the Electrodeless Ring Discharge," Journ. Appl. Phys., Vol. 33, p. 2780-88 (1962)

5. E. P. Gray and D. E. Kerr, "The Diffusion Equation with a Quadratic Loss Term Applied to Electron-Ion Volume Recombination in a Plasma," Annals of Physics, Vol. 17, pp. 276-300 (1962)

6. V. I. Solunskii and B. L. Timan, "Volume Recombination in the Presence of Ambipolar Diffusion in a Gas Discharge Plasma," Soviet Physics-Techn. Physics, Vol. 9, pp. 207-10, (1964)

7. H. U. Eckert, "The Diffusion Controlled Electrodeless Discharge in a Finite Length Cylinder," Report LR 18428, Lockheed-California Company (January, 1965)

8. E. Jahnke and F. Emde, Tables of Functions, B. G. Teubner, Berlin 1938, pp. 204-5

9. S. C. Brown, Basic Data of Plasma Physics, J. Wiley, New York, 1959, p. 50

10. M. A. Herlin and S. C. Brown, "Microwave Breakdown of a Gas in a Cylindrical Cavity of Arbitrary Length," Phys. Rev. Vol. 74, p. 1650-56, (1948)

11. L. Gould and L. W. Roberts, "Breakdown of Air at Microwave Frequencies," Journ. Appl. Phys., Vol. 27, pp. 1162-70 (1960)

12. A. D. MacDonald, D. U. Gaskell, and H. N. Gitterman, "Microwave Breakdown in Air, Oxygen, and Nitrogen," Phys. Rev., Vol. 130, pp. 1841-50, (1963)

13. E. W. McDaniel, Collision Phenomena in Ionized Gases, John Wiley & Sons, New York, 1964, pp. 473-79

14. H. Schlumbohm, "Messung der Driftgeschwindigkeiten von Elektronen und Positiven Ionen in Gasen," Zeitschr. f. Physik, Vol. 132, pp. 317-27 (1965)

15. W. Scharfman and T. Morita, "Focused Microwave Techniques for Measurement of the Ionization Rate and Collision Frequency," Journ. Appl. Phys., Vol. 35, pp. 2016-20 (1964)

16. W. B. Sisco and J. M. Fiskin, "Basic Hypersonic Plasma Data of Equilibrium Air for Electromagnetic and Other Requirements," Electromagnetic Effects of Reentry, edited by W. Rotman and G. Meltz, Pergamon Press, New York, 1961

17. R. W. B. Pearse and A. G. Gaydon, The Identification of Molecular Spectra, 3rd Ed., Chapman & Hall, London, 1963, p. 112

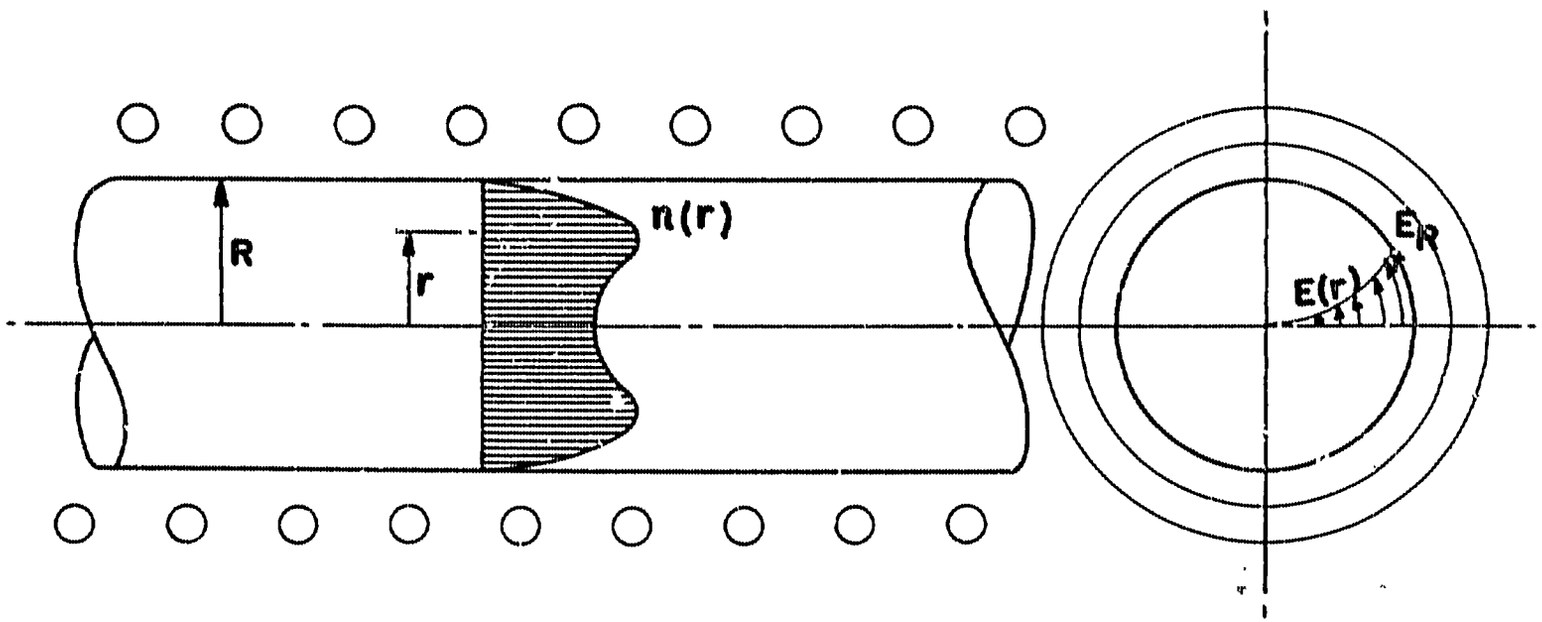


Figure 1. Outline of Inductive Discharge

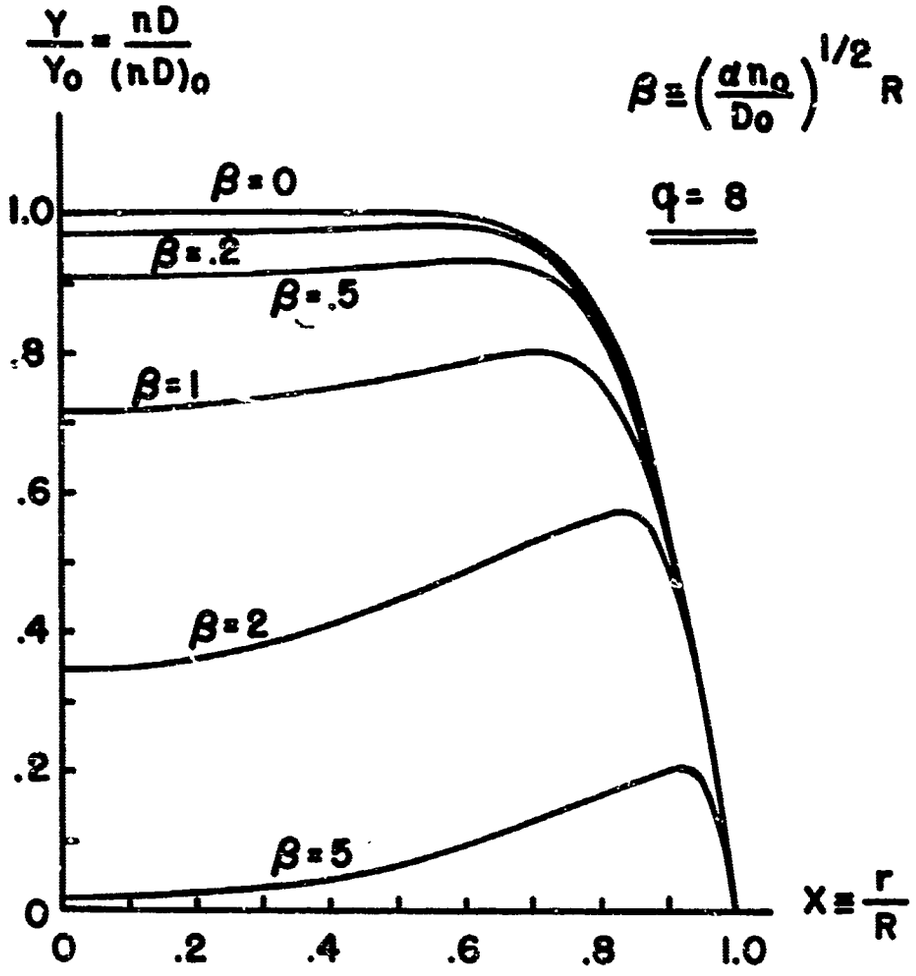


Figure 2. Effect of Volume Recombination upon Radial Distribution of Product Electron Density Times Diffusion Coefficient

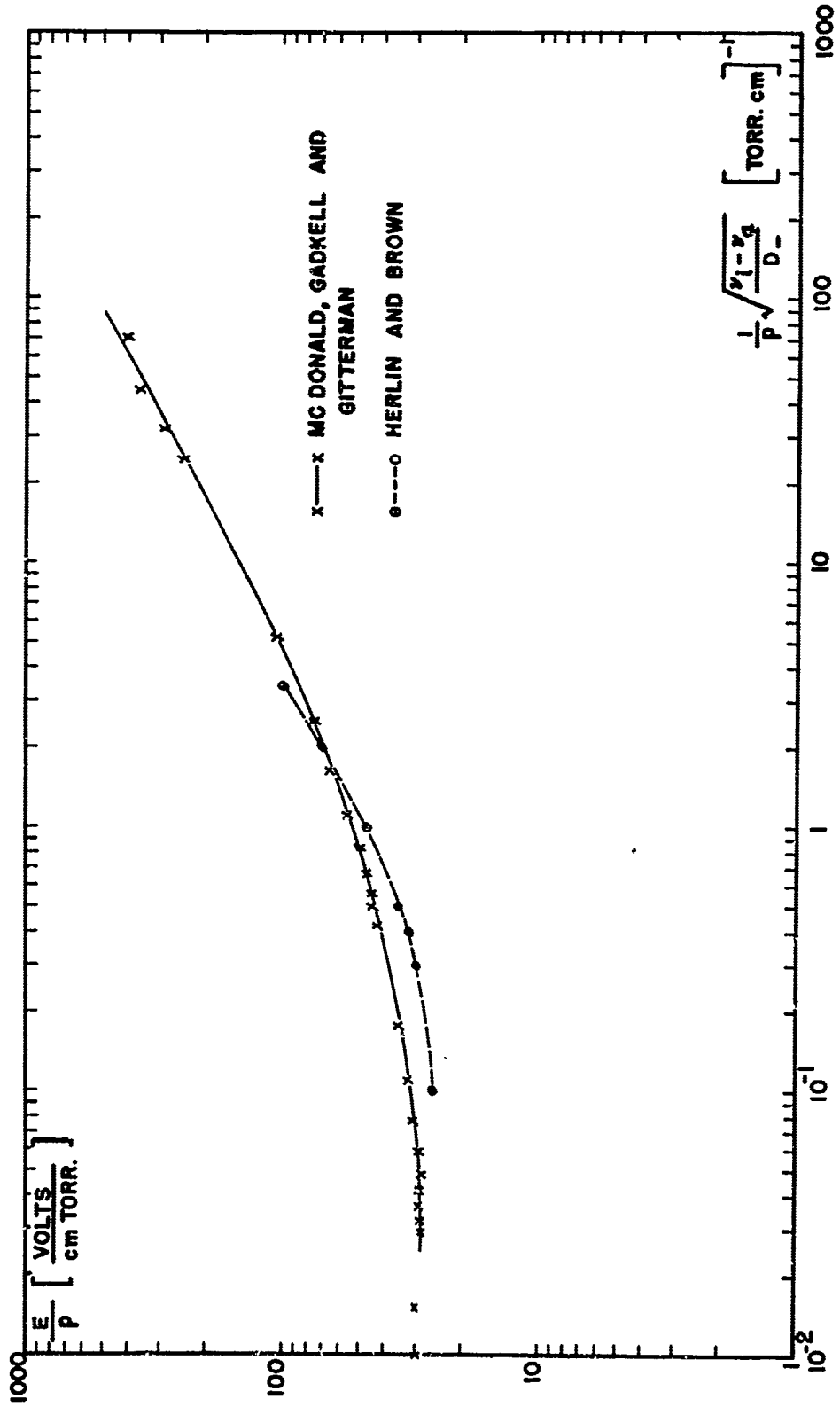


Figure 3. Ionization Function for Diffusion Controlled Discharges in Air from Microwave Breakdown Tests

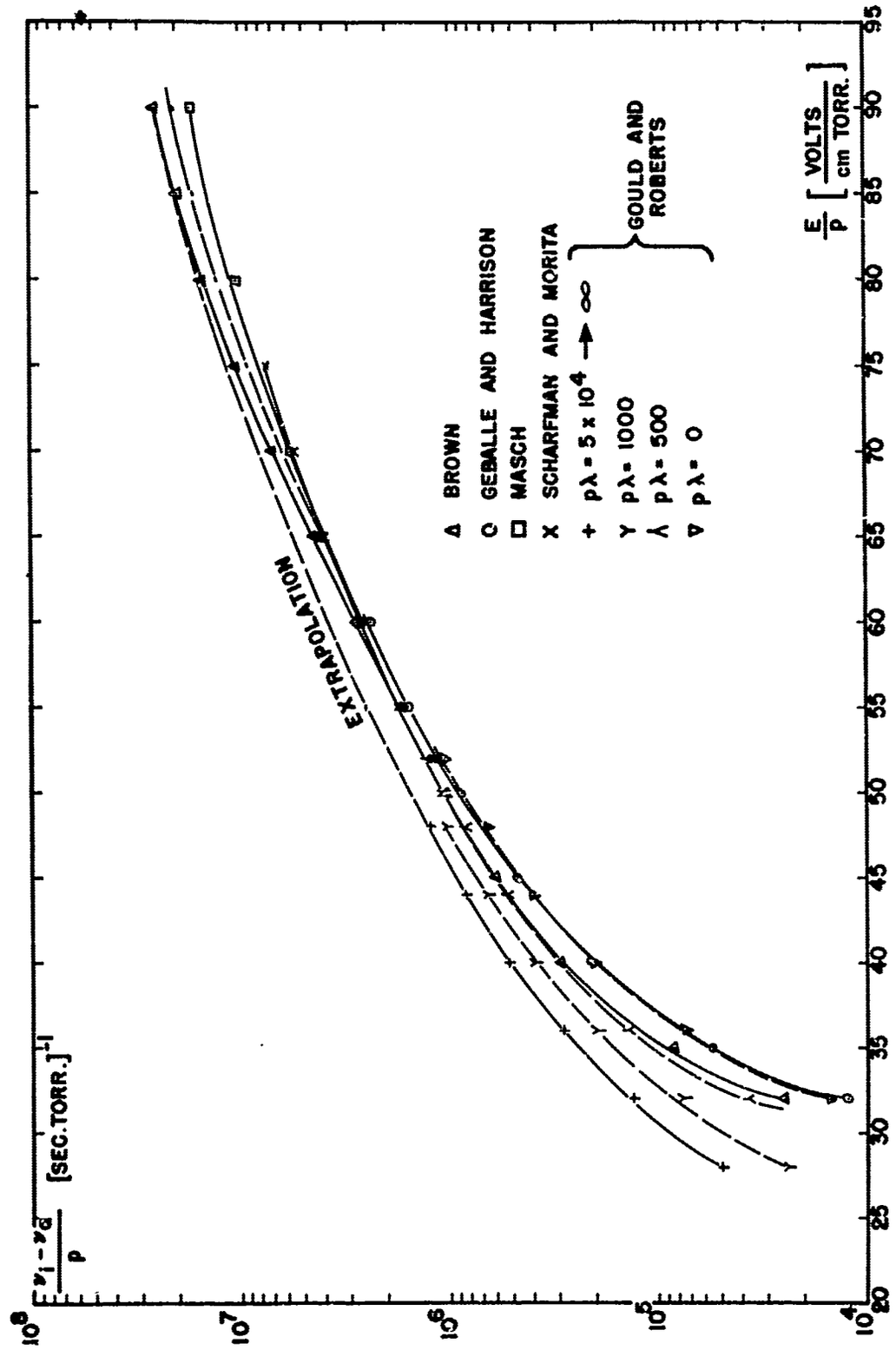


Figure 4. Net Ionization Frequency in Air

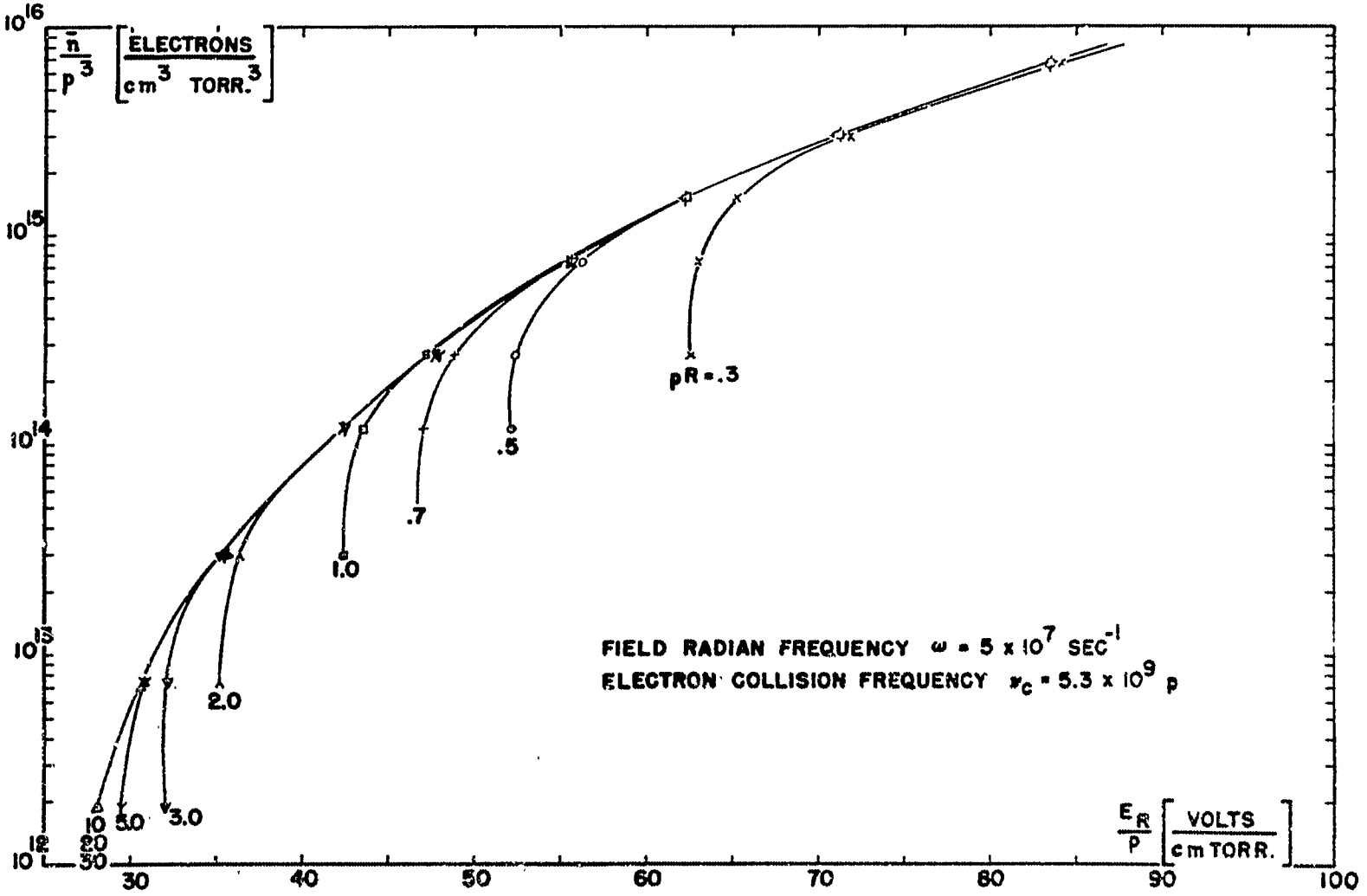


Figure 5. Electrodeless Discharge in Air. Effective Electron Density as Function of Pressure-Reduced Maintenance Field for Various Tube Radii

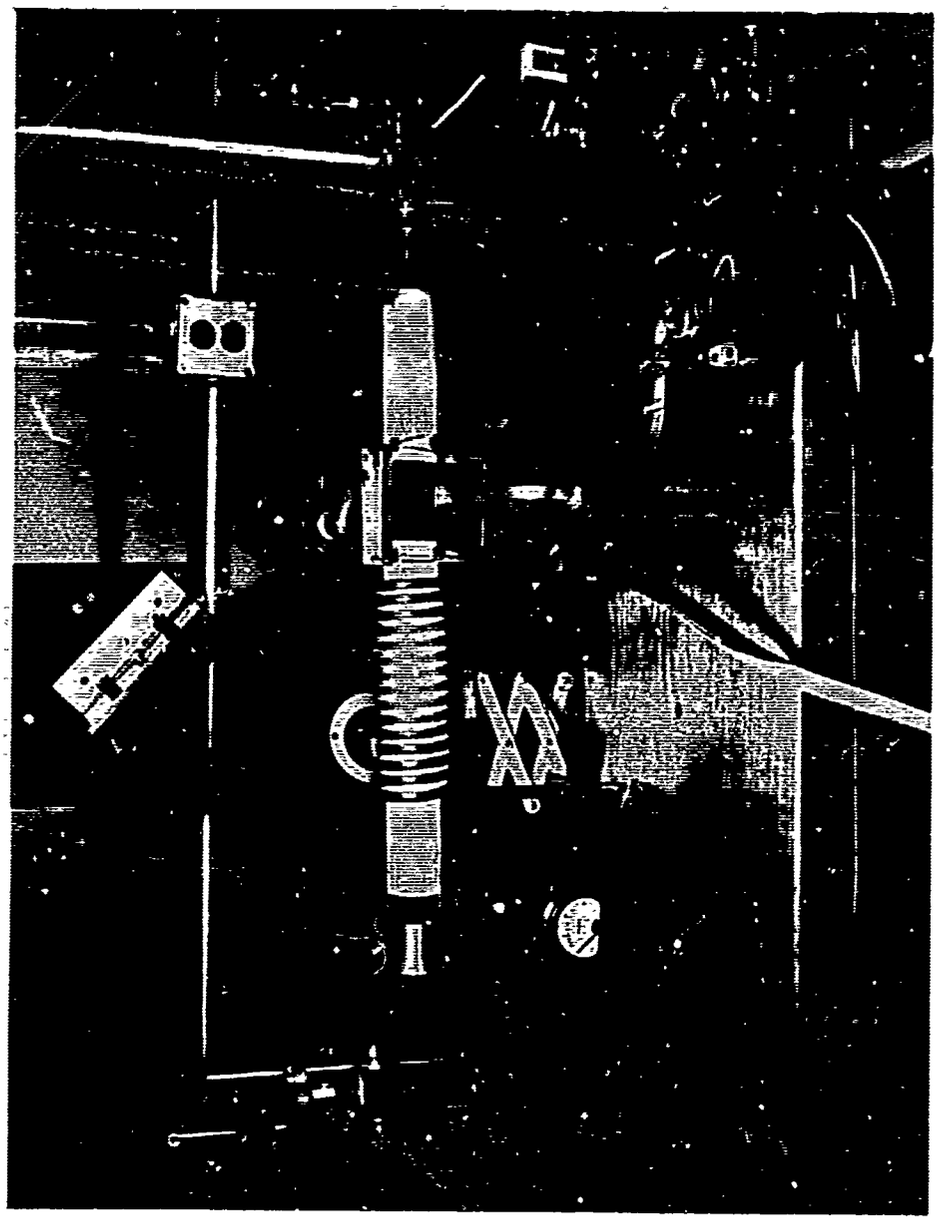


Figure 6. Test Arrangement for Seeding Experiments

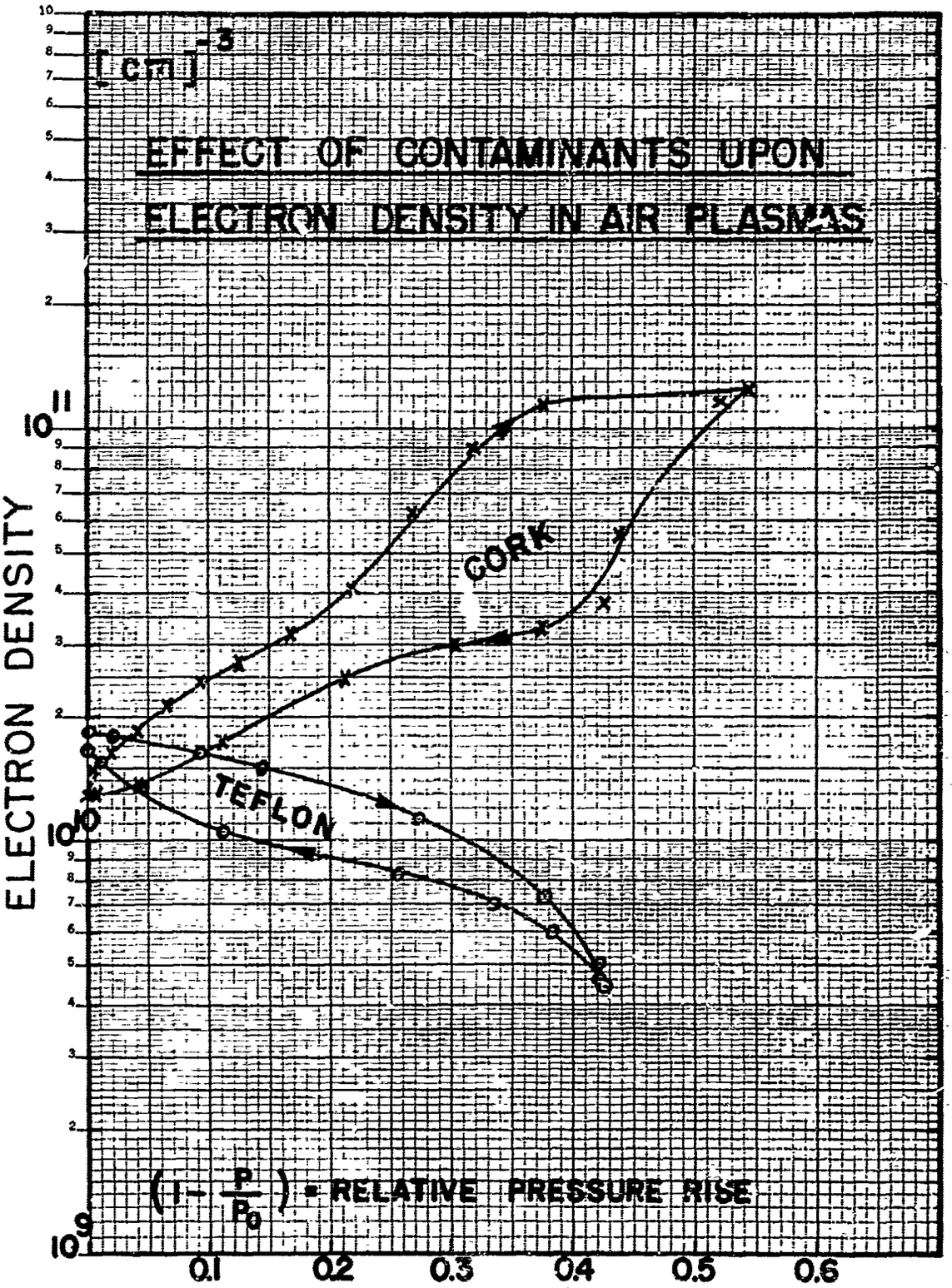


Figure 7. Effect of Contaminants upon Electron Density in Air Plasmas

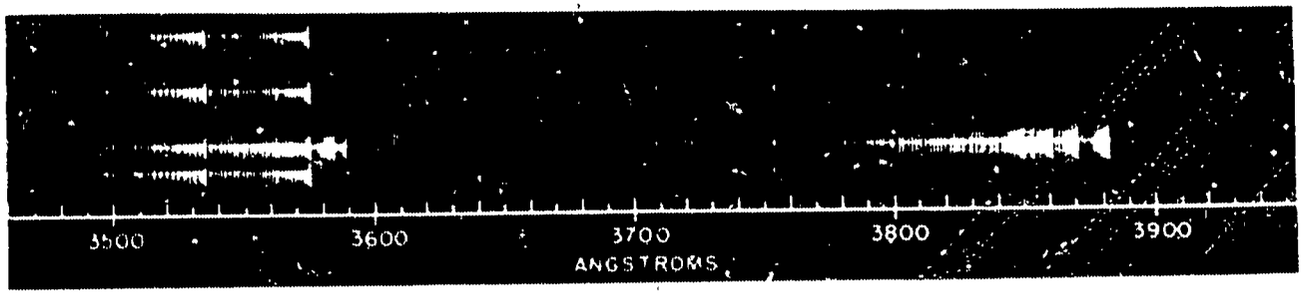


Figure 8. Appearance of CN Bands at 3883 Å and 3590 Å in Air Plasma Contaminated with Hydrocarbons

III. SHOCK TUBE SIMULATION OF RE-ENTRY PLASMA FLOWS AND THEIR MICROWAVE NOISE EMISSION*

James E. Hartsel+
Ross Caldecott
ElectroScience Laboratory
(formerly Antenna Laboratory)
Department of Electrical Engineering
The Ohio State University
Columbus, Ohio

ABSTRACT

The thermal noise emitted by the plasma sheath is of great importance in communicating with hypersonic vehicles. In order to study this problem it is essential to know the flow properties about the vehicle in considerable detail, particularly those of the thermal boundary layer. The flow fields of models mounted in the free stream of a hypervelocity shock tube have been carefully studied and compared with flight conditions in order to simulate experimentally typical re-entry plasma flows over an antenna.

In the past the shock tube has been widely used to simulate re-entry heat transfer at the stagnation point and can be applied to the communications problem in this region with little difficulty.

---

* The research reported in this paper was sponsored in part by Contract No. AF 33(657)-10523 between Air Force Avionics Laboratory, Electronic Warfare Division, Electromagnetic Environmental Branch, Propagation Group, Wright-Patterson Air Force Base, Ohio and The Ohio State University Research Foundation.

+ Aerodynamic Laboratory, Department of Aeronautical and Astronautical Engineering, The Ohio State University.

However, in practice an antenna is usually located away from the stagnation region to avoid the "blackout" problem. In the present study, points away from the stagnation region have also been measured in the shock tube, and it is found that a reasonable degree of simulation can be obtained. The boundary layers on shock tube models will be similar in nature to those on re-entry vehicles, and will possess the same dissociation and ionization effects, even though the free-stream Mach number will be considerably lower and flow field geometry slightly different from the flight case.

A simple model based on the existence of guided waves in the boundary layer has been adopted to explain the electromagnetic layer properties, in particular the noise temperature of a small flush mounted antenna.

THE BASIC NOISE PROBLEM

Much attention has been given to the radio blackout produced by the hypersonic plasma sheath, while the problem of plasma generated noise has tended to be overlooked. A blacked out signal is of somewhat academic interest. In practice, in an important communications link, steps will be taken to maintain an adequate signal level. This will be done by careful placement of the antenna, by use of a transmission frequency above plasma cut-off, or by resorting to one of the available methods of plasma control such as the use of a strong magnetic field. Once a sufficient signal level has been obtained, it is the signal-to-noise ratio which becomes important in determining system performance.

Plasma generated noise may be of two types, modulation or thermal. Modulation noise is caused by variations in the plasma sheath resulting from vehicle motion, operation of control jets, the proximity of other high power r.f. systems and so on, and appears as unwanted modulation or an r.f. signal passing through the plasma layer. It affects equally signals transmitted and received by the hypersonic vehicle. It is also very much dependent on the particular system configuration and for this reason will not be discussed further here.

Thermal noise on the other hand is generated within the plasma itself and is caused by the thermal motion of the free electrons. It is normally only important when a signal is being received by the hypersonic vehicle. In the transmitting case the beam area of a distant receiving antenna is generally such that the plasma sheath occupies only a very small part of it. A proportionally small amount of the thermal plasma noise is then coupled into the distant receiver. In the case of a very large receiving antenna this might not always be true, in which case the effect of the plasma generated thermal noise would have to be considered for both directions of transmission. The present discussion will, however, be confined to the case when the receiver is on board the hypersonic vehicle.

Noise temperature will be used here rather than noise power since this keeps the discussion largely independent of the receiver characteristics. The two are of course related by the familiar linear equation:

(1) $P = kTB$

where P is the noise power in watts

k is Boltzmann's constant (1.38×10^{-23} joules/°K)

T is the noise temperature in degrees Kelvin

B is the bandwidth in cycles per second.

At the receiver input terminals, T will be made up of the equivalent receiver noise temperature T_R and the antenna noise temperature T_A. T_A will depend, among other things, on the plasma sheath. Figure 1 shows the situation for a simple antenna aboard a re-entering vehicle. Noise will be contributed by the ground, the atmosphere, the cosmic background and the plasma sheath. There will also be a contribution from any lossy portions of the antenna structure. When low noise receivers are used, noise sources other than the plasma may well be significant and are discussed in many papers on low noise antenna systems, for example Reference 1. For the present purpose it will be assumed that the contribution from all these may be neglected and that the only contribution to the antenna temperature is from the plasma. The antenna noise temperature will then be given by

$$T_A = \alpha(1-R)T_P \,. \tag{2}$$

In this equation T_P will be the physical temperature of the plasma if it is close to thermal equilibrium which is generally the case; otherwise it will be the electron temperature. α is the emission coefficient of the plasma. For thermal equilibrium it is also the absorption coefficient for the signal and includes loss by reflection at the outer plasma boundary where the signal is reflected back into the plasma. R is the power reflection coefficient of the antenna.

The importance of the plasma with regard to system noise will depend on the magnitude of the antenna noise temperature compared to the receiver noise temperature. The deterioration D in signal-to-noise ratio due to noise alone but excluding the effect of signal loss may be written as

$$(3) \qquad D = \frac{T_R + T_A}{T_R}$$

or substituting from Eq. (2)

$$(4) \qquad D = 1 + \alpha(1-R) \cdot \frac{T_P}{T_R} \quad .$$

At first sight it would seem that a high reflection coefficient at the antenna would be an improvement. However, there is an additional deterioration due to signal loss which is given by

$$(5) \qquad D' = \frac{1}{(1-\alpha)(1-R)} \quad .$$

Multiplying Eqs. (4) and (5) gives the overall deterioration D_o in signal-to-noise ratio

$$(6) \qquad D_o = D\,D' = \frac{1}{(1-\alpha)(1-R)} + \frac{\alpha}{1-\alpha} \cdot \frac{T_P}{T_R} \quad .$$

From this it is evident that a high reflection coefficient is harmful. Assuming for the moment that it is possible to keep the antenna matched over a wide range of plasma conditions, Eq. (4) may be written

$$(7) \qquad D = 1 + \alpha \cdot \frac{T_P}{T_R} \quad .$$

The effect of plasma noise then depends only on α and the ratio T_P/T_R. However, plasma temperatures are measured in thousands of degrees Kelvin while the noise temperatures of modern receivers may be below one hundred degrees. Quite small values of α may thus produce a significant effect. This is illustrated using decibel scales in Fig. 2. Signal loss is also shown plotted against itself in the figure to illustrate its relative importance. It is evident from the figure that in practically all cases when the signal loss is in the range from 0.1 to 10db, plasma noise is of prime importance.

SHOCK TUBE SIMULATION OF HYPERSONIC PLASMAS

Evidently the noise level is sensitive to quite small changes in the plasma. It is thus necessary to know the plasma conditions accurately if the noise problem is to be properly evaluated. Unfortunately the plasma is by no means a simple uniform layer. It is bounded at the outer edge by the non-equilibrium region associated with the shock front and at the vehicle surface by a boundary layer. Since, in practice, antennas are not generally placed at the stagnation point but at some position further aft, to avoid the most severe plasma conditions, the effects of flow expansion and possible boundary layer turbulence must also be considered. Some form of experimental program is thus virtually essential, which brings up the question of whether the flight conditions can be accurately simulated in the laboratory.

Since the problem is basically aerodynamic, the development of facilities to simulate hypersonic flows has been one of the major efforts of the engineering approach to the problem. Hypersonic wind tunnels can develop sufficiently high Mach numbers but generally cannot approach the high total enthalpies encountered in actual flight. Thus such facilities do not produce the real gas chemistry which is the cause of re-entry communications difficulties. Plasma tunnels are another possibility, but flow conditions are often difficult to determine, and high enthalpies cannot always be obtained. Impulse facilities, such as the shock tunnel and the shock tube, are receiving much attention and use. The shock tunnel can produce the high Mach numbers and enthalpies needed for flight simulation, but care must be exercised in determining the free stream flow conditions since the rapid expansion through the nozzle may "freeze" the flow composition in a non-equilibrium state.

The hypervelocity shock tube has been used extensively for stagnation point heat transfer studies [2,3,4] and also for measuring thermal noise emission.[5] It is an excellent device for creating clean, high density plasmas for communications studies. However, it has not been used for complete flow field studies since the free stream Mach number is relatively low in the operating range where hypersonic stagnation conditions are simulated. The hypervelocity shock tubes at The Ohio State University Aerodynamic Laboratory can duplicate

the inviscid stagnation point conditions over a great portion of the re-entry map. However, the stagnation point of a blunt body is only a limited region in the flow field, and the larger question is what degree of simulation can be obtained in flow field regions away from the stagnation region?

Answering this question is the purpose of the present study, with the primary objective being the use of shock tube generated flows to measure thermal noise emission on a blunt body downstream of the stagnation region. If the shock tube can be employed for noise studies of this type, it may then be possible to examine the effect of the boundary layer on noise emission. The boundary layer on the aft region of a blunt body is thicker than that at the stagnation region and may have a pronounced effect on the noise level reaching the antenna. The effect of the thermal boundary layer on microwave noise measurements has been observed on the wall of the shock tube[6] and it would be of considerable interest to observe the effect of boundary layers such as those found on models mounted in the shock tube free stream.

The present problem is primarily one of similitude. The body selected is the hemicylindrically blunted flat plate at zero incidence. It is a simple two-dimensional body for which considerable wind tunnel data is available in the open literature and possesses a flat afterbody for uncomplicated antenna mounting. The parameters that are investigated experimentally are shock detachment distance, shock

shape, and pressure distribution over the body. Since the shock tube can easily produce the required total enthalpy of the flow, the three parameters mentioned should indicate the degree of inviscid flow similitude.

The experimental work was performed in normal air in the supersonic free jet of a four-inch diameter hypervelocity shock tube. The tube uses helium as a driver gas, which is heated by an electrical arc discharge from a capacitor bank with a maximum energy storage capacity of 200,000 joules. The general layout of the shock tube facility and the Schlieren system used in the present study is presented in Fig. 3.

The flow pattern about a typical model in the free jet test region is shown in Fig. 4. The model must be located near the tube exit in order to remain within the conical supersonic free jet, the extent of which is determined by the Mach angle μ_2 of Region 2. The free stream flow, Region 2, is considerably different from the free stream encountered in hypersonic flight, even though stagnation conditions on the model may be identical. Region 2 has been shock heated by the traveling normal shock to an elevated temperature and is partially dissociated and ionized for the range of conditions of this study.

The speed of sound in Region 2 is considerably increased by the initial shocking process. Thus, even though the flow velocity may be quite high, the Mach number remains in the moderate

supersonic range. In hypersonic flight the flow reaches the stagnation point condition by passage through a single, strong, normal shock. To reach the same stagnation condition in the shock tube, the flow passes through two shocks, and therefore each of these must be weaker than the corresponding hypersonic flight shock wave. Since the bow shock about the shock tube model is weaker than its flight counterpart, the change of flow variables across it will be less severe. An important hypersonic similitude parameter which is affected by this difference in free stream conditions is the normal shock density ratio, k. The variation of the shock tube free stream Mach number, M_2, and the density ratio across the normal portion of the bow shock, k, is presented in Fig. 5.

The effect of the shock tube free stream dissociation and ionization on non-equilibrium phenomena behind the model bow shock deserves consideration, particularly the question of relaxation to equilibrium behind the bow shock. Species recombination for flow near the body surface should not depend on the free stream conditions as long as equilibrium is reached at the stagnation point, since all flow over the afterbody near the surface will be in equilibrium near the stagnation region. Since the shock tube free stream is already raised to a high energy level, one would intuitively feel that relaxation would be faster behind the bow shock in the shock tube than it would

be in the flight case where the free stream is "cold". This has been investigated recently in the present facility, and results obtained indicate that relaxation is faster with a dissociated free stream.[7]

The mere fact that relaxation behind the bow shock in the shock tube is faster than in a simulated flight condition is not sufficient grounds for assuming that relaxation phenomena do not affect the shock tube model flow field. The models commonly used in the shock tube are usually much smaller than full-size hypersonic vehicles. Therefore the relative importance of non-equilibrium relaxation must be investigated by considering typical model sizes.

A good index of the relative importance of relaxation behind the normal portion of the bow shock is the comparison of relaxation distance to the shock detachment distance. The relaxation distance, d_e, is the distance behind the shock at which the flow properties are within 10% of their equilibrium values. This is a common parameter in relaxation studies and is presented in Fig. 6 for the shock tube model bow shock. The diameter selected for the calculation is 3/8 inch, the smallest model used in the present study. The relaxation distance curves are based on a constant flow velocity behind the bow shock equal to the velocity immediately behind the shock, while in the actual case the velocity will decrease as the flow senses the presence of the model. Therefore the curves represent an upper limit on d_e.



The shock detachment distances for the axisymmetric body (sphere) are from Reference 8, and those for the two-dimensional curve (cylinder) are based on present results. Figure 6 does show that at low pressures and low shock speeds a major portion of the nose region for this small model size can be in non-equilibrium, particularly for the axisymmetric model. For the two-dimensional model and test conditions of the present study, the stagnation region of the flow about the model was definitely in equilibrium. Since the equilibrium distance is inversely proportional to the initial pressure P_1, non-equilibrium effects in the stagnation region can be virtually eliminated by choosing a high enough value of P_1. The problem of recombination equilibrium during the expanding portion of the flow over the body is therefore assumed to be unrelated to the free stream conditions except by the fact that the limiting pressure for the expanding flow is the free stream pressure in the shock tube, P_2.

The test program included four measurements: shock stand-off distance, shock shape, body pressure distribution, and thermal noise emission from the shock layer at some body station away from the stagnation point. The first three measurements were made using the single pass Z-type Schlieren system described in Reference 8 and shown in Fig. 3. The pressure measurements of this study are of the indirect type, inferred from Schlieren photographs of the Mach lines emanating from the model surface. Small

tape slices were attached to the surface of the blunt plate model along the centerline, with the leading edge of each slice aligned parallel to the leading edge of the plate. The Mach lines generated by these small disturbances on the surface were photographed and the Mach angle μ was measured as a function of body station. The flow in the immediate vicinity of the afterbody surface has expanded from stagnation point equilibrium, an expansion that is assumed to be isentropic. This allows the Mach number distribution to be immediately converted into a pressure distribution by the use of standard "real gas" air tables. Pressure data were obtained only at lower velocities and enthalpies and relatively high initial pressures ($P_1 \approx 15$ mm Hg) so that the assumption of equilibrium expansion would allow the use of equilibrium values of the local speed of sound. This precaution was taken to insure the validity of the indirect pressure measurement technique. The present data for both the nose and afterbody of the blunt plate are compared with several other results in Fig. 7.

The degree of similarity between the shock tube conditions and those of free flight is perhaps best illustrated by an example. Since it is the plasma temperature and electron density which are important in determining the noise emission, these were calculated for the specific antenna location used and for a typical shock speed and pressure namely $M_s \approx 15$ and $P_1 = 1.0$ mm Hg. The corresponding

flight conditions were then calculated and found to be approximately V_∞ = 23,000 feet per second at an altitude of 110,000 feet. Assuming for the moment that it is important to simulate the stagnation region, this choice of altitude and velocity will give both flow fields the same total enthalpy. However, the shock layer on the flying plate at this altitude will be more expanded at S/D = 3 than that of the model, and thus the inviscid surface conditions will not be equal. If the inviscid surface conditions are to be equal, the body location of the antenna on the flying plate will necessarily be closer to the shoulder than that of the model. Using the blunt wing blast wave pressure equation of Reference 10 and the flight shock wave properties of Reference 11, it is found that the correct location for simulation on the flying plate is approximately S/D = 1.0. Thus inviscid surface conditions on the shock tube model at P_1 = 1.0 mm Hg, M_S = 15, and S/D = 3 are equal to conditions on the flying plate at V_∞ = 23,000 fps, altitude = 110,000 ft. and S/D = 1.0. There may be an infinite number of flight velocities, antenna locations, and altitudes giving equal thermodynamic conditions, but by matching the total enthalpy and stagnation pressure, the isentropic expansion from the stagnation point of both the flying plate and shock tube model to the same pressure means that the velocities will be equal at the antenna locations. This may be important in studying the boundary layer effect since it means that the local Reynolds number

at the antenna, based on distance from the stagnation region, is now entirely determined by the relative size of the two bodies.

Using an integral method, the flow properties across the shock layer for the two antenna locations have been calculated and are presented in Fig. 8. This result shows the absence of the sharply defined entropy layer near the shock tube model afterbody. In the flight case, however, the flow that has come through the near-stagnation region of the body forms a layer over the afterbody with severe gradients in the flow properties occurring beyond this layer as the bow wave is approached.

THERMAL NOISE MEASUREMENTS

The noise measurements were made at a frequency of 10 Kmc/s, the model used being shown in Fig. 9. The antenna consists of a dielectric loaded, open ended waveguide and is located three body diameters downstream of the blunt plate leading edge. It is shown surrounded by a choke ring in the figure, and measurements were made both with and without this ring. Connection to the measuring system was by way of the waveguide port seen in the lower left hand corner.

Equation (2) shows that for the measured antenna temperature T_A to be related to the plasma temperature, it is necessary to know both the absorption coefficient of the plasma, α, and the reflection

coefficient of the antenna, R. Over most of the range of measurement the plasma density was such that α could be taken as unity. The error introduced at low velocities by this assumption will become apparent on examining the experimental data. It was, however, necessary to measure the antenna reflection coefficient.

The experimental technique used is illustrated in Fig. 10. In order to obtain both the noise temperature and the reflection coefficient, a pair of measurements is necessary. For the first of these a sensitive radiometer was connected directly to the antenna. The radiometer consisted of two traveling wave tubes followed by a detector and an oscilloscope. It had a bandwidth of about 700 Mc/s and an integration time of about 5 μ sec, this latter being the maximum consistent with the desired time resolution. The radiometer was calibrated before and after each shot using a known noise source and a precision attenuator. Then, with appropriate allowance for transmission loss in the model and connecting waveguide, the observed noise temperature is given by

(8) $$T_1 = \tau(1-R)\, T_P \ .$$

T_1 was measured and plotted as a function of shock velocity for an initial pressure P_1 of 1 mm Hg. A second series of tests was then run using the second experimental arrangement shown in Fig. 10.

This time the observed noise level was a combination of the noise entering the antenna and that originating from a known noise source and reflected by the antenna. The observed noise temperature is given by:

$$(9) \qquad T_2 = \frac{\tau^2 R T_N}{4} + \frac{\tau(1-R) T_P}{2} \quad .$$

Pairs of temperatures T_1 and T_2, measured at the same shock velocity, were then substituted into Eq. (8) and (9) and the corresponding values of T_P and R calculated.

The oscilloscope noise traces fall into two distinctly different groups, depending on the shock velocity. Figure 11 presents one sample trace from each category to illustrate this effect. Both are measurements of antenna noise alone, that is of T_1. For low speed runs ($M_s \leq 11$) the temperature is nearly constant during the flow time and the buildup time is short. For speeds above $M_s = 11$ there is a definite overshoot in temperature followed by a gradual decay to a relatively constant value for the duration of the test time. There are two possible reasons for this phenomenon, both of which probably contribute to the effect. One is the passage of the traveling normal shock over the body, which produces a transient non-equilibrium overshoot in temperature. This overshoot is quite high in magnitude, but due to its extremely short duration, the effect may only be partially felt by the radiometer, which has a rise time of several microseconds.

However, some contribution must expected. The other reason is the time dependent buildup of the flow, particularly the boundary layer, after the passage of the traveling normal shock over the body. As the boundary layer builds up, the field of view of the antenna is increasingly affected and the recorded temperature level will decrease, since the antenna sees the entire boundary layer but only a limited depth of the shock layer. This is due to the "blackout" caused by the high electron density and plasma frequency at the higher speed runs.

In order to study this boundary layer effect further, two completely separate sets of measurements were made. The first set was made using a simple open ended waveguide antenna. For the second set the choke ring shown in Fig. 9 was added. The reduced temperature data from both sets are shown in Fig. 12 and the reflection data in Fig. 13. Referring to Fig. 12 the choked antenna temperature is only slightly lower than the plasma temperature in the midportion of the velocity range, indicating relatively little boundary layer effect. At low velocities it falls short due to the thin plasma; the assumption that the absorption coefficient α is equal to unity is no longer valid. At high velocities it again falls short due to the increasing influence of the boundary layer. The unchoked antenna on the other hand shows a markedly lower temperature over the whole of the velocity range

indicating a strong boundary layer dependence. The temperature overshoot referred to earlier in connection with Fig. 11 is also indicated in Fig. 13. It falls short of the non-equilibrium temperature behind the moving normal shock because of the limited rise time of the radiometer mentioned previously. However, it is considerably above the plasma equilibrium temperature at the antenna location indicating that it is not simply a boundary layer effect.

The part played by the boundary layer can perhaps be clarified by reference to Fig. 14. Within the boundary layer there exist both a temperature gradient and an electron density gradient which increase up to the equilibrium values at the outer edge of the layer. For dense plasmas there will also be a point along this gradient where the plasma frequency equals the measuring frequency. At this point the conductivity of the plasma is high. In the unchoked case this layer, where $\omega_p \triangleq \omega$, forms the lossy wall of a waveguide tee. The antenna couples almost entirely to this layer, and the observed noise temperature is essentially the layer temperature. When a choke is added a short circuit is thrown across this "waveguide", and the antenna is forced to look outwards. The conductivity of the plasma is still high, and so the reflection coefficient of the choked antenna will be higher than for the unchoked case. However, when allowance is made for the reflection coefficient, as was done in

these experiments, the observed noise temperature will be much closer to the equilibrium value for the choked antenna.

CONCLUSIONS

It has been shown that in situations where partial transmission through the plasma sheath is possible, plasma generated thermal noise is of the utmost importance in determining the performance of a receiving system aboard a hypersonic vehicle. It has also been demonstrated that small models mounted in the free stream of a shock tube can be successfully used for the study of plasma noise emission at points away from the stagnation region, provided care is exercised in scaling the relevant parameters. Experimental noise studies have shown that at high plasma densities the antenna noise temperature is closely related to the characteristics of the thermal boundary layer.

REFERENCES

1. Caldecott, R. and W. H. Peake, "Designing Low Noise Antennas," Electronics, January 20, 1961.

2. Nerem, R. M., "Measurements of Aerodynamic and Radiative Heating at Super-Orbital Velocities," The Ohio State University Aerodynamic Laboratory Report 1598-1, January 1964.

3. Nerem, R. M. and G. H. Stickford, "Radiative and Convective Heating During Hypervelocity Re-Entry," AIAA Journal, Vol. 2, 1156-1158, 1964.

4. Rose, P. H. and W. I. Stark, "Stagnation Point Heat Transfer Measurements in Dissociated Air," Jour. Aero. Sci., Vol. 25, No. 2, February 1958.

5. Shaffstall, E. L., "A Measurement of the Noise Temperature of a Shock Induced Plasma at 420 mcps and 690 mcps," Report 1573-3, 1 December 1963, Antenna Laboratory, The Ohio State University Research Foundation; prepared under Contract AF 33(657) -10523, Research and Technology Division, Wright-Patterson Air Force Base, Ohio. AD 427 067

6. Caldecott, R., J. D. Lee, and R. M. Nerem, "Development and Application of an Arc-Driven Hypervelocity Shock Tube," presented at the 8th Midwestern Mechanics Conference, Case Institute of Technology, April 1963.

7. Nerem, R. M. and J. E. Hartsel, "Normal Shock Relaxation Phenomena for Blunt Bodies in Shock Tube Generated Flows," submitted for presentation at the 5th. Shock Tube Symposium, White Oak, Silver Spring, Maryland, April 28-30, 1965.

8. Graber, B. C., "An Experimental Study of Real Gas Effects on Shock Detachment Distances and Shock Shapes for a Family of Blunt Axisymmetric Bodies," Research and Technology Division, Flight Dynamics Laboratory, Wright-Patterson Air Force Base, Ohio, TDR-64-130, October 1964.

9. Gregorek, G. M. and K. D. Korkan, "Hypersonic Blunt Body Similitude in a Perfect Gas," Flight Dynamics Laboratory TDR-64-92, June 1964, Research and Technology Division, Wright-Patterson Air Force Base, Ohio

10. Lee, John D., "Pressures on the Blunt Plate Wing at Supersonic and Hypersonic Speeds," Flight Dynamics Laboratory TDR-64-102, July 1964, Research and Technology Division, Wright-Patterson Air Force Base, Ohio.

11. Huber, Paul W., "Hypersonic Shock-Heated Flow Parameters for Velocities to 46,000 Feet per Second and Altitudes to 323,000 Feet," National Aeronautics and Space Administration Technical Report R-163, 1963.

12. Russo, A. J., "Estimates of Attenuation and Reflection of Telemetering Signals by Ionized Flow Fields Surrounding Typical Reentry Bodies," National Aeronautics and Space Administration Technical Note D-1778, August 1963.

13. Bachynski, M. P., French, I. P., and Cloutier, G. G., "Antenna Noise Temperature in Plasma Environment", Proc. IRE, Vol. 49, No. 12, pp. 1846-1857, December 1961.

14. Hartsel, J. E. "A Shock Tube Study of the Blunt Body Shock Layer and Plasma Sheath Thermal Emission", Ohio State University, Report 1573-9, Contract AF 33(657) -10523, Antenna Laboratory, The Ohio State Research Foundation, Columbus, Ohio, 15 March 1965.

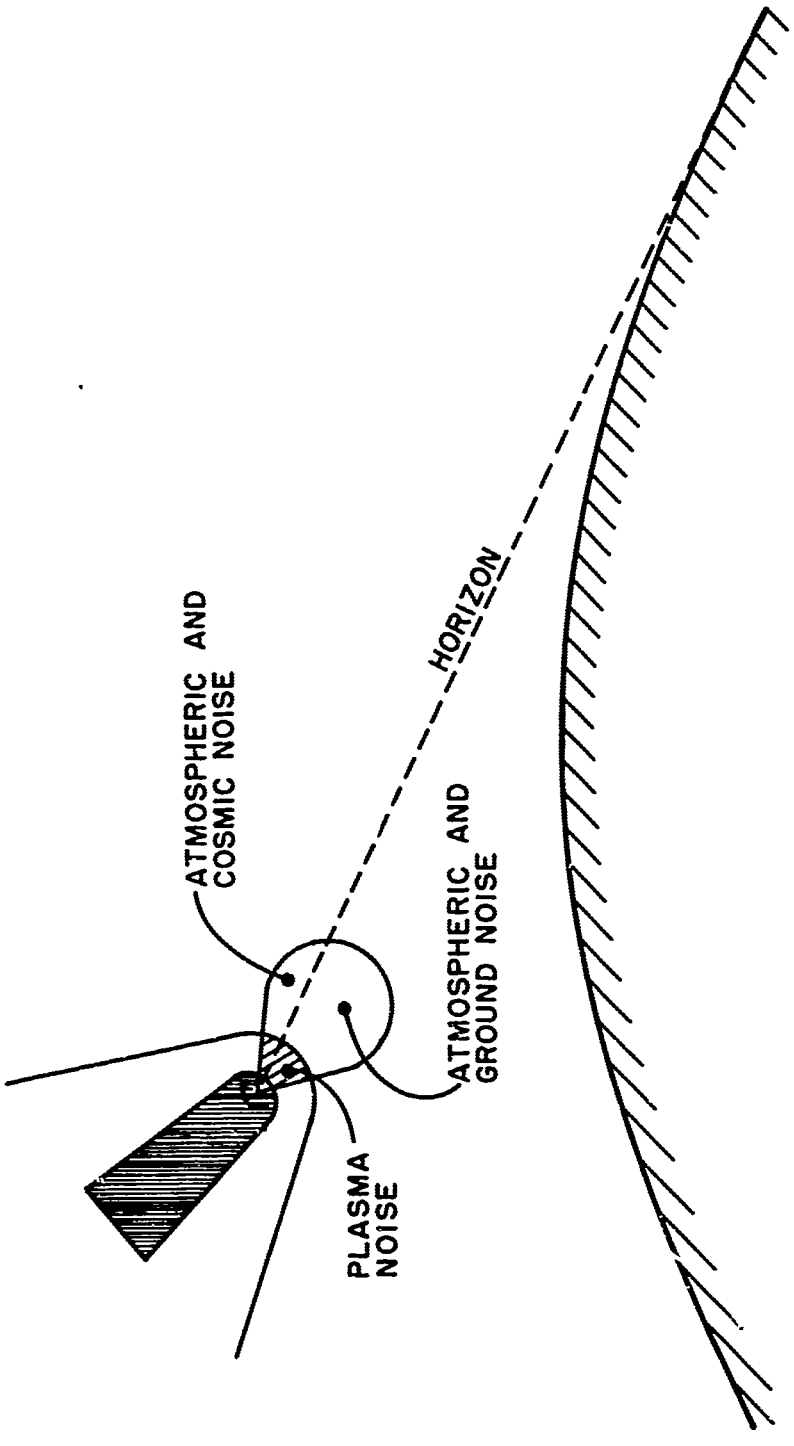


Fig. 1. Sources of antenna noise.

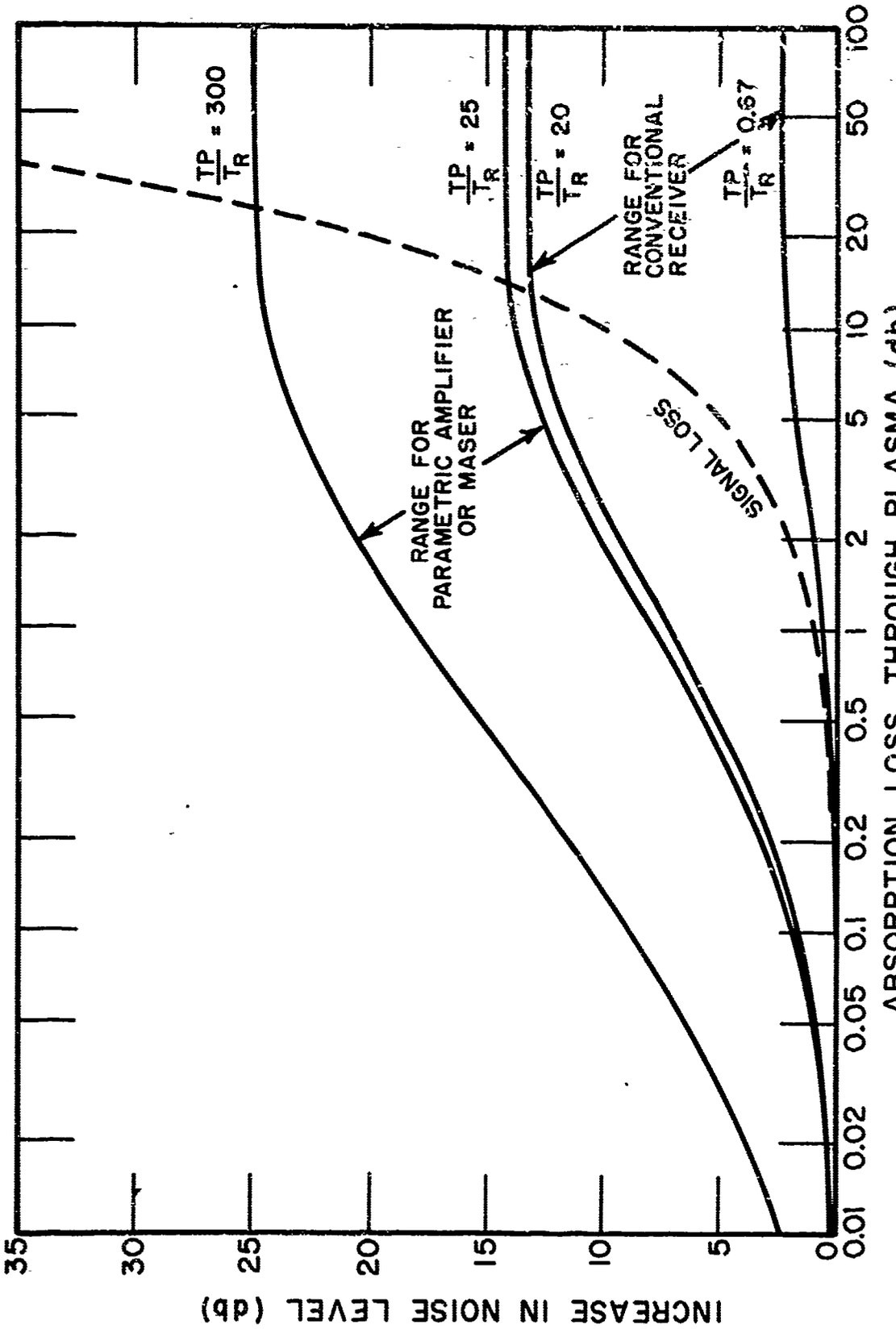


Fig. 2. Increase in noise level as a function of plasma temperature and absorption.

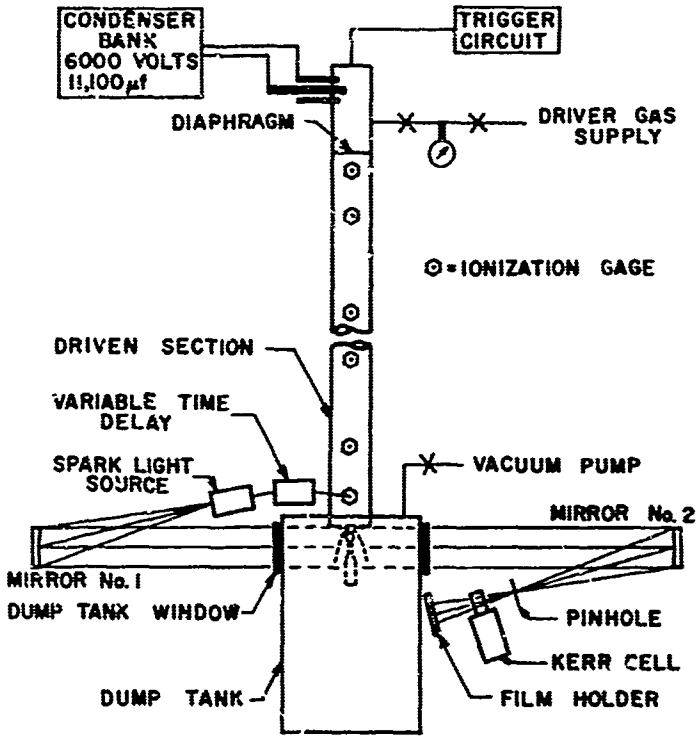


Fig. 3. Layout of shock tube and Schlieren system.

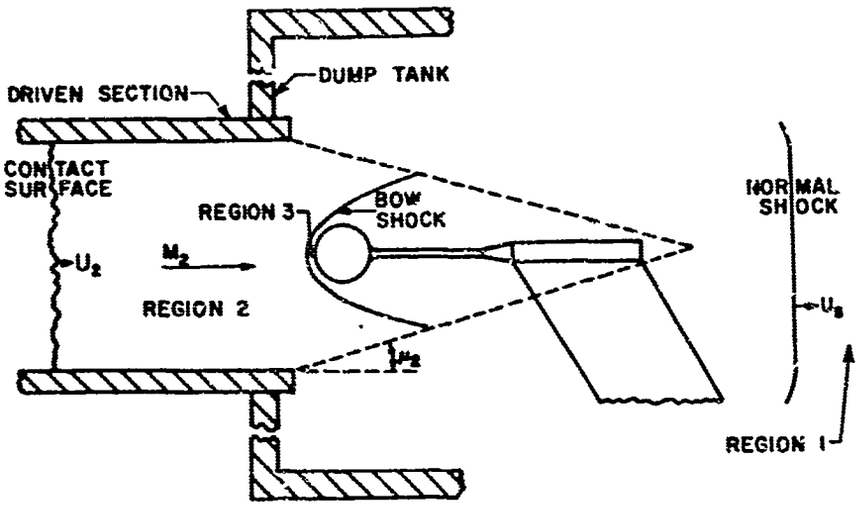


Fig. 4. Flow pattern about a typical model in the shock tube free jet test region.

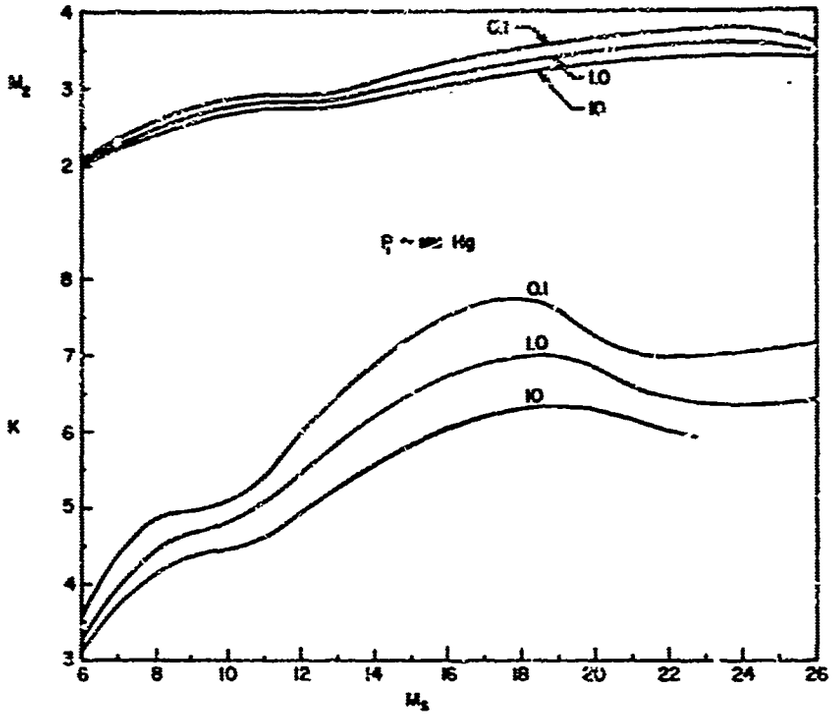


Fig. 5. Free stream Mach number M_2 and density ratio K across the normal portion of the bow shock for the range of shock tube conditions of the present investigation.

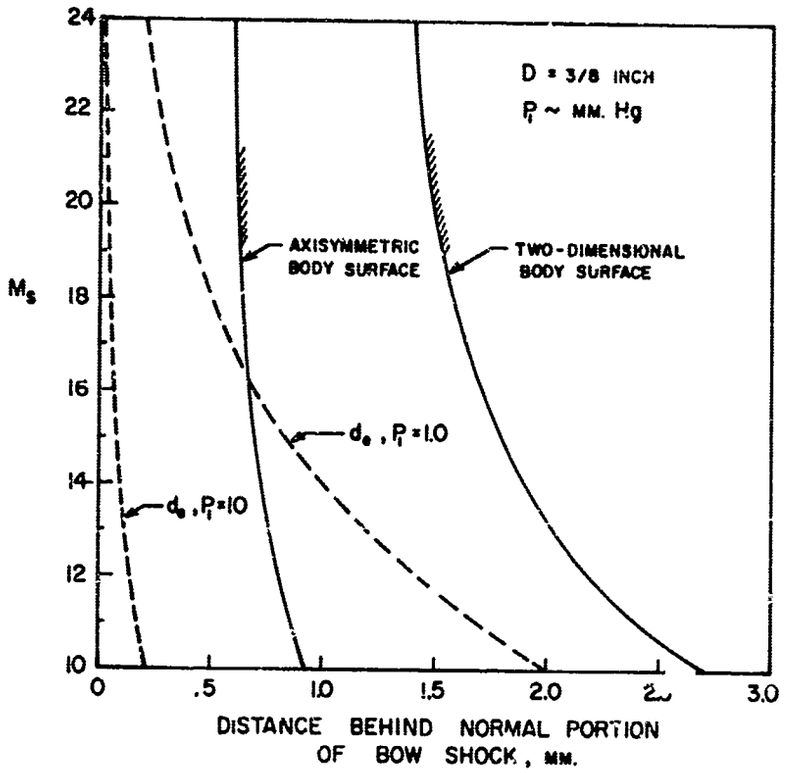


Fig. 6. Distance behind stagnation region normal shock for flow to equilibrate (d_e) and approximate location of blunt body stagnation surfaces.

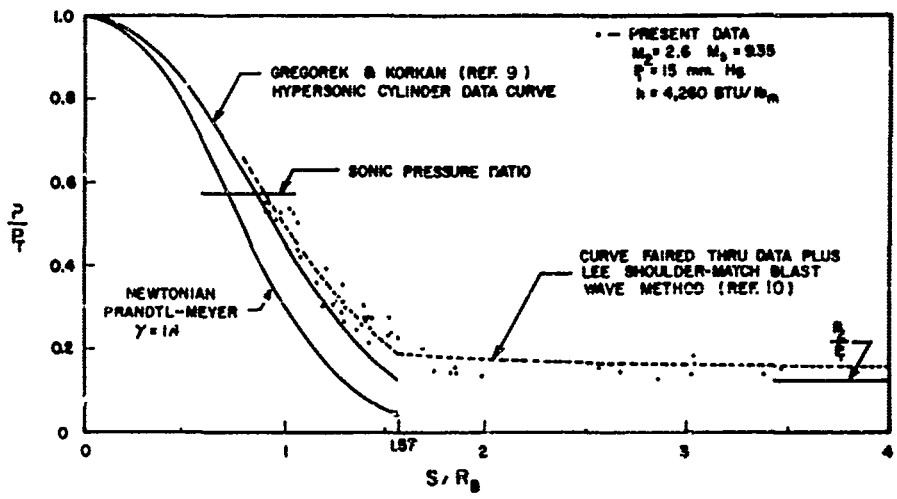


Fig. 7. Pressure distribution on a blunt flat plate.

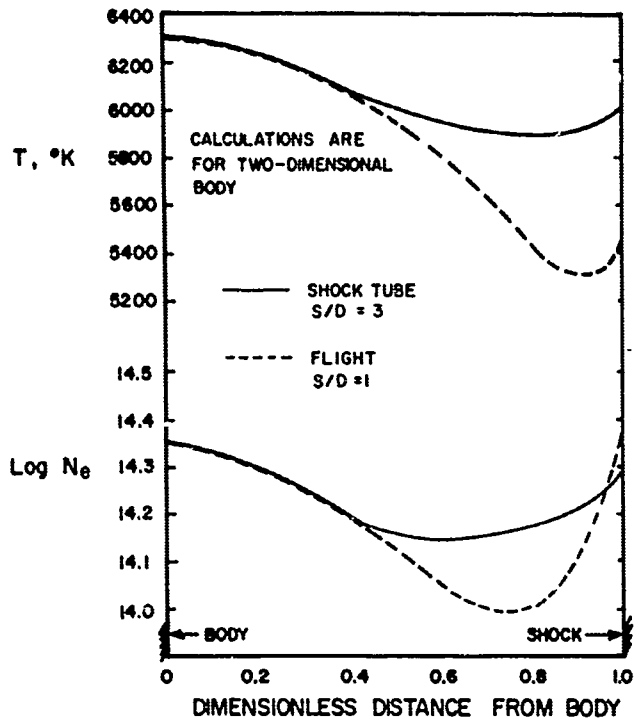


Fig. 8. Calculated variation of properties across the shock layer at the respective antenna locations for the flight and shock tube conditions of the similitude example.

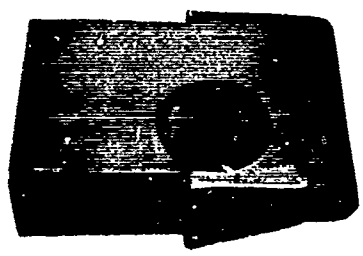


Fig. 9. Model used for thermal noise measurements.

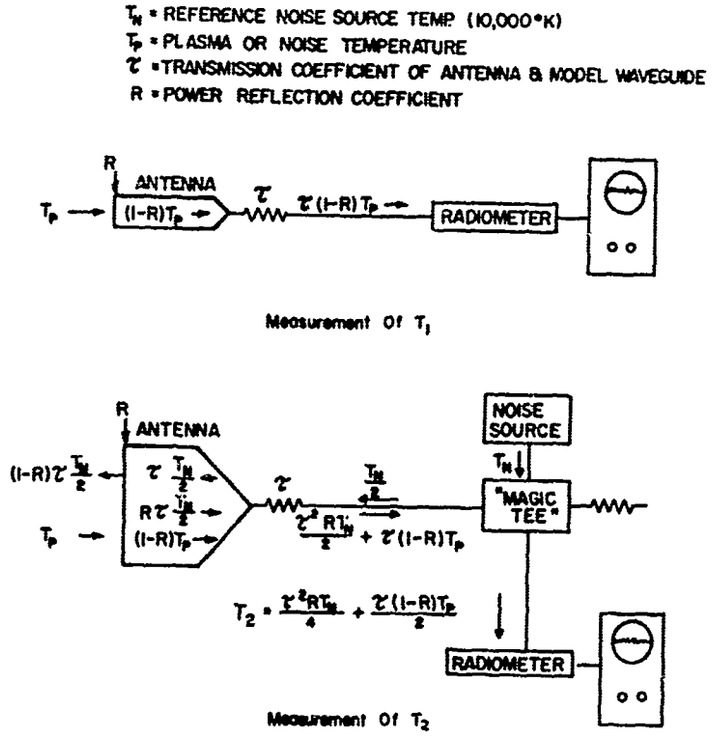


Fig. 10. Schematic diagram of the plasma noise measurement method.

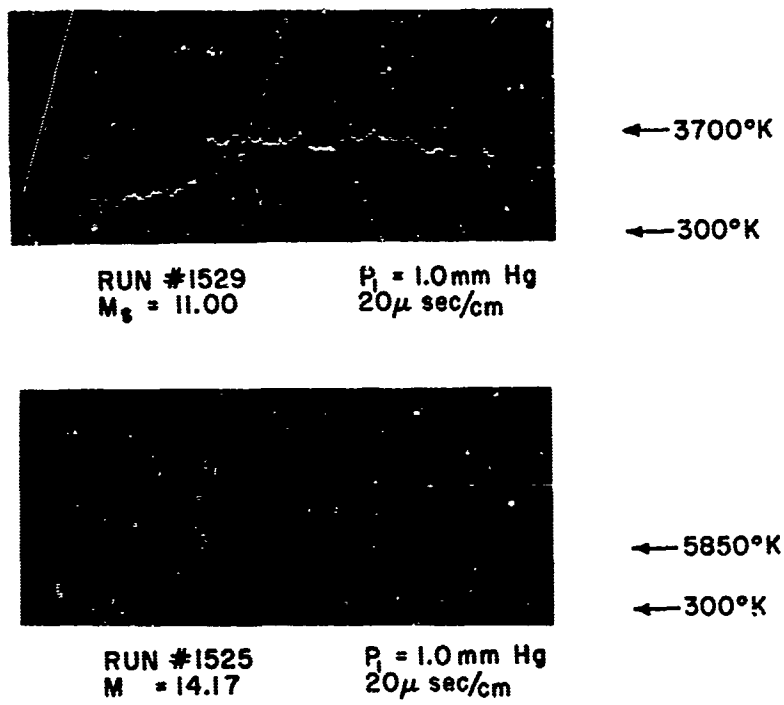


Fig. 11. Sample recordings of noise temperature T_1 showing the temperature overshoot phenomenon at higher shock speeds.

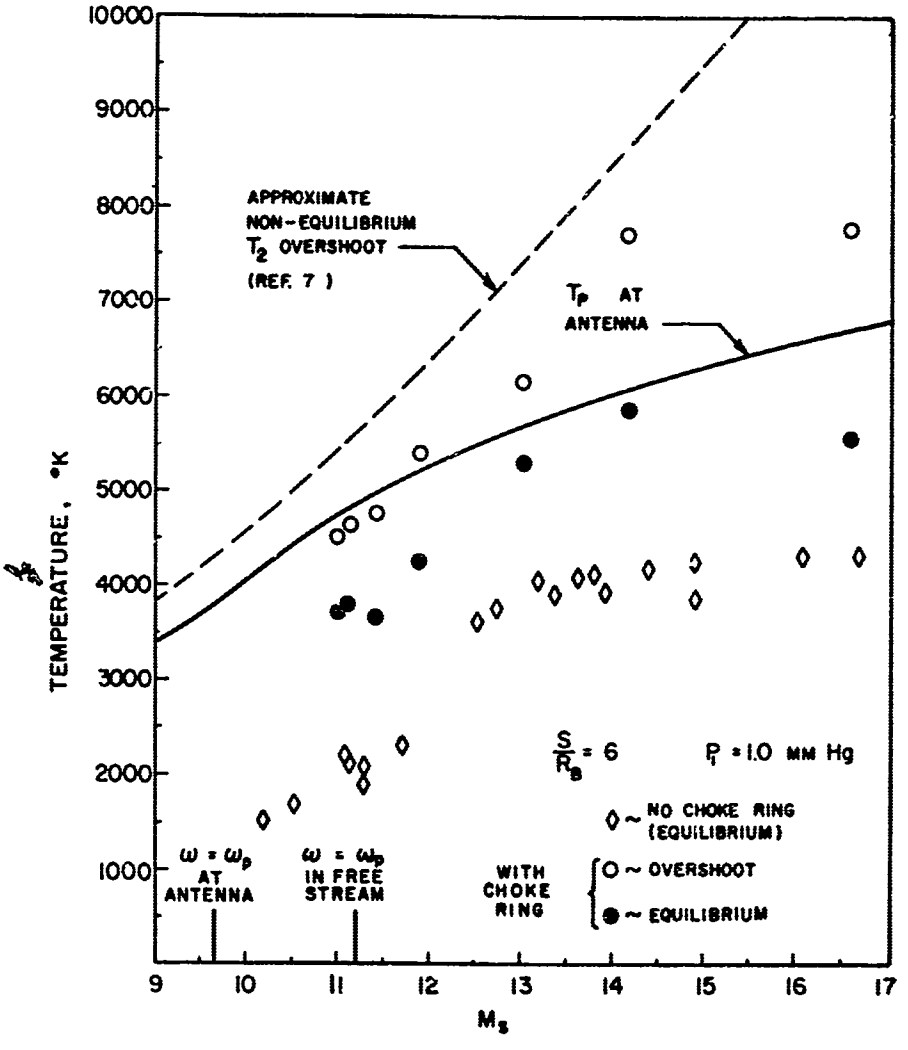


Fig. 12. Measured noise temperature at X-band on the blunt plate afterbody.

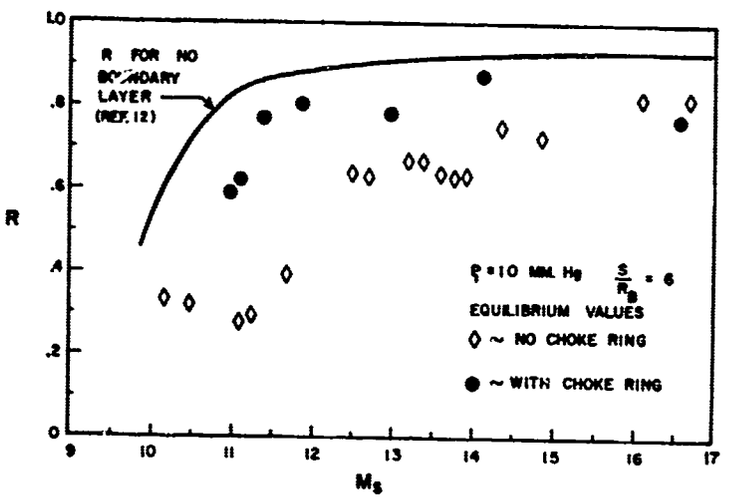


Fig. 13. Measured reflection coefficient at X-band on the blunt plate afterbody.

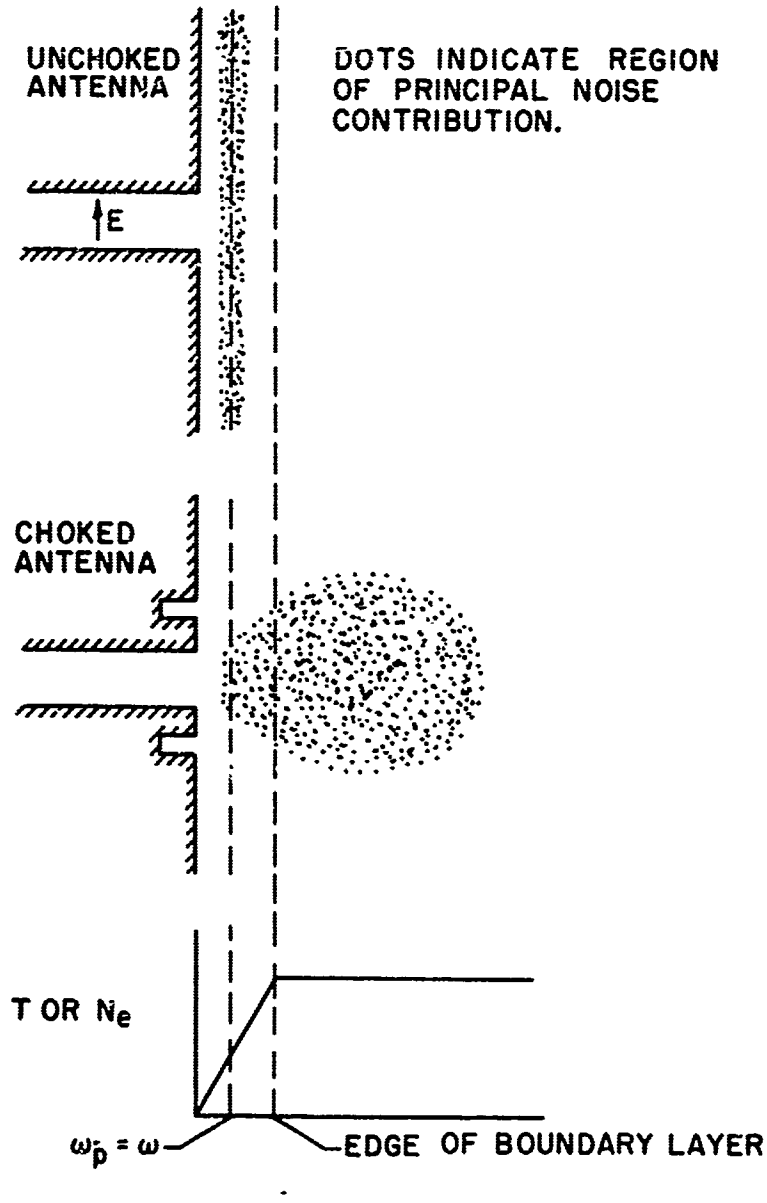


Fig. 14. Showing the effect of a choke on antenna noise temperature.

IV. AN EXPERIMENTAL STUDY OF PLASMA-COVERED SLOTTED-CYLINDER ANTENNAS

N. V. Karas and J. D. Antonucci

Air Force Cambridge Research Laboratories
Bedford, Massachusetts

Abstract

The radiation characteristics of axial slots on a cylinder which is covered by a layer of plasma has been studied by means of a plasma simulation technique. The relative index of refraction of less than unity between the plasma and free space is maintained for the model by an analog tank which represents "free-space" by a high dielectric constant liquid and the plasma by a lower dielectric material. This technique differs from a previous simulation method in that the models can be immersed into the tank, rather than being kept external. This modification allows the study of nonplanar geometries of complex shapes.

Antenna patterns of axial slots on cylinders of various radii and thickness of plasma covering were observed to have good agreement with theory for radiation in the equatorial plane. These measurements are being extended to radiation from finite bodies, such as the finite cone and cylinder. In addition, the effects of varying radii of curvative upon the admittance properties of the radiators are under study.

1. INTRODUCTION

The effects of plasma sheaths and rocket exhausts on electromagnetic radiation from space vehicles have been the subject of much research. Since plasmas have complicated structures and the vehicles have complex geometries, analytic solutions are not always possible. Many simplifying assumptions and approximations have to be made. An experimental technique that would more realistically simulate plasma conditions and provide the means for checking theoretical predictions has long been sought.

Among the variety of devices suggested and used in plasma simulation have been lumped electric elements and mechanical analogs.[1] Artificial dielectrics whose electrical characteristics are similar to those of a plasma have also been used,[2-3] among them a medium comprised of periodically spaced lattice of metal rods, and another a parallel-plate guide carrying the fundamental TE_{01} mode.

Some simulation techniques have limited application. For example, an artificial medium made of metal spheres or consisting of holes in plates or dishes may have a propagation constant equivalent to that of a plasma but a relative magnetic permeability that differs from unity. A conductive solution of an acid or salt may have the proper attenuation constant but a refractive index greater than unity. The degree of applicability of these simulation techniques is therefore limited since only one or two of the scalar

parameters of a plasma are simulated.

This paper describes a technique of plasma simulation in which the relative index of refraction of less than unity between the plasma and free space is maintained by using two contiguous real dielectric media. Free space is represented by a liquid of high dielectric constant, and the plasma by a material of lower dielectric constant. The technique differs from a previous simulation method[4] in that here the experimental models are not outside the liquid dielectric but immersed in it. The modification allows for studying nonplanar geometries of complex shapes.

2. THEORY

For weak signal interactions and in the absence of static magnetic fields, the plasma can be represented as an isotropic, linear, lossy dielectric whose magnetic permeability μ_o is unity. Under these restrictions the plasma has a complex index of refraction whose real part is less than unity.[5] Then

$$\epsilon_o = \epsilon_o \left(1 - \frac{\omega_p^2}{\nu^2 + \omega^2} + j \frac{\omega_p^2 \nu / \omega}{\nu^2 + \omega^2} \right) .$$

where

ϵ_o = dielectric constant of free space

ω_p = plasma frequency

ν = collision frequency

ω = operating frequency

ω_p = dielectric constant of plasma.

If $\nu \approx 0$,

$$\frac{\epsilon_p}{\epsilon_o} = 1 - \frac{\omega_p^2}{\omega^2}.$$

Further, if $0 < \frac{\omega_p}{\omega} < 1$,

then $0 < \frac{\omega_p}{\epsilon_o} < 1$,

or $n_r < 1$,

where the relative refractive index, n_r, equals $(\epsilon_p/\epsilon_o)^{1/2}$.

Since real dielectrics always have refractive indices greater than unity while lossless plasmas always have refractive indices less than unity, real dielectrics cannot be substituted directly for the plasma in a simulation experiment. The present technique is therefore based upon a double substitution in which the free-space region is replaced by a liquid of high refractive index and the plasma by (including air) of lower refractive index. It is readily shown below that the radiation pattern and normalized aperture impedance of a suitably scaled model of a dielectric clad antenna depends on the ratio of the constants of the cladding layer and the surrounding medium, rather than only upon absolute values.[6]

From the dimensionless form of Maxwell's equations, it is seen

that the scaling relations for any electromagnetic problem depend on certain dimensionless combinations of the parameters that characterize the media:

$$\mu \epsilon \ell^2 f^2 = A \tag{1}$$

$$\mu \sigma \ell^2 f = B \tag{2}$$

where

ℓ = characteristic length of model,

f = frequency,

σ = conductivity,

μ = magnetic permeability,

ϵ = dielectric constant, and

A and B are constants.

The relative spatial relations of the fields in corresponding regions of two systems, A and B, will be preserved, provided that:

$$\mu_A \epsilon_A \ell_A^2 f_A^2 = \mu_B \epsilon_B \ell_B^2 f_B^2 , \tag{3}$$

and

$$\mu_A \sigma_A \ell_A^2 f_A^2 = \mu_B \sigma_B \ell_B^2 f_B^2 \,. \tag{4}$$

Here the subscripts A, B refer to systems A and B respectively.

The constraints are now imposed that $\mu_A = \mu_B (= \mu_o)$ and $f_A = f_B$. Then,

$$\epsilon_A / \epsilon_B = \ell_B^2 / \ell_A^2 \,, \tag{5}$$

and

$$\sigma_A / \sigma_B = \ell_B^2 / \ell_A^2 \,. \tag{6}$$

The proper scaling relations will therefore be maintained in the two systems, provided that all dimensions are scaled in proportion to the characteristic lengths and that the ratios of dielectric constants and conductivities for corresponding points in the two systems be kept constant in accordance with Eqs. (5) and (6). For two sets of corresponding regions in each system (indicated by the additional subscripts 1 and 2 respectively), Eqs. (5) and (6) also impose the related constraints:

$$\epsilon_{A1}/\epsilon_{A2} = \epsilon_{B1}/\epsilon_{B2}, \tag{7}$$

and

$$\sigma_{A1}/\sigma_{A2} = \sigma_{B1}/\sigma_{B2} . \tag{8}$$

It should be noted that equations (5) through (8) involve only ratios of dielectric constants and conductivities. An antenna system, consisting of plasma-free space interfaces, can therefore be simulated by another system in which the free space ($\epsilon_{A1} = \epsilon_o$) is replaced by a material of high dielectric constant ($\epsilon_{B1} > \epsilon_o$) and the plasma ($\epsilon_{A2} < \epsilon_o$) replaced by free space or air ($\epsilon_{B2} = \epsilon_o$). The characteristic dimensions, as well as the wavelength, are then scaled in accordance with Eq. (5). Both systems are assumed lossless so that the conductivity σ is everywhere zero. The physical model then consists of an anechoic (reflection-free) chamber filled with a high dielectric material in which a scale model of the antenna under test is immersed. The plasma is represented by a low-dielectric constant or air layer over the antenna. It should be noted that this simulation is only correct at a single frequency since the plasma is dispersive while real dielectrics are not. Furthermore, this simulation technique is not applicable for frequencies at which the dielectric constant of the plasma is zero or negative.

3. EXPERIMENTAL RESULTS

Besides the physical restrictions enforced by electromagnetic

requirements, there are mechanical restrictions on the types of real dielectric materials that can be used to simulate free space. The medium simulating free space may not be a solid since a solid does not accommodate insertion of a model. A uniform granular composition is acceptable only for static tests like measurements of impedance because such tests require no movement of the model. A liquid appears to be the most suitable medium since it allows for both static and dynamic experimental tests.

A greater choice is available for selecting the medium to simulate the plasma. It may be a solid, gas, or liquid. In the case described in this paper, a liquid dielectric was chosen to simulate free space, and air to simulate the plasma. Plexiglas, whose dielectric constant approximates that of the liquid dielectric, was used as a separator between the two media.

A schematic of the experimental setup is shown in Figure 1. The dimensions of the metal tank that contains the liquid dielectric are 2.5 ft by 2.5 ft by 4.5 ft, corresponding to dimensions of 37 by 37 by 67 wavelengths (measured in the dielectric) at the operations frequency of 9500 Mcps. The tank has a capacity of about two hundred gallons of liquid dielectric. Its inside walls are lined with microwave absorber, spiked to minimize reflections, which is protected by a plastic liner since it would otherwise dissolve in the liquid dielectric.

Since the liquid dielectric occupies a large experimental volume, there are many safety factors to be considered. It must be noncorrosive; its vapors must be nontoxic; its flash and flame points must have high temperature thresholds. Also, for electromangetic reasons, it must

have a low loss tangent to prevent any marked signal attenuation.

The liquid dielectric selected for the medium to simulate free space was a secondary plasticizer for vinyl chloride and other resins, HB-40 (Monsanto Chemical Company). It does not attack metal or plexiglas but does attack plastics such as polystyrene. At 10K Mcps, HB-40 has a dielectric constant of 2.4, and a loss tangent of 0.0017.[7]

Experimental tests completed to date have yielded the radiation patterns of a plasma-clad axially slotted cylinder such as shown in Figure 2. The results are compared to the theoretical radiation patterns which are computed from an analysis of the plasma-clad slotted cylinder by Wait.[8]

The radiation patterns in Figure 3 of the unclad axially slotted cylinder of two-inch diameter (Model I--see Table 1 for dimensions of all models), show that the free-space pattern and the simulated environment pattern closely agree with theory, although the two experimental beamwidths are slightly narrower from about $\pm 45^{\circ}$ to $\pm 180^{\circ}$.

The radiation patterns for this same cylinder with a four-tenths inch simulated plasma coating (Model II) are shown in Figure 4. The theoretical curves predict the main effects of the lossless plasma layer to be a narrowing of the beamwidth and a slight change in the shape of the sidelobes. The experimental patterns exhibit the narrowing effect caused by the plasma layer and also show the altered sidelobes.

Figure 5 shows the radiation pattern of the two-inch diameter cylinder (Model III), but now the plasma thickness has been increased

to one inch. The effect of the plasma layer is to narrow the main beam slightly. The experimental pattern closely follows all the variations in the theoretical pattern. For purposes of clarity the experimental pattern of the beam without the plasma has been omitted.

Next, the diameter of the cylinder was increased to three inches and the plasma thickness set at one-half inch (Model IV). The beamwidth narrowing caused by the plasma is quite noticeable (Figure6) but there is a larger divergence between theory and experiment than shown by the previous models.

The beamwidths of the experimental patterns for both unclad and plasma-clad models were narrower than predicted by theory. This is partly because the theoretical curves were derived for an infinitely thin slot, whereas the experimental slots had a finite width. In addition, the following two experimental conditions contributed to the narrowing of the experimental beam:

1) The separation between transmitter and receiver is limited by the longitudinal dimension of the tank. The far field requirement for a plane wave across a receiving aperture is given by $L = 2D^2/\lambda$ where D is the effective aperture and L is the transmitter-receiver separation. Unfortunately, for the cylinders with diameters of three inches and above, this criterion for phase and amplitude uniformity across the receiving aperture could not be met within the available tank size.

2) Unwanted reflections often have adverse effects on the radiation pattern of any antenna; in an enclosed area such as a tank, these adverse effects are accentuated. Since microwave absorber ordinarily is matched to free space, its absorption capability in another medium decreases, and reflections correspondingly increase. Radiated energy that hits the side walls of the tank at almost grazing incidence and is not absorbed may combine with the direct radiation and cause a considerable amplitude taper across the receiver aperture.

The amplitude across the receiving aperture of the three inch diameter cylinder varies by about 1.5 db, having a minimum value at the edges. The radiation patterns of the cylindrical antennas show a beam narrowing caused by this tapered amplitude front, as well as by their inherent directivity. This effect causes a deviation between the experimental results and the theory which assumes a uniform amplitude across the aperture.

The limitations imposed by the far field requirements and by excessive reflections from the side walls may be overcome by placing the receiving antenna under test in the near field of a transmitting antenna whose aperture is comparable in dimension with the cross-section of the tank. The fields in this near-zone of the transmitter can be made uniform in both phase and amplitude by suitable antenna design,[9] thereby eliminating the far-field restriction. Further, this plane wave launcher also collimates the radiated energy so that it is normally incident upon the back wall of the tank,

thereby eliminating the grazing reflections from the side walls. A suitable design for such a plane wave launcher could consist of a large parabolic cylindrical reflector which is illuminated by resonant line source feed.

4. EXTENSIONS OF THE TANK PLASMA SIMULATION TECHNIQUE

Since the experimental models are totally immersed in the simulation medium, nonplanar model shapes, whose complicated geometry makes them difficult to analyze theoretically, can be studied experimentally. Figure 7 shows a few of many possible configurations that can be used to determine plasma effects on radiators that are located on finite bodies. Several of these models are now under investigation.

An advantage of the plasma simulation method is that the normalized impedance of a simulation model can be directly compared with the impedance of a similar plasma-clad radiator, and the effects of the plasma on the normalized aperture impedance of an antenna determined. The use of plexiglas as a separator between the air and the liquid dielectric allows investigation of many classes of plasma problems. Among these are the case of a plasma composed of several stratified layers, each layer having a different dielectric constant (Figure 8a), and the case of a plasma that does not touch the surface it envelopes (Figure 8b).

5. SUMMARY

Antenna patterns of axially slotted cylinders of various radii and

various thicknesses of plasma-simulating media have shown good agreement between experimental results and theoretical predictions, in the equatorial plane. The described plasma simulation technique is being used to determine the influence of plasma on normalized aperture impedance and its role in the radiation patterns of nonplanar and finite bodies such as cones and cylinders. The effects of varying radii upon the admittance properties of the radiators are also being studied, as is the feasibility of using the plasma-simulation technique to reproduce the effects of a time-varying or turbulent medium on electromagnetic energy.

REFERENCES

1. R. N. Bracewell, Analogues of an Ionized Medium: Applications to the Ionosphere, Wireless Engineer, Vol. 31, pp 320-326, December 1954.
2. W. Rotman, Plasma Simulation by Artificial Dielectrics and Parallel Plate Media, IRE Trans. on Antennas and Propagation, Vol. AP-10, No. 1, pp 82-95; January 1962.
3. K. E. Golden, Plasma Simulation with an Artificial Dielectric in a Horn Geometry, pp 587-594, IEEE Trans. on Antennas and Propagation, Vol. AP-13, No. 4, July 1965.
4. G. Tyras, P. C. Bargeliotes, J. M. Hamm, R. R. Schell, An Experimental Study of Plasma Sheath Effects on Antennas, Report AFCRL-65-53, Univ. of Arizona, Contract AF19(628)-3834, December 1964. Also G. Tyras et al, Radio Science Journal of Research, NBS, USNC-URSI, Vol. 69D, No. 6, June 1965.
5. E. H. Holt and R. E. Haskell, Foundations of Plasma Dynamics, pg. 334, The Macmillan Co., New York; 1965.
6. Stratton, Electromagnetic Theory, pp. 488-490, McGraw-Hill Book Co., Inc., 1941.
7. Von Heppel, Dielectric Materials and Applications, MIT Technology Press, April 1958.

8. J. R. Wait, Electromagnetic Radiation from Cylindrical Structures, pp 125-141, Pergamon Press, 1959.

9. W. A. Cummings, Radiation Measurements at Radio Frequencies: A Survey of Current Techniques, Proceedings of the IRE, pp 705-735, Vol. 47, No. 5, Part 1; May 1959.

TABLE 1

Model	Physical Dimensions (inches)			Electrical Dimensions			
	d	t	λ_m	$\frac{d}{\lambda_m}$	$\frac{t}{\lambda_m}$	A	B
I	2.00	--	0.80	2.50	--	8	--
II	2.00	0.40	0.80	2.50	0.50	8	11
III	2.00	1.00	0.80	2.50	1.25	8	16
IV	3.00	0.50	0.80	3.75	0.62	12	16

Frequency of operation = 9500Mcps

Also: a = outer radius of metal cylinder

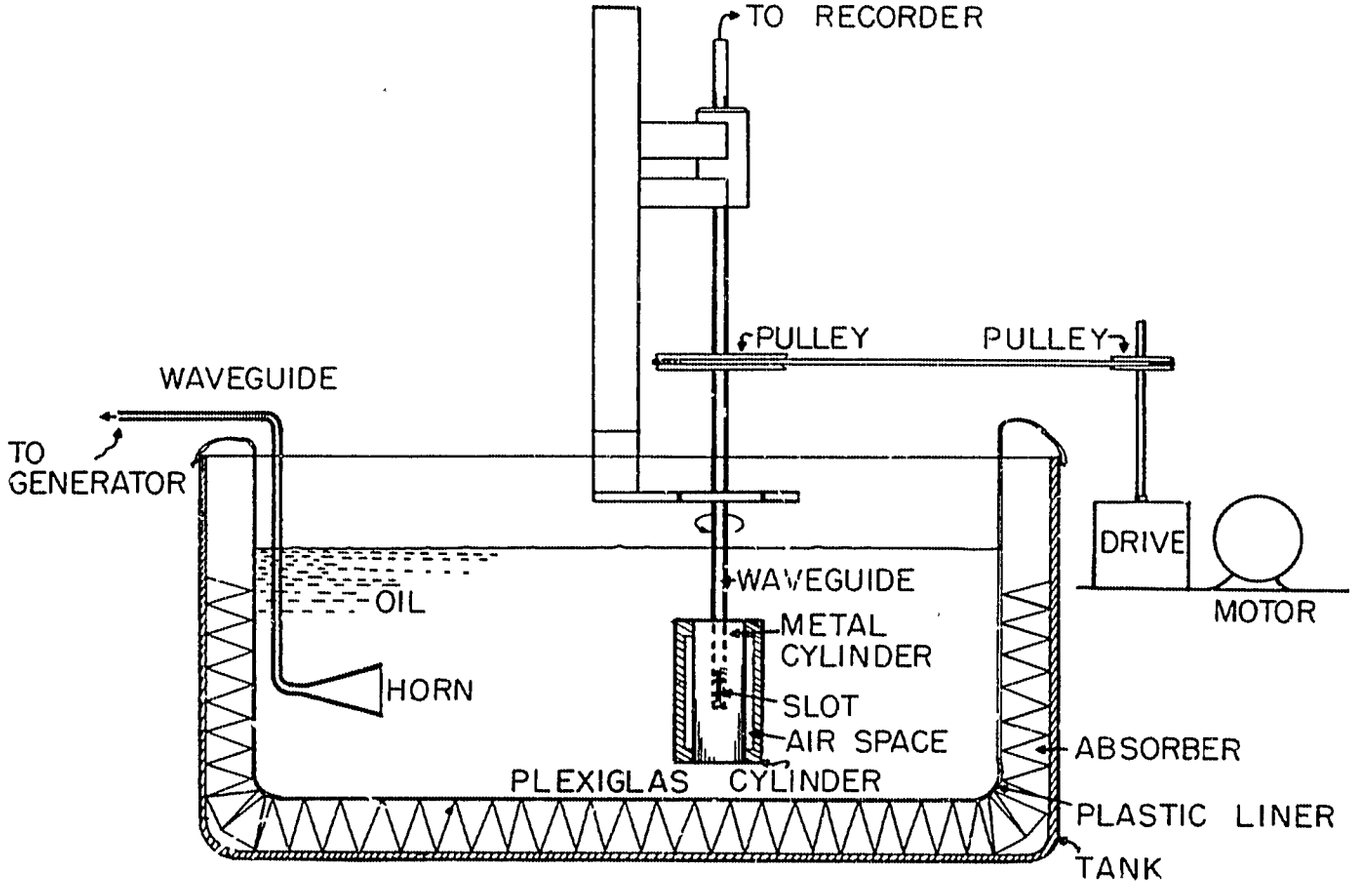
t = thickness of plasma layer (b-a)

b = outer radius of metal cylinder plus cladding dielectric layer

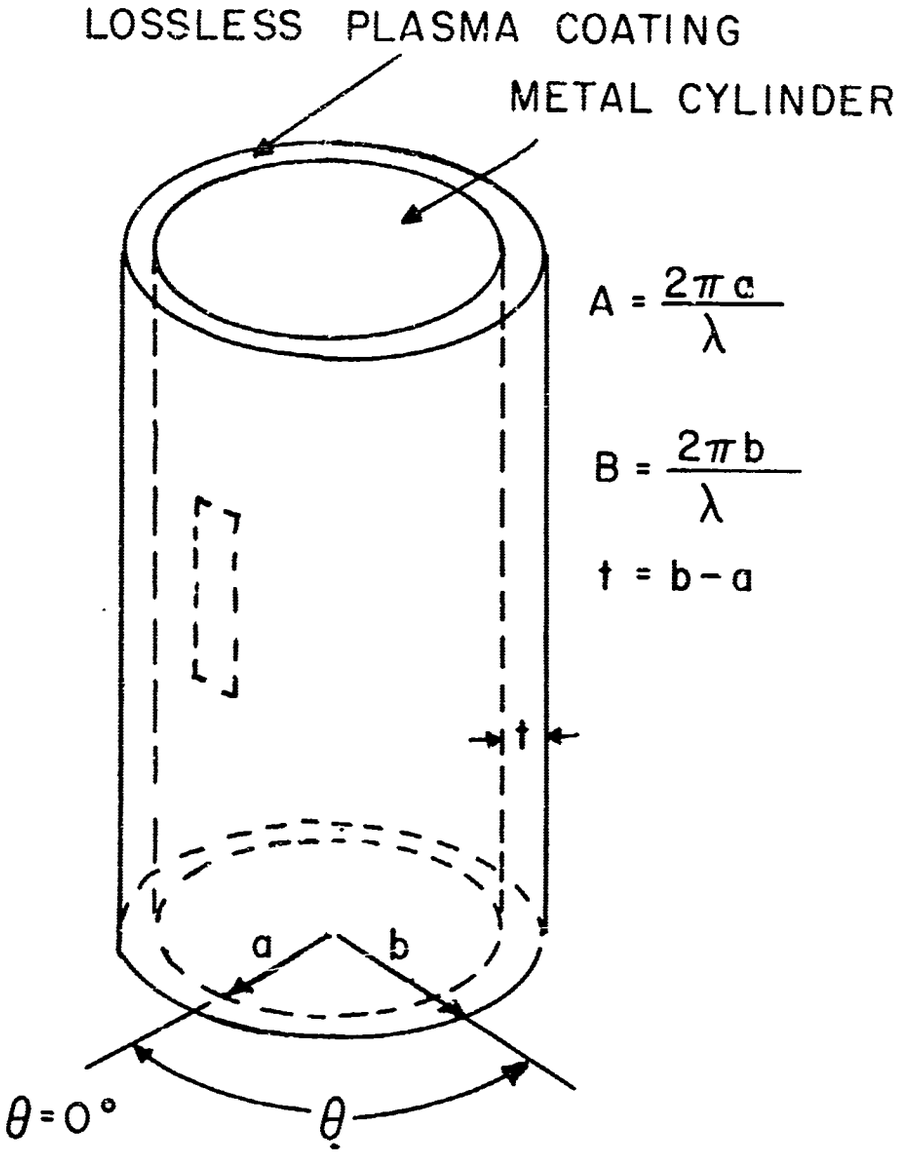
d = diameter of metal cylinder

λ_m = wavelength in the medium

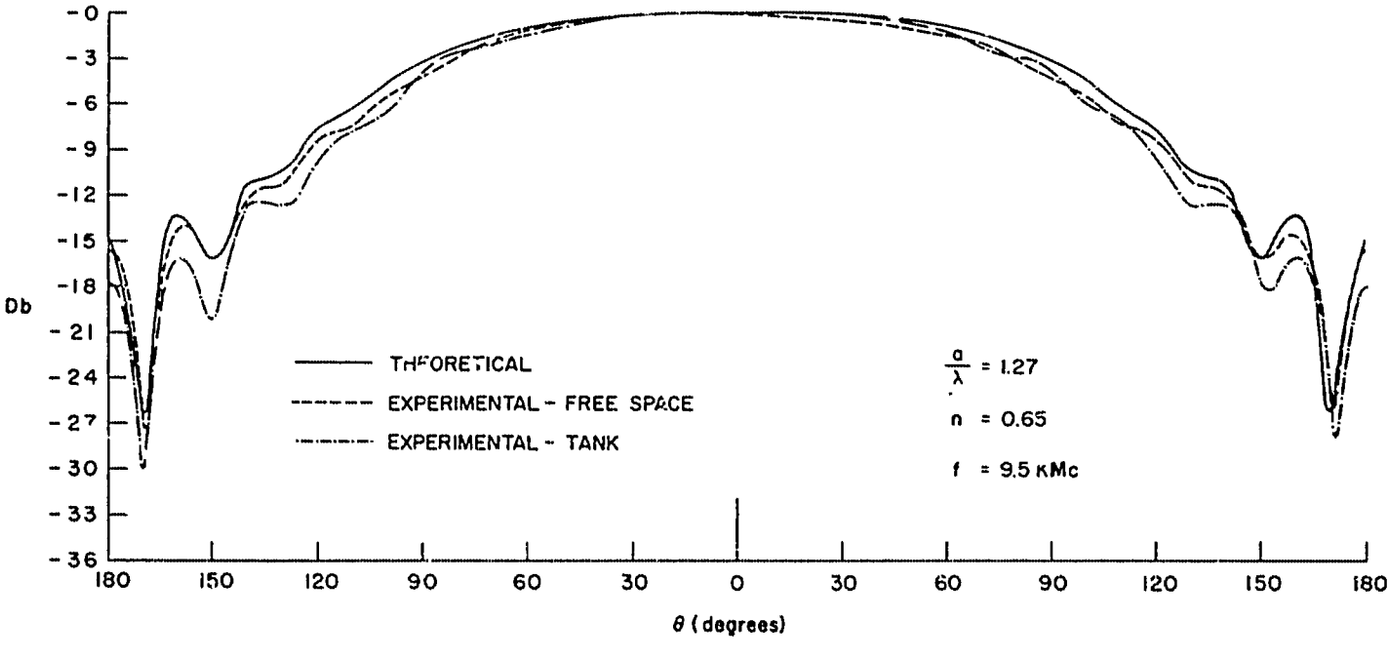
$A = \frac{2\pi}{\lambda_m} a$; $B = \frac{2\pi}{\lambda_m} b$



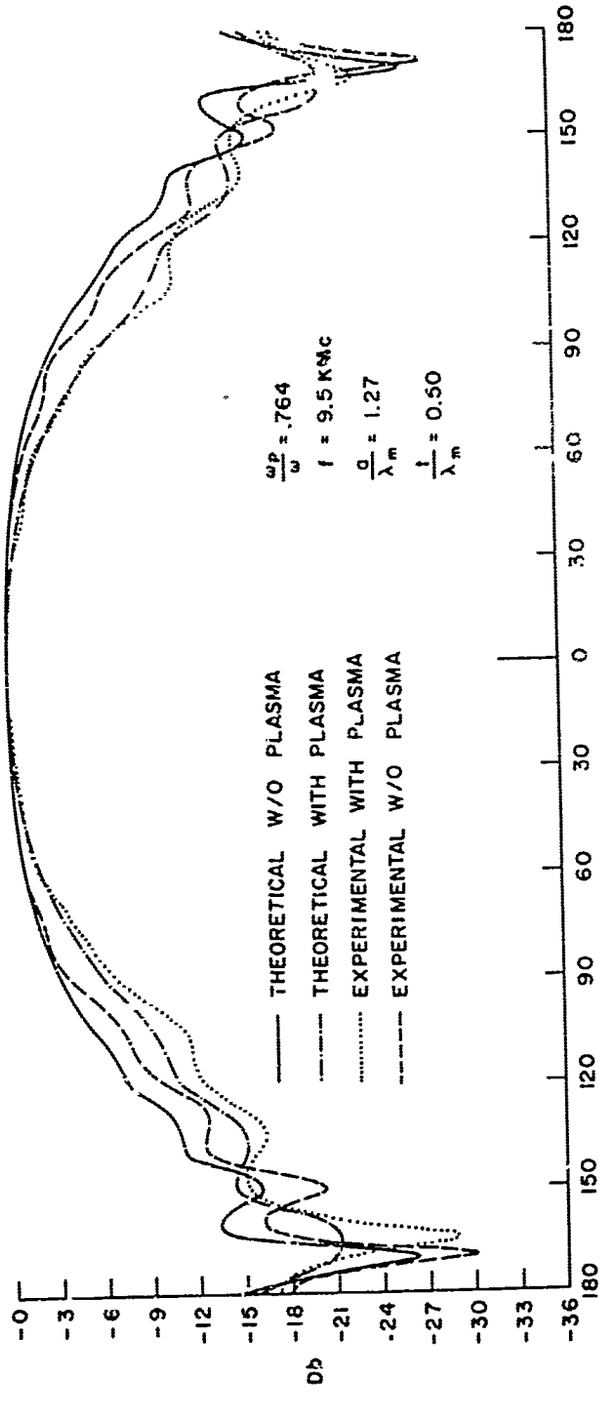
1. **Liquid Dielectric Tank for Plasma Simulation**



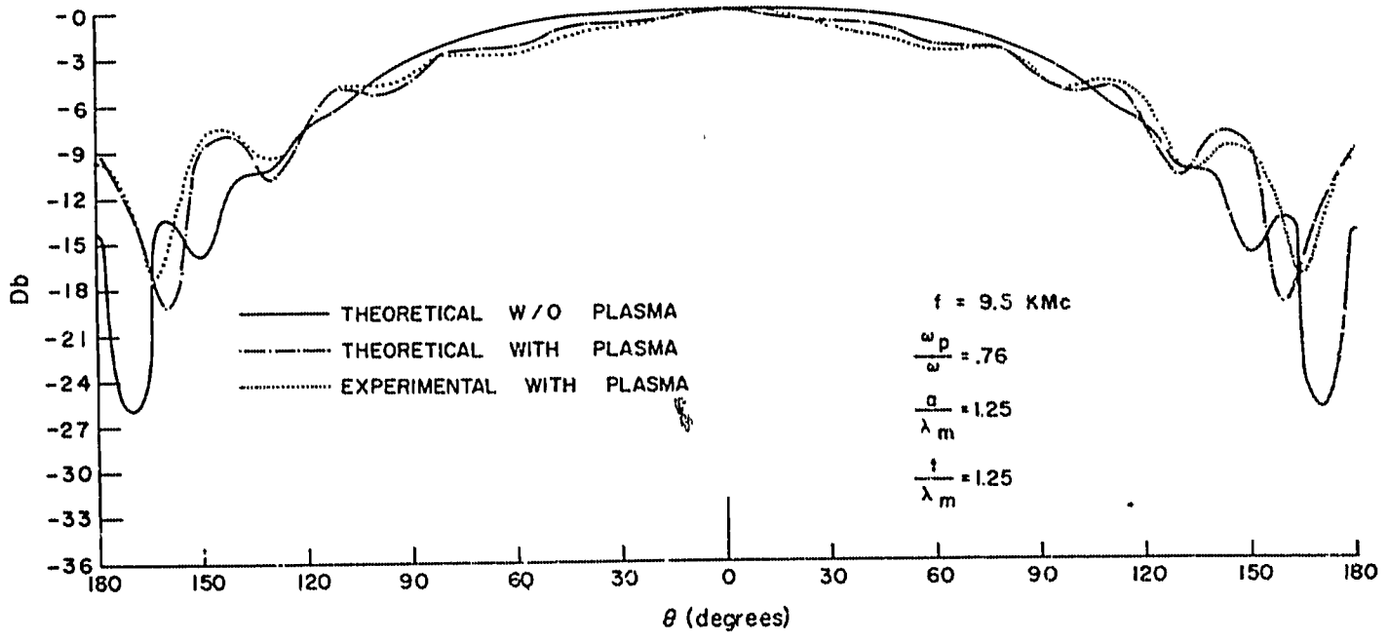
2. Plasma-Clad Axially Slotted Cylinder Model



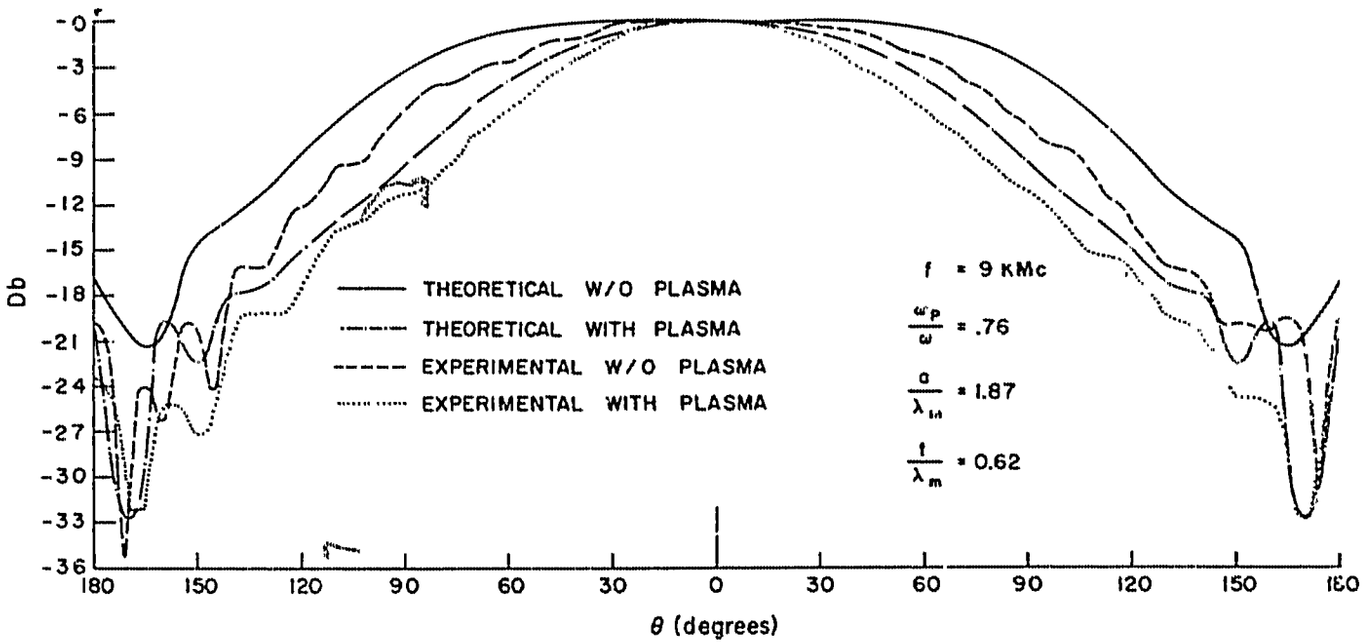
3. Radiation Patterns, Axially Slotted Cylinder ($A \approx 8$)



4. Radiation Patterns, Axially Slotted Cylinder with and Without Plasma ($A \approx 8$, $B \approx 11$)



5. Radiation Patterns, Axially Slotted Cylinder, with and Without Plasma ($A \approx 8$, $B \approx 16$)



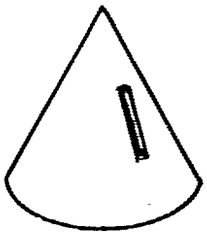
6. Radiation Patterns, Axially Slotted Cylinder, with and without Plasma (A ≈ 12, B ≈ 16)



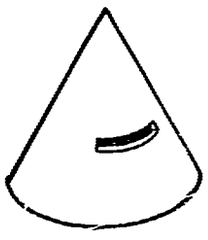
GAP EXCITED
CYLINDER



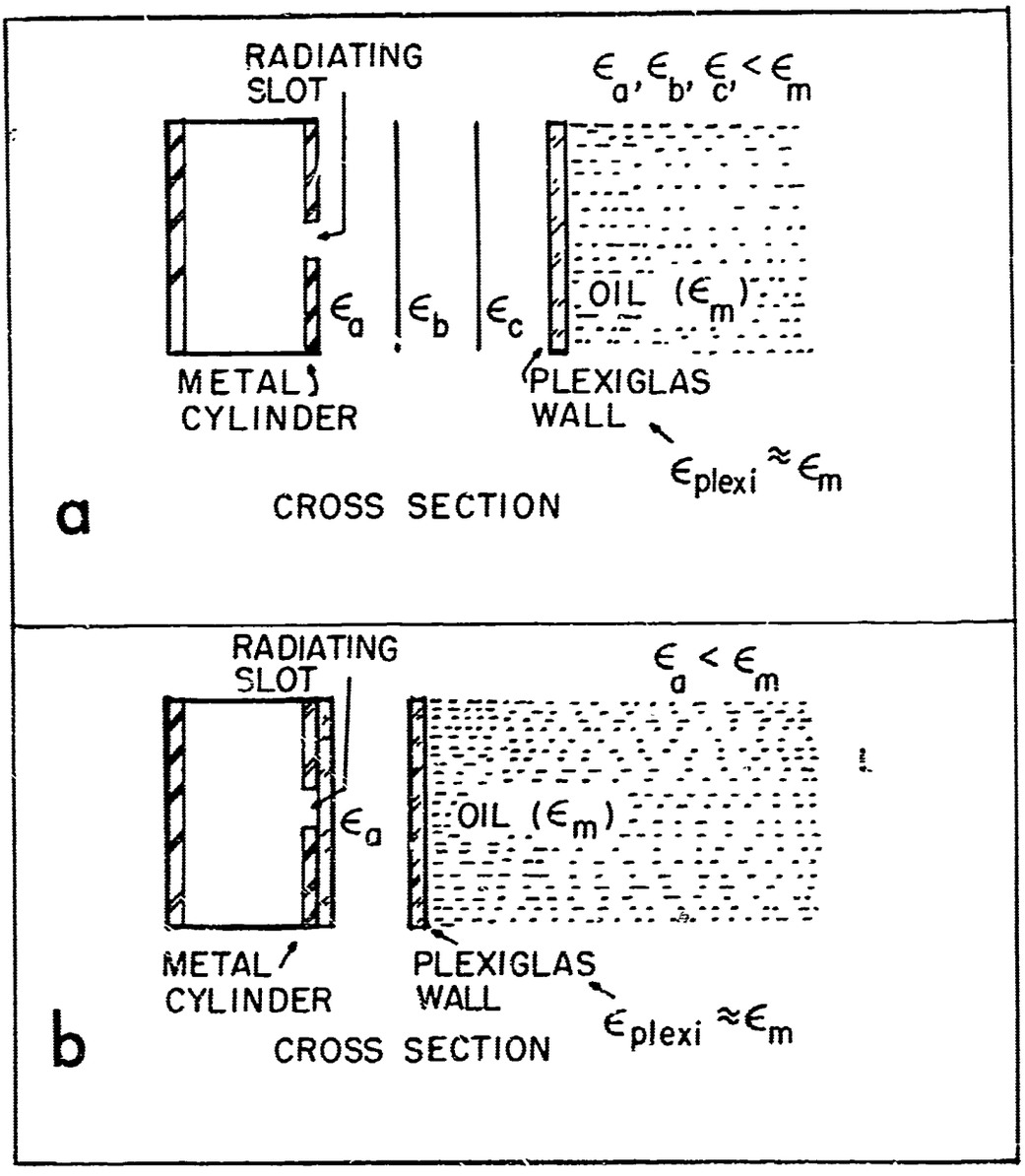
GAP EXCITED
CYLINDER-HEMISPHERE



LONGITUDINAL SLOT ON CONE



CIRCUMFERENTIAL SLOT ON CONE



8. Simulation of Plasma Layer:

(a) Stratified, (b) Noncontacting

V. INTERACTION OF ELECTROMAGNETIC WAVES WITH THE EXHAUST FLAME OF LAUNCH VEHICLES

G. Hasserjian
and
C. A. Clark

THE BOEING COMPANY
Aerospace Group
Seattle, Washington

ABSTRACT

Electromagnetic phenomena influencing the radio link performance between a launch vehicle and ground stations in the presence of the rocket exhaust flame are identified and the state of the art analyses of these phenomena are reviewed. The propagation problem, through and about the inhomogeneous plasma, is considered in detail and a geometrical optics approximation for a laminar exhaust flow is discussed considering reflection, diffraction and refractive phenomena. An integrated computer program is described which automates the computational steps of this approximation. Limitations and restrictions of the approximation are discussed and a sample computation is presented.

ACKNOWLEDGEMENT

This work is being supported by the National Aeronautics and Space Administration of the United States Government under Contract NAS 8-5608.

I. INTRODUCTION

Uninterrupted radio links between a launch vehicle during a powered flight and ground stations are essential requirements for modern day space exploration. Military launch vehicles also have similar requirements. However, such links are generally distorted due to the vehicle's exhaust flame which represents a dispersive plasma environment for the electromagnetic waves. In some instances this environment completely interrupts the radio communication link due to the highly attenuating and reflecting plasma. These critical periods occur generally at high altitudes where ground stations may not have a clear line of sight to the vehicle antenna due to the large extent of the exhaust. The most critical periods occur, however, during the staging sequence of the vehicle. In the latter instance, the exhaust generally envelopes the vehicle establishing the dispersive plasma medium between radiating antennas and receiving stations for all look directions.

In evaluating radio system performance on such vehicles, it is necessary to properly evaluate the characteristics of the plasma environment, analyze the electromagnetic behavior of the system, and attempt to alleviate the possibility of losing communication with the vehicle. A similar system evaluation and corresponding alleviating steps arise in reentry vehicle system design commonly referred to as the reentry blackout problem. In both instances, two basic steps are needed in the analysis. The first is to predict the electrical properties of the plasma, and the second is to evaluate the performance of a radiating

antenna and the propagation of its electromagnetic fields in the presence of this plasma. This paper describes an approach to the analysis of the propagation of the radiated fields of antennas in the presence of flame plasma and is a radical improvement to techniques employed previously. Because chemical and gas dynamic analyses of flames are not fully refined, flame attenuation estimates have been based on crude approximations. To alleviate possible conflict between the two disciplines and with the principal intent of providing a more accurate predictive tool, the work described in this paper was undertaken. The method of analysis and the resulting computer program may not only be applied to inhomogeneous plasmas, but may also be applied to problems involving propagation through other isotropic media.

A review of significant electromagnetic phenomena, associated with flame effects is presented first to place them in perspective. The state of the art approach to the analysis of these effects is then briefly reviewed and their relative effects on a radio system are compared. The propagation of the radiated fields through and around the flame is discussed in detail. The technique employed for this analysis considers the geometrical optics approximation supplemented by a diffraction approximation. The limitations and restrictions of these approximations are discussed and an integrated computer program is described which automates the computational steps of the approximations. Finally, a sample computation obtained by the use of the computer program is presented and discussed.

II. SIGNIFICANT ELECTROMAGNETIC PHENOMENA

The significance of the electromagnetic phenomena influencing the transmission of the information between a transmitter on the vehicle and receivers on the ground depends on the configuration of the exhaust. One may classify them into two configurations; the staging plume configuration and the main engine plume configuration. In the former, the antenna may be entirely enveloped by the exhaust plasma and in some cases be in contact with it. In the second configuration, the main engine plume may be sufficiently far away so that the antenna is not affected directly. Therefore, the dominant effects for each configuration will in general be different.

The significant electromagnetic phenomena may be categorized into two groups. The first group may be identified as "Near Zone" phenomena and the second group as "Far Zone" or "Propagation" phenomena. Near Zone phenomena play a dominant role in the staging plume configuration, while Far Zone phenomena are significant in both configurations. Propagation phenomena are considered in detail in the following sections, with emphasis on the main plume configuration, while Near Zone field effects are only reviewed here.

NEAR ZONE FIELD EFFECTS

In the staging plume configuration, antenna plasma interaction play a significant role in the performance of the communication system. This interaction may be categorized into effects due to antenna impedance change and nonlinear response of the plasma medium.

The impedance of an antenna may change radically due to the changing ionization of the gas and thus alter the power transfer between the transmitter and the external medium. If the field intensity around the antenna is sufficiently low, it possible to estimate the effect of the impedance change which may be in the range of one to ten decibels on the radiated power depending on the type of antenna and the value of the pertinent parameters. Theoretical expressions for antenna impedance in a lossy dielectric, having properties characteristic of a plasma, are available in the literature for dipole antennas,[1],[2] loop antennas,[3] annular slots[4] and waveguide fed slots[5] and apertures[6]. The validity of the expressions is frequently limited to media having low or moderate loss. Furthermore, these analyses assume the plasma to be a linear medium which it is not. However, if the power levels are sufficiently low, the above referenced analyses should yield adequate engineering results. Traveling wave or array type of antenna in the presence of plasma have not been adequately studied to the best knowledge of the authors. This class of antennas may be radically affected by the plasma due to the self and mutual impedance change of the individual elements, if they are of the Yagi or array type. In the case of tapered dielectric and corrugated structure type of traveling wave antennas, dominant effects will be due to the different wave number of the plasma.

Nonlinear effects of the plasma may also be significant and have a marked effect on the communication link. At relatively low power levels and at high altitudes plasma enhanced antenna breakdown may occur increasing the ionization of the gas sharply. This causes

a sharp increase in the reflected power degrading transmitter performance. It also results in larger rf energy absorption by the plasma and causes antenna pattern distortion. Consequently, it is necessary to operate the antenna below the power level at which breakdown occurs. The breakdown power level is dependent upon gas density, gas velocity, the ionization level prior to breakdown, the radio frequency and the configuration of the antenna. This phenomenon has been studied theoretically and experimentally by many workers and is reported adequately[7], [8], [9], so that is is possible to make engineering estimates on maximum allowable power for a given system.*

As noted before, the plasma is by no means linear, even at power levels far below breakdown. There is coupling of electromagnetic energy to the gas resulting in a change of the ionization. In addition, the plasma collision frequency may be a function of the applied field and may only be assumed constant for extremely low signal levels. Such nonlinearities cause phase and amplitude distortion in the radiated signal and hence an effective loss in the communication link. There have been some analytical and experimental results reported in the literature[10], [11] on this problem. However, the authors have been unable to find adequate results to obtain engineering estimates of this effect on a radio link.

---

*More recent results were reported in a NASA sponsored workshop on Voltage Breakdown in Electronic Equipment at Low Air Pressures, held at JPL, August 18-20, 1965. An additional phenomenon, noted in this workshop, which might interrupt communication is DC discharge. This phenomonon is known to occur during the staging phase of the vehicle's flight. A discussion of this phenomenon is beyond the scope of this paper.

FAR ZONE FIELD EFFECTS

At distances sufficiently far from an antenna, the field intensities may be relatively low and have a wave behavior. Therefore, it is reasonable to consider wave phenomena in a linear plasma. This phenomenon of propagation of electromagnetic energy through the plasma medium, is by far the dominant factor influencing the communication link. To analyze the effect of this phenomenon, it is necessary to know the electrical properties of the plasma as a function of space and time. If field intensities are sufficiently low and one is justified in assuming a constant collision frequency for the charged particles of the plasma, it is then possible to describe it as a linear, isotropic, inhomogeneous and time varying dielectric medium. It is reasonable to also assume that the time variation is slow. To analyze the propagation through such a medium, it is necessary to consider attenuation, refraction, diffraction and scattering of the electromagnetic waves. The scattering analysis requires a description of the irregularities of the medium, at least statistically. Such an analysis is beyond the scope of this paper however. A brief discussion of several analytical approaches is given elsewhere[12]. We need to emphasize, however, that if the plasma is very dense along the normal path of propagation, the contributions from volumetric scattering to the far zone field become dominant. Otherwise, the average field strengths may be obtained by evaluating propagation by accepting a laminar description of the medium.

Serious discrepancies may arise by ignoring the scattering from the medium irregularities in the staging plume configuration. However, similar scattering in the main engine plume configuration has secondary effects except in regions where antenna pattern nulls may occur

from the laminar analysis. For a thorough analysis of the system, it is necessary that scattering from the irregularities be considered. However, the laminar analysis will yield the average value of the fields in the medium and is a necessary first step to the scattering analysis due to the irregularities of the medium.

The above review of significant electromagnetic phenomena leads us to the justification of the assumptions and approximations developed below in the analysis of radio wave propagation in the presence of exhaust flame. We therefore state that the approximations described below are applicable to any plasma medium which has laminar inhomogeneities described deterministically for a given time in terms of spatial coordinates. The approximations also require that an effective complex dielectric constant be computed from the plasma parameters for a given signal frequency. To make the propagation analysis more tractable, we further assume that all pertinent dimensions of the exhaust are large in comparison to the signal wavelength.

The assumptions listed here are not very restrictive. There are a large class of vehicles whose main engine exhausts fall within the limitations of the required assumptions stated above. In many other circumstances our approximations will yield results describing first order effects.

Subject to these assumptions, the problem reduces to the analysis of the electromagnetic fields of an antenna with a prescribed radiation pattern, in the presence of an inhomogeneous medium with a complex refractive index. The sketch in Fig. 1 is a schematic illustration

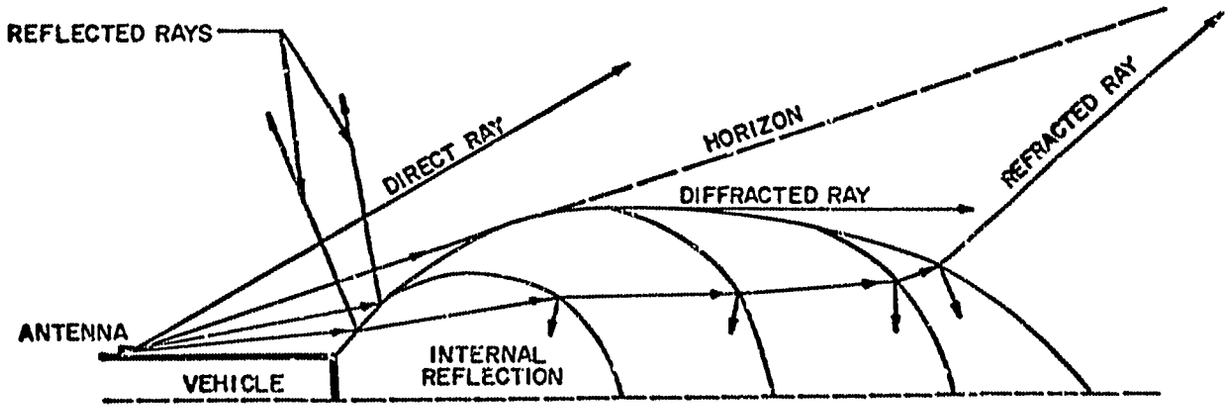


FIGURE 1 - An Illustration of the Geometry and Electromagnetic Phenomena

of the geometry of the problem and the electromagnetic phenomena that need to be considered. The three dimensional geometry of the vehicle and plume would be the figure of revolution of that portion of the sketch. The dashed line in the figure indicates the radio horizon of the plume and divides the field into two regions. Above the horizon, the total field consists of the sum of the direct rays, the reflected rays and the refracted rays. Below the horizon, the field is the sum of the diffracted and refracted rays. It is possible to carry out a geometrical optics approximation to compute the total field, including polarization and amplitude, provided the routine computational steps can be entrusted to a large digital computer. In the section III, we discuss the approximations that were developed for this study and in the section following we describe the integrated computer program that can implement the details of the computation.

III. THE GEOMETRICAL OPTICS APPROXIMATION

The determination of the effects of reflection, diffraction and refraction on radio wave propagation about the exhaust plasma is subject to a large number of parameters. These include geometry, signal frequency and medium constants and their spatial variation. We can employ the geometrical optics approximation if the distribution of the plasma is such that it can be subdivided into convenient subsections, the boundary surfaces of which have large dimensions in comparison to the signal wavelength. The term "geometrical optics" is used here to imply that the results are correct asymptotically as $k_o \to \infty$, where k_o is the

free space wave number of the signal, and that the ray nature of the electromagnetic wave can be utilized in the approximation. The diffraction analysis, described in a latter part of this section, is not a geometrical optics approximation in the true sense, but it is a complementary step to the approximation of the entire problem.

In considering propagation through the plume, we assume that its subsections consist of plasma having thick lossy subsections, thin lossy sections and sections with low loss: the latter constituting the major portions of the plume. For thick lossy sections we assume the reflected fields dominate, for thin lossy sections we approximate the section by a layered medium in the region of the incident ray tube for the computation of transmitted fields. Under these assumptions, the geometrical optics computations are performed for a lossless plasma and analytically continued to the lossy case.

The field intensity at a given observation point, which is assumed to be at a large distance from the vehicle, is the vector sum of the direct, the reflected, diffracted and the refracted fields. We describe below the necessary approximations and the resulting expressions to evaluate these fields. The assumed geometry is that shown in Fig. 1.

THE REFLECTED FIELD

A ray tube, originating from the antenna and incident to the plume boundary will be reflected from and transmitted through this boundary. Depending on the altitude of the vehicle, this plume boundary may be sharp or diffuse. To compute the reflected field, the reflecting

boundary, the plane of incidence and angle of incidence is first evaluated from the known geometry. The principal radii of curvature of the reflecting surface and the density gradients of the plasma are evaluated next. From these results, a "divergence coefficient" is computed. From the known plasma characteristics in the region of the boundary, transverse electric (TE) and transverse magnetic (TM) "reflection coefficients" are also evaluated. Finally, the reflected fields are determined within the limits of the geometrical optics approximation. This approximation, however, fails near grazing angles of incidence. For this reason, the computations for angles larger than 85° are performed by the diffraction formulas discussed later.

In the geometrical optics approximation, the reflected electric and magnetic fields are given by

$$\vec{E}_r = \vec{E}_{rs}\, D_s \exp\left[ik_o\,(r_1 + r_2)\right]$$
$$Z_o\, \vec{H}_r = \vec{t}_r \times \vec{E}_r \qquad (1)$$

where $\vec{E}_{rs}$ is the electric field at the reflecting boundary, D_s is the "Divergence Coefficient", k_o is the wave number, r_1 is the distance from the source to the point of reflection, r_2 the distance from this point to the observation point, $Z_o = \sqrt{\mu_o/\epsilon_o}$ is the free space wave impedance, and $\vec{t}_r$ is the unit vector in the direction of the reflected ray.

The electric ffeld components on the surface can be evaluated simply from the plane wave analysis, yielding the expression

$$\vec{E}_{rs} = R_e(\vec{E}_{is}\cdot\vec{b})\,\vec{b} + R_m(\vec{t}_i \times \vec{b})\cdot\vec{E}_{is}(\vec{t}_r \times \vec{b}) \qquad (2)$$

where $\vec{b}$ is the unit vector normal to the plane of incidence, $\vec{t}_i$ is the unit vector in the direction of the incident ray, $\vec{E}_{is}$ is the incident field at the reflecting surface, R_e and R_m are the reflection coefficients for the TE and TM waves respectively.

The Divergence Coefficient

This coefficient is simply a geometrical factor expressing the degree of divergence of a tube of ray due to reflection from a curved surface. It is related to the cross section of the incident ray tube $A(r_1)$ and the cross section of the reflected ray tube $A(r_2)$, at a distance r_2 from the reflection point, simply by

$$D_s = \sqrt{A(r_1)/A(r_2)}. \tag{3}$$

Fock has developed expressions for this coefficient for a general convex surface[13] with principal radii of curvature ρ_1 and ρ_2. The result for $r_2 \to \infty$ is

$$\frac{A(r_2)}{A(r_1)} = \frac{1}{\cos\theta}\left\{\cos\theta\left(1+\frac{1}{r_1^2}\right)+\frac{2}{r_1}\left[\left(\frac{1}{\rho_1}+\frac{1}{\rho_2}\right)\cos^2\theta+\frac{\sin^2\theta}{\rho_o}\right]+\frac{4\cos^2\theta}{\rho_1\rho_2}\right\}.$$

In the expression θ is the angle of incidence and ρ_o is the boundary radius of curvature in the plane of incidence.

The Reflection Coefficients R_e and R_m

These coefficients are a function of the characteristics of the medium and their gradients in the reflection region. As was stated before, the plume boundary may be sharp or diffuse. If it is sharp, the required expressions are simply the standard Fresnel reflection coefficients. However, we wish to employ an analytic expression which is

general enough to account for reflections from a diffuse boundary with its sharp boundary limit the Fresnel reflection coefficients. This can be accomplished adequately by considering the generalized "Epstein Profile" for the variation of the dielectric constant and the corresponding wave solution for such a layered medium. A general discussion of such a solution may be found in several books[14],[15],[16]. The authors have shown elsewhere,[17] that a transitional layer of plasma having an electron density and collision frequency variation, described respectively by

$$f(z) = \frac{e^{mz}}{1 + e^{mz}}$$

$$g(z) = \frac{(V_o/V_1) + e^{mz}}{1 + e^{mz}}, \tag{5}$$

can also be solved. These functions appear in the Appleton-Hartree expression, for the plasma relative dielectric constant, as

$$\epsilon_r(z) = 1 - \omega_1 f(z)/[1 + i V_1 g(z)]. \tag{6}$$

In the expressions above z is the coordinate along the normal to the reflecting boundary, which is taken to be at z = 0 the center of the transition layer, $\omega_1 = (\omega_p/\omega)^2$ with ω_p as the plasma frequency deep in the layer and ω the signal frequency, $V_o = \nu_i/\omega$ and $V_1 = \nu_f/\omega$ with ν_i and ν_f being the values of the collision frequency at the extremities of the layer. The parameter m describes the thickness of the layer and is inversely proportional to it. The reflection and transmission coefficients

for such a layer, for a TE wave, are given in terms of Gamma functions as

$$R_e = A^{(1-\gamma)} \frac{\Gamma(\gamma-1)\Gamma(1-\beta)\Gamma(\alpha-\gamma+1)}{\Gamma(1-\gamma)\Gamma(\gamma-\beta)\Gamma(\alpha)}$$

$$T_e = A^{(1-\gamma+\beta-\alpha)} \frac{\Gamma(\alpha-\gamma+1)\Gamma(1-\beta)}{\Gamma(\alpha-\beta+1)\Gamma(1-\gamma)} \tag{7}$$

where

$$A = \frac{1 + iV_1}{1 + iV_o}$$

$$\alpha = 1 + i(k_o/m)[\cos\theta - (\cos^2\theta - N)^{1/2}]$$

$$\beta = 1 + i(k_o/m)[\cos\theta + (\cos^2\theta - N)^{1/2}] \tag{8}$$

$$\gamma = 1 + i2(k_o/m)\cos\theta$$

$$N = \omega_1/(1+iV_1)$$

For small m, which corresponds to a thick layer, the reflection and transmission coefficients for the TM case are identical to those in (7). For large m, a sharp transition or a thin layer, the expression in (7) will again hold if the exponents α and β are replaced by

$$\alpha' = 1 + i(k_o/m)\,[(1-N)\cos\theta - (\cos^2\theta - N)^{1/2}]$$

$$\beta' = 1 + i(k_o/m)\,[(1-N)\cos\theta + (\cos^2\theta - N)^{1/2}] \tag{9}$$

Additional corrections are needed for intermediate values of m. In the limit as $m \to 0$, the boundary becomes very diffuse hence the reflection coefficient approaches zero exponentially. In this range, reflections are secondary and the transmitted fields are computed according to the approximations of the refracted fields which penetrate the plume.

THE DIFFRACTED FIELD

At grazing angles of incidence, plume boundary electromagnetic phenomena cannot be described in the geometrical optics sense, particularly when these boundaries are relatively sharp and are of high density. There are cases of exhaust plumes where diffraction phenomena are significant in the region of the plume horizon (see Fig. 1). An exact formulation of the problem is not possible, we therefore consider the results obtained for the solution of a sharply bounded spherical plasma region with a source external to it. We seek appropriate approximations for the fields about the horizon defined by the tangent line to the surface drawn through the source. The basic problem has been studied extensively by many authors in connection with radio propagation on the earth's surface. Logan has reported an extensive review of these works[18] and has generalized the results providing adequate approximations so that the geometric optics approximations for the illuminated region are continued smoothly into the diffraction or shadow region.

The assumptions therefore are that in the region of incidence the boundary can be described by a spherical surface and that the tangential component of the electric and magnetic fields are related by a constant at the boundary. Improvements to the latter are possible but are not considered here. Logan's results are given below for the case of a source at a relatively large distance from the surface and an observation point at infinity.

Figure 2 illustrates the geometry in the plane of incidence. The boundary shown in the figure is the local spherical approximation of the actual plume boundary, in the region of incidence, with a radius of

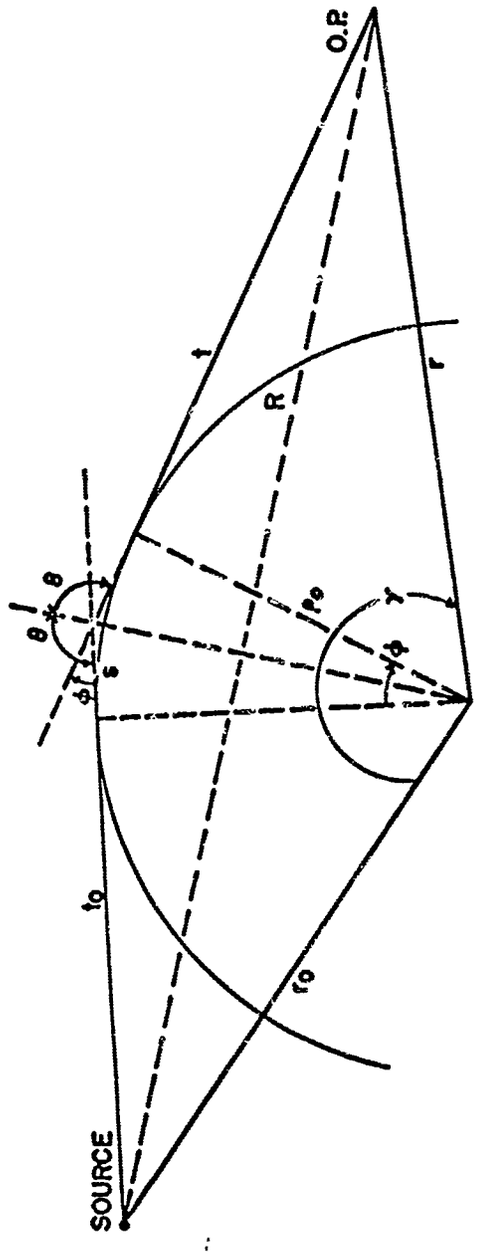


FIGURE 2 - Geometry of the Diffraction Approximation

of curvature ρ_o. For linear boundary conditions we employ the surface impedance expressions

$$Z_{TM} = (k_o/k)\,[1-(k_o/k)^2]^{1/2}$$
$$Z_{TE} = (k_o/k)\,[1-(k_o/k)^2]^{-1/2} \tag{10}$$

for the TM and TE waves respectively, with k representing the complex wave number in the plasma medium. In the development below, the above impedance expressions appear in the term

$$q = i(k_o\rho_o/2)^{1/3}Z. \tag{11}$$

The terms $y_o = (k_o\rho_o/2)^{1/3}(t_o/\rho_o)$, t and r are assumed to be approaching infinity, and the angle of incidence, θ, is generalized to also describe the diffracted ray beyond the horizon. $s = \rho_o\phi$ is approximated by $s \cong (-2\rho_o\cos\theta)$ is used for $80° < \theta < 100°$ since this is the range of interest here and it appears in the parameter

$$x = (k_o\rho_o/2)^{1/3}(s/\rho_o). \tag{12}$$

For a radial dipole of the electric or magnetic type, Logan's results for the total field about the plume horizon can be expressed by

$$U(r,\gamma) \cong \frac{\exp ik_o(R+W)}{4\pi R}\left[\frac{t_o \sin 2\theta}{\rho_o} - \cos 2\theta\right]^{-1/2}\frac{V_{11}(x,q)}{\sqrt{y_o}} \tag{13}$$

where

$$W = \begin{cases} 2t_o(1-\sin^2\theta) + \rho_o(2\theta + \sin 2\theta - \pi), & \theta > \frac{\pi}{2} \\ t_o(1-\sin\theta) - (\rho_o/3)\cos^3\theta, & \theta < \frac{\pi}{2} \end{cases}$$

For $\theta > \pi/2$, (the shadow region)

$$V_{11}(x,q) \cong -\frac{\exp(i\pi/4)}{\sqrt{\pi}} \int_{-\infty}^{\infty} \exp(ixt)\, \frac{v'(t)-qv(t)}{w_1'(t)-qw_1(t)}\,dt \tag{14}$$

which may be evaluated by its residue series.

For the horizon region, $\pi/2 - \epsilon < \theta < \pi/2 + \epsilon$, ($\epsilon$ may be considered to be approximately 10°),

$$V_{11}(x,q) \cong V_2(x,q) + \begin{cases} \sqrt{y_o}\, K\,(x\sqrt{y_o}) & ,\theta > \frac{\pi}{2} \\ \sqrt{y_o}\, \exp(-ik_o W) - \sqrt{y_o}\, K\,(-x\sqrt{y_o}), & \theta < \frac{\pi}{2} \end{cases} \tag{15}$$

$$V_2(x,q) \cong -\frac{\exp(i\pi/4)}{\sqrt{\pi}} \left\{ \int_{-\infty}^{\infty} e^{ixt}\, \frac{v'(t)-qv(t)}{w_1'(t)-qw_1(t)}\,dt + \frac{1}{2x} \right\} \tag{16}$$

In the expressions above $w_1(t) = u(t) + iv(t)$ and $w_1'(t)$ are the Airy functions and their derivatives respectively, and

$$K(\tau) = \frac{\exp(-i\tau^3 - i\pi/4)}{\sqrt{\pi}} \int_{\tau}^{\infty} \exp\,(is^2)\,ds. \tag{17}$$

The evaluation of (16) is rather involved. However, for (x/q) small the approximation

$$V_2(x,q) \cong -\exp(i\pi/4) \left\{ \left(\frac{-i}{2q\sqrt{\pi}}\right) \left[1 + \frac{ix}{2q} + \frac{1}{6}\left(\frac{ix}{q}\right)^2\right] + \frac{x}{3q^3}\, p'(x) + p(x)\left[1 + \frac{ix}{q} + \frac{1}{2}\left(\frac{ix}{q}\right)^2\right] + \ldots \right\} \tag{18}$$

can be used. Logan has evaluated p(x) numerically[19] and given tables for $-1.6 < x < 1.6$.

In evaluating $V_{11}(x,q)$, it should be sufficient to use the expression given in (15) without carrying the evaluation deep into the shadow region. In this region, the diffracted fields are of second order to the refracted fields unless the medium is a very dense plasma. The use of an impedance boundary condition requires further study. It should be possible to derive more accurate linear boundary conditions for various possible ranges of plasma parameters. Such improvements can be readily introduced into the general expressions given above.

The evaluation of the diffracted fields of any antenna, (the results above are for dipoles) can be performed by expressing the source field in terms of the linear combination of TE and TM waves in the plane of incidence and normalizing the expressions in (13) by the field intensity of the source at a distance t_o.

IV. FIELDS IN THE EXHAUST FLAME

The analysis of the fields in the exhaust plasma is based on the geometric optics approximation of Maxwell's equations. Before applying this approximation, it is necessary to classify the kind of medium and the applicability of the approximation. If the exhaust plasma and the signal frequency is such that there is significant transmission through it, then it is reasonable to approximate this into three subsections: sections having low losses, thin sections having high losses, and thick sections also with high losses. Transmitted fields through the first two can then be computed by the geometric optics approximation if the thin lossy section is approximated by parallel boundaries. Since the transmitted fields through thick lossy sections will be of second order, only reflected fields from their boundaries need be considered. The evaluation of the fields (their amplitude, phase

and polarization) is performed by integrating a set of linear first order differential equations. Ray paths are determined from the variation of the real part of the propagation constant k, but the amplitude of the field is evaluated for complex k because of analyticity with respect to k. In the analysis multiple reflections are ignored. A brief review of the development of the required differential equations is given below.

Kline[20] has shown that the geometric optics approximation of the field $\vec{E}$ is the first term of the asymptotic series

$$\vec{E}(x,y,z) = \left[\exp ik_o S(x,y,z)\right] \sum_{n=0}^{\infty} \vec{E}_n(x,y,z)/(ik_o)^n \qquad (19)$$

for large k_o. This assumes a single family of phase fronts $S(x,y,z)$ for the fields. Substituting (19) in Maxwell's differential equations and equating terms of equal powers of k_o, one obtains the Eiconal Equation

$$|\nabla S|^2 - (k/k_o)^2 = 0 \qquad (20)$$

and the Vector Transport Equation for the first term

$$2\nabla S.\nabla \vec{E}_o + \nabla^2 S\, \vec{E}_o + 2\,(\vec{E}_o.\nabla k/k)\nabla S = 0 \qquad (21)$$

The ray directions are the trajectories normal to the phase fronts $S(x,y,z)$ and thus from (20) we have

$$\nabla S = \vec{k}/k_o = \eta \vec{t} \qquad (22)$$

where η is the index of refraction and $\vec{t}$ is the unit vector along the ray. It is easy to show that the nonlinear partial differential equation in (20) is satisfied by the following set of linear first order differential equations:

$$\frac{d\vec{x}}{dx} = \nabla S/\eta = \vec{t}$$
$$\frac{d}{ds}\left(\eta \frac{d\vec{x}}{ds}\right) = \nabla\eta \qquad (23)$$

where $\vec{x} = (x,y,z)$ is the position coordinate of the ray and ds is the differential length along the ray path. The above set is used in our computation in the form

$$\frac{d\vec{x}}{ds} = \frac{\vec{k}_r}{k_r} \quad ; \quad \frac{d\vec{k}_r}{ds} = \nabla k_r \qquad (24)$$

where k_r is the real part of the complex k, since we require real paths and geometry. The set of six differential equations define a ray path for given initial values, medium constants and boundary conditions (Snell's law gives the boundary conditions) sufficient for the computation of the field intensities.

The vector transport equation, given in (21), contains information on the polarization and amplitude of the field. It is easier to demonstrate the significance of the terms of this equation by dissociating the vector quantities from the scalar ones.

We consider the geometric optics term $\vec{E}_o$ and the relations

$$\vec{p} \equiv \vec{E}_o/E_o, \quad \vec{p}\cdot\vec{t} = 0 \qquad (25)$$

where $\vec{p}$ is the unit polarization vector. From (21) we have, after division by E_o,

$$\frac{d\vec{u}}{ds} + \vec{p}\,\frac{1dE_o}{E_o ds} + \frac{v^2 S}{2\eta}\vec{p} + \left(\frac{\nabla k}{k}\cdot\vec{p}\right)\vec{t} = 0 \tag{26}$$

Since $\vec{p}$ is orthogonal to $\vec{t}$ and $(d\vec{p}/ds)$, (26) yields the set of equations

$$\frac{1}{E_o}\frac{dE_o}{ds} + \frac{v^2 S}{2\eta} = 0, \tag{27}$$

$$\frac{d\vec{p}}{ds} + \left(\frac{\nabla k}{k}\cdot\vec{p}\right)\vec{t} = 0 \tag{28}$$

also,

$$\vec{p}\cdot\frac{d\vec{t}}{ds} = \frac{\nabla k}{k}\cdot\vec{p} \tag{29}$$

Equation (27) describes the amplitude dependence of the field term E_o and (28) describes the polarization dependence. A closer examination of (27) reveals that conservation of energy is implied. Therefore, it does not account for reflections in regions where the change in k might be small but finite. We make this requirement since difference equations are to be used in our application and also we wish to avoid using boundary conditions as much as possible. Equation (27) represents the differential equation

$$\frac{1dE_o}{E_o ds} = -\frac{1}{2}\left[v\cdot\vec{t} + \frac{1}{k}\frac{dk}{ds}\right]. \tag{30}$$

It is shown elsewhere[21] that to account for finite but small changes in k, the amplitude transport equation should be

$$\frac{1}{E_o}\frac{dE_o}{ds} = -\frac{1}{2}\left[v\cdot\vec{t} + \left(\frac{\lambda}{k}\right)\frac{|\nabla k|^2}{\nabla k\cdot\vec{t}}\right] \tag{31}$$

Physically, the term $\nabla.\vec{t}$ accounts for the change of amplitude due to the divergence of the ray tube. The last term in both equations account for energy density change, but the last term in (31) also accounts for change in energy due to partial reflections.

Thus, given the initial direction, amplitude and polarization of a wave we can obtain the total field anywhere in the plasma, subject to the assumptions made, by integrating the following set of ten linear, first order, ordinary differential equations.

$$\frac{1}{E}\frac{dE}{ds} = ik - \frac{1}{2}\left[\nabla.\vec{t} + \frac{\nabla k.\vec{t}}{k}\left(\frac{|\nabla k_r|}{\nabla k_r.\vec{t}}\right)^2\right]$$

$$\frac{d\vec{p}}{ds} = -\left(\vec{p}.\frac{\nabla k_r}{k_r}\right)\vec{t} \qquad (32)$$

$$\frac{d\vec{x}}{ds} = \frac{\vec{k_r}}{k_r}, \quad \frac{d\vec{k_r}}{ds} = \nabla k_r$$

The numerical evaluation of the term $\nabla.\vec{t}$ can be performed either for each differential step Δs or after a complete ray has been traced. In either case a minimum of three rays are required to evaluate the divergence of a ray tube.

V. THE COMPUTER PROGRAM

The approximations described above are included in the computer program as subroutines. The major portion of the program, however, consists of input storage, processing and logic subroutines. The program processes the input information in order to obtain characteristic parameters required by the subroutines. These include incident field

strength and polarization from the antenna, plume geometry, propagation constants in the plume and receiver position with respect to the transmitting antennas. From these parameters, the program determines the region of the required radiation field and then carries out the necessary computations and prints out the results.

The basic function of the computer program is to evaluate the radiation fields of four types of rays when called for. These rays are; the direct ray from the antenna, the reflected ray from the plume boundary, the diffracted ray around the plume boundary and the transmitted ray through the plume. The field is divided into two regions, the shadow region and the illuminated region. In the former, the present program evaluates the transmitted and diffracted rays. In the latter, it evaluates the direct and reflected rays. For some angles there may only be a direct ray while for angles close to the shadow boundary the diffraction calculation may be required in addition to or in place of the reflected plus the direct ray calculation.

Figure 3 illustrates the control for performing these calculations in the proper sequence. The field strengths for all rays radiated from the antenna are determined from antenna pattern tapes. The angle θ_m, is the minimum angle of incidence below which only the direct ray computations are made. This angle of incidence is determined by the tangent ray to the vehicle surface and the angle normal to the plume boundary. The reflected ray calculation is performed if the angle of incidence satisfies $\theta_m < \theta_i < 85°$. The direct and reflected

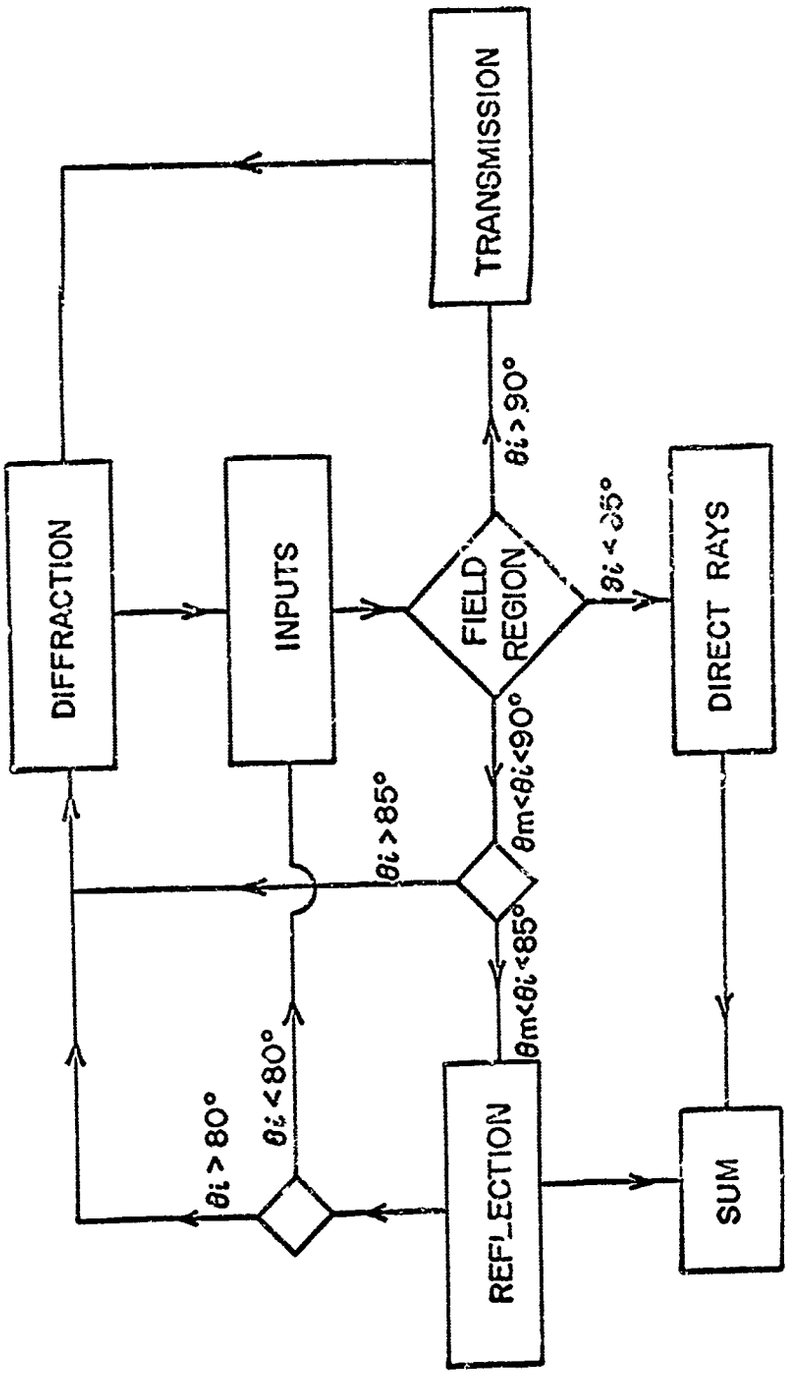


FIGURE 3 - Integrated Computer Program Flow Chart

rays are summed vectorially. The reflected ray is the product of the antenna pattern factor in the direction of the incident ray, the reflection coefficient, and the divergence factor. The reflection coefficient subroutine contains the Fresnel formulas and the Epstein profile reflection formulas. Both computations use the "Plume Program" to obtain the basic parameters. The "Plume Program" also has a procedure for fitting the "exponents" of the Epstein profile to the actual electron density and collision frequency for both polarizations. An alternate procedure for computing the reflection coefficient is to consider direct integration of the "Ricatti Equations". However, it is necessary to weight the computer time for the two approaches. The divergence factor is a real number less than unity and requires geometric information from the "Geometry Subroutine" for its calculation. The latter computes the angle of incidence, point of incidence, distance from the antenna, and parameters describing the curvature of the boundary.

If the angle of incidence is too close to 90°, the geometrical optics procedure of adding the direct and reflected rays is no longer valid and a diffraction calculation must be used. For an overlapping region of $80° < \theta_i < 85°$, both calculations are performed and compared (not added). The diffraction calculations are carried for $\theta_i > 80°$. This subroutine requires parameters from the antenna pattern tapes, the radius of curvature and the deflection angle from the "geometry subroutine," and a surface impedance from the "Plume Subroutine".

For the shadow region, $\theta_i > 90°$, the transmission calculations are performed followed by the diffraction calculations. The total field is the sum of the two contributions. The transmission program contains a number of subroutines that are called for under various circumstances. The most important subroutine is the "Ray Tracing - WKB" program (our nomenclature for the geometric optics approximation). If the losses are not excessive this program computes the exit direction and field strength of a given incident ray. All parts of the Vector Transport Equation are not included in this program as yet but will be in the near future. Because of possible discontinuities and high loss regions within the plume, provisions are made to compute complex propagation vectors and complex field vectors across a discontinuity or a layered medium. The point of incidence and exit of the rays across such a layer is assumed to be displaced by the thickness of the layer only. Multi-layered transmission line equations are used for the transmission and reflection coefficients.

A two dimensional linear interpolation program is included to relate the reflection or transmission direction vectors to the incident vector. This is employed to limit the computation to the required look direction. Provisions are also made for sequencing the calculations in any desired order. A control card may be introduced to require various parts of the computation to be executed independent of the others. There is also a plotting routine which can be used to plot the constant electron density and collision frequency contours, the internal shock line, and the plume boundary lines. These additional

functional subroutines add to the flexibility of the program and also aid in checking the computations during the development and alterations of the program.

At the date of the writing of this paper, the entire program has been assembled but a complete run on a large booster plume has not been successful. The difficulties have been minor and routine. A fully operative program should be available in the very near future. All subroutines have operated successfully and several computations on reflection, diffraction and transmission have been obtained separately. We have chosen to present, in the next section, the results of a computation which considers the case of a high altitude exhaust which has no sharp boundaries. The results show a definite necessity for computing exhaust flame effects in the manner suggested here.

VI. A SAMPLE COMPUTATION AND CONCLUSIONS

The results of a sample computation, obtained by the computer program, are illustrated in Fig. 4. The chosen example is a vehicle exhaust at high altitude which has a very diffuse and expanded plume. The Mach lines in the figure also represent constant electron density and collision frequency contours. Ray paths are shown in the figure which were computed for a telemeter frequency of 250 Mc.

Because of the low density of the plasma, it was anticipated that reflections would be negligible and that the deviation of the ray

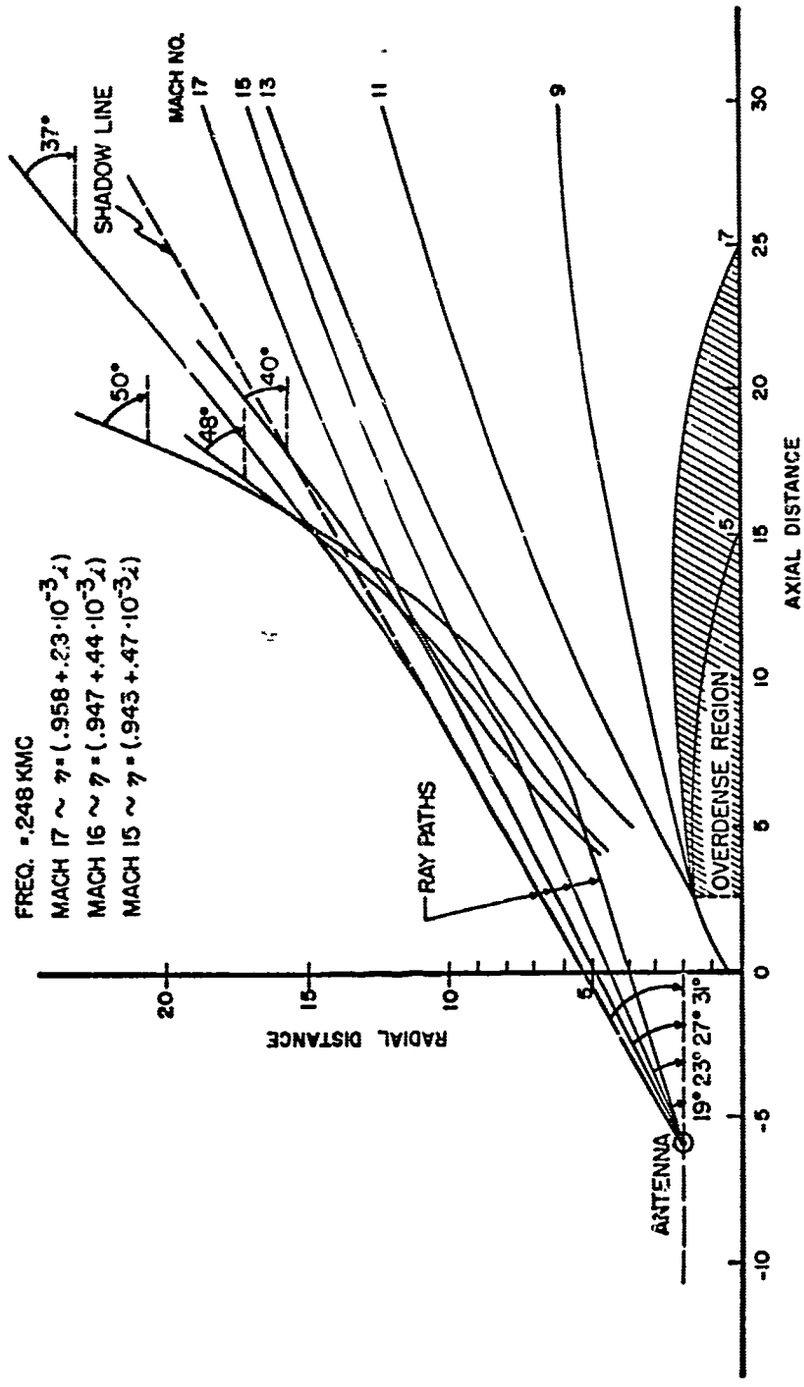


FIGURE 4 - An Example of an Exhaust Plume and Computed Ray Paths

paths from the line of sight path would be slight. As is shown in the figure, the rays deviate radically from the line of sight path in the region close to 30° from the vehicle axis. These results indicate an effective shadow region for look angles less than 30°. This is an entirely unexpected result since overdense regions of the plasma occur within a two degree cone about the vehicle axis.

The example shown is a simple plume case in which reflection and diffraction effects are not significant. The computer program, however, has the capacity to process the case of more complex plumes which have mixing and internal shock regions. At this time, plume description data storage and processing subroutines of the program are limited to axisymmetric plumes. Consideration is being given to multi-nozzle plumes which may not have such symmetry. The present program is also capable of processing, by a slight modification, an interstaging plume configuration which can be approximated by a single plume having its own symmetry axis at an arbitrary angle to the vehicle axis.

The above described analytical approach and the associated computer program to carry out the computational routines, represent a practical approach to the analysis of wave propagation through inhomogeneous plasma. There are further necessary improvements to the analysis to account fully for electromagnetic phenomena associated with a communication link in an exhaust flame environment. There is a definite need to develop analytical methods to account for the nonlinearities of the plasma at power levels below breakdown. A laminar description of the plasma is not sufficient either. Irregularities in the exhaust

must also be accounted for, at best, by a statistical description of the medium. Examination of some flight data has shown periodic modulations of signals in the lower audio range which show correlation with the rocket chamber resonances. These imply periodic variations in the density of the plasma and the boundary of the plume. Preliminary analyses have been conducted to account for the internal irregularities of the plasma and its boundaries. These analyses assume the laminar medium results as the average field and the scattered field from the irregularities of the medium as secondary fields. It is anticipated that an analysis of the nonlinear effects of the plasma will also require the results of the laminar and linear medium analysis as a first order result for an iterative solution. Therefore, the results reported here represent a significant step to a full analysis of electromagnetic interaction of radio frequency waves with the exhaust gases of a launch vehicle.

REFERENCES

1. Tai Tsun Wu, "Theory of the Dipole Antenna and the Two Wire Transmission Line", Journal of Math. and Physics, Vol. 2, July-August, 1961.

2. D. W. Gooch, C. W. Harrison, R. W. P. King and T. T. Wu, "Impedance and Admittance of Long Antennas in Air and in Dissipative Media," Technical Report No. 353, Cruft Laboratory, Harvard University, Cambridge, Mass., January, 1962.

3. Chin-Lin, Chen, "The Small Loop Antenna in a Dissipative Medium," Technical Report No. 369, Cruft Laboratory, Harvard University, Cambridge, Mass., May 1962.

4. Janis Galejs, "Admittance of Annular Slot Antennas Radiating into a Plasma Layer," Research Report No. 356, Applied Research Labs., Sylvania Electric Systems, Waltham, Mass., July, 1963.

5. Janis Galejs, "Slot Impedance for Plasma Layers," Research Report No. 347, Applied Research Labs., Sylvania Electric Systems, Waltham, Mass. July, 1963.

6. Janis Galejs, "Admittance of a Waveguide Radiating into a Stratified Plasma," Research Report No. 347, "Applied Research Labs., Sylvania Electric Systems, Waltham, Mass., June, 1963.

7. S. C. Brown, "High Frequency Gas Discharge Breakdown," Proc. IRE, Dec. 1961, pp. 1493-1501.

8. J. B. Chown, "Study of Plasma Induced Breakdown at Low Pressure," Final Report SRI Project No. 3309, Stanford Research Inst., Menlo Park, Calif. July 1961.

9. W. J. Linder, "The Power Handling Capacity of a Microwave Antenna in a Hypersonic Environment," Document D2-90111, The Boeing Company, Seattle, Wash. August, 1962.

10. Kun-Mu Chen, "Interaction of a High Intensity EM Field with a Low Density Plasma," IRE Transactions on Antennas and Propagation, Vol. AP-10, Jan. 1962.

11. E. B. Barrett, R. F. Whitmer, S. J. Tetenbaum, "Nonlinear Interaction of an Electromagnetic Wave with a Plasma Layer in the Presence of a Static Magnetic Field, III Theory of Mixing, IV Experimental Results," Physical Review, Vol. 135, July 1964, pp. A374-389.

12. G. Hasserjian, "Electromagnetic Interaction with the Exhaust Plume," Document D5-11418-2, The Boeing Company, Seattle, Wash., August, 1964.

13. V. A. Fock, "Fresnel Reflection and Diffraction Laws," Uspekhi Fizicheskikh Nauk, Vol. 36, 1948, pp. 308-319. English Translation, "Diffraction, Refraction and Reflection of Radio Waves, Thirteen papers by Fock, V. A." edited by N. A. Logan, ASTIA Document AD117276, June 1957.

14. K G. Budden, Radio Waves in the Ionosphere, Cambridge University Press, Cambridge, England, 1961.

15. L. M. Brekhovskikh, Waves in Layered Media, Academic Press, New York, 1960.

16. V. L. Ginzburg, Propagation of Electromagnetic Waves in Plasma, Gordon and Breach, New York, New York, 1961.

17. G. Hasserjian, "A Plasma Layer Having an Epstein Variation for Both the Electron Density and Collision Frequency," Technical Note 2-5463-50-105, June 15, 1965, The Boeing Company, Seattle, Wash.

18. N. A. Logan and K. S. Yee, "A Mathematical Model for Diffraction by Convex Surfaces," Electromagnetic Waves, edited by R. E. Langer, The University of Wisconsin Press, Madison, Wisconsin, 1962, pp. 139-180.

19. N. A. Logan, "General Research in Diffraction Theory," Vol. I and II, Technical Report LMSD-288087 and 288088, Lockheed Aircraft Corp., Sunnyvale, California, Dec. 1959.

20. M. Kline, "Electromagnetic Theory and Geometrical Optics," Electromagnetic Waves, edited by R. E. Langer, The University of Wisconsin Press, Madison, Wisconsin, 1962, pp. 3-31.

21. G. Hascerjian, "The Geometrical Optics Approximation of Electromagnetic Fields in Inhomogeneous Media," Technical Note No. 2-5463-50-119, The Boeing Company, Seattle, Washington, August 5, 1965.

VI. INFORMATION LOSS CAUSED BY REENTRY PLASMA DISPERSION*

J.F. Fox and T.R. McPherron

Space and Missile Engineering Division
McDonnell Aircraft Corporation
St. Louis, Missouri

ABSTRACT

Modulation degradation of C-Band signals passing through a simulted reentry plasma is discussed. A rectangular (1" x 4" x 20") glow discharge was used to simulate a reentry plasma. Peak plasma frequency was variable from 2.0 to 6.4 gcps and the collision frequency remained constant at 9.4×10^8 second^{-1} resulting in a maximum attenuation of 15 db to a 4 gcps signal. Experiments with single pulses, time variant plasmas, and a PCM-AM (non-coherent) system showed no detectable frequency sensitive phase shift or attenuation for typical telemetry bandwidths. A nanosecond pulse experiment showed slight pulse widening. Based on these experimental results, the performance of several PCM systems is compared to serve as an aid in the selection of an optimum modulation technique.

INTRODUCTION

Aerospace vehicles may experience partial or total loss of radio communication during their atmospheric reentry phase. In addition to signal attenuation, fluctuations in the plasma parameters caused by flow field turbulence and ablation products may cause phase and amplitude changes in the signal resulting in degradation of the modulation or intelligence on the signal.

*This work was partially supported by USAF, WPAFB, Contract AF33(615)-1198.

Loss in information could also be caused by the dispersiveness of the plasma producing nonlinear phase and amplitude response. Dispersive effects have been studied and experimentally observed for waveguide propagation.[1,2] The analysis has been extended to the plasma case and distortion predicted for certain plasmas under very restrictive conditions.[3] These conditions require the signal frequency to be greater than twice the plasma frequency and the plasma to be collisionless so that only phase shift effects are produced. It has been hypothesized that degradation effects increase as the plasma frequency is approached since the propagation characteristics become more nonlinear. Since this region is difficult to treat analytically, an experimental program was initiated to determine the intelligence degradation of SHF telemetry signals caused by plasma dispersiveness. The intent was to determine possible optimum modulation techniques to provide maximum information transfer during marginal reentry transmission conditions. Upon completion of these tests the study was extended to include a wide bandwidth signal employing a nanosecond pulse.

PLASMA/ELECTROMAGNETIC ENVIRONMENT

The realistic reentry plasma/electromagnetic environment was investigated to determine the required simulation characteristics. For propagation tests it is necessary to simulate the plasma electron concentration and collision frequency magnitudes and gradients as well as the plasma thickness. Current literature was reviewed to determine representative ranges for these parameters.

The flow field around a typical body is characterized by four flow regions - stagnation, intermediate, aft body, and wake. The regions of interest are the intermediate and aft body since these contain the usual propagation paths as determined by antenna location on the vehicle. The majority of analyses have been performed for cylindrical bodies with spherical nose caps. The electron concentration has an exponential decay across the flow field while the collision frequency remains approximately constant. For blunt bodies such as Gemini and Apollo, the peak electron concentration is greater and varies from zero to a peak and returns to zero as the flow field is traversed. The collision frequency remains relatively constant. For slender or pointed vehicles, the peak electron concentration is lower and the plasma is very thin. The electron concentration has an exponential decay while the collision frequency remains relatively constant.

Summarizing the reentry plasma characteristics obtained in the regions of interest for electromagnetic wave propagation, it is obvious the plasmas are highly dependent on the shape of the reentry vehicle. The peak electron concentrations in the regions of interest range from 10^9 to 10^{13} electrons per cubic centimeter for corresponding collision frequencies of approximately 10^9 per second. The profile of collision frequency remains relatively constant. However, the electron concentration may remain relatively constant as in the case of the blunt vehicle but may vary over several orders of magnitude in an inch or less for the case of the sharp cone, and, to a lesser extent, for the cylindrical body. Plasma thicknesses range from many inches for blunt bodies to fractions of an inch for slender bodies.

REENTRY COMMUNICATION SYSTEMS

As a part of determining the realistic plasma-electromagnetic environment of reentry vehicles, present telemetry systems were reviewed. The primary objectives were to determine types of modulation, power level, carrier frequency, and pulse width or bandwidth of typical systems. A summary of these characteristics is given in Table I. In addition to the systems shown in the table, use is made of FM/FM for continuous data telemetry and AM for voice communication. This brief review indicated a wide range of communication system parameters. Frequencies are predominantly VHF, but S and X band are utilized. Of particular interest for this study was the range of pulse widths which are typically of the order of several microseconds. System types vary, but it is to be noted that PCM is used for Gemini and Apollo.

PLASMA GENERATOR

The interaction of an electromagnetic signal and plasma is controlled by the magnitude and distribution of the plasma electron concentration and collision frequency, the ratio of the electromagnetic frequency to these plasma parameters, and the plasma dimensions. Data presented previously showed the wide range of magnitudes and gradients of electron concentration possible depending upon the vehicle configuration. However, collision frequency was primarily dependent upon altitude and exhibited only small gradients. Therefore, to provide simulation of reentry plasma parameters, the plasma should contain gradients of electron concentration with a near constant collision frequency. The plasma thickness should be in the range of one to several inches. Absolute magnitudes of electron

concentration and collision frequency depend on the electromagnetic frequency chosen in order that these magnitudes be capable of producing large attenuations of the signal at the chosen frequency.

Plasma generation can be accomplished in both static and dynamic facilities. Dynamic plasmas are generated in shock tubes, shock tunnels, plasma jets, and free flight ranges. These facilities give good simulation of such features as aerodynamic flow about a scaled model, gas and electron temperature, electron concentration, and collision frequency. Some undesirable features characteristic of such generators are short test time, small plasma volume, inability to reproduce the plasma, and generally high operating cost.

Static plasmas are produced by impressed radio frequency fields, low pressure flames, arc discharges, and glow discharges. These plasma sources do not give realistic flows and are also marginal in free electron concentration and the collision frequencies obtainable. The most desirable features are continuous operation, ease of instrumentation, good reproducibility, and low operating cost. Large plasma volumes can be shaped so that plasmas of varying thicknesses are possible. A more detailed account of the applicability of various plasma generators for telemetry studies is given in Ref. 4. Review of the advantages and disadvantages of these facilities indicates the glow discharge to be well suited for telemetry studies.

Glow discharge is a complex phenomenon with several distinct regions of various characteristics. The region utilized for electromagnetic interaction studies is the positive column which is characterized by equal

numbers of electrons and positive ions, thermal nonequilibrium, low voltage gradients, and ambipolar diffusion as the dominant loss mechanism. The principal problem is obtaining a high electron concentration in a large volume so that a reasonable approximation to a plasma slab is obtained. McDonnell has developed the rectangular glow discharge facility shown in Fig. 1 which fulfills the requirements for electromagnetic interaction studies.[4] The rectangular geometry was chosen to best utilize the plasma volume obtained and to approximate a plasma slab for correlation to theoretical analyses.

The main part of the glow discharge facility is fabricated from 3/4 inch silicone laminate. One wall is pyrex plate glass (12 x 24 x 1 1/4 inches) to permit visual observation of the plasma. The instrumentation ports are pyrex ground glass sockets which allow diagnostic equipment to be easily moved to different test regions. The system can be evacuated to a minimum pressure of less than 1 μ Hg without using a cold trap or diffusion pump.

The primary design feature of the facility is its double or hollow cathode permitting passage of large currents without arcing. The cathode consists of two plane parallel stainless steel plates (5 x 11 inches). Current density at the cathode is increased as much as a thousand times that observed in a glow discharge using a single cathode. Sustaining voltage is considerably lower than that observed in a normal glow discharge.[5,6,7] The anode (7/8 x 11 inches) is also planar and made of stainless steel. The electrodes are well polished to prevent "hot spots" and subsequent arcing.

The discharge is maintained by a power supply capable of 3000 volts at 20 amperes. A 125 ohm, 625 watt, wire wound, ballast resistor is used for circuit stability.

The plasma instrumentation is shown in Table 2. The discharge characteristics measured were voltage drop, current, and gas pressure.

For this study program, the primary requirement of the glow discharge was to produce plasma frequencies greater than the transmitting frequency so that significant attenuation resulted. The discharge performance was optimized as a function of test gas, pressure, and allowable current flow before arcing. Argon at a pressure of 100 μ Hg yielded a uniform plasma slab at currents up to five amperes. However, the electron concentration resulted in an inadequate attenuation of 25% for an S-band signal. Helium at 600 μ Hg produced higher attenuations, but the discharge constricted into two distinct columns which tended to become unstable. Plexiglass inserts were placed in the facility to reduce the vertical plasma dimension from 12 to 4 inches. With this configuration helium at 600 μ Hg with currents up to 5 amperes proved satisfactory and was used throughout the tests. The volt-ampere characteristics showed the discharge to be operating in the normal glow region with a voltage drop of 440 volts for currents up to 5 amperes.

The facility plasma characteristics are summarized in Table 3. Electron concentration is a linear function of current from 0.3 to 5 amperes. The remaining parameters are independent of current. A complete description of the plasma and discharge parameters and the instrumentation techniques is given Ref. 8.

COMMUNICATION EQUIPMENT

The communication equipment was designed to be compatible with the plasma facility and to meet the objective of investigating basic phenomena of signal degradation caused by a reentry plasma medium. Simulation parameters desired were:

(a) Pulses transmitted by amplitude and frequency modulation,
(b) Power levels of the order of a few watts to milliwatts,
(c) Transmission frequency in the proper range to produce high levels of attenuation for a wide range of ω with respect to ω_p to obtain parametric data,
(d) SHF carrier frequency for a realistic relationship between wavelength and plasma thickness and small antenna size compared to the plasma dimensions, and
(e) Monitoring of the signal time function and frequency spectrum to determine frequency sensitive phase shift and attenuation.

The communication system block diagram fulfilling these requirements for telemetry signals is shown in Fig. 2. The transmission channel was matched to minimize reflections by adjusting the facility wall thickness to a multiple of one-half wavelength.

The block diagram for the nanosecond pulse experiment is shown in Fig. 3, and Fig. 1 is a photograph of the experimental configuration. The technique to generate the nanosecond pulse was developed for low power applications.[9]

EXPERIMENTAL RESULTS

The three basic phases of experimentation with telemetry signals were degradation studies with static plasmas, time-variant plasmas, and PCM-AM (non-coherent) system performance tests. Primary emphasis was placed on static tests with detailed examination of time function and frequency spectrum data to determine frequency sensitive channel characteristics.

A carrier frequency of 4 gcps was selected as giving acceptable performance with respect to attenuation and antenna size. The maximum attenuation at this frequency was 15 db. The ranges of the modulation function parameters were based upon present practical communication requirements as well as the practicality of laboratory instrumentation. It was desirable to investigate a group of signals with wide variation of frequency spectral spacing. Such signals reveal nonlinear effects of the medium as well as the basic effects of the medium on the Fourier components. A practical signal which satisfies these requirements results from square pulse modulation. Both amplitude and frequency modulation were investigated. The pulse widths examined varied from 5 to 1000 μs while pulse repetition rate varied from 500 to 50,000 cps. The transmitted power levels were on the order of milliwatts. Plasma characteristics were varied over the range from $.5\omega \leq \omega_p \leq 1.6\omega$ for a $\nu/\omega = 0.37$. Most of these tests were performed with the antennas operating in the near field.

A sample of the data is shown in Fig. 4. Frequency spectrum and time function data are presented for both a plasma and no plasma case. Gains were adjusted in the plasma case (f_p = 5.3 gcps) to accentuate any nonlinear effects thus not showing the true channel attenuation which was 9 db. The case shown is an amplitude modulated pulse of width 5 μs with a repetition rate 50,000 pps. The marker on the frequency spectrum photograph indicates the frequency spread between the center of the photograph and marker which for this case was 1.2 mcps. The upper trace on the time function photograph is the transmitted pulse while the lower trace on the photograph is the received signal.

The data presented is characteristic of the entire modulation degradation experiment for telemetry signals. No distortion of the modulation function was observed during the entire test sequence for static plasma conditions. These results indicate that typical telemetry signals would not exhibit detectable nonlinear phase shift or attenuation during reentry.

Experiments with time variant plasmas were performed to investigate the effects of changes in the plasma characteristics on a propagating microwave signal. Such changes in reentry plasmas may occur because of ablation materials or flow field turbulence. A lack of data on the frequency and magnitude of such variations led to an investigation over a wide range of frequencies from very low to tens of kilocycles.

Variations in the glow discharge tube current were accomplished by an electronically controlled, current shunting amplifier connected in parallel with glow discharge tube. Since the circuit power supply was a constant current source, variations in the amplifier current produced equal variation in discharge current and electron concentration.

Samples of the data are presented in Fig. 5. The upper trace in each photograph shows the discharge tube current with modulation function. The modulation functions shown are a 5 kcps sine wave and a square pulse of 250 microseconds duration and repetition rate of 1 kcps. Only part of the sine function is shown since the amplifier was biased in cut-off for static operation. The variation in the tube current is from 0.4 to 2.0 amperes in each case. The lower traces show the received microwave signal, a 1 kcps square wave. In both cases the amplitude of the received signal follows the modulation function. The high frequency fluctuations

appearing on the received signal during pulse modulation were apparently caused by an instability induced in the plasma as a result of the sharp change in current level. These fluctuations were definitely not caused by striations in the plasma.

Similar data was taken for sine wave modulation functions varying from 100 cps to 50 kcps and for random noise of 20 kcps bandwidth. The results show the production of possible error effects by changing the signal energy, the apparent position of the leading edge of the pulse, or the apparent pulse width.

Experiments with a PCM-AM (non-coherent) system were also performed to verify the conclusions formulated on the basis of the single pulse studies. The criterion of performance was probability of error. Tests were performed with both variable and fixed decision thresholds. Reduction in the system signal to noise ratio caused by insertion of the plasma was shown to be equivalent to increasing channel attenuation.

Since these experiments had shown no detectable distortion, a test was performed to determine the effect on a very wide bandwidth signal. This test was limited to pulse modulation. Photographs of the received signal for various plasma conditions are shown in Fig. 6. The upper set of photographs was taken with gains held constant to accentuate attenuation characteristics, while the lower set was taken with gains adjusted to accentuate distortion effects. The sweep rate for all photographs was 1 nanosecond per centimeter. Attenuation characteristics were as expected with approximately 12 db loss for a discharge current of 4 amperes.

Distortion effects were not as pronounced as anticipated. The wide variation in attenuation and phase shift characteristics over the signal bandwidth led to an expectation of appreciable degradation. The observed distortion was limited to a slight increase in pulse width (10-20%) at discharge currents producing plasma frequencies near the transmitting frequency. However, due to synchronizing difficulties it could not be conclusively determined that the pulse broadening was caused by plasma effects.

A computer program is presently being written to theoretically predict degradation for arbitrary pulse shapes and plasma conditions. Theoretical verification of these results will then be attempted.

PREDICTION OF SYSTEM PERFORMANCE

The experimental results of the preceding section were used to predict the effects of such plasma conditions on various pulse code modulation (PCM) systems. Digital systems were selected for study because of their extensive usage and superior performance to analog systems. Pulse code modulation was analyzed because of its use in present vehicles and its theoretically superior information capability. Since no dispersion was detected for signals of telemetry bandwidths, only the attenuating effects of the plasma were considered.

The performance of PCM systems in the presence of Gaussian noise has been well documented (e.g., Ref. 10). Probability of binary digit error is the usual criterion of performance. Amplitude, frequency, and phase modulation were investigated. Both coherent and non-coherent detection, that is, the presence or absence of a reference carrier at the receiver, were analyzed.

In a PCM-AM (non-coherent) system the information is carried on the amplitude of the signal. A signal of the form E cos ωt is transmitted for a "one" and nothing is transmitted for a "zero" No reference carrier is available at the receiver and the signal plus noise is processed by a matched filter with the decision as to a "one" or "zero" made by a threshold device. The conditional probabilities of error are:

$$P(1/0) = \int_{U_D}^{\infty} \frac{U}{\sigma^2} \exp(-U^2/2\sigma^2)\, dU,$$

$$P(0/1) = \int_{o}^{U_D} \frac{U}{\sigma^2} \exp\left(-\frac{U^2 + 4E}{2\sigma^2}\right) I_o\left(\frac{2U\sqrt{E}}{\sigma^2}\right) dU.$$

The terms in the above equations are defined in the glossary at the end of the paper. Assuming an equal probability that a one or zero is transmitted, the total probability of error is:

$$P_e = \frac{1}{2} P(1/0) + \frac{1}{2} P(0/1),$$

If the maximum signal energy is $2\sqrt{E}$, the optimum threshold is approximately $\sqrt{E}$. Probability of error as a function of signal to noise ratio is shown in Fig. 7 for optimum threshold conditions, that is, the threshold adjusts itself to always remain one-half the signal level of a "one". The effects of an attenuating plasma on system probability of error may be considered in the following manner. If optimum threshold conditions are maintained, the probability of error for a plasma condition can be read directly from the curve of Fig. 7 by adjusting the signal level with the appropriate plasma transmission coefficient, assuming only the signal changes and not the noise. If the decision threshold is fixed,

that is, independent of signal level, the new probability of error must be calculated from:

$$P_e = \frac{1}{2} \exp\left(-\frac{E}{\sigma^2}\right) + \frac{1}{2}\left\{1 - Q\left[2K\sqrt{\frac{E}{\sigma^2}}, \sqrt{\frac{E}{\sigma^2}}\right]\right\},$$

where K is the voltage transmission coefficient of the plasma and the Q-function is defined and tabulated in Ref. 11.

The PCM-AM (coherent) system differs from the non-coherent system in that a local phase and frequency reference is maintained at the receiver and mixed with the incoming signal. The conditional probabilities of error are:

$$P(1/0) = \frac{1}{\sigma\sqrt{2\pi}} \int_{U_D}^{\infty} \exp\left(-\frac{U^2}{2\sigma^2}\right) dU,$$

$$P(0/1) = \frac{1}{\sigma\sqrt{2\pi}} \int_{-\infty}^{U_D} \exp\left(-\frac{(U - 2\sqrt{E})^2}{2\sigma^2}\right) dU.$$

The optimum threshold for this system is $\sqrt{E}$. Its relative performance is shown in Fig. 7. In a plasma environment, the performance for variable threshold conditions can be determined in the same manner as for the non-coherent case. Under fixed threshold conditions the probability of error is given by:

$$P_e = \frac{1}{2}\left\{1 + \operatorname{erf}\left[\frac{1-2K}{\sqrt{2}}\sqrt{\frac{E}{\sigma^2}}\right]\right\} + \frac{1}{2}\left[1 - \operatorname{erf}\sqrt{\frac{E}{2\sigma^2}}\right].$$

The PCM-FM (2 channel) system transmits a signal E cos $\omega_1 t$ for a "one" and E cos $\omega_2 t$ for a "zero". Detection is accomplished by a two channel receiver having each channel tuned to one of the carrier frequencies. If the outputs are arranged such that the output from the "zero" channel is subtracted from the output of the "one" channel, the optimum threshold level is "zero". The decision in favor of a "one" or "zero" depends

upon whether the difference between the two channels is positive or negative. The inherent advantage of this system is that the decision threshold is independent of signal level. The conditional probabilities of error are:

$$P(0/1) = \int_0^\infty \frac{U_1}{\sigma^2} \exp\left(-\frac{U_1^2 + 2E}{2\sigma^2}\right) I_o\left(\frac{U_1\sqrt{2E}}{\sigma^2}\right) \int_{U_1}^\infty \frac{U_o}{\sigma^2} \exp\left(-\frac{U_o^2}{2\sigma^2}\right) dU_o\, dU_1 ,$$

$$P(1/0) = \int_0^\infty \frac{U_o}{\sigma^2} \exp\left(-\frac{U_o^2 + 2E}{2\sigma^2}\right) I_o\left(\frac{U_o\sqrt{2E}}{\sigma^2}\right) \int_{U_o}^\infty \frac{U_1}{\sigma^2} \exp\left(-\frac{U_1^2}{2\sigma^2}\right) dU_1\, dU_o .$$

Since threshold is independent of signal level, the probability of error for a plasma case may be read directly from the curve in Fig. 7.

In the PCM-PM (differentially coherent) system the information is carried on the phase of the carrier with the "one" and "zero" functions 180° out of phase. The differentially coherent system detects the phase shift between successive binary digits. The probability of making an error when the previously transmitted digit is used as a reference is:

$$P_e = \frac{1}{2} \exp\left(-\frac{E}{\sigma^2}\right) .$$

Since threshold is independent of signal level, system performance in a plasma environment can be determined by referring to the proper curve in Fig. 7.

The relative performance of these systems under the conditions producible in the glow discharge facility is shown in Fig. 8. A 10 db signal to noise ratio was assumed for no plasma conditions. These results illustrate the superior performance given by phase modulation and the greatly improved performance possible by maintaining optimum threshold for AM systems.

If pulse distortion effects were considered, the total probability of error would depend on the particular binary sequence under consideration. The same analysis would be followed with effects of pulse overlap or channel memory added to the signal levels in the conditional probability integrals with no change in the threshold level or limits of integration.

CONCLUSIONS

The results of this program show no detectable degradation of the modulation function for signals of typical telemetry bandwidths propagating through a plasma representative of reentry conditions. A slight increase in pulse width was observed in the nanosecond pulse experiment. Theoretical verification of this result will be attempted. The glow discharge facility performed very satisfactorily and additional tests relative to the plasma transmission problem are planned.

GLOSSARY

$P(1/0)$	probability that a "one" is detected when a "zero" is transmitted
$P(0/1)$	probability that a "zero" is detected when a "one" is transmitted
U	signal voltage
U_D	decision threshold
σ^2	noise power
E	average signal energy
I_o	modified Bessel function
P_ϵ	probability of error
K	voltage transmission coefficient of plasma

REFERENCES

1. R.S. Elliot, "Pulse Waveform Degradation Due to Dispersion in Waveguide", IRE Transactions on Microwave Theory and Techniques, October 1957, pages 254-257.

2. A.C. Beck, "Microwave Testing with Millimicrosecond Pulses", IRE Transactions, Vol. MTT-2, April 1954, pages 93-100.

3. R. Marquedant, C.M. Knop and H. Hodara, "Performance of Digital Signals Through Plasmas", IEEE Transactions on Communication Systems, March 1964, pages 74-86.

4. McDonnell Aircraft Corporation Report A220, "Analysis of Plasma Generators", January 1964

5. M.A. Townsend, "A Hollow Cathode Glow Discharge with Negative Resistance", Applied Sci. Res. Sec. B., 5, 75, 1955.

6. A.D. White, "New Hollow Cathode Discharge", J. Appl. Phys. 30, 711, 1959.

7. E.O. Johnson and L. Malter, "A Floating Double Probe for Measurements in a Gas Discharge", Phys. Rev. 80, #1, 58, October 1950.

8. T.R. McPherron, P.J. Anderson, A.F. Ruehl, "Study and Experimentation on Modulation Degradation by Ionized Flow Fields", Technical Report AFAL-TR-65-10, February 1965.

9. J.K. Pulfer and B.G. Whitford, "A Simple Method of Generating Nanosecond Pulses at X-Band", Proc. of the IRE, May 1961.

10. S. Reiger, "Error Probabilities of Binary Data Transmission Systems in the Presence of Random Noise", Convention Record of the IRE, Part 8, 1953.

11. J.I. Marcum, "Table of Q-Functions", Rand Report No. RM-339, January 1, 1950.

ACKNOWLEDGEMENTS

The writers wish to particularly acknowledge the work of P.J. Anderson in the plasma instrumentation and diagnostics, A.F. Ruehl for communication system analysis and experimental design, and G.L. Elder for assistance in performing the experimental work. Other members of the Advanced Electronic Techniques Department at McDonnell also assisted in the program. C.A. Hines of the Air Force Avionics Laboratory monitored the portions of the work performed under contract.

TABLE I. REENTRY TELEMETRY SYSTEMS

Vehicle	Frequency mcps	Transmitted Power Watts	System	Data Rate $msec^{-1}$	Pulse Width Microsecond
ASSET	238	6	PDM/FM or PDM/FM/FM	0.90	100-700
ASSET	9320	100	PPM/AM	0.90	0.75
Gemini (Real Time)	230	2	PCM/FM	51.2	19.5
Gemini (Delay Time)	259	2	PCM/FM	112.6	8.9
Apollo	225-260 2280	10 5	PCM/FM	51.2	19.5

TABLE II. PLASMA INSTRUMENTATION

Instrument	Parameter Derived
Double Langmuir Probe	Electron Concentration Plasma Repeatability Electron Concentration Gradients
	Electron Temperature Electron - Neutral Collision Frequency
K_a Band Microwave Interferometer	Electron Concentration
Photoelectric Cell	Plasma Repeatability
Thermocouple	Gas Temperature

TABLE III. PLASMA CHARACTERISTICS

Characteristic	Range
Electron Concentration	2×10^{10} to 5.5×10^{11} cm^{-3}
Plasma Frequency	2.0 to 6.5 gcps
Electron-Neutral Collision Frequency	$(9.4 \pm .3) \times 10^{8}$ $sec.^{-1}$
Size	1 x 4 x 20 inches
Electron Distribution	Approximately sine in 1 and 4 inch axes. Uniform in 20 inch axis.
Collision Frequency Distribution	Approximately constant
Gas Temperature	Approximately 350°K
Electron Temperature	42,000 ± 5000°K
Electron Concentration Reliability	Better than 85%

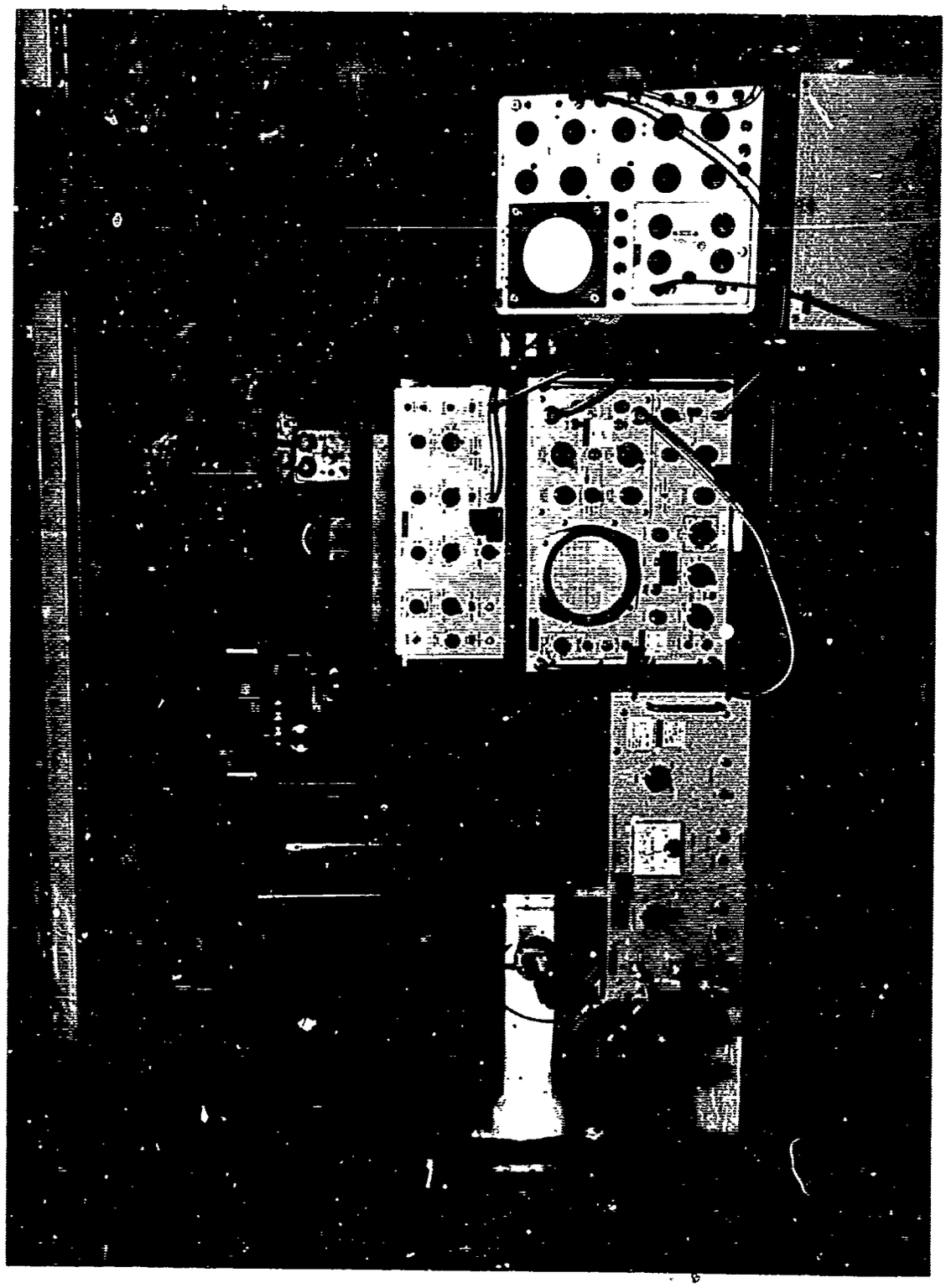


FIGURE 1 NANOSECOND PULSE EXPERIMENTAL CONFIGURATION

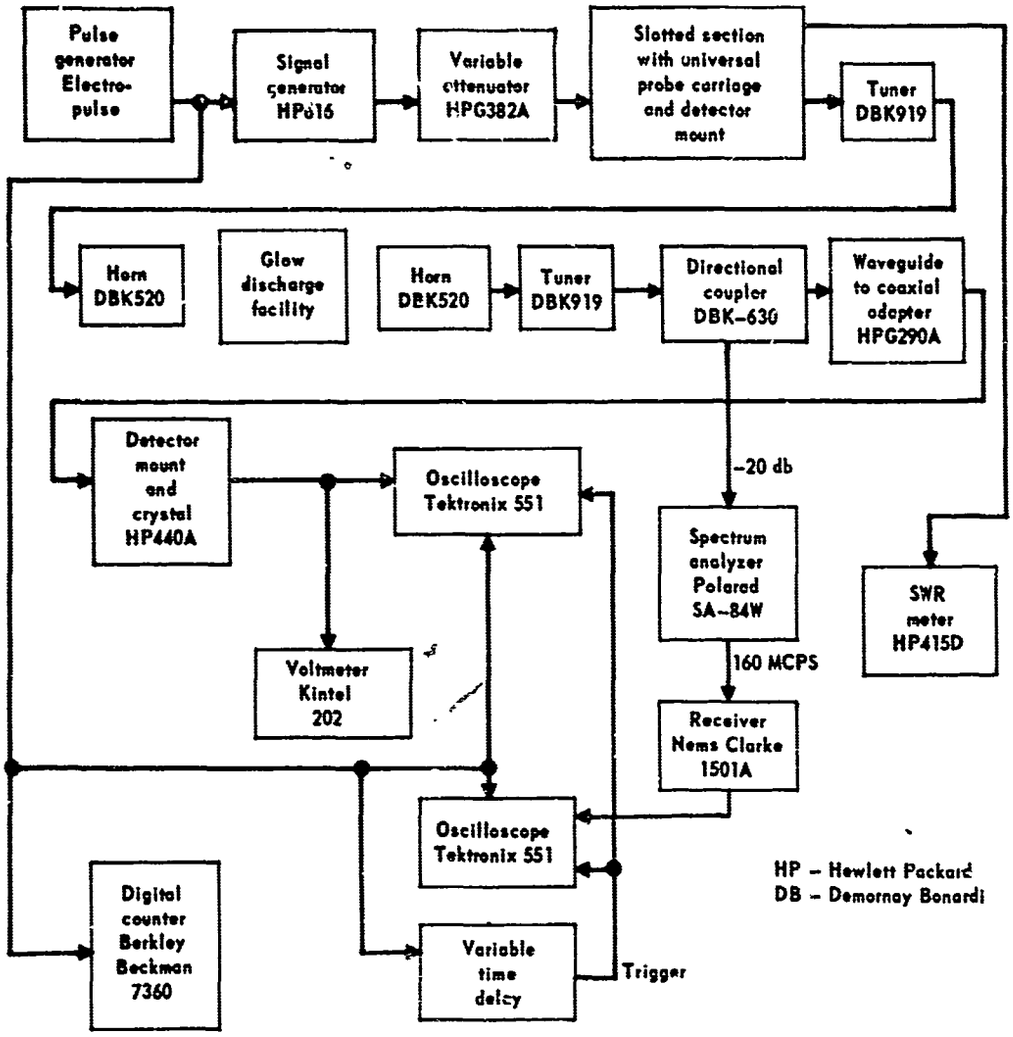


Figure 2. Block diagram for telemetry tests.

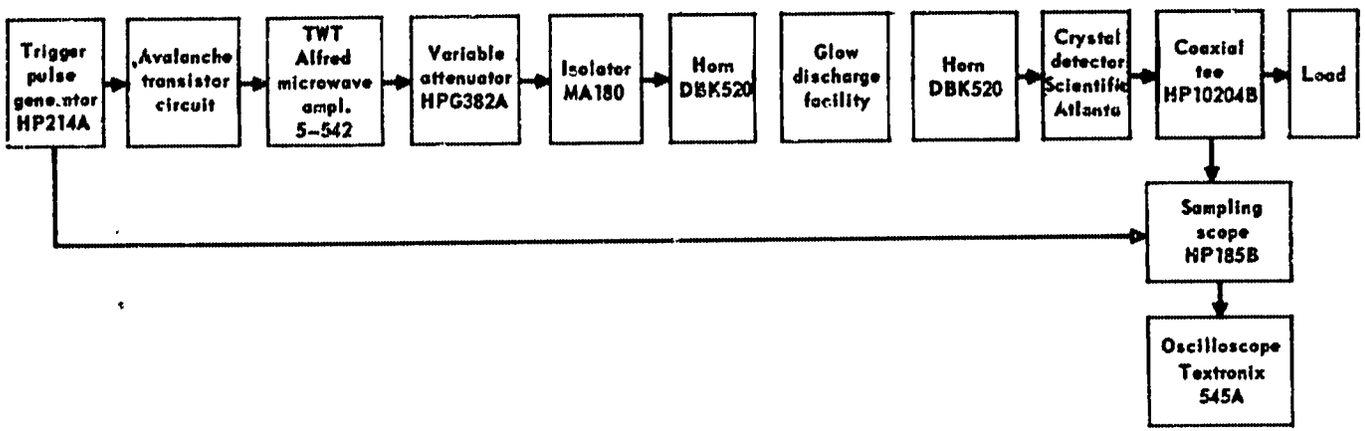


Figure 3. Block diagram for nanosecond experiment.

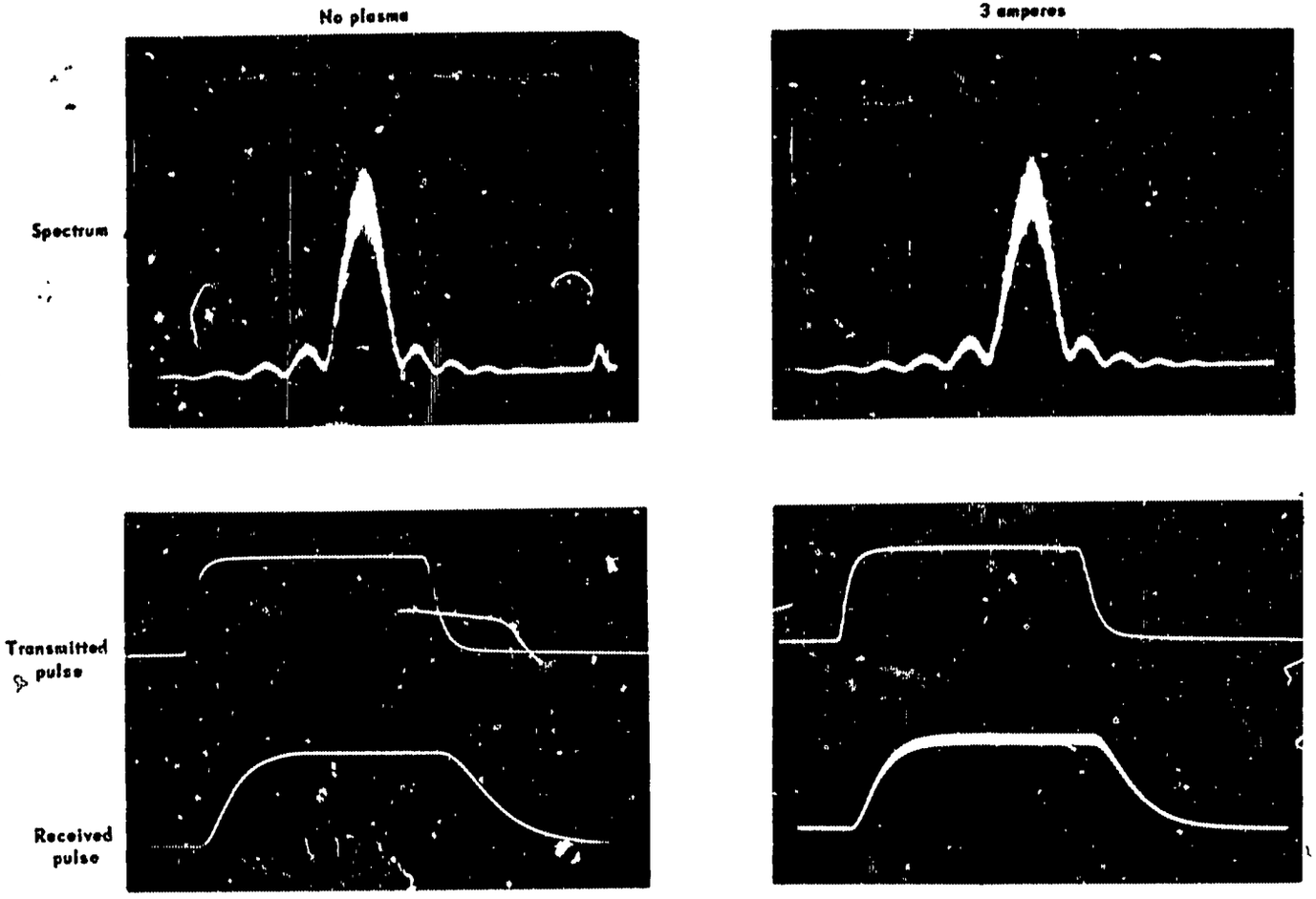
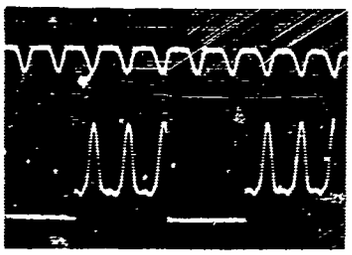


Figure 4. Experimental spectrum and time function photographs.

Discharge current

Frequency – 5 kcps

Received microwave signal



Discharge current

Pulse width – 250 μs

Received microwave signal



Figure 5. Time varian. plasma experimental photographs.

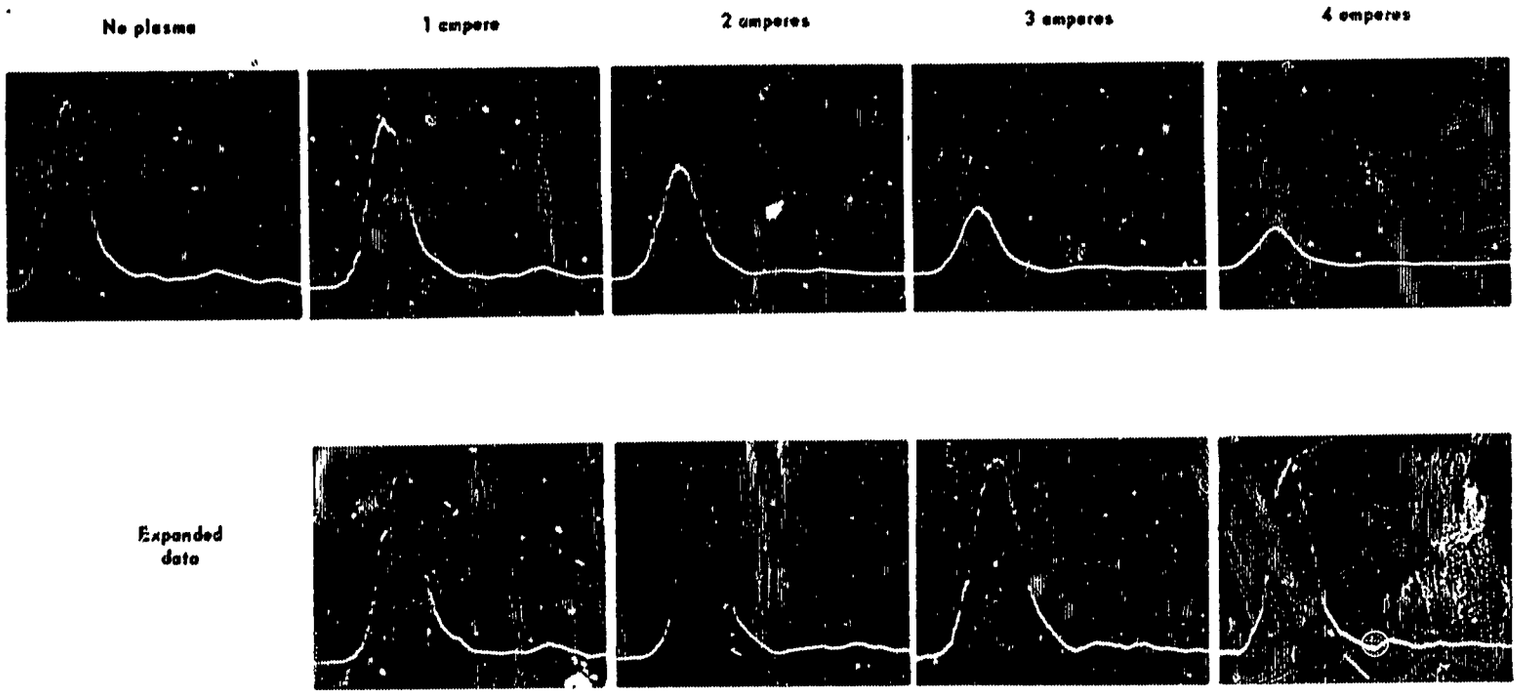


Figure 6. Nanosecond time function photographs.

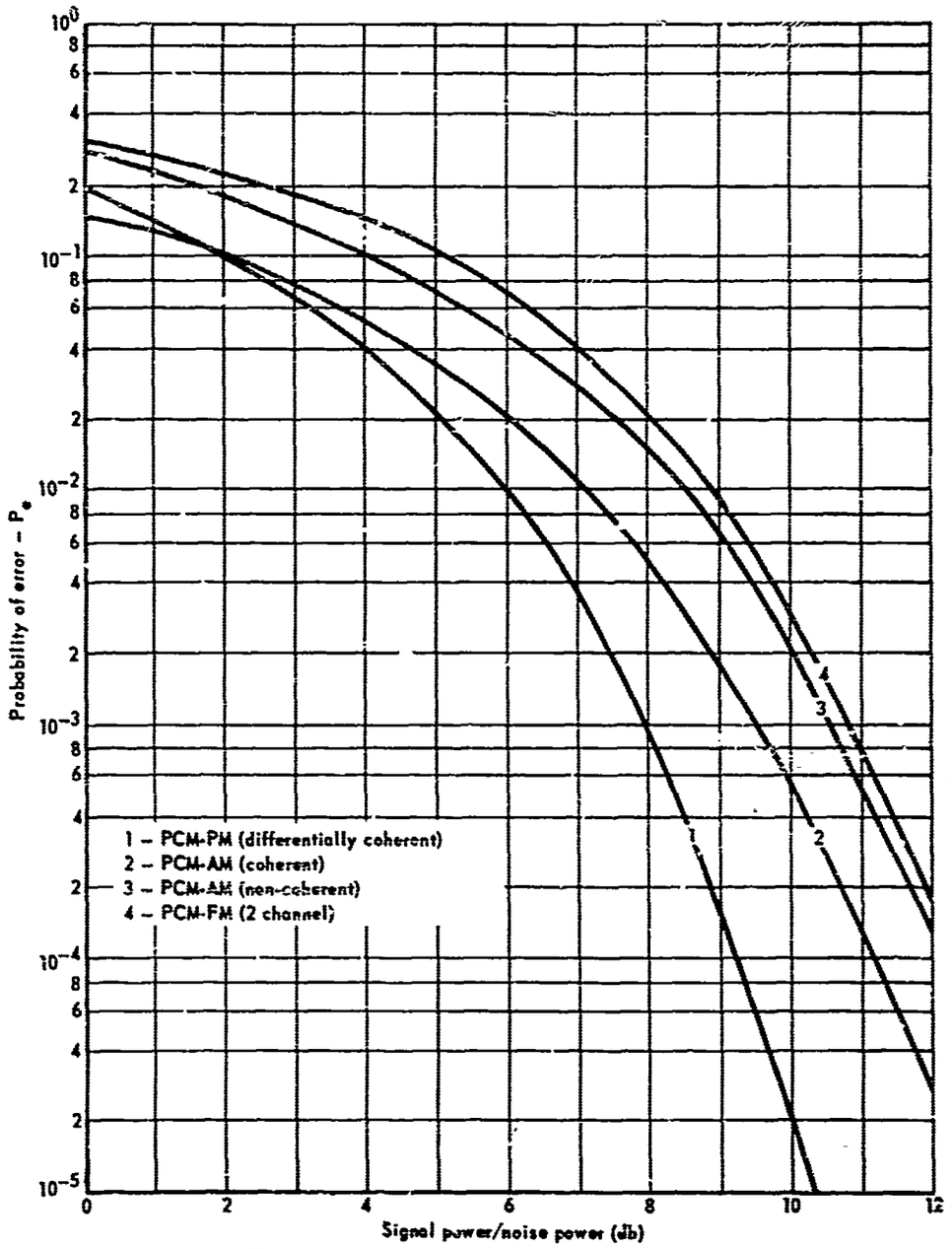


Figure 7. Performance characteristics of selected PCM systems.

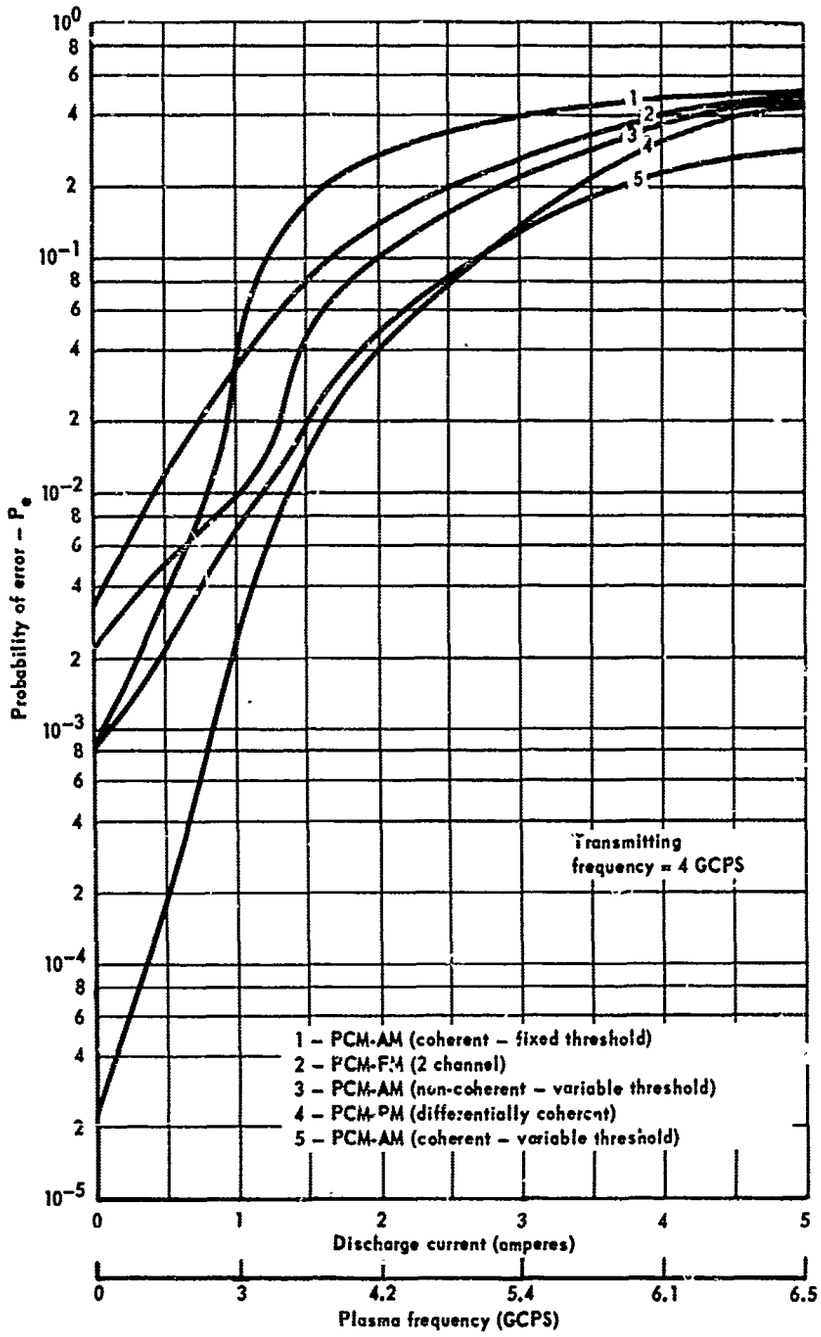


Figure 8. Predicted performance characteristics for 10 db initial signal to noise ratio.

VII. DEVELOPMENT OF A PROBE FOR THE MEASUREMENT OF POINT VALUES OF ELECTRON DENSITIES IN SUPERSONIC FLOWS*

By Manlio Abele
Hector Medecki

General Applied Science Laboratories, Inc.
Merrick and Stewart Avenues
Westbury, L. I., New York

ABSTRACT

dynamic requirements which dictate the geometry of the cavity and the mode of interaction of the electromagnetic field with the flow itself.

The cavity probe techniques appear to be particularly convenient for measuring a broad range of several orders of magnitude in electron densities even when the plasma frequencies are larger than the operating frequency of the cavity. Consequently, standard microwave techniques with S and X band cavities can be used to measure electron densities up to values which would require the use of millimeter wavelengths with conventional interferometeric techniques.

* Sponsored by the National Aeronautics and Space Administration, Goddard Space Flight Center, Contracts NAS5-3929 and NAS5-9881.

A high sensitivity is obtained with this probe technique due to the large values of Q which can be achieved with a resonant cavity.

Specific cavity arrangements are presented, ranging from configurations where the ionized gas is allowed to pass through the cavity to configurations where the probe measures the electron density of the flow passing over its external surface.

Probes operating over the range 10^{8} to 10^{14} e/cm^{3} have been developed and used in measurements conducted in a shock tube facility. The results are presented and compare with the data obtained with other techniques.

ACKNOWLEDGEMENTS

The authors wish to acknowledge the contribution of Mr. Robert Byrne for the continuous discussion during the development of the probes and to Mr. David Attwood for his participation in the experimental part.

I. INTRODUCTION

The classical microwave interferometer is one of the most widely used techniques in the study of the plasma properties of an ionized gas. The measurement is conducted without perturbing the medium and a relatively simple correlation is established between phase and attenuation measurements and the electron density and electron collision frequency of the plasma. The basic disadvantages of these techniques are the upper limit of plasma frequency which must be lower than the frequency of the electromagnetic wave and the long path of propagation in the medium which is required when the plasma frequency becomes very small. Thus only the average properties of the plasma can be determined on the basis of such measurements.

In the microwave range resonant structures can be built with large values of Q and dimensions of the same order of the wavelength of the electromagnetic field. Due to the high precision by which resonant frequency and Q can be measured resonant cavities have been widely used in the study of electric properties of materials. The high Q and the relatively small dimensions suggest the possibility of using cavities in the measurement of the electric properties of an ionized gas. In actual flight conditions and large simulation facilities the flow dimensions are usually large compared to the dimensions of resonant microwave structures in the centimeter wavelength range. Consequently quasi local values of the electric properties of the flow can be measured with these techniques. The main disadvantage is that

the resonant microwave structure probe has to be located in the flow. The ensuring flow perturbation depends on the aerodynamic and fluid dynamic properties of the flow itself. Thus, to minimize the flow perturbation, the probe shape has to be designed according to the aerodynamic and fluid dynamic properties at the point where the probe is located. In a flow situation an extremely wide range of electron densities is found. To obtain the desired sensitivity in the measurement of the plasma properties different approaches to the mode of interaction between the electromagnetic field and the plasma must be taken according to whether the plasma frequency is small or large compared to the operating frequency of the probe. It is the purpose of this paper to discuss the basic properties of the interaction mechanism between the field of a resonant structure and the plasma, which lead to the selection of the mode of operation. Furthermore some of the fluid dynamic and plasma dynamic effects arising in the perturbation of the flow induced by the probe will be discussed.

II. CLOSED CAVITY PROBES

The design of a specific microwave resonant structure as a plasma probe depends on the aerodynamic and plasma dynamic properties of the ionized medium where the probe is located. The range of resonant frequencies and the mode of operation of the probe depend on the electric properties of the ionized gas. The region of interaction between gas and electromagnetic field of the probe has to be minimized in order to obtain a quasi local measurement of the plasma properties. Furthermore the shape of the probe has to be selected in such a way as to minimize the perturbation of the physical properties of the ionized gas.

Before discussing the restrictions imposed by the aerodynamic and plasma dynamic conditions on the probe design it is convenient to analyze some basic types of microwave resonant probes in the presence of a plasma which is characterized by a plasma frequency ω_p and an electron collision frequency ν. In this analysis a cold plasma model is assumed, i.e. plasma oscillations are not taken into accunt. With a sufficiently small intensity of the electromagnetic field and a large operating frequency of the probe, a linear theory can be used in the analysis of the electron motion in the plasma. With no DC magnetic field, the plasma is characterized by a complex index of refraction x which is given by

$$x^2 = 1 - \frac{\omega_p^2}{\omega^2} \frac{1}{1 - i\frac{\nu}{\omega}} \qquad (1)$$

The plasma frequency is related to the electron density n through the equation

$$\omega_p^2 = \frac{ne^2}{m\epsilon_o} \qquad (2)$$

where e, m are the electric charge and mass of an electron and ϵ_o is the dielectric constant of a vacuum.

In general the calculation of the resonant frequency and Q factor of a microwave structure in the presence of the plasma is extremely involved and numerical methods of solution have to be used in each particular case. Nevertheless, some of the basic properties of the interaction of the plasma with the electromagnetic field can be readily discussed on the basis of a perturbation theory.

Consider first a microwave structure, without plasma, which resonates at a frequency ω_o for a given mode of operation and let $\overline{E}$ be the local value of the electric field. In the presence of the plasma, if a small perturbation of the field is induced by the plasma itself, the resonant frequency is shifted to a new value $\omega_o + \Delta\omega$. $\Delta\omega$ is given by:

$$\frac{\Delta\omega}{\omega_o} \sim \frac{i}{2\omega_o \epsilon_o} \frac{\int_V \vec{E}\cdot\vec{j}\, dV}{\int_V E^2 dV} \qquad (3)$$

where V is the volume occupied by the electromagnetic field. In Eq. (3) $\vec{j}$ is the electric current density induced in the plasma. By virtue of Eq. (1)

$$\vec{j} = - i\epsilon_o \omega_p^2 \frac{\vec{E}}{\omega_o - i\nu} \qquad (4)$$

One observes that the $\frac{\Delta \omega}{\omega_o}$ is a complex quantity. The real part of Eq. (3) gives the actual shift of the resonant frequency and the imaginary part is related to the change in the Q factor through the equation:

$$\Delta \left(\frac{1}{Q}\right) = 2 \text{ Im} \left(\frac{\Delta \omega}{\omega_o}\right) \qquad (5)$$

It is important to observe that the perturbation equation (3) does not necessarily imply that the plasma is underdense ($\omega_p < \omega_o$). In the case $\omega_p \ll \omega_o$ the plasma may occupy a large fraction of the total volume V without introducing a large perturbation on the field distribution. On the other hand if $\omega_p > \omega_o$ the perturbation in the field distribution is still small provided that the penetration depth of the electromagnetic field inside the plasma is sufficiently large compared to the dimensions of the plasma region. Specifically the plasma region must have everywhere a linear dimension which is small compared to the quantity c/ω_p where c is the speed of light in a vacuum.

In the particular case of a uniform plasma Eq. (3) yields

$$\text{Re} \left(\frac{\Delta \omega}{\omega_o}\right) \sim K \frac{\omega_p^2}{\omega_o^2 + \nu^2} \; ; \; \Delta \left(\frac{1}{Q}\right) \sim 2 K \frac{\nu}{\omega_o} \frac{\omega_p^2}{\omega_o^2 + \nu_2^2} \qquad (6)$$

where

$$K = \frac{1}{2} \frac{\int_{V_p} E^2 dv}{\int_{V} E^2 dv} \qquad (7)$$

V_p is the volume of the plasma region. K may be defined as the sensitivity of the probe. Eq. (7) shows that K increases as the plasma volume V_p increases. By means of Eq. (6) and a measurement of both the resonant frequency shift and the Q of the probe one obtains the value of ω_p and ν.

From Eq. (6) one observes that as long as the collision frequency ν is small compared to ω_o, the shift of the resonant frequency is dominant compared to the decrease of the Q of the probe. Therefore, due to the large values of Q which can be attained in a microwave structure this scheme of interaction is particularly appealing for the measurement in an underdense plasma over a wide range of electron densities.

With this scheme of interaction two basic types of resonant structures can be used. One corresponds to a cavity where the plasma is inserted in the cavity itself through a suitable channel. The second scheme is an open nonradiating structure located inside the plasma.

A typical example of the first type of probe is a cylindrical cavity of radius r_2 and height z_o as shown in Fig. 1a.

Assume a uniform plasma confined in the cylindrical region of radius r_1 coaxial with the cavity. In the fundamental TM_{010} mode of operation the resonant frequency and the change in the

Q of the cavity are given by the complex values of ω which satisfy the equation:

$$\varkappa \frac{J_1\left(\frac{\omega}{c}\varkappa r_1\right)}{J_0\left(\frac{\omega}{c}\varkappa r_1\right)} = \frac{J_1\left(\frac{\omega}{c} r_1\right) Y_0\left(\frac{\omega}{c} r_2\right) - J_0\left(\frac{\omega}{c} r_2\right) Y_1\left(\frac{\omega}{c} r_1\right)}{J_0\left(\frac{\omega}{c} r_1\right) Y_0\left(\frac{\omega}{c} r_2\right) - J_0\left(\frac{\omega}{c} r_2\right) Y_0\left(\frac{\omega}{c} r_1\right)} \tag{8}$$

where J, Y are the Bessel functions of the first and second kind respectively.

In the absence of the plasma ($\varkappa = 1$), the solution of Eq. (8) is $\omega_o \, c \, \frac{x_o}{r}$ where x_o is the first root of $J_o(x) = 0$.

Assume now that the plasma is strongly underdense ($\omega_p \ll \omega_o$). In this case Eq. (8) reduces to

$$\frac{\Delta\omega}{\omega_o} \sim \frac{1}{2 J_1^2(x_o)} \left(\frac{r_1}{r_2}\right)^2 \left[J_o^2\left(x_o \frac{r_1}{r_2}\right) + J_1^2\left(x_o \frac{r_1}{r_2}\right)\right] \frac{\omega_p^2}{\omega_o^2} \frac{1}{1 - i\frac{\nu}{\omega}} \tag{9}$$

As mentioned before a small perturbation of the field inside the cavity is found even in an overdense plasma provided that

$$\frac{\omega_o}{c} |K| \, r_1 \ll 1 \tag{10}$$

This implies that the radius r_1 of the plasma cylinder is small compared to r_2 and to the penetration depth of the electromagnetic field in the plasma.

When Eq. (10) is satisfied one has

$$\frac{\Delta\omega}{\omega_o} \sim \frac{1}{2\,J_1^2(x_o)} \left(\frac{r_1}{r_2}\right)^2 \frac{\omega_p^2}{\omega_o^2} \frac{1}{1 - i\,\frac{\nu}{\omega_o}} \qquad (11)$$

From Eqs. (9) and (11) one observes that this $\frac{\Delta\omega}{\omega_o}$ depends on the product $\omega_p^2\, r_1^2$. Thus the probe measures the electron density per unit length in the axial direction. It is worthwhile pointing out that in the TM_{010} mode the plasma is found in the region of maximum value of the electric field, which is the ideal condition for a strong effect of the plasma on the resonant frequency.

This technique is used to measure electron density in a variety of experimental conditions (Refs. 1 and 23).

An application to a supersonic flow condition is shown in Fig. 1b. The region A corresponds to the cylindrical transmission cavity and the plasma is injected coaxially with the cavity through the channel B. One observes that the channel has a slightly divergent conical shape dictated by aerodynamic considerations which will be discussed in the next section. Also the external conical shape is determined by the flow field Mach number. In the central part of the cavity the confinement of the plasma is obtained with a thin dielectric window.

This probe departs somewhat from the scheme of Fig. 1a because the cavity is not a completely closed structure. When the plasma is underdense the electromagnetic field penetrates into the channel B and some radiation losses occur at both ends

of the channel itself. As a consequence the Q of the cavity depends also on the radiation losses. Neglecting the effect due to the small conical divergence, one may consider the channel as a section of a cylindrical waveguide which is excited in a TM_{01} mode. Therefore it is necessary to keep the radius of the channel small compared to the value which corresponds to the cutoff condition. Furthermore the length of both sections of the channel has to be long in order to minimize the intensity of the field at both ends of the probe. Unfortunately, a long narrow inlet channel is undesirable from the flow point of view, and a compromise solution has to be adopted which optimizes the electromagnetic requirement without introducing a serious perturbation of the flow.

It is worthwhile pointing out that the energy loss through the channel may become quite large when the plasma becomes overdense. In this case the above-mentioned cutoff considerations does not apply any more. A surface wave is excited at the boundary of the plasma and a large energy absorption is found in the plasma even if no substantial radiation occurs at both ends of the probe.

As a consequence the use of this probe is limited to underdense plasmas. The operating frequency of the cavity shown in Fig. 1b is in the X band. Thus the maximum values of electron densities which can be measured with this probe is in the $10^{11} \div 10^{12}$ e/cm^3 range.

The total range of electron densities n that can be measured depends on the particular technique which is used in

measuring the output signal of the cavity. With an amplitude measurement the minimum measurable frequency shift can be defined as half the bandwidth of the resonance curve of the cavity in the absence of the plasma. Thus if Q_o is the value of the Q of the cavity without plasma, one has:

$$n_{min} \sim \frac{n_c}{2\ K\ Q_o} \tag{12}$$

where n_c is the critical value of electron density which corresponds to $\omega_p = \omega_o$, and K is defined in Eq. (7). In order to maximize the value of K it is necessary to increase the volume of the interaction region, i.e. the radius of the channel. For the probe of Fig. 1b $Q_o \sim 2\text{x}10^3$; $K \sim .27$. Thus $n_{min} \sim 10^8$ e/cm^3.

This electron density range can be extended to lower values with a differential technique in the measurement of amplitude and phase of the cavity output.

Due to the complicated geometry of the probe an exact calculation of the shift of the resonant frequency as a function of the plasma properties cannot be performed. Thus, calibration techniques must be used. In the range of low electron densities the probe may be calibrated by introducing in the channel a dielectric medium of dielectric constant close to unity.

In this case the frequency shift has the opposite sign compared to the shift produced by a strongly underdense plasma.

Nevertheless on the basis of the perturbation theory the results can be extrapolated to the equivalent dielectric constant of a plasma, according to Eq. (1).

Another technique which appears to be particularly suitable for extremely low electron densities is the use of an electron beam inserted in the cavity where the electron density is known on the basis of accelerating beam and current. A very good coincidence between the results obtained with these two techniques has been found. In the higher range of electron densities the calibration is performed with an independent measurement of the plasma properties with a microwave interferometric techniques in the flow where the probe is located. Fig. 2 shows the characteristics of the probe of Fig. 1b. The solid line corresponds to the shift of the resonant frequency obtained on the basis of the above-mentioned calibration techniques used is the low electron density range. The experimental points correspond to the calibration performed with the interferometric technique.

The same cavity of Fig. 1a could be used in the range $\omega_p \geq \omega$ without the severe decrease in the Q which appear in the TM mode by exciting the cavity in the TE_{011} mode. In this case no current is flowing from the plasma to the cavity walls. For the TE_{011} mode the resonant frequency and the change in Q of the cavity are given by the complex solutions of

$$\frac{1}{k_1}\frac{J_1(k_1 r_1)}{J_0(k_1 r_1)} = \frac{1}{k_2}\frac{J_1(k_2 r_1)\,Y_1(k_2 r_2) - J_1(k_2 r_2)\,Y_1(k_2 r_1)}{J_0(k_2 r_1)\,Y_1(k_2 r_2) - J_1(k_2 r_2)\,Y_0(k_2 r_1)} \qquad (13)$$

where

$$k_1^2 = \frac{\omega^2}{c^2} K^2 - \frac{\pi^2}{z_o^2} \; ; \; k_2^2 = \frac{\omega^2}{c^2} - \frac{\pi^2}{z_o^2} \tag{14}$$

In the particular case of $r_1 << r_2$ and ω_p of the same order of ω or smaller, Eq. (13) reduces to:

$$\frac{\Delta \omega}{\omega_o} = \frac{1}{16} \frac{x_1^2}{J_o^2(x_1)} \left(\frac{r_1}{r_2}\right)^4 \frac{\omega_p^2}{\omega_o^2} \frac{1}{1 - i \frac{\nu}{\omega_o}} \tag{15}$$

where x_1 is the first root of

$$J_1(x) = 0 \tag{16}$$

and ω_o is the resonant frequency of the cavity without plasma. It is of interest to compare Eq. (15) with Eq. (11). One observes that due to the high power of the coefficient r_1/r_2 in Eq. (15), the TE_{011} mode provides a smaller sensitivity in the range of extremely small electron densities.

If one assumes now in Eq. (13) that the plasma is strongly overdense ($\omega_p >> \omega$) and $\nu/\omega << \omega_p^2/\omega^2$, the absolute value of $k_1 r_1$ may become large compared to unity. In this case in Eq. (13):

$$\frac{1}{k_1} \frac{J_1(k_1 r_1)}{J_o(k_1 r_1)} \sim \frac{1}{\bar{k}_1} \tag{17}$$

where

$$\bar{k}_1 \sim \frac{\omega_p}{c} \left(1 - i \frac{\nu}{\omega}\right)^{-\frac{1}{2}} \tag{18}$$

Thus the cavity of Fig. 1a is equivalent to a coaxial cavity with an inner conductor of radius r_1 where the penetration depth δ of the electromagnetic field is

$$\delta = \mathrm{Re}\left(\frac{1}{\bar{k}}\right) \sim \frac{c}{\sqrt{2}\,\omega_p} \sqrt{\left|1 + \frac{\nu^2}{\omega^2}\right|^{\frac{1}{2}} + 1} \qquad (19)$$

The value of δ determines the shift in the resonant frequency of the cavity and the imaginary part of $\bar{k}^{-1}$ determines the change in Q of the cavity.

III. OPEN STRUCTURES PROBES

In the cylindrical cavity probe discussed in the previous section, when the plasma is strongly overdense and $\delta \ll r_1$, the effect of the plasma is to confine the electromagnetic field in the region $r_1 < r < r_2$. This property suggests the possibility of using an open cavity technique to measure high electron densities. The plasma itself closes the cavity when $\omega_p \gg \omega$ and the mode of operation of the cavity is selected in such a way as to minimize the energy losses due to radiation and the contact between plasma and external surface of the cavity.

Two possible schemes of open cylindrical cavities are shown in Fig. 3. Fig. 3a shows a probe where the cylindrical surface of the cavity is exposed to the ionized gas. For a strongly overdense plasma and a TE_{011} mode, the frequency shift and the change in Q of the cavity are given by

$$\mathrm{Re}\left(\frac{\Delta\omega}{\omega_o}\right) \sim -K_1 \frac{\omega_o}{\omega_p}\sqrt{\left(1+\frac{\nu^2}{\omega_o^2}\right)^{1/2}+1}\,; \quad \Delta\left(\frac{1}{Q}\right) \sim 2K_1 \frac{\omega_o}{\omega_p}\sqrt{\left(1+\frac{\nu^2}{\omega_o^2}\right)^{1/2}-1} \tag{20}$$

where

$$K_1 = \frac{x_1^2 c^3}{\sqrt{2}\,\omega_o^3 r_o^3} \tag{21}$$

and x_1 is the first root of Eq. (16) and

$$\omega_o = c\sqrt{\frac{\pi^2}{z_o^2}-\frac{x_1^2}{r_o^2}} \tag{22}$$

ω_o is the resonant frequency of a perfectly conducting cylindrical cavity of radius r_o and height z_o in the TE_{011} mode. An identical behavior is found in the scheme of Fig. 3b where one of the bases of the cylinder is exposed to the plasma on the plane surface of a wedge. Again for the TE_{011} mode and a strongly overdense plasma Re $(\Delta \omega/\omega_o)$ and $\Delta(1/Q)$ are given by Eqs. (20) where

$$K_1 = \frac{\pi^2 c^3}{\sqrt{2}\ \omega_o^3 z_o^3} \tag{23}$$

The schemes shown in Fig. 3 correspond to operation in a supersonic flow. Nevertheless it is apparent that the same open cavity technique can be used in a stagnation region or in a zero velocity region of the flow, where a probe of the type of Fig. 1 could not be used (Ref. 4).

The maximum value of electron density which can be measured with the probes of Fig. 3 depends on the Q of the cavity. Again if the minimum measurable frequency shift is defined as half the bandwidth of the resonant curve of the close cylindrical cavity. Thus if Q_o is the value of Q for the closed cavity the maximum value of electron density is

$$n_{max} \sim 8\ n_c\ K_1^2\ Q_o^2 \tag{24}$$

The order of magnitude of $8\ K_1^2$ is about unity in a practical case. Thus Eq. (24) shows that n_{max} may be higher than n_c by several orders of magnitude and with a relatively

low value of Q_o. The most serious limitation in the maximum value of n which can be measured arises from fluid dynamic and plasma dynamic boundary problems at the surface of the window of the cavity. As mentioned before the open cavity technique is limited to the range of overdense plasmas. This limitation is eliminated with a different technique which uses an element of nonradiating dielectric waveguide as a resonant structure (Ref. 5). Assume for instance a circular dielectric waveguide of radius r_o, length z_o, index of refraction x_d. A uniform plasma is assumed in the outside region $r > r_o$. The dispersion equation for the $TE_{o,m}$ mode is

$$\frac{1}{x}\frac{J_1(x)}{J_o(x)} = -\frac{1}{y}\frac{K_1(y)}{K_o(y)} \tag{25}$$

where

$$x = r_o\left(\frac{\omega^2}{c^2}x_d^2 - m^2\frac{\pi^2}{z_o^2}\right)^{\frac{1}{2}} ; \quad y = r_o\left(m^2\frac{\pi^2}{z_o^2} - \frac{\omega^2}{c^2}x^2\right)^{\frac{1}{2}} \tag{26}$$

K_1, K_o are the modified Bessel functions of the second kind. No radial propagation occurs as long as

$$m\frac{\pi}{z_o} > \frac{\omega}{c}x \tag{27}$$

If condition (27) is satisfied in the range of small electron densities ($\omega_p \ll \omega$) Eq. (25) yields

$$\mathrm{Re}\left(\frac{\Delta\omega}{\omega_o}\right) \sim K\,\frac{\omega_p^2}{\omega_o^2}\,\frac{1}{1+\frac{\nu^2}{\omega_o^2}}\;;\;\Delta\left(\frac{1}{Q}\right) \sim 2K\,\frac{\omega_p^2}{\omega_o^2}\,\frac{\nu}{\omega_o}\,\frac{1}{1+\frac{\nu^2}{\omega_o^2}} \qquad (28)$$

where

$$K = \frac{1}{1-\frac{y_o}{x_o}\,\frac{F'(x_o)}{G'(x_o)}\,x_d^2} \qquad (29)$$

ω_o is the resonant frequency without plasma ($x = 1$). x_o, y_o are the values of x, y for $\omega = \omega_o$ and

$$F'(x) = \frac{d}{dx}\left(\frac{1}{x}\,\frac{J_1(x)}{J_o(x)}\right)_{x_o}\;;\;G(y_o) = \frac{d}{dy}\left(\frac{1}{y}\,\frac{K_1(y)}{K_o(y)}\right)_{y_o} \qquad (30)$$

Thus the resonant frequency shift for $\omega_p \ll \omega$, is proportional to the electron density of the plasma, as in the previously discussed cavity probes. In the range of large electron densities

$$\frac{\omega_p^2}{\omega^2}\left|\frac{1}{1-i\,\frac{\nu}{\omega}}\right| \gg 1 \qquad (31)$$

Eq. (25) reduces to:

$$\begin{cases} \mathrm{Re}\,\dfrac{\Delta\omega}{\omega_1} = -K_2\,\dfrac{\omega_1}{\omega_p}\sqrt{\left(1+\dfrac{\nu^2}{\omega_1^2}\right)^{1/2}+1} \\ \\ \Delta\dfrac{1}{Q} = 2K_1\,\dfrac{\omega_1}{\omega_p}\sqrt{\left(1+\dfrac{\nu^2}{\omega_1^2}\right)^{1/2}-1} \end{cases} \tag{32}$$

where

$$K_1 = \frac{x_1^2\, c^3}{\sqrt{2}\,\omega_1^3\, r_o^3\, x^2} \tag{33}$$

x_1 is the first root of Eq. (16) and ω_1 is resonant frequency of the element of waveguide when the external surface ($r = r_o$) is assumed to be a perfect conductor. As expected in this higher range of ω_p the behavior of the waveguide is identical to the open cavity. In conclusion this type of probe may operate in a wide range of electron densities from the underdense to the overdense conditions. Fig. 4 shows an example of a dielectric probe which is designed to operate in a zero velocity region. The operating frequency is in the X band, and the length of the probe is three times the waveguide wavelength ($m = 6$). The dielectric medium used in this probe is boron nitride ($\kappa_d \sim 2$). Two metallic plates are mounted at both ends of the probe in order to reduce the radiation losses. In order to have a unique relation between resonant frequency and plasma properties, considerable care has to be taken in the

dielectric probe to have the required mode separation over the entire range of resonant frequencies. The mode separation has to be maintained over a value of $\Delta\omega$ as large as possible in the total range of electron densities. Furthermore the sensitivity of the probe must be as large as possible in the upper range of electron densities where the most severe reduction in the Q of the probe has to be expected. With the chosen dielectric medium these considerations have suggested the hollow structure of Fig. 4 for the dielectric waveguide which is supposed to measure a range of electron densities between 10^{10} e/cc and 10^{14} e/cc. In addition Fig. 4 shows an array of three metallic wires imbedded in the dielectric medium to eliminate the modes which do not belong to the TE_{01} type. The excitation of the TE_{01m} mode is performed through the coupling of the dielectric rods to the narrow side of a rectangular waveguide which operates in the fundamental TE_{01} mode as shown in Fig. 4. The measured Q of the probe without plasma is 2.10^3. Fig. 5 shows the theoretical characteristic of the hollow dielectric probe. In the range of low electron densities the calibration has been performed by surrounding the probe with a dielectric medium of dielectric constant close to unity with the same technique followed in the closed cavity probe. In the upper range of electron densities a calibration has been performed by measuring the resonant frequency of the probe with coaxial metallic cylinders of different radii which surround the dielectric medium. In this measurement the calibration is performed by identifying the gap between the inside surface of the metallic cylinder and the external surface of the dielectric waveguide

with the penetration depth δ defined in Eq. (19). In the middle range the probe calibration requires an independent measurement of the plasma properties. The probe of Fig. 4 has been designed for operation in a large environment situation where the probe dimensions are of no particular importance. If the dimensions of Fig. 4 are scaled down for an operating frequency in the 30 Gc range this technique appears to be particularly suitable for laboratory experiments in shock tube and shock tunnel facilities (Ref. 6).

IV. FLUID DYNAMIC AND PLASMA DYNAMIC CONSIDERATIONS

If a microwave probe is to operate in a supersonic flow two fluid mechanical effects have to be considered, those of compressibility and of viscosity. The gas should reach the region of interaction with the electromagnetic field of the probe without suffering a significant perturbation.

Consider first the probe of Fig. 1b where the flow is allowed to pass through the cylindrical cavity. The external shape of the cavity has to be designed in such a way to avoid a detached shock. Thus the angle at the leading edge depends upon the Mach number and the angle of attack at which the probe is supposed to operate. This specific probe is designed to operate at $M \geq 2.5$ and maximum angle of attack of 5°. Inside the channel viscous effects can lead to a perturbation of the flow situation which in turn affects the electron density distribution in the interaction region. Furthermore if proper allowance is not made for the boundary layer growth in the channel a choking of the passage may result leading to a normal shock standing ahead of the probe entrance. This effect can be minimized by compensating for the effective reduction in stream area. This can be accomplished by using a slightly divergent channel which is just enough to compensate the boundary layer growth. Since the boundary layer effect can only be assessed approximately it is necessary to perform aerodynamic measurements of the channel flow to assess the magnitude of the flow field perturbation. Measurements of the static pressure were performed at several stations along a channel with half the diameter of the final design shown in Fig. 1b at a free stream Mach number $M = 2.5$ and several Reynolds numbers. A

typical result is shown in Fig. 6. It is seen that the flow is not choked and that actually the internal passage is slightly overexpanded. This condition corresponds to the maximum Reynolds number at which the probe is supposed to operate. The minimum Reynolds number at which the probe may operate without serious fluid dynamic effects has not been determined due to the lack of adequate facilities.

The open cavity probes shown schematically in Fig. 3, which are designed for measurements of electron densities in supersonic flow conditions, are similarly affected by compressibility and viscosity. The configuration of Fig. 3a will produce a flow perturbation due to the shock formed at the apex of the cone. However, for many ionized flow fields of practical interest, preliminary calculations employing equilibrium thermodynamics have indicated that the perturbations caused by the shock for cones with semi-vertex angles less than 10° is less than a factor of 2 in electron density. Non-equilibrium chemistry considerations should lead to even lower values of the estimated perturbations in electron density. In addition to the perturbations caused by the shock, one must examine those caused by the boundary layer which is built up on the cone and its afterbody. Preliminary calculations of the boundary layer growth over a 10° semi-vertex angle cone, three inches long, have indicated that for conditions similar to those for which the internal cavity probe was developed, that portion of the boundary layer where the electron density differs significantly from that external to the boundary layer is on the order of 1/10 of the boundary layer thickness and extended about 4/10 mm above the surface of the cone. The configuration shown in Fig. 3b will

have negligible effects of shock perturbations of the electron density for flow conditions where viscous interaction effects are not large. The calculated boundary layer thicknesses will be larger than those for the cone differing roughly by a factor of $\sqrt{3}$ for the same length over which the boundary layer is allowed to grow.

In addition to the fluid dynamic perturbations induced by the probe, the electron density distribution in the interaction region may be affected by the plasma boundary conditions at the wall of the probe. In the range of electron densities of interest in a fluid dynamic problem, the Debye shielding distance is always extremely small compared to the dimensions of the interaction region, for both overdense and underdense plasma. The plasma sheath at the surface of the probe may become important only when the mode of operation of the probe involves an electric current flowing from the wall to the plasma, particularly in the case of an overdense plasma. For this reason the TE_o modes have been selected for both the open cavities and the dielectric probes. Also, it is worthwhile pointing out that the TE_o modes of operation avoid a possible coupling mechanism between the electromagnetic field and the plasma oscillations in the plasma sheath.

The most serious perturbation of the electron density distribution in the interaction region appears to be due to the diffusion of the charged particles, ions, and electrons, toward the wall of the probe. The walls act as a sink for the charged particles which recombine at the wall. Thus, the electron density at the surface of the probe becomes very small compared to the density in the unperturbed region. It is apparent that the

thickness of the layer close to the wall, where the electron density decay is important, must be small compared to the dimensions of the interaction region. Consider the flow of the ionized gas inside a cylinder of radius r_o as in the case of the closed cavity probe. Assume that temperature, density and flow velocity $\vec{u}$ are uniform. The diffusion equation for the electron density may be written in the form

$$\nabla^2 n - \frac{1}{D}\vec{u}\cdot\nabla n + \frac{K_d}{D}[1-f(n)] = 0 \qquad (34)$$

in a situation where the ionization processes are due to collision between neutral particles. K_d is a positive constant which depends upon the pressure and temperature of the gas. D is the ambipolar diffusion coefficient and f(n) depends upon the chemistry of the ionization reactions in the gas. Eq. (34) must be solved with the boundary conditions of a vanishing electron density at the wall of the channel ($r = r_o$), and an assigned distribution of n_e at the entrance of the channel. At larger distances from the channel entrance the radial distribution of electron density depends primarily on the parameter

$$\alpha = r_o\sqrt{\frac{K_d}{Dn_e}} \qquad (35)$$

where n_e is the equilibrium electron density at the assigned values of pressure and temperature of the channel flow. If $\alpha \gg 1$ the electron density is almost uniform across the channel

and the electron density decay is confined to a small layer close to the wall of thickness.

$$\lambda_D \sim \frac{r_o}{\alpha} \tag{36}$$

λ_D may be defined as the electron diffusion length. If $\alpha \ll 1$ a strongly nonuniform distribution has to be expected and the electron density at the axis of the cylinder (r = 0) becomes small compared to n_e. The equilibrium electron density n_e may be assumed to be equal to the free stream value. Thus a probe operating in a situation where $\alpha \ll 1$ would measure an electron density which is much smaller than n_e. Figure 7 shows the asymptotic radial distribution for the particular case of a reaction between atomic oxygen and nitrogen where

$$f(n) = \frac{n^2}{n_e^2} ; \quad K_d = k_d n_o n_N \tag{37}$$

k_d is the ionization reaction rate; n_o, n_N are the oxygen and nitrogen densities respectively. With assigned values of K_d and n_e it is apparent that the perturbation decreases as r_o increases and D decreases.

In the case where $\alpha \ll 1$, the decay of electron density along the axis z of the channel may be computed assuming $K_d = 0$ in Eq. (34). If a uniform electron density n_e is assumed at the entrance of the channel (z = 0) the solution is

$$n = 2n_e \sum_{n=0}^{\infty} \frac{1}{x_n} \frac{J_o\left(x_n \frac{r}{r_o}\right)}{J_1(x_n)} e^{-\gamma_n^2} \tag{38}$$

where

$$\gamma_n = \frac{1}{2}\sqrt{\frac{u^2}{D^2} + \frac{x_n^2}{r_o^2}} - \frac{u}{D} \tag{39}$$

and x_n are the roots of the equation $J_o(x) = 0$. From Eq. (38) one observes that the electron density decreases rapidly within a distance of the order of the cylinder diameter even for relatively large values of ur_o/Dx_n. As mentioned in Section II, the ratio between length z_1 and radius r_o of the channel section upstream of the cavity must be sufficiently large to minimize the radiation losses. Consequently from Eq. (38) and the requirements of a strong attenuation of the TM_{01} mode in the channel, the ratio z_1/r_o must satisfy the condition

$$\frac{1}{x_o} \ll \frac{z_1}{r_o} \ll 4\,\frac{ur_o}{Dx_n^2} \tag{40}$$

at least for the first few roots x_n.

In the case of the open cavities and the dielectric probe the electron diffusion toward the surface is equally important. Thus the combined fluid dynamic and plasma dynamic considerations require that the penetration depth of the electromagnetic wave at the maximum measurable electron density be large compared to the thickness of the layer where n departs significantly from the free stream value.

These fluid dynamic and plasma dynamic considerations show that the probe calibration must be performed in the same range of Mach number, Reynolds number and electron diffusion length

as those of the flow in which the probe is supposed to operate. For the internal cavity probe calibration a shock tube was used to generate the plasma. Measurements were made immediately behind the incident shock where the Mach number was approximately 2.5 and a range of densities from $10^{-6} \times 10^{-4}$ k_o/m^3. Simultaneous measurements of the electron density were made using the probe and a microwave interferometer (Ref. 7). Typical results of this calibration are those shown previously in Fig. 2. The calibration of the dielectric probe which is intended for a zero velocity application is being conducted again with a microwave interferometer in the region behind the reflected shock in a conventional shock tube. The preliminary results are shown in Fig. 5.

V. CONCLUSIONS

The microwave cavity probe techniques offer the advantage that measurements of both underdense and overdense plasmas can be performed. Thus, even extremely large electron densities of the order of 10^{14} e/cc can be measured using conventional microwave circuits in the centimeter wavelength range. The relatively small size of a microwave resonant structure in this wavelength range allows the measurement of quasi local values of electron densities over a wide range of flow situations. Several orders of magnitude in the electron density can be measured by a probe due to the sensitivity which can be achieved in a microwave resonant cavity. The design of a probe and its mode of operation is dictated by the range of flow conditions in which the probe is intended to be used. Several practical probe geometries can be designed which minimize the flow perturbation induced by their presence and in particular do not significantly change the local value of electron density in the region of interaction with the electromagnetic field.

REFERENCES

1. Labitt, M. and Herlin, M. A., Application of the Resonant Cavity Method to the Measurement of Electron Densities and Collision Frequencies in the Wake of Hypervelocity Pellets, MIT Lincoln Laboratory Technical Report No. 248, October 17, 1961.

2. Labitt, M., Measurement of the Diameter of the Electronic Wake of Hypersonic Pellets, MIT Lincoln Laboratory Technical Report No. 342, January 20, 1964.

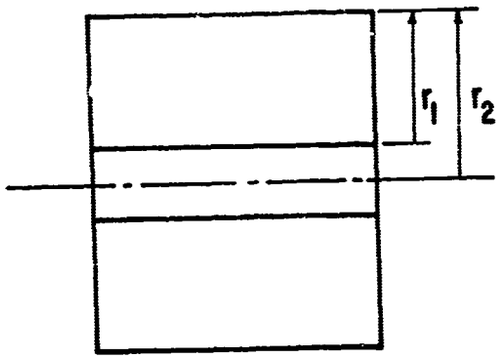
3. Abele, M., Byrne, R. and West, J., Preliminary Design of an Electron Probe, GASL Technical Report No. 188, October 5, 1960.

4. Lederman, S., Abele, M. and Visich, M., Microwave Techniques Applicable to Shock Tube Measurements, Proc. of the First International Congress on Instrumentation in Aerospace Simulation Facilities, September 1964.

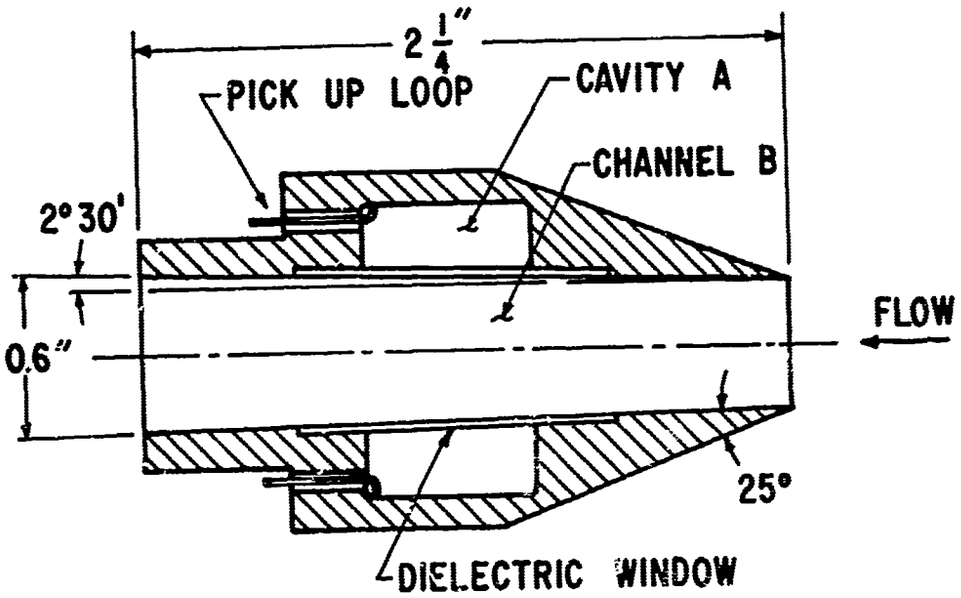
5. Development of a Probe to Measure the Electron Density in Separate Flow Regions Surrounding the Apollo Vehicle, GASL Proposal No. 9-440 (Technical), September 15, 1964.

6. Robson, P. N. and Stewart, R. D., Surface Wave Probe for Measuring Electron Densities in a Gaseous Plasma, Electronic Letters, Vol. 1, No. 1, March 1965.

7. Abele, M., Byrne, R. and Medecki, H., Development of a Probe for the Measurement of Point Values of Electron Densities in Supersonic Flows, GASL Technical Report No. 527, September 1965, NASA Contract NAS5-3929.



Ia



Ib

FIG. I CYLINDRICAL CAVITY PROBE

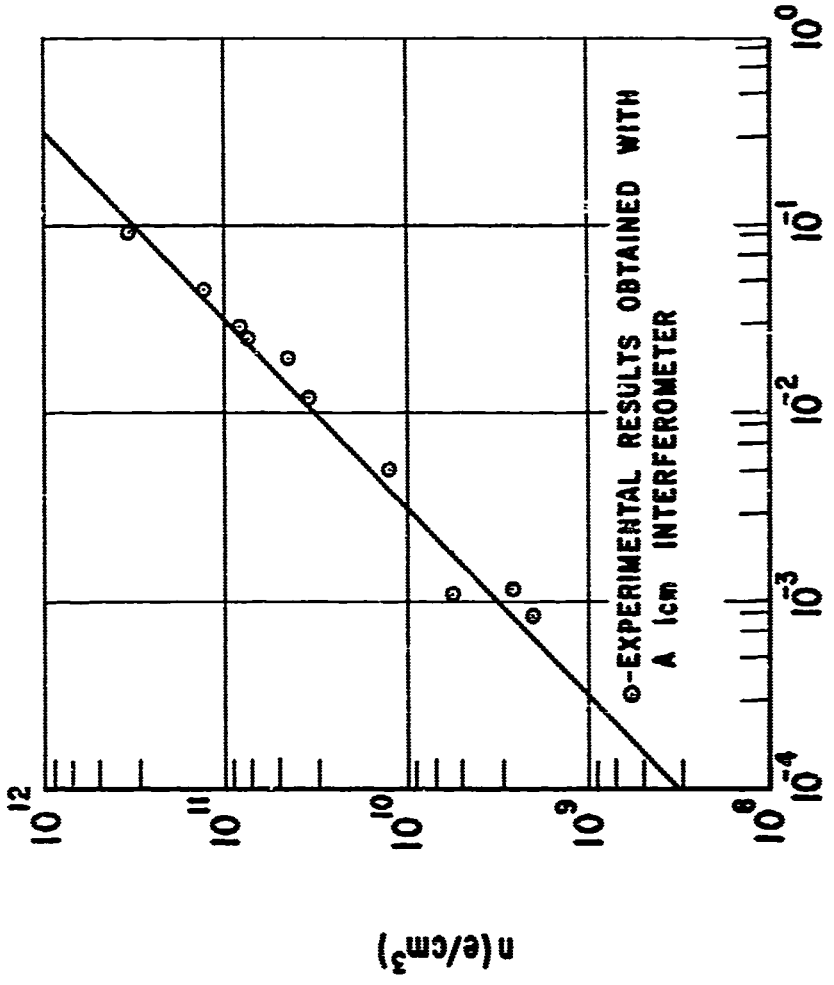


FIG. 2 CHARACTERISTIC OF THE CYLINDRICAL CAVITY PROBE

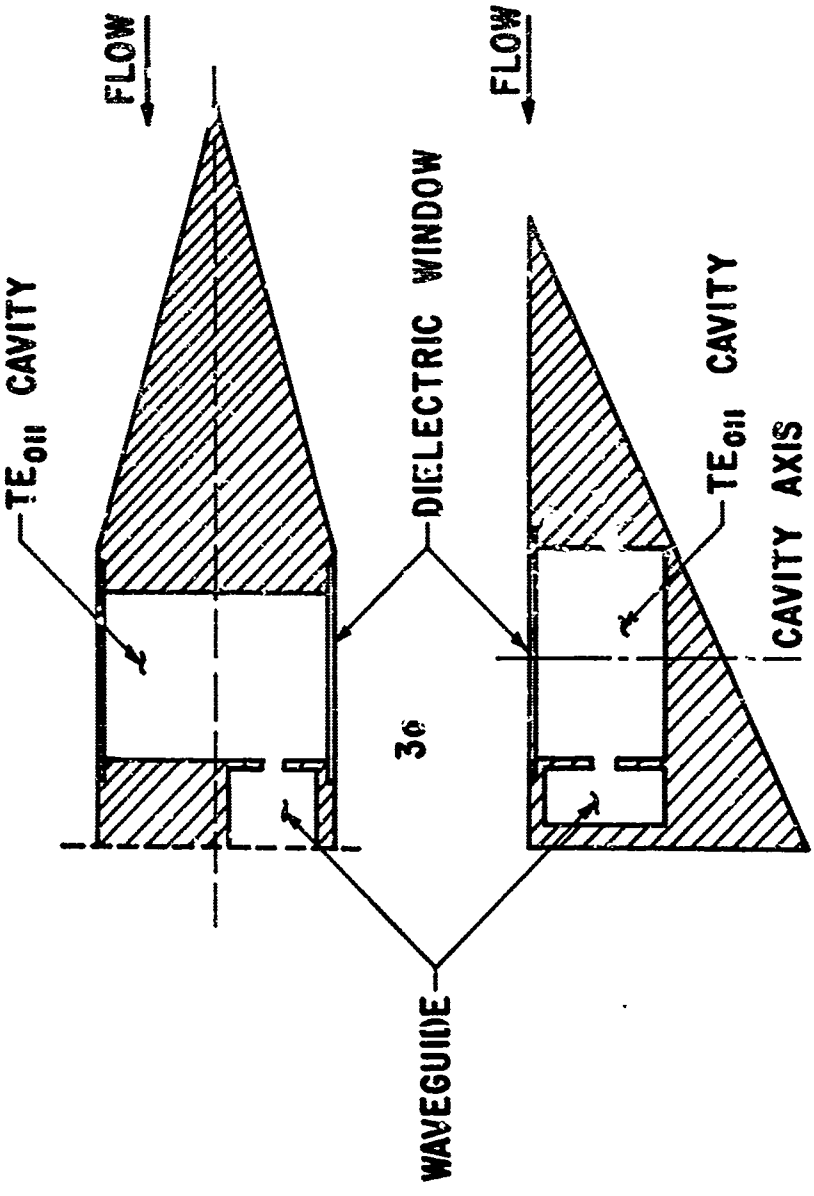


FIG. 3 OPEN CAVITY PROBE

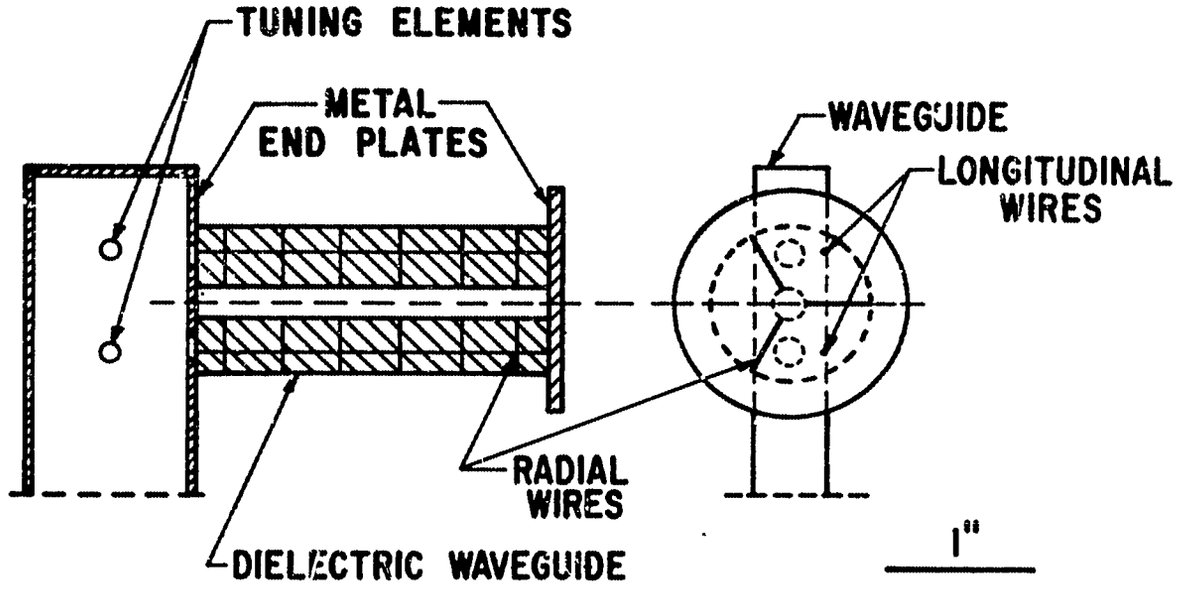


FIG. 4 DIELECTRIC PROBE

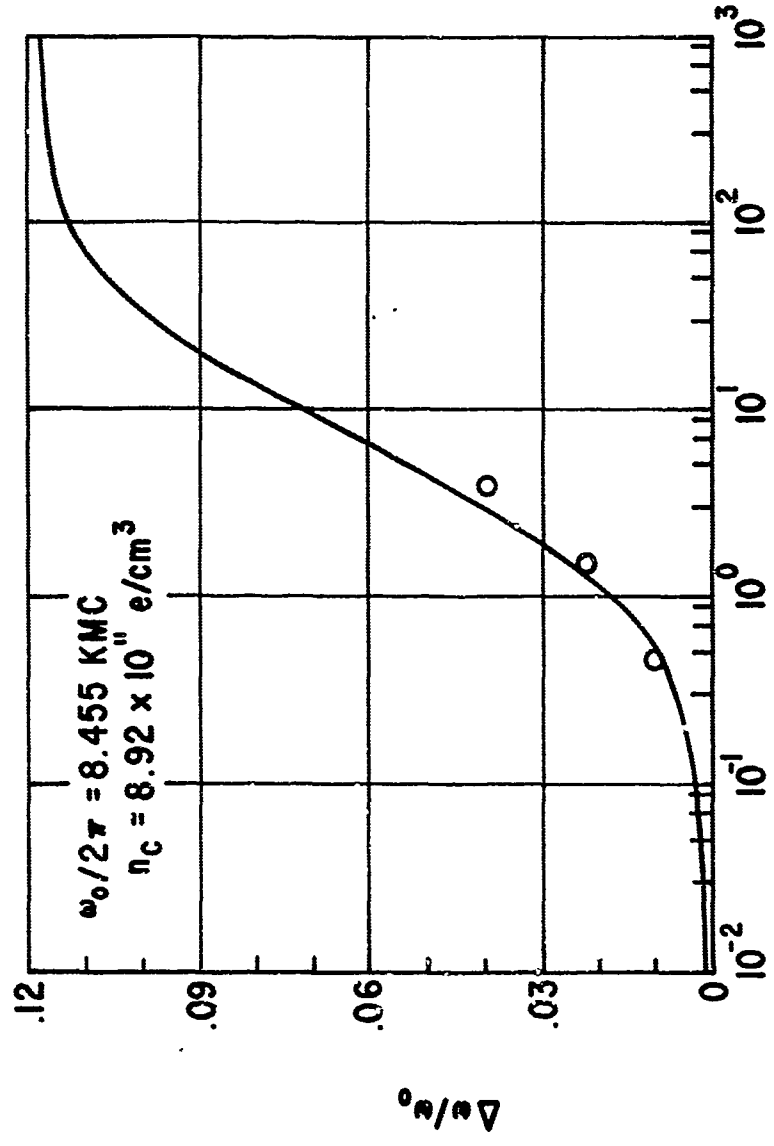


FIG. 5 CHARACTERISTIC OF THE DIELECTRIC PROBE

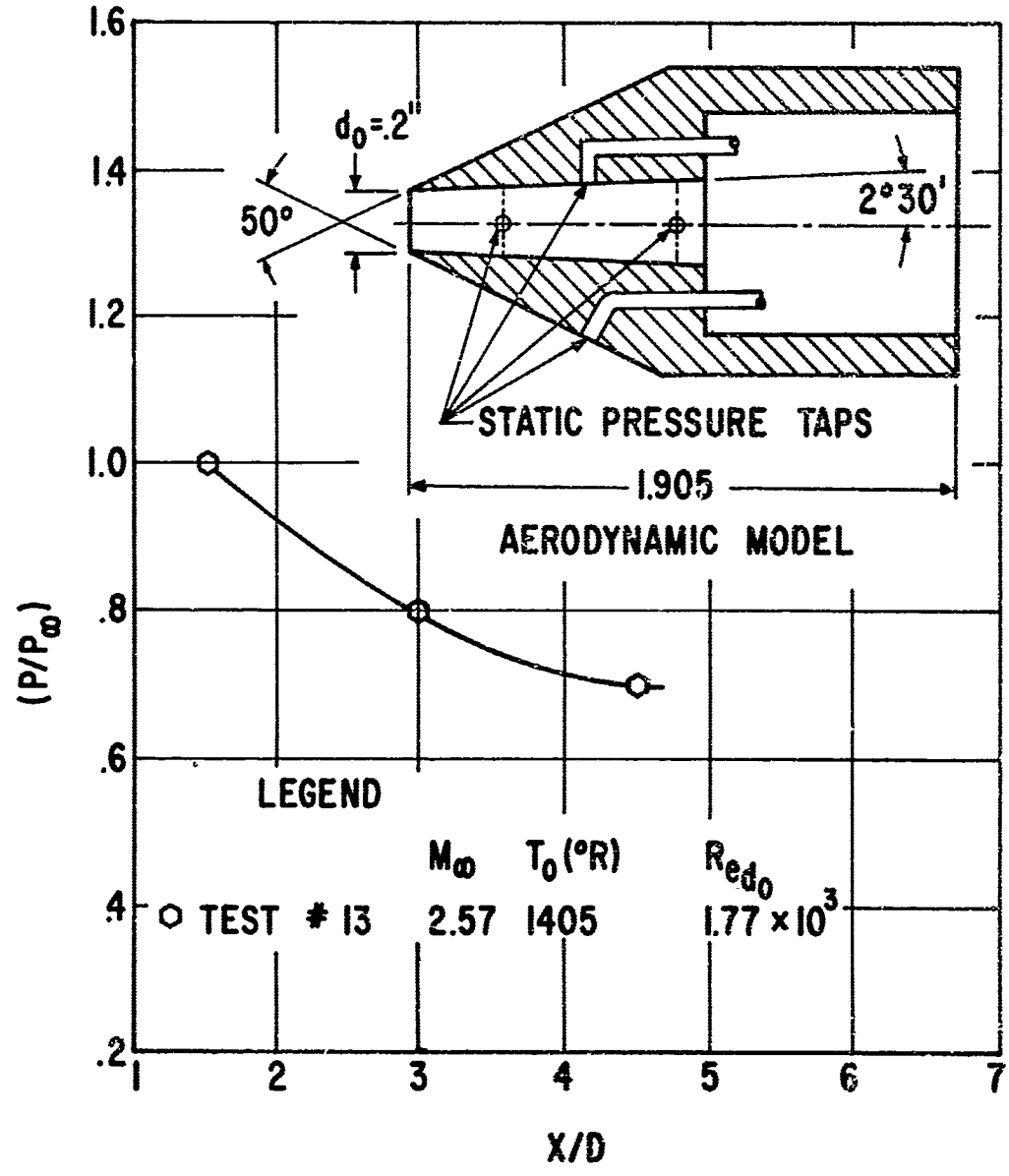


FIG. 6 STATIC PRESSURE DISTRIBUTION IN THE INLET CHANNEL OF THE CYLINDRICAL CAVITY

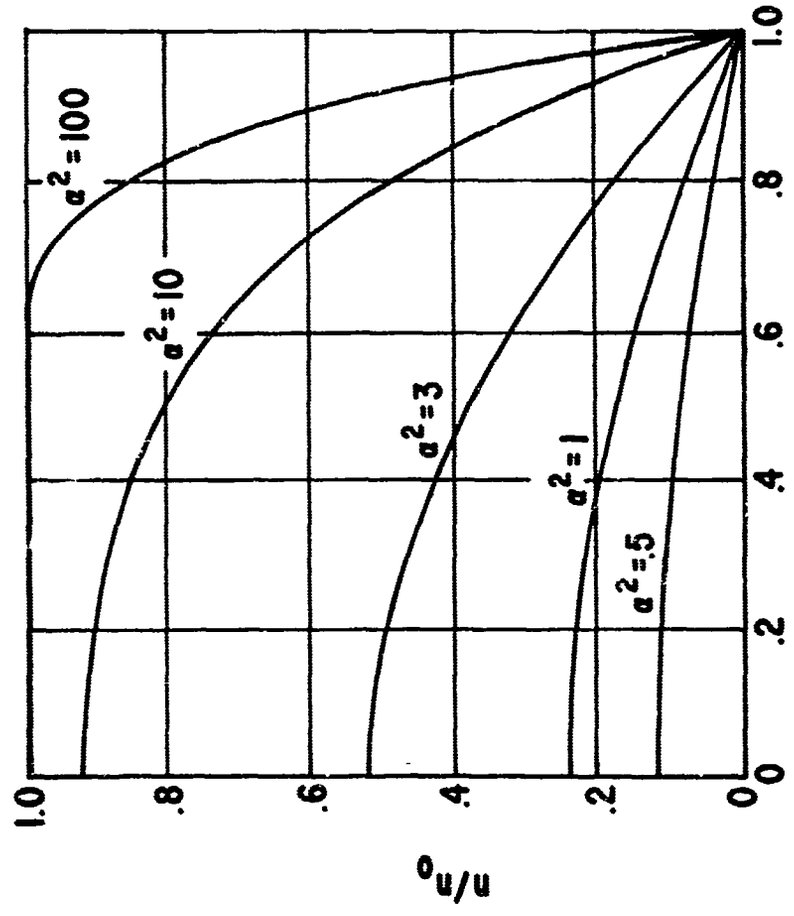


FIG. 7 RADIAL ELECTRON DENSITY DISTRIBUTION IN A CYLINDRICAL CHANNEL

VIII. MEASUREMENT OF PLASMA PARAMETERS USING A RADIAL TRANSMISSION LINE

John H. Mullen
Louis N. Medgyesi-Mitschang
Research Division
McDonnell Aircraft Corporation
St. Louis, Mo.

ABSTRACT

This report presents a new method for measuring the electron density and collision frequency of plasmas. This diagnostic technique which is applicable to low as well as high density plasmas, minimizes the usual field problems associated with microwave plasma diagnostic schemes. The effect of plasma non-uniformity on this technique has been calculated. Spectrographic measurements and thermodynamic partition function calculations were found to be consistent with the plasma parameters measured with the present technique.

INTRODUCTION

The measurement of plasma parameters, particularly the plasma electron density, has been a persistent problem in the plasma diagnostic field. Ever since the plasma-induced blackout of reentry telemetry was recognized, the importance of this problem has increased. Various diagnostic techniques, such as Langmuir probes, have been proposed along with spectrographic and electrical techniques.

The most direct approach to the problem has involved transmitting electrical signals through a plasma medium and observing the subsequent plasma-induced attenuation and phase shift. From a theoretical point of view this scheme should work. However, it is difficult to implement experimentally since it requires the signal wavelengths to be

comparable to the plasma dimensions and assumes very little refraction and reflection. For the usual laboratory plasma, the signal frequencies are restricted to the X band region or higher. But such frequencies require high density plasmas, which are difficult to generate. Furthermore, high density plasmas have high density gradients, which lead in turn to considerable experimental errors.

The diagnostic scheme presented here is compatible with high as well as low density plasmas and is optimum with respect to the usual cylindrical laboratory plasma geometry. Furthermore, since the basic diagnostic apparatus is a radial transmission line, the electromagnetic wave equations for the diagnosing signal can be solved exactly. Thus, the correlating analysis, while not simple, is capable of good resolution. The usual field problems connected with fringing, leakage, and non-uniform phase fronts are minimized because of the geometry of the structure. The question of the effect of non-uniformity in the plasma on this measurement technique has also been considered and appropriate compensations can be made for it in many cases.

GENERAL APPROACH

This diagnostic technique involves the correlation of the impedance in a radial transmission line with the plasma electron density and collision frequency. The correlation between these quantities involves matching the boundary conditions of the electro-magnetic fields at the plasma air interface of the radial transmission line. From this correlation a theoretical plasma impedance is then compared with the experimentally measured values, providing the correlating link between the measured plasma impedance and the plasma electron density and collision frequency.

EXPERIMENTAL APPARATUS*

The experimental aspects of this diagnostic scheme best illustrate the underlying features of the technique. The implementation of this method is shown in Fig. 1. A radial transmission line is placed around the plasma at the point of diagnosis. The device is equipped with a radially calibrated slot and probe, connected to a crystal detector measuring the VSWR and the location of the field maxima and minima of the radial line. A tuner is provided for the probe to ensure increased sensitivity without requiring increased power from the signal source. The radial line is excited with a 95% TEM mode by a gradually tapered section from a shallow auxiliary cavity which is fed from six loop feeds as shown in Fig. 2. Sufficient attenuation is placed in the tapered section to make certain the generator wave impedance matches the wave characteristic impedance of the slotted section.

MEASUREMENT OF THE EXPERIMENTAL PARAMETERS

The VSWR and the location of the field maxima and minima in the radial line, as in uniform transmission lines are functions of the line termination. In this apparatus the termination is the plasma column. It can be considered in the electrical sense as a dielectric. While such a termination may be difficult to synthesize in terms of lumped parameters, its effect on the radial line can be measured in the same way as a conventional load.

The measurement procedure of the VSWR and the location of the field maxima and minima on a radial line is identical to that on a uniform transmission line, such as a coaxial cable or waveguide. The interpretation of the data for these parameters however is different. In this

*The experimental apparatus used in these studies was conceived, designed and constructed under McDonnell's independent research and development program. All patent and proprietary rights therein are retained by McDonnell Aircraft Corporation.

difference lies the dissimilarity between the uniform and non-uniform transmission lines. The radial transmission line is a non-uniform transmission line. The distinguishing feature between the two types of lines is that in a non-uniform transmission line the propagation constant and the characteristic impedance of the line are functions of the spatial dimension of the line in the direction of propagation. In the radial line this is the radial direction. The functional variation of the characteristic impedance with radius is given by Fig. 3. The VSWR measured on a radial line must be normalized with respect to this variation. The normalized VSWR is given by

$$VSWR = (VSWR)_r \frac{G_o(k_o r_{max})}{G_o(k_o r_{min})}, \quad k_o = \frac{2\pi}{\lambda}$$

where $(VSWR)_r$ is the VSWR measured on the radial line and r_{max} and r_{min} refer to the location of the field maxima and minima, respectively. The functional dependence of $G_o(k_o r)$ is given by Fig. 3.

Since the propagation constant varies on the radial line, the phase shift is non-linear, so that the conventional phase shift associated with the Smith Chart is not applicable. Hence, the data from the radial line cannot be plotted on a Smith Chart directly even though the VSWR has been normalized. For this type of work, a radial transmission line calculator (Fig. 4) has been devised by the author[1]. This calculator compensates for the non-uniformity of the phase shift. Using the calculator, the measured data can be reduced directly to an impedance. It is convenient for data correlation to transform all the experimentally determined impedances to the plasma air interface. This transformation is most conveniently accomplished on the calculator itself [7].

THEORETICAL ASPECTS

To correlate the experimental data with the plasma parameters, it is necessary to match the experimentally determined impedance on the radial line, transformed to the plasma-air interface, with the theoretical plasma impedance at the same point. The schematic representation of the fields in a radial transmission line terminated by a plasma column if given in Fig. 5. The sense of the EM fields shown correspond to a TEM mode excitation. This excitation was chosen because it greatly simplifies the analysis. The experimental apparatus was optimized to minimize the effect of the other modes.

First the analysis will be performed for the case of a homogeneous plasma load. Next a non-uniform plasma termination will be considered. These results will then be compared to provide an upper and lower bound on the electron density measurements on the radial transmission line.

HOMOGENEOUS PLASMA COLUMN

The plasma wave impedance equals the air wave impedance at the plasma-air interface. If the wave impedance on the non-plasma side of the interface is chosen, the expression has to include the reflections at the interface, considerably complicating the expression. On the other side of the interface the reflection terms drop out. The resulting wave impedance expression is just the ratio of the electric and magnetic fields in the plasma. The electromagnetic fields in the plasma can be determined from Maxwell's equations with the appropriate boundary conditions. Maxwell's equations in a complex dielectric medium assuming sinusoidal time variations are[2,3].

$$\nabla \times \vec{H} = \vec{D} + \vec{I} = (j \omega \epsilon_0 \epsilon_r + c) \vec{E} \tag{1}$$

$$\nabla \times \vec{E} = - \mu_0 \vec{H} \tag{2}$$

The boundary conditions at the plasma-air interface are:

$$E_{tang1} = E_{tang2} \tag{3}$$

$$H_{tang1} = H_{tang2} \tag{4}$$

But since the radial line is excited with a TEM mode, the electric and magnetic fields in the non-plasma region of the line are given by[4]

$$E_z = AH_0^{(1)}(kr) + BH_0^{(2)}(kr) \tag{5}$$

$$H_\phi = \frac{j}{377}\left[AH_1^{(1)}(kr) + BH_1^{(2)}(kr)\right], \tag{6}$$

where H represents Hankel functions and $k = \frac{2\pi}{\lambda}$. The constants A and B refer to the magnitudes of the inward and outward traveling waves in the radial line.

Solving Maxwell's equations (Equations 1 and 2) simultaneously, one obtains

$$\nabla \times \nabla \times \vec{E} = (\omega^2 \mu \epsilon_0 \epsilon_r - j\omega \mu_0 \sigma)\vec{E} \tag{7}$$

Since the electric field may exist only in the Z-direction as a consequence of Equations 3 and 5, the double curl reduces to:

$$\nabla \times \nabla \times \vec{E} = -\frac{1}{r}\left[\frac{dE_z}{dr} + r\,\frac{d^2E_z}{dr^2}\right] \tag{8}$$

Then Equation 7 reduces to Bessel's equation

$$\frac{d^2E_z}{dr^2} + \frac{1}{r}\frac{dE_z}{dr} + k^2E_z = 0 \tag{9}$$

where k is the complex propagation constant in the plasma column, given by

$$k^2 = \omega^2 \mu_0 \epsilon - j\omega \mu_0 \sigma \tag{10}$$

The parameters ϵ and σ are the permittivity and conductivity of the plasma, respectively. For a homogeneous plasma ϵ and σ are defined as

$$\epsilon = \epsilon_0 \left(1 - \frac{\omega_p^2}{\nu^2 + \omega^2}\right) \tag{11}$$

$$\sigma = \epsilon_0 \left(\frac{\omega_p^2 \nu}{\nu^2 + \omega^2}\right) \tag{12}$$

The solution of Equation 9 gives the electric field inside the plasma column in terms of the zeroth order Bessel function with a complex argument

$$E_z = A' J_0 (kr) \tag{13}$$

where A is an arbitrary parameter which will drop out. Substituting Equation 13 into Equation 2 gives the magnetic field intensity within the plasma as

$$H_\phi = \frac{jkA'}{\omega \mu_0} J_1 (kr) \tag{14}$$

The wave impedance on the plasma side of the interface is given by the ratio of the electric and magnetic fields:

$$Z = -\frac{j\omega \mu_0}{k} \left(\frac{J_0(kR)}{J_1(kR)}\right) \tag{15}$$

The complex argument, kR, of the zero and first order Bessel functions is related to the plasma parameters in the following way,

$$k = (\omega\mu_o\epsilon_o)^{1/2}\left\{\omega^2\left(1 - \frac{\omega_p^2}{\nu^2+\omega^2}\right)^2 + \left(\frac{\omega_p^2\nu}{\nu^2+\omega^2}\right)^2\right\}^{1/4}(\cos\phi + j\sin\phi) \qquad (16)$$

where

$$\phi = \frac{-1}{2}\tan^{-1}\left(\frac{\omega_p^2\nu}{\omega(\omega^2+\nu^2-\omega_p^2)}\right). \qquad (17)$$

Thus the plasma impedance reduces to a complex function of ν and ω_p, represented mathematically as

$$Z = U(\omega_p;\nu) + j\,V(\omega_p;\nu) \qquad (18)$$

where U and V are real functions of ω_p and ν. The rf frequency, ω, is not included in the functional notation above because the radial line is operated at constant frequency for each set of experiments. The numerical evaluation of Equation 18 was done by a computer program.

NON-HOMOGENEOUS PLASMA COLUMN

The previous analysis assumed that the plasma was uniform throughout. While this approach is often justifiable for low and medium density diffusion plasmas, it neglects the effect of the walls of the plasma container on the electron density. If this effect is taken into account, then the plasma will be non-uniform. The effect of non-uniformity in the plasma on the electron density measured by the present technique will now be discussed.

In general, the electron density in a cylindrical plasma is maximum at the center and zero at the walls. The rate at which the electron density drops off from its maximum value is impossible to predict in general. However, for diffusion plasmas where the diffusion coefficient is constant throughout a cylindrical geometry, the zeroth order Bessel

function, $J_0\left(2.405\ \frac{r}{R}\right)$, has been found to describe the non-homogeneity in electron density[5,6]. This electron distribution is given in Fig. 6. In order to simplify the analysis, a parabolic distribution (Fig. 6) was chosen instead of the Bessel function. A comparison of these two curves shows that the former closely approximates the Bessel function. Furthermore, both functions satisfy the boundary condition at the walls of the plasma container.

The analysis for this case with a non-homogeneous plasma is similar to the foregoing case with a homogeneous plasma. For this case the defining equation for the plasma frequency is

$$\omega_p = 5.63 \times 10^4 \left\{N_0\left(1 - \frac{r^2}{R^2}\right)\right\}^{1/2} \tag{19}$$

where N_0 is the maximum electron density at the center of the plasma column; R is the radius of the plasma column. Thus the dielectric constant and the conductivity of the plasma, Equations 11 and 12, respectively become:

$$\epsilon = \epsilon_0 \left[1 - \frac{\omega_0^2}{\nu^2 + \omega^2}\left(1 - \frac{r^2}{R^2}\right)\right] \tag{20a}$$

$$\sigma = \epsilon_0 \frac{\omega_0^2 \nu}{\nu^2 + \omega^2}\left(1 - \frac{r^2}{R^2}\right) \tag{20b}$$

$$\omega_0 = 5.63 \times 10^4 \sqrt{N_0}$$

Using these modified expressions for ϵ and σ in the complex propagation constant k (Eq. 10), the differential equation giving the electric field

in the plasma column becomes

$$\frac{d^2E_z}{dr^2} + \frac{1}{r}\frac{dE_z}{dr} + \left\{\left[\left(\frac{\omega}{c}\right)^2 - \left(\frac{\omega}{c}\right)^2\left(\frac{\omega_o^2}{\nu^2+\omega^2}\right) - j\,\frac{\omega}{c^2}\left(\frac{\omega_o^2\nu}{\nu^2+\omega^2}\right)\right]\right. \tag{21}$$

$$\left. + \frac{r^2}{R^2}\left[\left(\frac{\omega}{c}\right)^2\frac{\omega_o^2}{(\nu^2+\omega^2)} + j\left(\frac{\omega}{c^2}\right)\frac{\omega_o^2\nu}{(\nu^2+\omega^2)}\right]\right\} E_z = 0.$$

This equation is of the second order having two possible solutions. Since the roots of the indicial equation are both zero, the two solutions have the form

$$E_{z_1} = \sum_{n=0}^{\infty} C_n r^n \,, \; C_o \neq 0 \tag{22a}$$

$$E_{z_2} = \sum_{k=0}^{\infty} C_k r^k + (\text{constant})\, E_{z_1} \ln r \tag{22b}$$

where the C's are found by substitution of these series solutions into Equation 21. The second solution is singular at r = 0, and thus physically inadmissible. Substituting the first solution into Equation 21 gives

$$\sum_{n=0}^{\infty} C_n \, ?r^n + \left\{\left(\frac{\omega}{c}\right)^2 - A\right\}\sum_{n=0}^{\infty} C_n r^{n+2} \tag{23}$$

$$+ \frac{A}{R^2}\sum_{n=0}^{\infty} C_n r^{n+4} = 0$$

where

$$A = \left(\frac{\omega_o^2}{\nu^2+\omega^2}\right)\left[\left(\frac{\omega}{c}\right)^2 + j\,\frac{\omega\nu}{c^2}\right] .$$

Equating coefficients of like power, the following recursion relationships are obtained

$$C_o = \text{arbitrary}$$

$$(n)^2 \frac{C_n}{C_o} + \left\{\left(\frac{\omega}{c}\right)^2 - A\right\} = 0 \qquad , n = 2 \tag{24}$$

$$(n)^2 \frac{C_n}{C_o} + \left\{\left(\frac{\omega}{c}\right)^2 - A\right\} \frac{C_{n-2}}{C_o} + \frac{A}{R^2} \frac{C_{n-4}}{C_o} = 0, \; n = 4, 6, 8 \ldots\ldots$$

Note since all C_n's with odd numbered subscripts are zero, it is convenient for the latter calculations to redefine the coefficient in the recursion relationships as

$$\frac{C_n}{C_o} = a_{2n} + j\, b_{2n} \tag{25}$$

Rewriting Equation 24 using the previous definition and equating the real and imaginary parts to zero gives

$$a_o = 1 \qquad b_o = 0$$

$$a_2 = \frac{-D}{4} \qquad b_2 = \frac{F}{4} \tag{26}$$

$$16a_4 + Da_2 + Fb_2 = G = 0$$

$$16b_4 - Fa_2 + Db_2 + L = 0$$

$$4n^2 a_{2n} + Da_{2(n-1)} + Ga_{2(n-2)} + Fb_{2(n-1)} - Lb_{2(n-2)} = 0, \; n>3$$

$$4n^2 b_{2n} - Fa_{2_{(n-1)}} + Db_{2(n-1)} + La_{2(n-2)} + Gb_{2(n-2)} = 0$$

where

$$D = \left(\frac{\omega}{c}\right)^2 \left(1 - \frac{\omega_o^2}{\nu^2 + \omega^2}\right); \quad G = \frac{1}{R^2}\left(\frac{\omega}{c}\right)^2 \left(\frac{\omega_o^2}{\nu^2 + \omega^2}\right);$$

$$F = \frac{\omega\nu}{c^2}\left(\frac{\omega_o^2}{\nu^2 + \omega^2}\right); \quad L = \frac{F}{R^2}$$

The previous equations determine the coefficients of the series solution of the electric field. Thus

$$E_z = 1 + \sum_{n=1}^{\infty} a_{2n} r^{2n} + j \sum_{n=1}^{\infty} b_{2n} r^{2n} \tag{28}$$

Substituting Equation 28 into Equation 2 gives the magnetic intensity within the plasma as

$$H_\phi = \frac{2}{j\omega\mu}\left\{\sum_{n=1}^{\infty} n a_{2n} r^{2n-1} + j \sum_{n=1}^{\infty} n\, b_{2n} r^{2n-1}\right\} \tag{29}$$

The wave impedance on the plasma side of the interface is given by the ratio of the electric and magnetic fields,

$$Z = \frac{E_z}{H_\phi} = j\,\frac{\omega\mu}{2}\,\frac{1 + \sum_{n=1}^{\infty} a_{2n} r^{2n} + j \sum_{n=1}^{\infty} b_{2n} r^{2n}}{\sum_{n=1}^{\infty} n\, a_{2n} r^{2n-1} + j \sum_{n=1}^{\infty} n\, b_{2n} r^{2n-1}} \tag{30}$$

Rationalizing Equation 30, the real and imaginary parts of the plasma impedance for a non-uniform plasma are respectively,

$$Z_R = \frac{\omega\mu}{2}\left(\frac{U_o V_1 - U_1 V_o}{V_o^2 + V_1^2}\right) \tag{31a}$$

$$Z_I = \frac{\omega\mu}{2}\left(\frac{U_o V_o + U_1 V_1}{V_o^2 + V_1^2}\right) \tag{31b}$$

where

$$U_o = 1 + \sum_{n=1}^{\infty} a_{2n} r^{2n} \tag{32a}$$

$$U_1 = \sum_{n=1}^{\infty} b_{2n} r^{2n} \tag{32b}$$

$$V_o = \sum_{n=1}^{\infty} n a_{2n} r^{2n-1} \tag{32c}$$

$$V_1 = \sum_{n=1}^{\infty} n\, b_{2n}\, r^{2n-1} \tag{32d}$$

The previously deduced expressions were calculated for a wide range of plasma parameters using an IBM program.

EVALUATION OF THE PIASMA IMPEDANCE

The foregoing equations for the plasma impedance, Equations 15 and 31 for a uniform and a non-uniform plasma, respectively, were evaluated by a computer since the exact relationship between the plasma parameters and the plasma impedance is too involved to be expressed as an explicit function. Two IBM programs were developed to calculate the plasma impedance for the anticipated plasma parameters. Plasma electron densities of 10^{10} to $10^{15} cm^{-3}$ and collision frequencies of 10^{8} to 6×10^{13} sec^{-1} were chosen. The computed results are plotted on the Smith Chart given in Figs. 7 and 8. The plots are normalized to the real part of the characteristic impedance of the radial transmission line at the plasma-air interface (132 ohms). The various plasma parameters plotted correspond to constant collision frequency and electron density lines.

plasma frequency, then the impedance measured will contain no resistive part but will be a pure capacitive susceptance, which corresponds to a very high VSWR reading on the radial line. The resolution of the Smith Chart, however, decreases rapidly at high VSWR radii. Therefore, the excitation frequency must be equal to or lower than the plasma frequency. As the excitation frequency is lowered, the dimensions of the radial line must be comparably increased, in order to enable meaningful VSWR measurements to be made. Thus, the lower limit of the electron density capable of resolution with this method is set by the maximum physical dimensions of the radial line that can be accommodated and the uniformity of the plasma in axial direction.

EXPERIMENTAL RESULTS

Evaluation tests were performed on the diagnostic apparatus using four known solid dielectrics as loads for the radial transmission line. For this purpose dielectrics with dielectric constants of 2.1, 4, 9, and 15 were used. The dielectric loads tested were one inch in diameter. The wave impedance of these dielectrics was measured. From the measured wave impedance, the dielectric constants of the loads were determined. These results were then compared with the dielectric constant in the manufacturer's specifications. This comparison is shown in Fig. 9. The results show that at higher dielectric constants the error between the experimental and specified values is less than 10% which would indicate an error in electron density of approximately the same amount.

Next a series of tests were performed on a number of seeded and unseeded plasmas under varied flow and pressure conditions. A representative sampling of these measurements is summarized in Table 1. All

If the plasma load in the radial transmission line is uniform then the electron density is interpreted from Fig. 7. If the plasma is non-uniform, with the electron density profile given in Fig. 6, then the experimental results are interpreted from Fig. 8. Thus, for a given impedance, measured on the radial transmission line, two electron density correlations can be obtained. At low electron densities $N_e = 10^{11} cm^{-3}$, the average electron density of the non-uniform distribution N_o (using Fig. 8) is approximately 1.33 times as high as the density of the uniform plasma, N_e, (using Fig. 7). The ratio between N_o and N_e increases continuously, until at $N_e = 10^{13} cm^{-3}$, $N_o = 3.33\ N_e$. The change in the ratio N_o/N_e is to be expected since at high electron densities the effect of any non-uniformity in the plasma becomes important. It should be noted that the constant collision frequency lines on the impedance plots are not noticeably altered by the change of the plasma density profile.

It may seem that this method of interpreting the experimental data is ambiguous. In reality by having considered these two limiting cases for the electron density profile, this method is capable of yielding upper and lower limits for the electron densities measured.

The usefulness of the plasma impedance plots (Figs. 7 and 8) is limited to electron densities in excess of $10^{10} cm^{-3}$. This electron density corresponds to a plasma frequency which is identical to the excitation frequency of the uhf radial line (i.e., 960 Mc/Sec). For lower electron densities it is necessary to use a lower frequency to drive the radial line to obtain meaningful results. This requirement arises from the fact that, if the diagnosing signal's frequency is greater than the

measurements were made on a radio frequency plasma of one inch diameter. The exciting frequency of the radio frequency generator was 1 Mc and the rf power to the plasma was 10 kW.

When using argon, the electron density was measured using the radial transmission line method and spectrographically. A three meter Baird-Atmoic grating spectrograph was focused on a point in the center of the plasma immediately above the radial line. Because the transition probabilities of argon are readily available and relatively unambiguous, an accurate check was obtained. All electron densities measured using the radial line were approximately 20% lower than those measured spectroscopically. The spectrograph was not used to check the electron density using an air plasma because of the great difficulty in reducing the data. However, the radial transmission line technique should not be affected by the type of gas used in the plasma.

CONCLUSIONS

The radial line technique for measuring the electron density and collision frequency of laboratory plasmas has the following diagnostic characteristics:

- It is applicable to both high and low density plasmas;
- It can be adapted to uniform as well as non-uniform plasmas;
- It minimizes the customary difficulties with microwave measurements of a plasma, such as non-uniform phase fronts, refraction and reflection, and other field anomalies;
- It gave results on seeded and unseeded plasmas which were found to be consistent with spectrographic measurements and thermodynamic partition function calculations.

REFERENCES

1. J. H. Mullen, "Reflection Coefficient - Impedance Calculator for a Radial Transmission Line," PROC. National Electronics Conference 1960; p. 861-65.

2. H. Hodara, "Use of Magnetic Fields in the Elimination of Reentry Radio Blackout," PROC. IRE. (December 1961), p. 1830.

3. J. A. Stratton, "Electromagnetic Theory," (McGraw-Hill, 1941), p. 10-16.

4. S. Ramo and J. R. Whinnery, "Field and Waves in Modern Radio," (John Wiley and Sons, New York, 1953), p. 395-400.

5. S. C. Brown, "Basic Data of Plasma Physics," (MIT Press; Cambridge, Mass.), p. 47-50.

6. D. J. Rose and M. Clark, Jr., "Plasmas and Controlled Fusion," (MIT Press; Cambridge, Massachusetts), p. 70-75.

7. J. H. Mullen, L. N. Medgyesi-Mitschang, AFCRL-65-553, "Determination of Electron Densities Using a Radial Transmission Line," May 1965.

ACKNOWLEDGMENTS

The authors wish to express their sincere thanks to the Air Force Cambridge Research Laboratories, Office of Aerospace Research, United States Air Force, (Contract AF19(628)-2764) for their encouragement in this work.

Table 1 Preliminary seeding experiments

Gas	Seedant	Power into water jacket (kW)	System pressure (torr)	Seedant flow (cm^3/min)	Gas flow (lb/sec)	Weight seedant / Weight gas	Collision frequency (sec^{-1})	Electron concentration (electrons/cm^3)
Air	Water	2.9	0.31	0.3×10^{-1}	7.7×10^{-5}	1.2×10^{-2}	5.9×10^{9}	14×10^{10}
↑	↑	3.0	0.31	0.1×10^{-1}	7.7×10^{-5}	0.2×10^{-2}	5.5×10^{9}	13×10^{10}
↓	↓	3.1	0.31	0.5×10^{-1}	7.7×10^{-5}	2.6×10^{-2}	5.5×10^{9}	11×10^{10}
		2.9	0.30	1.0×10^{-1}	7.7×10^{-5}	4.8×10^{-2}	5.0×10^{9}	9.5×10^{10}
		2.9	0.32	1.4×10^{-1}	7.7×10^{-5}	6.7×10^{-2}	4.2×10^{9}	8.2×10^{10}
		2.8	0.33	1.8×10^{-1}	7.7×10^{-5}	8.6×10^{-2}	4.4×10^{9}	7.8×10^{10}
		2.8	0.33	2.2×10^{-1}	7.7×10^{-5}	11×10^{-2}	4.5×10^{9}	9.0×10^{10}
Air	Water	2.6	0.33	2.7×10^{-1}	7.7×10^{-5}	13×10^{-2}	4.8×10^{9}	8.1×10^{10}
Air	75%	2.1	0.32	0.8×10^{-1}	7.4×10^{-5}	3.7×10^{-2}	5.0×10^{9}	20×10^{10}
↑	Ethanol	2.2	0.32	1.1×10^{-1}	7.4×10^{-5}	4.6×10^{-2}	5.0×10^{9}	10×10^{10}
↓	in water	2.2	0.33*	1.3×10^{-1}	7.4×10^{-5}	5.6×10^{-2}	6.0×10^{9}	10×10^{10}
	↓	2.2	0.33*	1.5×10^{-1}	7.4×10^{-5}	6.6×10^{-2}	7.0×10^{9}	8.4×10^{10}
		2.2	0.34	1.8×10^{-1}	7.4×10^{-5}	7.6×10^{-2}	7.0×10^{9}	8.1×10^{10}
		2.1	0.34	2.0×10^{-1}	7.4×10^{-5}	8.7×10^{-2}	6.5×10^{9}	8.4×10^{10}
Air		2.0	0.34	2.3×10^{-1}	7.4×10^{-5}	9.8×10^{-2}	6.0×10^{9}	8.1×10^{10}
Argon	Ethanol	N.A.	0.42*	0.5×10^{-1}	1.6×10^{-4}	0.8×10^{-2}	1.0×10^{12}	10.0×10^{12}
↑	↑	1.1	0.42	N.A.	1.6×10^{-4}	N.A.	1.0×10^{12}	10.0×10^{12}
↓	↓	1.1	0.44*	0.2×10^{-1}	1.6×10^{-4}	0.4×10^{-2}	1.0×10^{12}	10.0×10^{12}
		1.0	0.46*	0.9×10^{-1}	1.6×10^{-4}	1.6×10^{-2}	0.05×10^{12}	1.5×10^{12}
		1.1	0.48	1.4×10^{-1}	1.6×10^{-4}	2.5×10^{-2}	0.058×10^{12}	1.0×10^{12}
		1.1	0.48*	1.9×10^{-1}	1.6×10^{-4}	3.4×10^{-2}	0.10×10^{12}	1.5×10^{12}
		1.1	0.48	2.4×10^{-1}	1.6×10^{-4}	4.3×10^{-2}	0.07×10^{12}	1.0×10^{12}
		1.1	0.48*	2.9×10^{-1}	1.6×10^{-4}	5.2×10^{-2}	0.05×10^{12}	0.39×10^{12}
		1.1	0.48*	3.1×10^{-1}	1.6×10^{-4}	5.6×10^{-2}	0.008×10^{12}	0.12×10^{12}
		1.0	0.48	3.5×10^{-1}	1.6×10^{-4}	6.2×10^{-2}	0.015×10^{12}	0.07×10^{12}
		1.0	0.48*	4.0×10^{-1}	1.6×10^{-4}	7.1×10^{-2}	0.030×10^{12}	0.15×10^{12}
		1.1	0.48*	4.5×10^{-1}	1.6×10^{-4}	8.0×10^{-2}	0.040×10^{12}	0.20×10^{12}
		1.1	0.48	5.1×10^{-1}	1.6×10^{-4}	9.1×10^{-2}	0.008×10^{12}	0.05×10^{12}
Argon	Ethanol	1.1	0.48*	5.6×10^{-1}	1.6×10^{-4}	10×10^{-2}	0.02×10^{12}	0.08×10^{12}

Data is preliminary and qualitative only. *Interpolated values N.A. – No data available.

GENERAL APPROACH

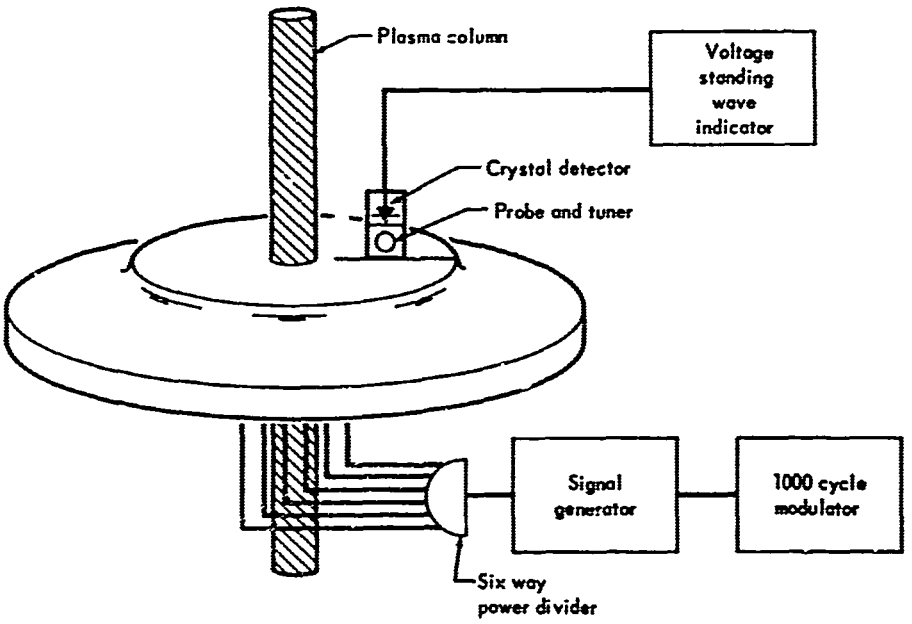


Fig. 1 Experimental apparatus for measurement of plasma parameters.

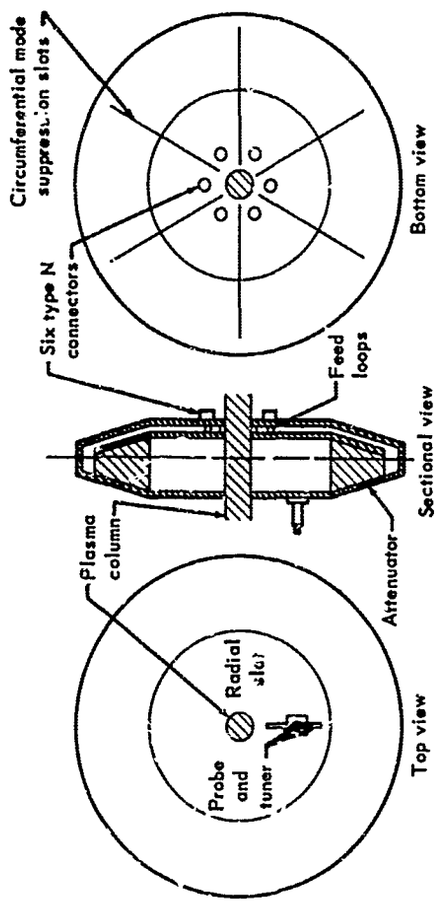


Fig. 2 Slotted radial transmission line

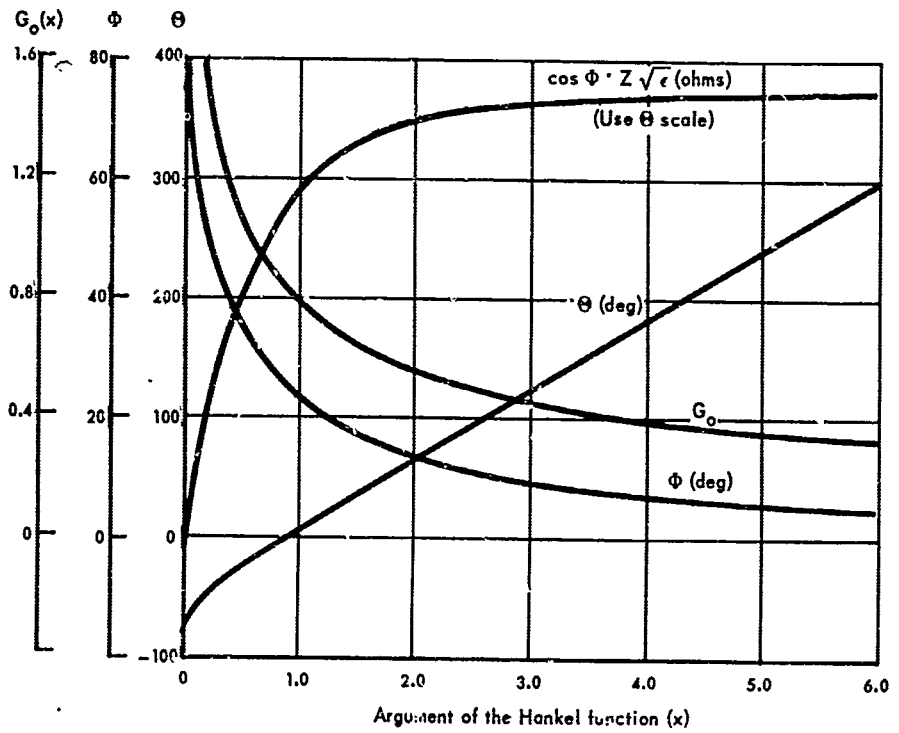


Fig. 3 Normalization chart for VSWR

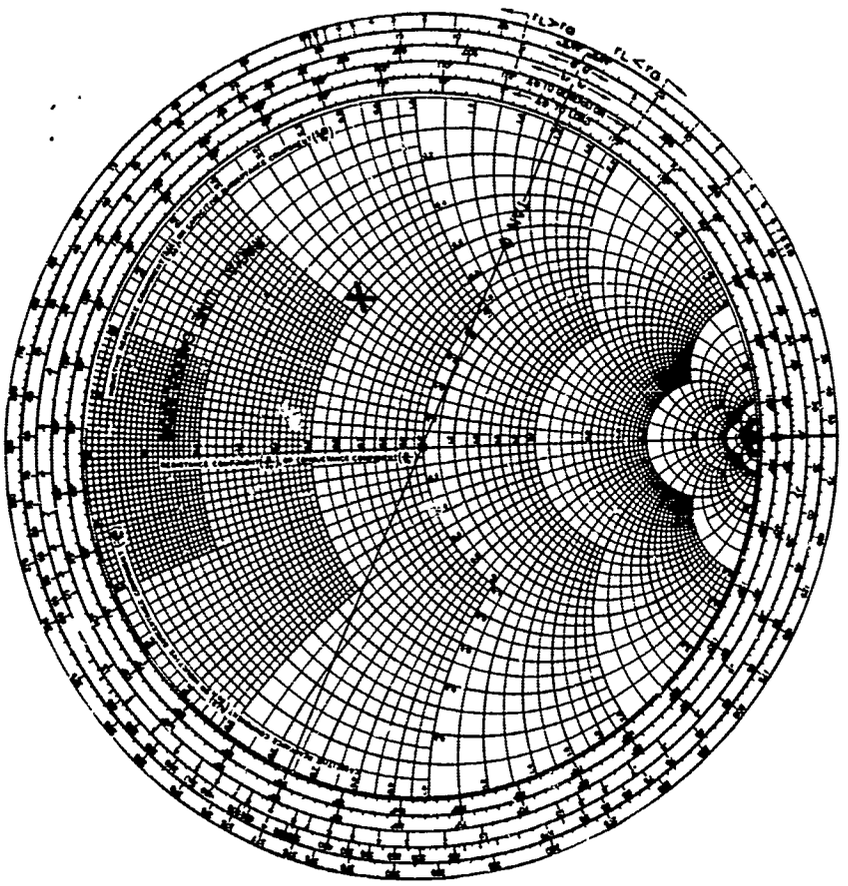


Fig. 4 Radial transmission line calculator

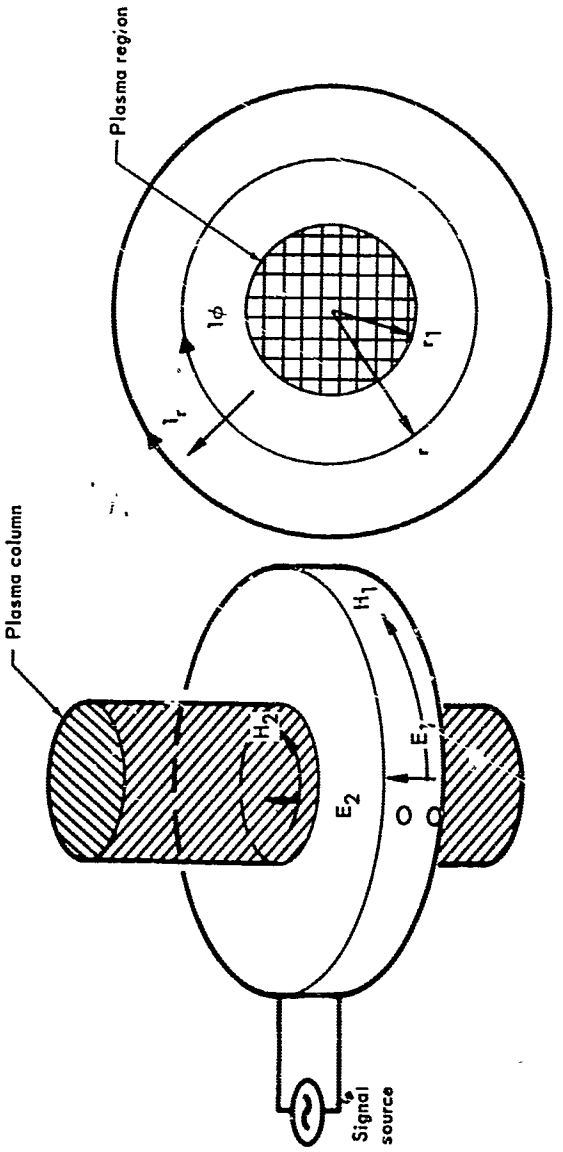


Fig. 5 Schematic for the radial line

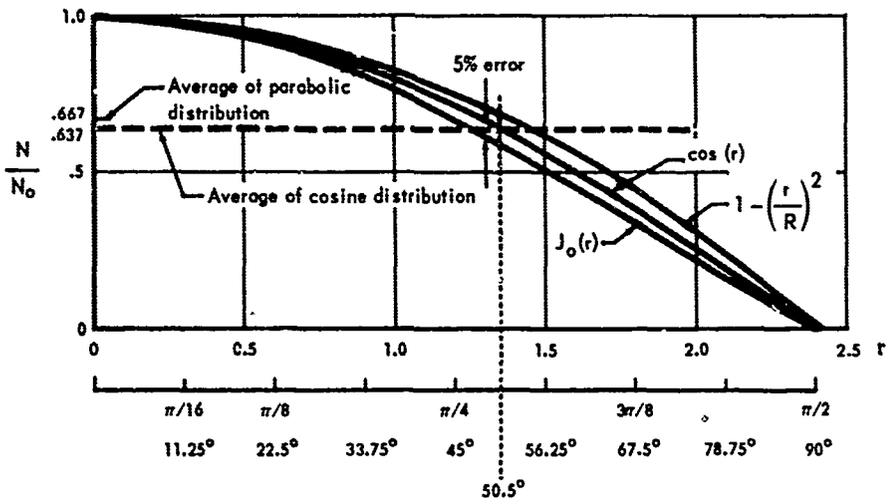


Fig. 6 Electron density distribution

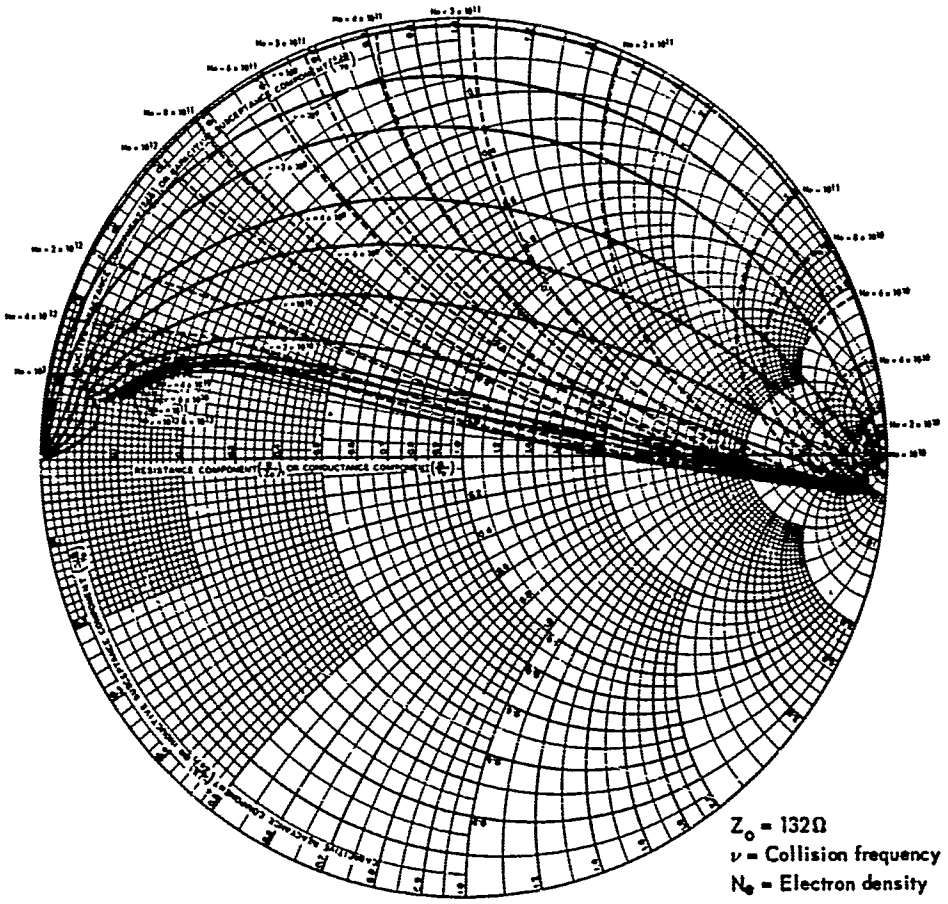


Fig. 7 Radial wave impedance for a uniform plasma

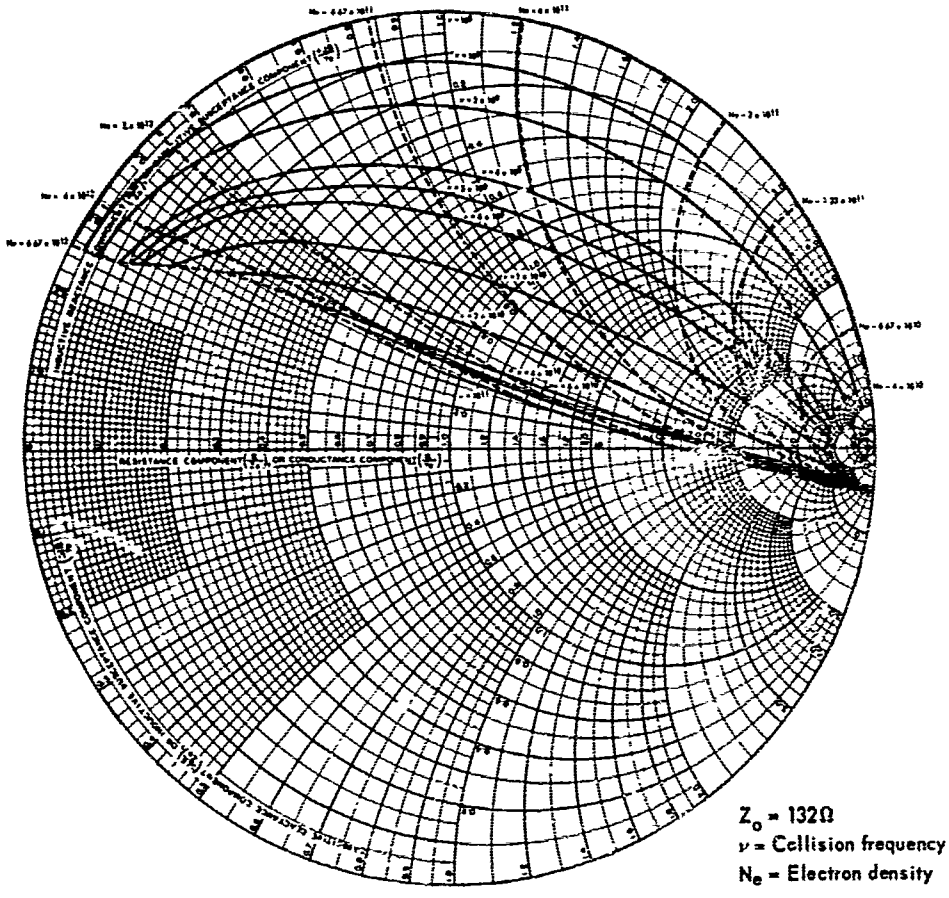


Fig. 8 Radial wave impedance for a non-uniform plasma

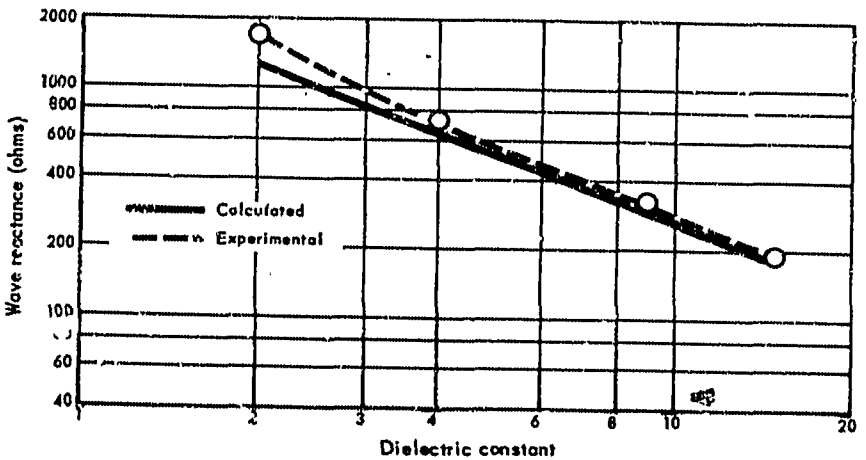


Fig. 9 Wave reactance as a function of dielectric constant

IX. REFLECTOMETER MEASUREMENT OF THE PLASMA SHEATH ENCOUNTERED DURING THE PROJECT ASSET FLIGHTS

R. J. Plugge
ElectroScience Laboratory
(formerly Antenna Laboratory)
Department of Electrical Engineering
The Ohio State University
Columbus, Ohio

ABSTRACT

The input impedance of an antenna was measured thoughout two flights of a hypersonic glide reentry vehicle, a VHF antenna in one case, and an X-band antenna in the other case. These data and a qualitctive discussion of their time history are presented here.

INTRODUCTION

The Asset vehicle is a hypersonic lifting re-entry vehicle designed to obtain basic aerodynamic, thermodynamic, and structural test data. A secondary objective of its flights was an evaluation of the effects of the plasma sheath on radio communication links between the vehicle and ground. The on-board measurement of the plasma effects was limited to a continuous impedance measurement of one antenna per vehicle. Data from two flights on different trajectories are shown here. One set of data was obtained from a VHF antenna, the other from an X-band antenna. *

This reflectometer experiment was conducted to determine the amount of mismatch introduced into the rf systems by the presence of the plasma sheath. As a secondary purpose, it was hoped that the

---

*The data on which this paper is based were furnished to this laboratory in the form of analog plots reduced from the original telemetry data. For some of the measured variables, several apparently inconsistent reductions were received. The reasons for the inconsistencies have not been fully resolved. Since the reflectometer was flown as an "add-on" experiment on a vehicle with a different primary mission, the antenna location was severely constrained. The chosen location made predictions of flow field conditions extremely difficult, so that it was almost impossible to determine what the reflectometer should have seen from theoretical considerations. The conclusions to be drawn from this experiment are therefore mostly of a qualitative nature. The present paper should be taken as a demonstration of the power of antenna measurements for the indication of flight conditions rather than as an accurate determination of the conditions of these particular flights.

effectiveness of antenna impedance measurements in providing vehicle flow field information would be demonstrated.

The plasma environment encountered during these flights caused impedance changes which appeared primarily as variations of the phase angle of the reflection coefficient. Thus, these results indicated relatively small reflection loss changes due to the plasma. The small reflection loss variation may be due to the particular VHF antenna used, which was mis-matched to the transmission line, or due to the fact that the plasma was of a relatively low density during the X-band measurement. Another possibility is that the denser plasma was located, for the most part, away from the antenna apertures. However, these results have shown that the reflection coefficient phase angle was still responsive to changes in the rf environment of the antenna, including the presence of the plasma sheath. This is taken to indicate that with suitable design and placement of the antennas, reflectometers can be useful tools for investigating plasma flow characteristics as well as the radio communication problems encountered during hypersonic flight.

A single impedance measurement determines values for only two variables. A vehicle's plasma sheath environment presents many more variables which affect the antenna impedance. Thus the main diagnostic value of impedance data from a single reflectometer is to support or reject plasma sheath models proposed on

the basis of aerodynamic knowledge. Since the plasma studies were a secondary objective of these flights, the communication links into which the reflectometers were inserted were not optimum for deducing plasma characteristics from impedance measurements. In particular, the VHF antenna was not readily amenable to theoretical analysis and both antennas were located at points on the vehicle where aerodynamic flow fields could not be accurately predicted. Therefore, because of the complexity of the aerodynamic and electromagnetic problems associated with this particular experiment no numerical results for the plasma parameters themselves were expected. Thus the data obtained are primarily of qualitative value, providing a demonstration of the responsiveness of these antennas to their environment.

EXPERIMENT DESCRIPTION

The shape of the vehicle and the antenna locations on its right flank are indicated in Fig. 1. It is apparent that the vehicle wing will greatly influence both the EM field and air flow in the vicinity of the antenna.

Both antennas were essentially linearly polarized, with the polarization parallel to the roll axis of the vehicle.

The VHF antenna[1] was a dielectric-loaded, cavity-backed, U-slot that was quite temperature sensitive. On the basis of the pre-flight temperature predictions and laboratory measurements of

the antenna, the antenna had been de-tuned to approximately a 12.4:1 VSWR prior to launch in the expectation that it would tune itself as a result of heating during the flight. However, it did not tune as much as expected. The X-band antenna[1] was an open-ended waveguide with a dielectric window.

The reflectometers were of a four-probe type[2] which provide both phase and amplitude data. The output data from the reflectometer are in the form of two voltages (V_1 and V_2). These voltages are the rectangular components of the reflection coefficient with reference to an arbitrary voltage plane (V-plane). When this V-plane is properly rotated for phase orientation, it is directly proportional to the reflection coefficient plane defined by Γ_R, Γ_i, or $|\Gamma|$, $\angle\Gamma$, the rectangular or polar coordinates of the Smith Chart.

The effective telemetry systems into which the reflectometers were inserted are shown in Fig. 2. These were conceptually the same for both frequencies except that the X-band transmitter was isolated from the antenna, whereas the VHF transmitter was not. This, of course, necessitated more calibration of the VHF system and increased its liability to error. Known loads were used to establish the loading effects on the VHF transmitter and the resulting reflectometer outputs. However, some variations seen in both the VHF and X-band data are presently unexplained and thus may indicate possible sources of error in the experimental system not accounted for

during calibration. The reader is therefore cautioned to accept these data as a demonstration of the sensitivity of antenna impedance measurements rather than as a necessarily accurate determination of the conditions during these particular flights.

The VHF communication link sampled was "blacked out" by the plasma sheath during a portion of the trajectory. Thus, the reflectometer data in both cases were telemetered via the X-band system or by delayed (tape) playback via the VHF system.

REFLECTOMETER DATA

The variations in the reflectometer data were primarily contained in one of the two output voltages on both flights. Thus, the variation of the reflection coefficient vs t, the time from launch, can be pictured qualitatively with the time history of only one voltage parameter. These are shown for the VHF and X-band antennas in Figs. 3 and 4, respectively.

The second voltage parameter of the VHF data remained at a nearly constant, relatively large value (-1.45) through the period where plasma induced effects were seen. Thus the impedance variations of the VHF antenna during this period were seen to be contained predominantly in phase angle variations which closely follow the curve in Fig. 3.

The reduced impedance data for the X-band antenna are shown in Fig. 5. The Smith Chart is normalized to the $TE_{1,0}$ wave impedance of the waveguide and the data are phase-referenced to the aperture of the antenna. The effects of the plasma sheath on the impedance of this antenna are also primarily seen in the changing phase angle of the reflection coefficient. In Fig. 5 there is a point indicating the impedance seen when a short circuit (aluminum foil) was placed at the vehicle skin. The data in Fig. 5 have not been corrected for the line loss from the reflectometer to the antenna aperture which is apparent in this short-circuit reference reading.

The X-band data is also shown plotted on the voltage plane in which it was measured in Fig. 6. The data points plotted in Fig. 6 and labeled 250+ through 600 are the average values determined by drawing a smooth curve through the impedance variations. The actual data points in the V_1, V_2 plane are shown in the inset. This inset and the V_2 trace shown in Fig. 4 illustrate that the actual antenna impedance measured oscillated from point 250 to approximately point 605 about the average values shown.

The point identification in these figures is the flight time in seconds.

Both the VHF and X-band data can be broken down into time points and periods which are of interest. A qualitative explanation of the time history of the antenna impedance follows.

THE VHF DATA

The slow change in impedance which occurred from lift off to t = 160 sec is at present unexplained. It could have been caused by an antenna temperature change, a change in the transmitter characteristics, or by drift in some part of the vehicle or data receiving systems. No other support for any explanation has so far been found.

Plasma induced variations of the impedance were observed from approximately $162 < t < 320$s. The vehicle angle of attack (α) was changed during a period prior to 180s in preparation for the glide phase of the flight. Deviation from free-space impedance conditions is noted to have begun at $t \simeq 162$s when α was slightly negative. The impedance continued to vary until $t \simeq 180$s. During the glide phase of the flight α was approximately 38°.

The impedance shows a relatively large phase change caused by the plasma when the angle of attack passed through zero degrees. It is also seen that as the angle of attack continued to increase, the impedance returned to nearly its free-space value before again indicating a phase variation. The rapid variation between 178 and 180s indicates the increasing effects of the dense plasma originating on the bottom of the vehicle at the higher angles of attack.

It is interesting to note that the signal strength data[3] showed a similar variation of the attenuation vs angle of attack during this

period. This signal strength variation has been seen[3] to indicate that plasma formed at the vehicle nose flowed first along the top of the wing past the antenna aperture at $\alpha \simeq 0°$ and then that it flowed above the antenna reducing the attenuation as the angle of attack increased. It also indicated that as the angle of attack continued to increase the dense plasma originating on the bottom of the vehicle flowed into the field of view of the antenna.

The "spike" in the data at 170.8s agrees with the time of retro fire and thus is attributed to reflection from the retro flame.

During the period $180 < t < 216$ a large positive angle of attack and dense plasma existed. Throughout this period the antenna "looked" at a dense "sheet" of plasma approximately at the wing edge. The plasma sheath also extended somewhat "upward" from the rear edge of the wing. Over the wing only a sparse, inhomogeneous plasma existed. The impedance seen during this 30-second period was essentially constant.

The inhomogeneous plasma over the wing, the dense plasma along the wing edge (side and back), the vehicle side, and the wing top are believed to have formed a type of trough waveguide during the time period $180 < t < 216$s. This trough would have redirected energy toward the top-rear of the vehicle. The trough and the direction of EM energy flow are illustrated on the right side of Fig. 7. The impedance seen during this period would thus have

resulted from the aperture coupling of the energy from the antenna into the trough waveguide mode.

A trough waveguide structure appropriate for the geometry of Fig. 7 has been investigated[4]. The combination of the angle subtended by the vehicle flank and the plasma sheath, the approximate plasma densities calculated for this flight period, and the operating frequency were seen to be sufficient to allow dominant mode propagation in this assumed trough waveguide model. It is hoped that the validity of this trough waveguide model will be substantiated by further analysis of the data.

During the time span $216 < t < 320$s a gradual change in the antenna impedance was measured, caused by the decrease in the plasma density resulting from the vehicle trajectory. By the end of this period the plasma density in the vicinity of the antenna had dropped to the point where it was no longer observable.

With the antenna again "seeing" free space, the impedance data indicate a reduced VSWR and a phase change from that seen at 160s. This resulted from the heating of the antenna which had occurred.

THE X-BAND DATA

The X-band data are shown in Figs. 4, 5, and 6. It was noted that impedance changes occurred both before and after the period in which plasma effects were expected.

At lift-off the antenna was only slightly mis-matched to free space. During the period $103 < t < 117$s a change in the reflection coefficient was noted. It was at first suspected that this might have been due to condensation in the air flow adjacent to the antenna. However, this is considered unlikely at the present time. Another unexplained impedance variation occurred at approximately 780s. Both these variations occurred at similar supersonic flight conditions.

Vehicle separation and the beginning of the glide phase occurred at 217.8s. The angle-of-attack transition ended by 228s. This vehicle also glided with a 38° angle of attack. The impedance measured was approximately constant from $219\text{s} < t \leq 250\text{s}$.

The trajectory and attitude data do not indicate any reason for believing that the impedance should have changed at $t = 250$s. The cause of the small phase angle variations beginning at $t = 250$s is unknown. There is insufficient calibration information available to remove the possibility of higher order mode contributions in the antenna window as it was heated. Also, a subliming ablative material existed on the top of the wing. A corner of this material, upstream

from this antenna aperture during the glide phase, is known to have peeled off and projected into the air stream at some point during the flight. This may have occurred here and produced ablation products which affected the antenna impedance.

The impedance variations are also noted to have continued long after plasma reflection induced variations would have been expected.

SUMMARY

The reflectometer data have shown that the input impedance of the antenna is sensitive to the density and position of the plasma sheath formed during re-entry. In addition the data have shown impedance sensitivity to the aerodynamic flow field characteristics and to antenna temperature, the latter being a side effect due to the characteristics of the particular antenna flown. When specifically designed for the purpose, an antenna and reflectometer system can be a useful tool for the study of both the aerodynamic flow field and radio communications in hypersonic flight, particularly when used in conjunction with other recorded flight data. The results obtained from these flights have prompted the study of a number of theoretical problems in this connection.

REFERENCES

1. Krah, J. W., "High Temperature Telemetry Antennas for Asset," OSU-RTD Symposium on EM Windows, Columbus, Ohio, Proceedings Vol. IV, 2-4 June 1964.

2. The design and operation of the reflectometers is discussed in: Bohley, P., R. Caldecott, R. McGown and R. C. Taylor, "Automatic Impedance Plotter for Missile Application," Report 1565-1, 1 February 1963, Antenna Laboratory, The Ohio State University Research Foundation; prepared under Contract AF 33(657)-10426, Research and Technology Division, Wright-Patterson Air Force Base, Ohio. AD 402-414. And also Bohley, P., R. Caldecott, R. McGown, and R. C. Taylor, "Measuring Missile Antenna Impedance in Flight," Electronics, McGraw-Hill Publishing Co., July 12, 1963.

3. Stolwyk, C. E. and C. A. Hinrichs, "Effects of Re-Entry Ionization on the Asset Communication System," IEEE-SEIG International Space Electronics Symposium, Las Vegas, Nevada, October 6-8, 1964. Also, Hinrichs, C. A., "Cursory Analysis of the ASV-1 Communication Link Performance," McDonnell Aircraft Corporation, Inter-Office Memo 411-151C-4211, 20 February 1964.

4. Dybdal, R. B., "Trough Waveguide Analysis of Glide Re-entry Vehicle," Report 2146-2, 15 April 1966, Antenna Laboratory, The Ohio State University Research Foundation; prepared under Contract AF 33(615)-3466, Systems Engineering Group, Research and Technology Division, Wright-Patterson Air Force Base, Ohio. (AD 486 778)

ACKNOWLEDGEMENTS

The research reported in this paper was sponsored in part by Contract Number AF 33(657)-1042 between Air Force Avionics Laboratory, Electronic Warfare Division, Electromagnetic Environment Branch, Propagation Group, Wright-Patterson Air Force Base, Ohio and The Ohio State University Research Foundation.

The reflectometer experiment was accomplished through the cooperation of the McDonnell Aircraft Corporation. It was designed by Messrs. R. Caldecott, R. C. Taylor, R. McGown, and P. Bohley of The Ohio State University ElectroScience Laboratory.

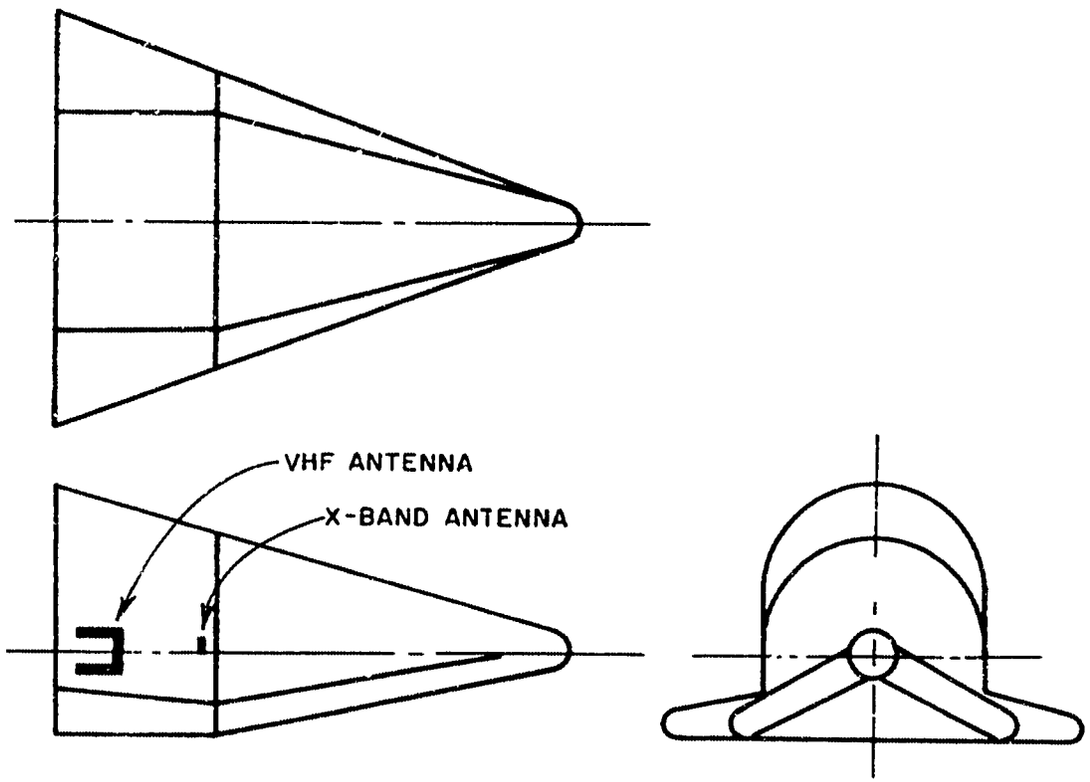


Fig. 1. The Asset vehicle showing the antenna locations.

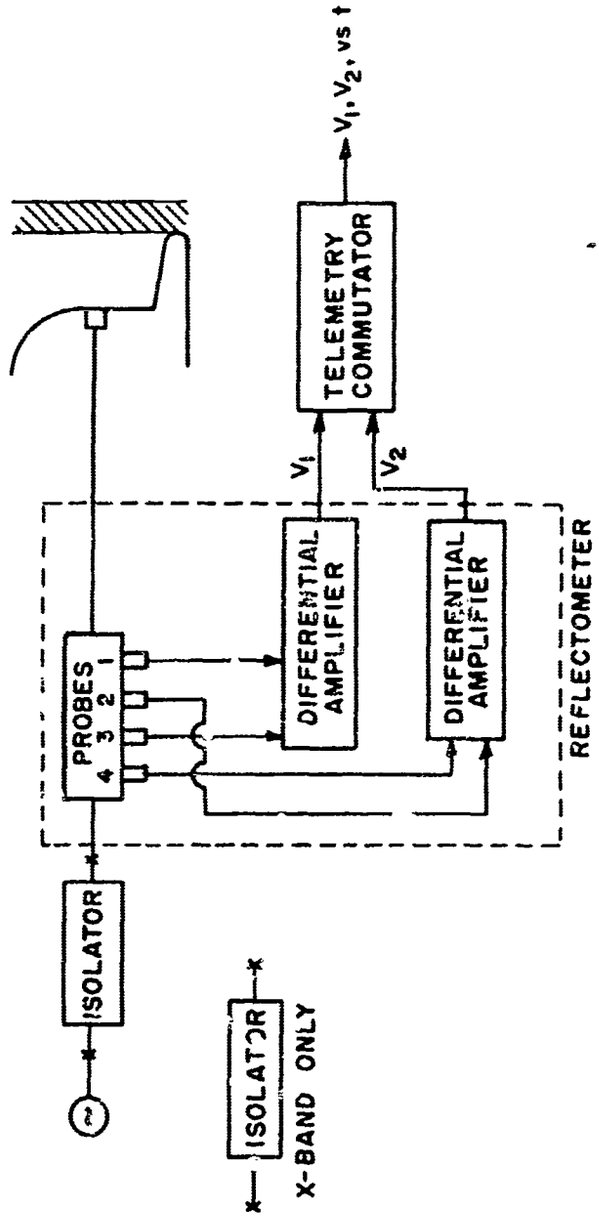


Fig. 2. Reflectometer system.

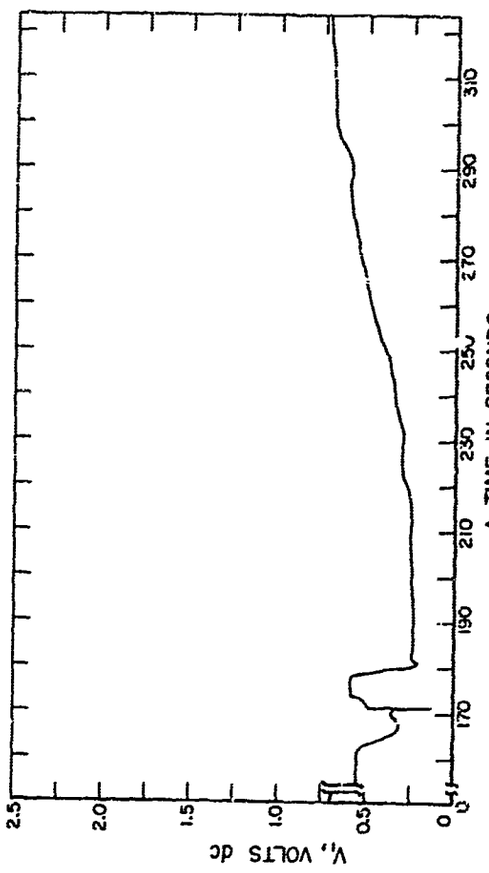


Fig. 3. Smoothed trace of one voltage versus time measured during the VHF measurement.

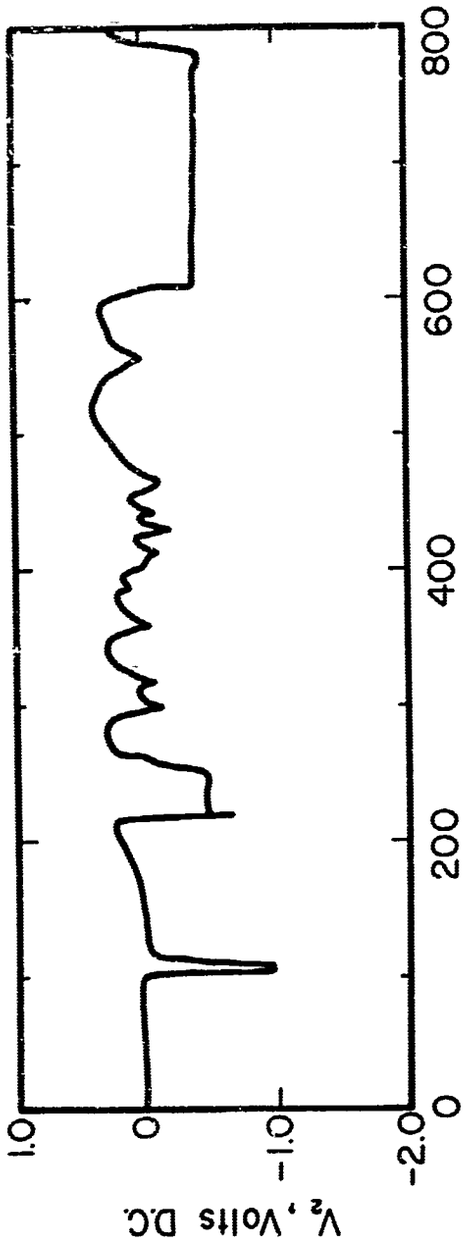


Fig. 4. Smoothed trace of one voltage measured versus time from launch during the X-band measurement.

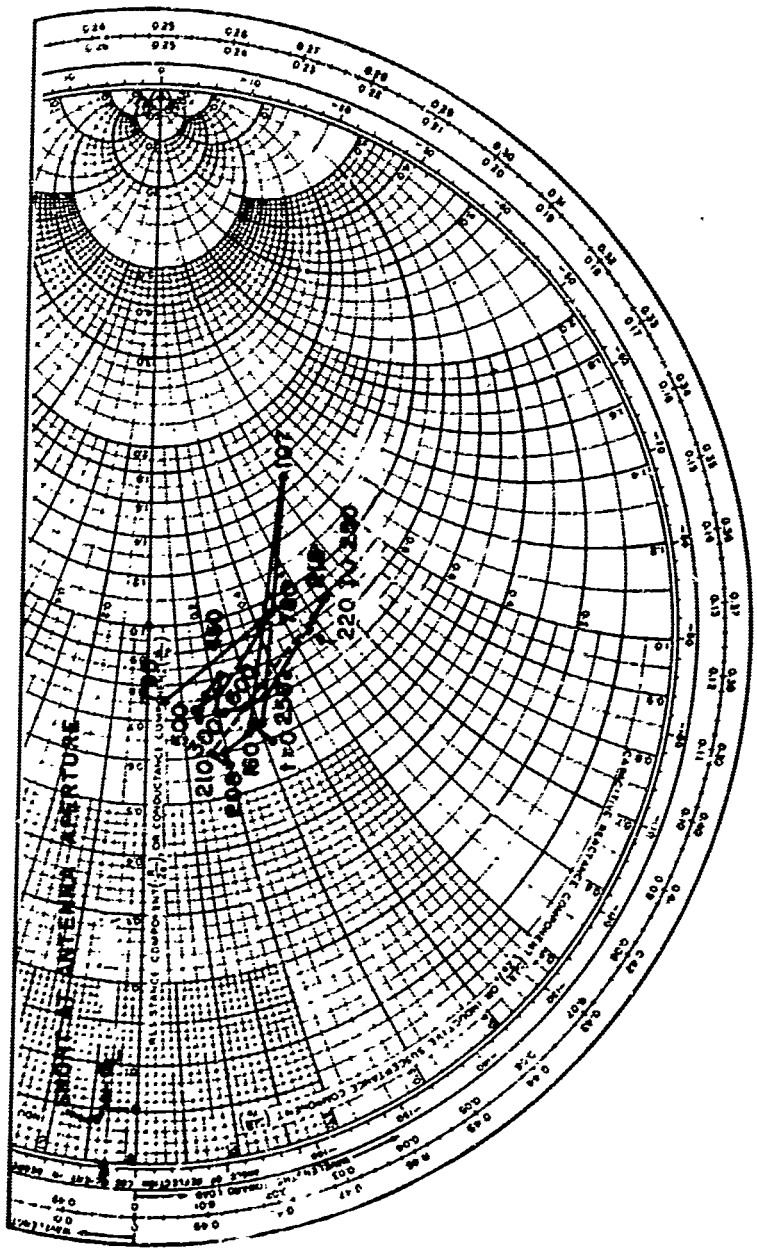


Fig. 5. X-band antenna impedance.

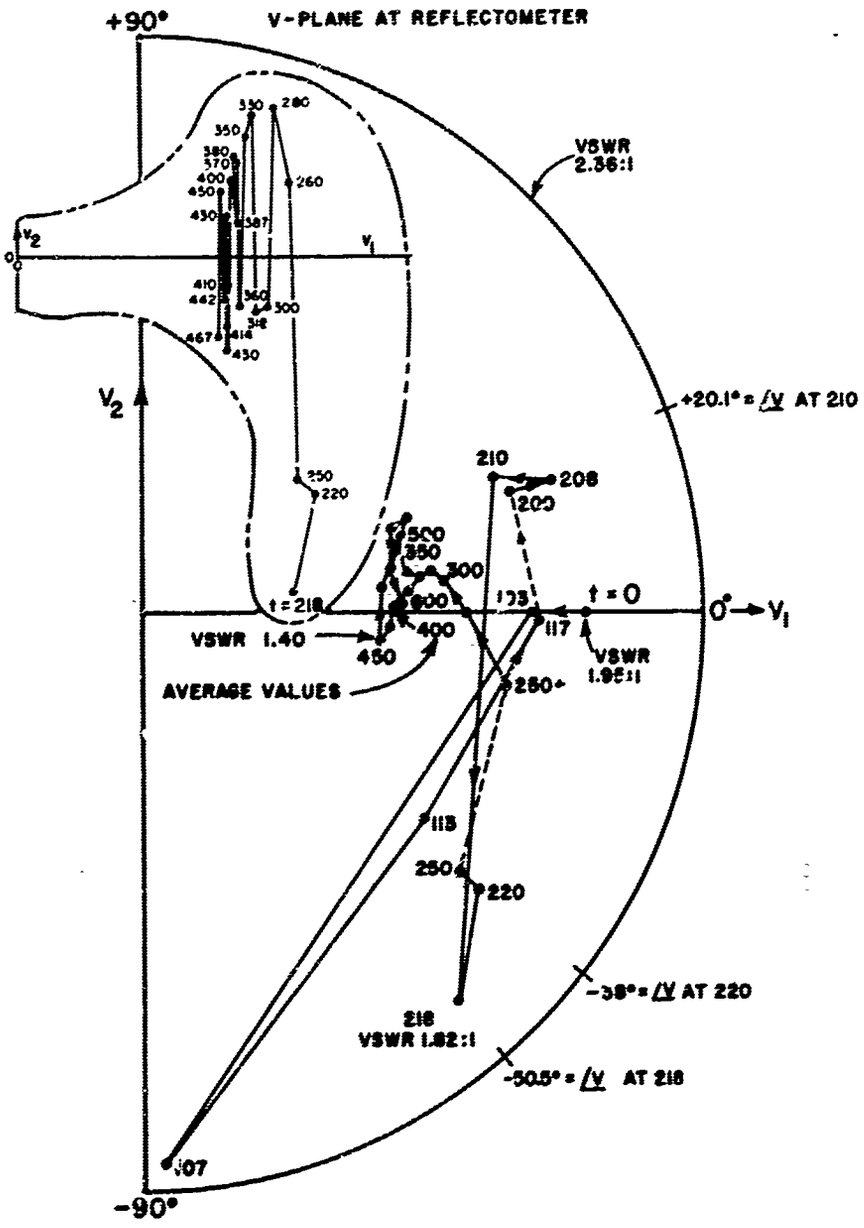


Fig. 6. X-band antenna impedance shown on the voltage plane.

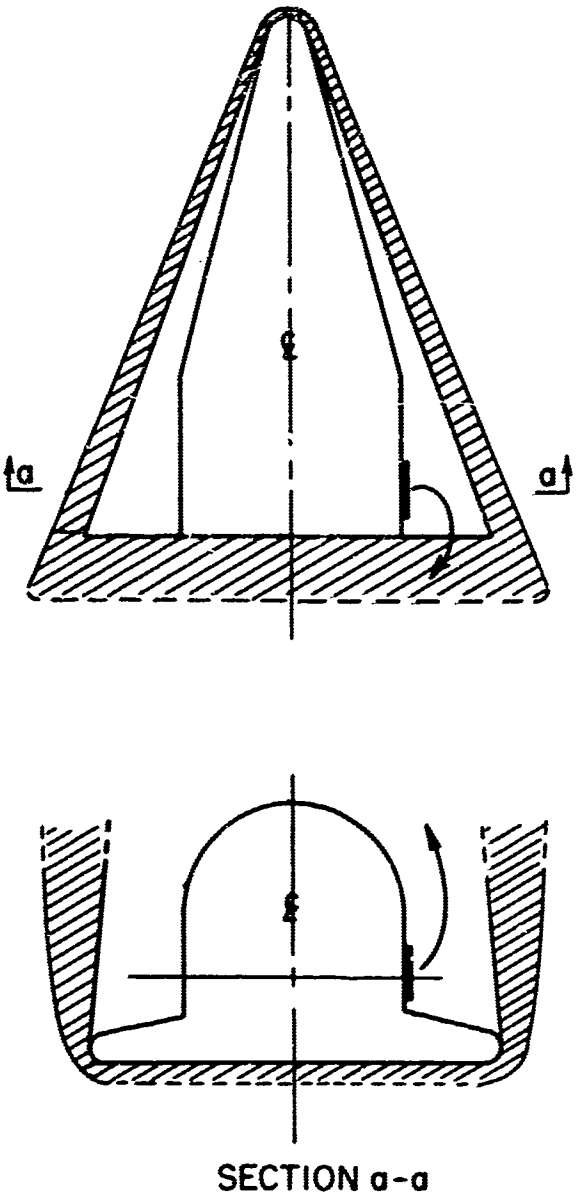


Fig. 7. Approximate flow for $\alpha \sim +40°$.

X. PLASMA SHEATH REDUCTION BY ELECTRON ATTACHMENT PROCESSES

A.I. Carswell and C. Richard

RCA Victor Company, Ltd.
Research Laboratories
Montreal, Canada

ABSTRACT

One promising technique for reducing the plasma sheath surrounding a re-entry vehicle involves the use of electronegative additives to "quench" the plasma by the process of electron attachment. Because of its very high cross-section for electron attachment, sulfur hexafluoride (SF_6) presents itself as a suitable material for plasma quenching and initial measurements on supersonic argon plasmas have served to support this. Because of the additional complexities of the possible reactions occurring in air plasmas seeded with electronegative gases, a laboratory experimental study of such systems has been undertaken. This paper presents recent findings on studies of nitrogen plasma flow systems which are seeded with SF_6, H_2O, O_2, CO_2 and NO. The apparatus developed for these studies is described and measurements at flow velocities up to about 10^4 cm/sec and for pressures between about 0.5 and 10 Torr are reported. The properties of the seeded afterglow plasmas are examined using electrical probing methods, optical spectroscopy and microwave techniques and the results of these diagnostics are discussed.

PLASMA SHEATH REDUCTION BY ELECTRON ATTACHMENT PROCESSES

A. I. Carswell and J. Richard
RCA Victor Company, Ltd.
Research Laboratories
Montreal, Canada

I. INTRODUCTION

It is well-known that the electron component of the plasma sheath surrounding a re-entry vehicle is the primary cause of the degradation in rf signal transmission. A possible technique for reducing the electron content of the plasma involves the use of electronegative additives. Such additives (e.g. the halogens) tend to replace the electrons in the plasma with heavier negative ions by the process of electron attachment. Since the more massive negative ions will only interact weakly with the high frequency rf field, an improvement in the signal transmission will be effected.

The laboratory study of such electron attachment processes has been pursued for many years under a variety of conditions and this information indicates that the process is a promising one for electron density reduction during re-entry. However, because of the very complex nature of the re-entry plasma, it is not possible to apply the existing data in such a manner that practical quantitative assessments can be made. The effects on the attachment process of phenomena in the flow field such as: shock-fronts, turbulence, chemical-kinetic reactions, ablation products etc. are extremely difficult to include in any analysis. Because of this, a series of laboratory investigations has been undertaken to examine the "quenching" efficiency of various electronegative additives in plasma flow systems having properties of relevance to re-entry conditions.

As in any attempt to simulate the re-entry environment in the

laboratory, the present systems cannot provide accurate simulation of all of the parameters, but by providing quantitative measurements of the important processes over a controllable range of conditions, much useful information can be obtained.

The results of earlier investigations on the seeding of supersonic argon plasma jets with electronegative gases have already been published[1,2] and in the present paper more recent measurements on the properties of nitrogen plasma flow systems seeded with SF_6, H_2O, CO_2, NO and O_2 are summarized.

During the course of the measurements in several flow systems, it has been found that the properties of the plasma are strongly influenced by changes in: wall conditions, gas purity, gas pressure and excitation power level. As a result, meaningful measurements can only be obtained if these factors are adequately controlled and monitored. This aspect influences the design of the apparatus and the diagnostic techniques, and some of these considerations are also presented in this paper.

II. ATTACHMENT PROCESSES

When an electron attaches to an atom to form a negative ion, energy is released since the energy of the stable negative ion is below that of the parent neutral atom. There are several mechanisms by which the attachment may take place.[3,4,5]

1. The radiative attachment of a free electron to a neutral atom,

$$e + A \rightarrow A^- + h\nu \qquad (1)$$

where the capture process is accompanied by the emission of radiation.

2. Capture of a free electron by an atom with a third body taking up the excess energy

$$e + A + B \rightarrow A^- + B + \text{kin.en.} \qquad (2)$$

3. Dissociative attachment, in which the electron is captured by a molecule with the excess energy going into dissociation of the molecule,

$$e + XY \rightarrow [XY]^{-*} \rightarrow X + Y^- \qquad (3)$$

4. Electron capture by a molecule with vibrational excitation of the molecule,

$$e + XY \rightarrow [XY]^{-*} \qquad (4a)$$

$$[XY]^{-*} + A \rightarrow [XY]^- + A + \text{kin.en.} + \text{pot.en.} \qquad (4b)$$

Concerning these various processes, it is known that the probability of radiative capture is quite small (of the order of 10^{-7} per collision) and that the probability of the 3-body capture process, being dependent on the availability of the third body, decreases with decreasing gas pressure.

The probability of the electron capture process can be expressed in several ways. The electron capture cross-section is defined in the conventional manner, and the electron attachment probability, h, used extensively in the earlier literature[6] is defined by:

$$h = \frac{\bar{\sigma}_a}{\bar{\sigma}_s} \qquad (5)$$

where $\bar{\sigma}_a$ and $\bar{\sigma}_s$ are respectively the average attachment cross section and average total scattering cross section for electrons.

In electron swarm experiments it is also convenient to define an

attachment coefficient. The change in electron concentration, n_e drifting under the action of a uniform field in an electronegative gas is given by:

$$dn_e = -\eta n_e dx \tag{6}$$

where η is the attachment coefficient representing the probability that an electron traversing unit distance (in the x-direction) will attach to a molecule. It can be shown[4-6] that η is related to $\bar{\sigma}_a$ by the expression

$$\eta = \frac{n_o \bar{\sigma}_a \bar{v}}{v_d} \tag{7}$$

where $\bar{v}$ and v_d are the electrons' average random and drift velocities respectively, and n_o is the number of electronegative molecules. Also, since $h = \lambda n_o \bar{\sigma}_a$, it is apparent that η and h are related by the expression:

$$\eta = \frac{h\bar{v}}{\lambda v_d} \tag{8}$$

where λ is the average electron mean free path.

For studies of the electron removal process in re-entry plasma it is desirable to examine electronegative materials having the greatest probability of electron attachment: i.e. materials having the greatest values of σ_a, h or η as tabulated in the existing literature.

Fig. 1 shows the attachment cross-sections, σ_a, for several of the gases used in the present investigation. Except for SF_6 the cross-sections shown are for dissociative attachment. These data illustrate the strong dependence of σ_a on the electron energy as well as the marked variation between different electronegative gases. The cross-sections exhibit a strong "resonance" behaviour being sharply peaked over a relatively narrow band of electron energies. An additional summary of some attachment cross-sections

is given in Table I.*

A comparison of the same gases on the basis of the attachment coefficient, η, is given in Fig. 2. Since η is a measure of the overall electron loss, independent of what the particular attachment process is, it is possible to have considerable differences in the relative values of η and σ_a depending on the range of electron energies. For example it is seen from Figs. 1 and 2 that although O_2 and H_2O do not show significant dissociative attachment at low energies, some non-dissociative attachment mechanism is significant enough to cause a large attachment coefficient (η/p) at low energy values.

Although the strong electronegativity of SF_6 is apparent in both Fig. 1 and Fig. 2, the complex variations of σ_a and η serve to illustrate some of the problems encountered in selecting, on the basis of existing data, the best electronegative gas for re-entry plasma quenching.

III. OTHER PROCESSES AFFECTING THE ELECTRON DENSITY

Except under very specially selected conditions, the electron density in any plasma will be affected by a number of processes in addition to attachment. In the examination of the attachment process in re-entry type plasmas it is, therefore, necessary to ascertain the relative importance of such interactions.

The various processes can be summarised in the form of an electron continuity equation of the form:

---

* An apparent typographical error in Ref. 14 leads to two values being cited for the cross-section of CO, viz: 2.7×10^{-18} and 2.7×10^{-19}, with the second one being correct and in agreement with Ref. 11. The incorrect value has been requoted in Refs. 5(p.285) and 15.

$$\frac{dn_e}{dt} = (\nu_i - \nu_a)n_e + \nabla.(D\nabla n_e) - k_r n_e^2 + Q(t) \qquad (9)$$

where

ν_i = ionisation collision frequency

ν_a = attachment frequency

D = diffusion coefficient for electrons

k_r = electron ion recombination rate

and $Q(t)$ = an unspecified time dependent ionization source included in some discussions of more complex systems[16].

Working with afterglows in the laboratory, it is often possible to distinguish between the various processes by their different dependence on the plasma parameters (e.g. electron density, gas pressure, container geometry).

In the design of a system for attachment studies, one of the aims would be to select, if possible, a combination of the parameters such that the attachment process dominates. If this can be done, equation (9) reduces to:

$$\frac{dn_e}{dt} = -\nu_a n_e \qquad (10)$$

giving an exponential time dependence for the electron density.

The attachment frequency, ν_a, is in general, further specified in terms of the two- and three-body attachment rate coefficients,[17] k_{2a} and k_{3a} giving:

$$\frac{dn_e}{dt} = -k_{2a}n_o(X)n_e - k_{3a}n_o(X)\, n_o(Y)n_e \qquad (11)$$

where $n_o(X)$ and $n_o(Y)$ are the number densities of the attaching molecules, X, and third bodies, Y. For a velocity independent cross-section the two-body rate coefficient and the cross-section are related by the expression

$$k_{sa} = \overline{\sigma_a}\,\overline{v} \tag{12}$$

Hence, from equation (7), if n_e and v_d are known, the attachment coefficient η can be computed from the rate constant k_{sa} or vice versa since

$$\eta = \frac{k_{sa} n_e}{v_d} \tag{13}$$

From the foregoing summary it is obvious that in a complex plasma such as that encountered during re-entry, or in a laboratory simulation facility, accurate measurements of the effectiveness of electronegative additives for electron removal will be extremely difficult to make. Experimental assessments of the relative magnitudes of the various terms in equation (9) have to be made over the range of plasma parameters of interest, and in general this is not readily accomplished - especially if there are electron sources in the plasma arising from chemical-kinetic reactions.

In the present investigation, continuous flow afterglow systems have been used so that the electronegative gas additives can be injected into a plasma whose salient properties can be measured before and after injection (i.e. upstream and downstream from point of seeding). In this way, the plasma source parameters are independent of the electronegative gas properties - a factor which cannot be achieved if the electronegative gas is introduced directly into the region where the plasma is being generated. The geometry of the apparatus has been kept simple (uniform cylinder) so that diffusion effects can be more readily assessed. The diagnostic techniques have been selected to provide good temporal and spatial resolution of the plasma properties.

Nitrogen has been used initially in the present experiments since it

is a gas which has properties of aerodynamic interest, but which does not give rise to many of the problems involved in analysing an air plasma. Some measurements have been made on air discharges, but as yet no quantitative seeding studies have been undertaken.

The nitrogen afterglow is useful for seeding studies, however, since it provides, in a region free from external fields, plasmas with electron densities two to three orders of magnitude lower than the primary discharge and electron temperatures at least an order of magnitude lower. Thus the present results with $5000°K < T_e < 15{,}000°K$ complement the temperature range previously studied[1,2] in the argon discharges where: $20{,}000°K < T_e < 100{,}000°$. Also, as in the re-entry plasma, the nitrogen afterglow mechanisms include plasma generation processes so that the quenching in the presence of electron production can be examined.

IV. APPARATUS

Fig. 3 shows a schematic diagram of one of the experimental arrangements used. The main body of the flow system consists of a pyrex tube 2.5 cm i.d. by 1.8 meters long. The high purity nitrogen (99.998%) gas is fed from a pressurized cylinder through a needle valve and is then excited by two external cylindrical electrodes connected to a 1 kw, rf power supply (13.5 Mc/sec). The discharge products proceed down the tube and towards the pumps. Electrical probes can be introduced into the flow as shown in the figure. These probes, inserted through O-ring seals, can be moved under vacuum and their length is sufficient to allow any point in the flow tube to be examined. Such an arrangement makes possible a continuous probing of a steady state flow.

The seed gases can be introduced either upstream or downstream of

the main discharge. The relative position of the downstream seeding can be varied by either adjusting the flow velocity or moving the rf excitation electrodes. Precision gauges and needle valves are used throughout the seed gas handling system for maximum control of the gas flow. Seeding ratios (seeding ratio = molecules of seed gas/molecules of N_2) as small as 10^{-4} can be measured readily. Flow velocities up to about 5×10^3 cm/sec have been attained with pressures ranging from 0.1 to 10 Torr.

Apart from electrostatic probe diagnostics, the experimental system also includes facilities for measuring optical emission from the afterglow. Two spectrometers are used to provide a detailed spectral analysis and the radiation from the afterglow can be directed into the spectrometers via a flexible optical fibre system so that, by scanning the fibre along the flow tube, any position of the afterglow can be examined. The scanning bench is fitted with an electrical position indicator so that plots of light output as function of position can be obtained directly on an X-Y recorder.

In addition to the spectral analysis spatial intensity variation of particular optical transitions of interest can be investigated with the aid of photomultipliers and a series of appropriate interference filters.

The interference filters used had a pass-band of approximately 100 Å and center frequencies were chosen to correspond with several of the most intense molecular nitrogen ion and neutral emission bands. (e.g. the first negative ($N_2^+[B^2\Sigma_u^+]$) 0-0, 0-1 and 0-2 bands at 3914 Å, 4278 Å and 4709 Å respectively, and the first positive ($N_2[B^3\pi_g]$) $\Delta v = 4$ series at approximately 5800 Å).

Microwave facilities are also available for making amplitude and phase measurements in the plasmas with both focussed and unfocussed

beams[18]. As yet, detailed microwave measurements of the afterglow plasma have not been made, chiefly because of the fact that at the low electron densities involved (e.g. 10^{10}/cc and lower) the spatial resolution of the microwave diagnostics is much poorer than that of the other techniques.

V. MEASUREMENTS ON PURE N_2

Since the quenching ability of seed gases was to be investigated by comparing the properties of seeded and unseeded nitrogen plasma flow fields, it was of importance to examine the properties of the pure nitrogen afterglow and to insure its reproducibility.

The nature of the early nitrogen afterglow is quite complicated and as yet, not fully understood, particularly with respect to the ion and electron production mechanisms in the so-called "pink" afterglow. In addition, the afterglow exhibits a rather "temperamental" behaviour being highly dependent upon gas pressure, impurity level, excitation power, temperature, wall conditions, etc. Hence measurements were made to determine the quantitative values and the spatial variations of the afterglow parameters in the present system. Electron (and ion) densities, electron, ion and gas temperatures, nitrogen atom, excited molecular neutral nitrogen (N_2^*) and excited molecular nitrogen ion (N_2^{+*}) relative densities were measured.[19]

Axial variations of the nitrogen afterglow properties were investigated over a range of velocities up to about 5×10^5 cm/sec and pressures between about one and ten Torr. Figures 4 and 5 show sample plots of the ion (and electron) density distribution and the electron temperature variations in the afterglow as obtained from double probe characteristics. The distribution shown in the curves presents the typical shape associated with the N_2 afterglow. The various regions of the afterglow are labelled in Fig. 4.

After the discharge region there is a tail flame which exhibits a rapid decay of ionization and electron temperature. A dark space follows where the ionization is extremely small ($< 10^7$/cc).

The pink glow in Fig. 4 shows two maxima in ionization at about 10 and 18 milliseconds after the discharge with ion concentrations of about 10^{10}/cc and 10^9/cc respectively.

The electron temperature (Fig. 5) shows a rapid decrease from a value of about 10^5 deg.K in the primary discharge to about 10^4 deg.K in the afterglow. It is interesting to note that because of the flow, the electron temperature shows its maximum at the downstream end of the discharge with lower values being recorded within the discharge itself. The rf fields used for generating the discharge were found to be present in the tail flame which extended about 10 cm from the electrodes as a visible "orange" discharge.

Experiments conducted in several systems under a variety of conditions have revealed the great sensitivity of the afterglow properties on the impurity level and wall conditions in the flow systems. With the present apparatus, it was found that the seeding of the nitrogen afterglow with SF_6 for example, could affect the tube walls in such a way that on subsequent running of a pure nitrogen flow, the afterglow intensity will be appreciably altered. Careful cleaning and handling of the system is required if reproducible results are to be obtained.

Figure 6 presents the axial variation of afterglow properties of pure N_2 as recorded by optical emission (using photo-multipliers and filters) at 3914 Å and 5780 Å and by double probe measurements. It is interesting to note that the structure of the afterglow as seen by the three measurables (N_2 ion emission, N_2 neutral emission and ion density) is virtually identical.

In general, such agreement was observed, whatever the detailed structure of the afterglow. The probe measurements, however, usually showed peaks which were more clearly resolved. This appears to indicate that the probes provide a somewhat better spatial resolution than the photomultiplier-systems (which integrate along their line of sight).

The simultaneous use of probe and optical emission illustrated in Fig. 6 provides a rapid means for making detailed analysis of the axial dependence of the afterglow and this method was also employed with the seeding investigations.

VI. MEASUREMENTS ON SEEDED FLOWS

Seeding experiments in nitrogen plasmas have been carried out using O_2, NO, CO_2, H_2O and SF_6. In the measurements to be described, the seed gas was introduced immediately downstream from the tail flame shown in Fig. 4. (approx. 15 cm from the discharge) and the seeded flow was investigated by the methods described above.

The general procedure consisted of examining the axial variation of the properties of the afterglow with the various diagnostic means for each different seeding ratio starting with the pure nitrogen and proceeding with increasing seeding rates. Sufficient time was given after any change of seeding rate (especially at low rates) in order to ensure that equilibrium had been reached in the flow system. Times of the order of one to five minutes were usually required. The reproducibility of the pure N_2 afterglow was checked before and after each run to ensure that apparatus contamination was not affecting the results.

6.1 O_2 Seeding

Figure 7 shows a sample variation of the intensity of the excited

ion emission (N_2^+ at 3914 Å) as the N_2 flow is seeded with O_2. It is noted then an O_2 concentration of about one percent (seeding ratio $\simeq 10^{-2}$) is sufficient to remove almost all traces of excited N_2^+ ion. Figure 8 presents a comparative plot of the decay in the afterglow of excited N_2 molecules, excited N_2^+ ions and the total ionisation as a function of the O_2 seeding ratio. This plot is typical of those obtained with the other seed gases. The first negative (e.g. 3914 Å) system is the first to show the effect of the seed gas, followed by the first positive system and closely by the total positive ion density.

Oxygen shows a dissociative attachment cross-section of 1.3×10^{-18} cm^2 at 6.7 ev, according to the two body process

$$e + O_2 \rightarrow O + O^-$$

Since the electron temperature prevailing in the afterglow is considerably less than 6.7 ev ($\sim$ 1 ev), it is unlikely that this mechanism can account for all of the observed quenching. It is possible that the three body process occurring around 1 ev and suggested by Hurst and Bortner[20] and Chanin et al[21] according to

$$e + O_2 + X(\text{third body}) \rightarrow O_2^- + X$$

is also effective. Studies made by Chanin et al have found a relatively high value for the over all attachment coefficient (η/p) in O_2 for low energy values (see Fig. 2).

6.2 NO Seeding

The quenching ability of NO was observed when employing the NO titration technique[22] to determine the ground state nitrogen above concentration in the nitrogen afterglow. Figure 9 illustrates the quenching

action on the first negative system (N_2^+ ion) along the afterglow for different NO seeding ratios. The quenching produced on the first positive system (N_2 molecule) and the total ion density is, as in the case of oxygen, comparable but slightly less.

Measurements performed by Bradbury[23] give NO an electron attachment probability of about 1/10 that of H_2O under the conditions prevailing in the present system. However, it is unlikely that electron attachment is the main reaction responsible for the observed quenching. It has been postulated[24] that the characteristics of the early N_2 afterglow can be explained by the interaction of a highly energetic (> 25.5 ev) loosely bound N_4 molecule interacting with atomic nitrogen and excited N_2 molecules. Therefore rapid removal of the atomic nitrogen by the NO could also be contributing to the plasma quenching.

6.3 CO_2 Seeding

Although the attachment cross section of CO_2 is not very large (Fig. 1), a strong quenching of the nitrogen afterglow by CO_2 was observed with considerable evolution of heat.

Figure 10 shows a sample variation of the total ion current along the afterglow for different CO_2 seeding ratios. The quenching of the two emission systems was found to be almost identical to that of Fig. 10. Here, a seeding ratio of about 1.5×10^{-3} is sufficient to reduce the ionisation to zero (i.e. to the background level).

The important electron attachment mechanism known to occur with CO_2 is dissociative attachment according to

$$CO_2 + e \rightarrow CO + O^-$$

which has a maximum measured cross-section of 4.5×10^{-19} cm^2 at 8.3 ev. Again, under the thermal conditions in the present system ($T_e < 1$ ev), the attachment alone is probably not sufficient to account for the quenching observed.

Milne et al[25], however, have found that near resonance vibrational energy transfer can take place between the vibrationally excited ground-state of N_2 and the ν_3 vibrational mode of CO_2, i.e.

$$N_2^* + CO_2 \rightarrow N_2 + CO_2^*$$

Since nitrogen molecules with large vibrational excitation are known to be present in the afterglow[26] this mechanism could also contribute to the afterglow quenching with CO_2.

6.4 H_2O Seeding

Water vapour is of considerable interest as a quenching agent owing to its high attachment coefficient at low E/p (Fig. 2) and its favourable effect on the recombination time. Both mechanisms result in the depletion of the free electron density in the plasma.

Figure 11 illustrates the strong quenching of the plasma produced by water vapour as seen by the 3914 Å filter. Seeding ratios of only 2×10^{-4} are sufficient to reduce the ionization by two orders of magnitude.

With H_2O as well as with SF_6, the low seeding ratios were achieved by preparing 10% mixtures of the seed gases in N_2. In order to assess the effects of the injected N_2 on the afterglow, pure N_2 was also seeded into the afterglow. Some reduction in ionization was observed, but it was several orders of magnitude smaller than that obtained with the H_2O-N_2 mixtures.

According to measurements by Muschlitz[27], two types of negative

ions (O^- and H^-) may result from the dissociative attachment following an electron-H_2O molecule encounter. OH^- may be produced by secondary reactions.

$$e + H_2O \rightarrow 2H + O^- \quad \text{(appearance potential: 6.3 ev)}$$

$$e + H_2O \rightarrow OH + H^- \quad \text{(appearance potential: 7.3 ev)}$$

$$H^- + H_2O \rightarrow OH^- + H_2$$

$$O^- + H_2O \rightarrow OH^- + O_2$$

Again, under the present conditions of operation, it is doubtful that the above dissociative attachment processes can account for the strong quenching measured. Measurements by Schulz[10] have shown that water vapour may not be efficient for electron attachment below about 2 ev energy. On the other hand, a large attachment coefficient (η/p) in water vapour has been measured, at low energies, by Kuffel[23] (see Fig. 2). According to Kuffel, this attachment is not of the dissociative type but is due to electrons attaching to large clusters of molecules - a concept also shared by Bradbury[23].

6.5 SF_6 Seeding

Among the electronegative gases, SF_6 presents one of the largest capture cross-sections for attachment of electrons. This cross-section is about 10^{-15} cm^2 for close to zero electron energy as shown in Fig. 1. A strong quenching should therefore be expected in the afterglow where the thermal condition is more favourable than it was for the previous seed gases. Results are shown in Fig. 12 where it is seen that complete quenching is achieved for a seeding ratio of about 10^{-5}.

The strong quenching of SF_6 can be seen by comparing the relative of efficiencies of the different seed gases for quenching the nitrogen afterglows. Figure 13 presents a composite plot of the relative quenching

of the nitrogen plasma by the various seed gases. The data plotted shows the reduction in the N_2^+ ion density as a function of the seeding ratio for SF_6, H_2O, CO_2, NO, O_2 and N_2.

As shown in Fig. 13, in the present studies, SF_6 is found to be the most effective quenching gas, followed by water vapour. This order corresponds to that expected on the basis of the value of the overall attachment coefficient at low energy (e.g. Fig. 2). The data of Fig. 13 is really a comparison of the quenching "per molecule" and on this basis, SF_6 is more effecient than H_2O. On the basis of quenching per unit mass, however, H_2O becomes equally effective since the molecular weights differ by almost an order of magnitude ($W_{H_2O} = 18$, $W_{SF_6} = 146$).

The quenching ability of CO_2 is less spectacular. CO_2 has been observed to be slightly more efficient than that of oxygen. As discussed above, this may be attributed to an efficient energy transfer between the vibrationally excited N_2 molecule and CO_2.

NO also proved to be a better quenching agent than O_2. In this instance, however, it is likely that the electron attachment is not an important process, but that most of the quenching is due to the reaction of NO with the ground-state nitrogen atoms which constitute a major reactant in the generation of the N_2 afterglow.

VII. CONCLUSION

The results presented in the previous section illustrate the relative quenching ability of several electronegative gases in the laboratory systems studied. Although such results do not provide all of the information required for assessing the effectiveness of seeding in a re-entry environment, they can provide useful data on several aspects of the problem.

It has been found that the electronegative additives in a complex plasma system do produce significant reductions in the ionisation over a wide range of conditions - even in the presence of electron production reactions. In the cases studied thus far, the results indicate also that a true plasma quenching is obtained, i.e. that the replacement of electrons by negative ions is rapidly followed by a charge neutralisation interaction which reduces the overall ionisation in the plasma.

In addition, it appears that the usefulness of the quenching process extends over a wider range of electron energies than might be expected from the known (resonance) attachment cross-sections of the various species (e.g. Fig. 1). In fact, it appears that in estimating the usefulness of such additives for re-entry applications, data on the attachment coefficient may be more useful that data on the specific attachment cross-sections.

As already pointed out, however, the attachment process is not the only property of the seed-gas which can determine its effectiveness for plasma quenching. The seed gas can have an effect on the electron-ion recombination time in the afterglow as has been reported by Kuhns[29] in water vapour and such processes must also be taken into account.

One limitation of the experiments already performed is the fact that, although the effectiveness of electronegative gases for plasma quenching has been demonstrated for a large range of electron temperatures (~ 5000°K in the present experiments, up to 10^5 deg.K in the rare gas experiments[1,28]), the ion and neutral gas temperatures employed have always been below about 1000°K.

There is the possibility of other effects at higher gas and ion energies which could limit the usefulness of the electron attachment process. For example, with large polyatomic attaching molecules such as SF_6, it is

possible that in the higher temperature plasmas the SF_6 molecules would be "fragmented" so that the large attachment cross-section of SF_6 would not determine the electron removal process. (Mass spectrometer studies in SF_6 seeded discharges[28] have shown a high degree of dissociation of SF_6 into SF_5, F_2 and F atoms.)

At higher gas and ion temperatures it is also known that the detachment rate of electrons from negative ions is increased[31-33] resulting in an apparent reduction of the attachment rate. Other interesting gas temperature effects on the attachment process in O_2 have been recently reported by Fite et al[34]. A measurement of the quenching of a combustion flame plasma by SF_6 seeding has been published recently[35] in which gas temperatures of the order of 3000°K were employed. The electron density reductions in the flames were found to be much smaller than those found in the present study. Although this may indicate the increase of detachment, the complexity of the flame plasma makes quantitative comparison difficult. The measurements are being continued in an effort to clarify the importance of ion and gas temperature effects on the attachment processes in re-entry plasma.

REFERENCES

1. A. I. Carswell and G.G. Cloutier, "Supersonic Plasma Streams Seeded with an Electronegative Gas" Phys.Fluids. Vol.7, p.602, (1964).
2. G.G. Cloutier and A.I. Carswell, "Plasma Quenching by Electronegative Gas Seeding", Phys.Rev.Letters, Vol.10, p.327 (1963).
3. H.S.W. Massey, Negative Ions Cambridge Un.Press, Cambridge, (1950).
4. E.W. McDaniel, Collision Phenomena in Ionised Gases John Wiley & Sons, New York, (1964).
5. J.B. Hasted, Physics of Atomic Collisions Butterworths, London (1964).
6. L.B. Loeb, Basic Processes of Gaseous Electronics Un. of California Press, Berkeley & Los Angeles, (1955).
7. M.A. Biondi and R.E. Fox, "Dissociative Attachment of Electrons in Iodine. III. Discussion" Phys.Rev. Vol.109, p.2012, (1958).
8. W.M. Hickam and R.E. Fox, "Electron Attachment in Sulful Hexafluoride Using Monoenergetic Electrons" J. Chem.Phys. Vol. 25, p.642, (1956).
9. (a) N.S. Buchelnikova, "Adhesion of Slow Electrons to SF_6 and CCl_4 Molecules", Soviet Phys. JETP, Vol.7, p.358, (1558).
   (b) N.S. Buchelnikova, "Cross-Sections for the Capture of Slow Electrons by O_2 and H_2O molecules and Molecules of Halogen Compounds", Soviet Phys. JETP, Vol.8, p.783, (1959).
10. G.J. Shulz, "Excitation and Negative Ions in H_2O" J.Chem.Phys. vol.33, p.1661, (1960).
11. G.J. Shulz, "Cross Sections and Electron Affinity for O^- Ions from O_2, CO and CO_2 by Electron Impact", Phys.Rev. Vol.128, p.178, (1962).

12. J.D. Craggs, R. Thorburn and B.A. Tozer, "Attachment of Slow Electrons in Oxygen", Proc.Roy.Soc., Vol.A240, p.473, (1957).

13. Asundi and J.D. Craggs, in Atomic Collision Processes, ed. M.R.C. McDowell North-Holland, Amsterdam, p.549, (1964).

14. J.D. Craggs and B.A. Tozer, "The Attachment of Slow Electrons in Carbon Monoxide", Proc.Roy.Soc. Vol. A247, p.337, (1958).

15. D.R. Bates, ed., Atomic and Molecular Processes Academic Press, New York p. 210, (1962).

16. W.B. Kunkel, "Analysis of Ionic Recombination Including Ion Production during Measurement", Phys.Rev., Vol.84, p.218, (1951).

17. L.M. Chanin, A.V. Phelps and M.A. Biondi, "Measurement of the Attachment of Low Energy Electrons to Oxygen Molecules", Phys.Rev. Vol.128, p.219, (1962).

18. A.I. Carswell and C. Richard, "Focussed Microwave Systems for Plasma Diagnostics", RCA Victor Rept. 7-801-32 Dec. (1964).

19. A.I. Carswell, C. Richard and A.K. Ghosh, "Electrochemical Properties of Seeded Plasma Flow Fields II", RCA Victor Rept. 7-801-39, June,(1965).

20. F.E. Bortner and G.S. Hurst, "An Apparatus for Measuring Electron Attachment: Results for Oxygen in Argon", Health Phys. Vol.1, p.39, (1958).

21. L.M. Chanin, A.V. Phelps and M.A. Biondi, "Measurement of Attachment of Slow Electrons in Oxygen", Phys.Rev.Letters, Vol.2 p.344, (1959).

22. K.P. Hartock, R.K. Reeves and G. Mannella, "Rate of Recombination of Nitrogen Atoms", J.Chem.Phys. Vol.29, p. 608, (1958).

23. N.E. Bradbury, "Formation of Negative Ions in Gases by Electron Attachment. Part II. CO_2, N_2O, SO_2, H_2S, H_2O" J.Chem.Phys. Vol.2, p.835, (1934).

24. A.B. Prag and K.C. Clark, "Excitation Mechanism for the Nitrogen Pink Afterglow", J.Chem.Phys. Vol.39, p.799, (1963).

25. E.L. Milne, M. Steinberg and H.P. Broida, "Vibroluminescence of CO_2 and N_2O in Active Nitrogen", J.Chem.Phys. Vol.42, p.2615, (1965).

26. A.M. Bass, "Absorption Spectrum of the Pink Afterglow of Nitrogen in Vacuum Ultraviolet", J.Chem.Phys. Vol.40, p.695, (1964).

27. E.E. Muschlitz Jr., "Formation of Negative Ions in gases by Secondary Collision Processes", J.Appl.Phys. Vol. 28, p.1414, (1957).

28. E. Kuffel, "Electron Attachment Coefficients in Oxygen, Dry Air, Humid Air and Water Vapour", Proc.Phys.Soc. Vol.74, p.297 (1959).

29. P.W. Kuhns, "Microwave Measurements of Steady State and Decaying Plasmas", IEE Trans. Vol. SET-8 p.173, (1962).

30. G.G. Cloutier, C. Richard, "Generation of Negative Ions in a Gas Discharge", RCA Victor Rept. 7-811-6, Nov. (1963).

31. A.V. Phelps and J.L. Pack, "Collisional Detachment in Molecular Oxygen", Phys. Rev.Letters, Vol. 6, p.111, (1961).

32. P.J. Chantry, J.S. Wharmby and J.B. Hasted in Proc. 5th Int. Conf. on Ionisation Phenomena in Gases, North Holland, Amsterdam, p.630, (1961).

33. R. Hackam and J.J. Lennon, "Microwave Measurements of Temperature Dependence of Electron Density Decay Rates in Oxygen and Oxygen-nitrogen Mixtures" Proc.Phys.Soc. Vol. 86, p.123, (1965).

34. W.L. Fite, R.T. Brackman and W.R. Henderson Proc. 4th Int. Conf. on Physics of Atomic Collisions Laval.Un. Aug. 1965.

35. J. Hoffman, E.A. Westbrook, "Flame Plasma Seeded with Sulfur Hexafluoride", Phys.Fluids, Vol. 8, p.1410, (1965).

ACKNOWLEDGEMENTS

The authors wish to express their appreciation to Dr. A.K. Ghosh and Mr. J. Sheppard for their contributions to the work described in this paper. This research was supported by the Advanced Research Projects Agency under Contract No. NOnr-4596(00).

TABLE I - Attachment Cross-Sections of Common Electronegative Gases.

Molecule	First Peak		Second Peak		Ref
	Energy (ev)	σ/s (cm^2)	Energy (ev)	σ/s (cm^2)	
I_2	~ 0	3.2×10^{-15}			5,7
$SF_6 \rightarrow (SF_6^-)$	~ 0	1.2×10^{-15}			4,8
$SF_6 \rightarrow (SF_5^-)$	~ 0.1	5.7×10^{-16}			9
CCl_4	0.02	1.3×10^{-16}	0.6	1.0×10^{-16}	9
HB_r	0.5	5.8×10^{-17}			9
H_2O	6.4	4.8×10^{-18}	8.8	1.3×10^{-18}	9,10
HCl	0.6	3.9×10^{-18}			9
O_2	6.7	1.3×10^{-18}			11,12
CO_2	4.3	1.3×10^{-19}	8.3	4.5×10^{-19}	11,13
CO	10.1	1.6×10^{-19}			11,14,15

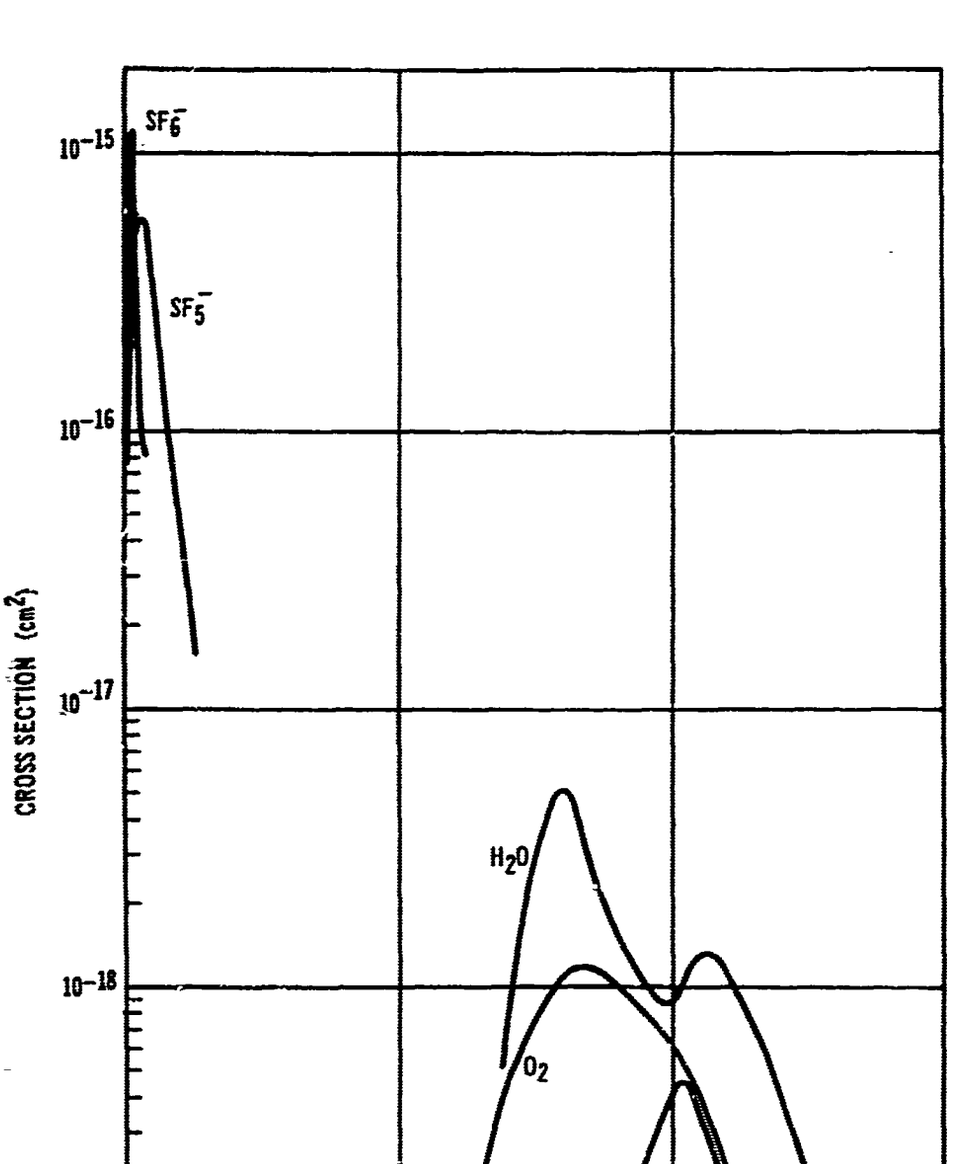

SF_6^-
SF_5^-
H_2O
O_2
CO_2
CO_2
CO
10^{-15}
10^{-16}
10^{-17}
10^{-18}
10^{-19}
CROSS SECTION (cm^2)
2
4
6
8
10
12
ELECTRON ENERGY (eV)

Figure 1.

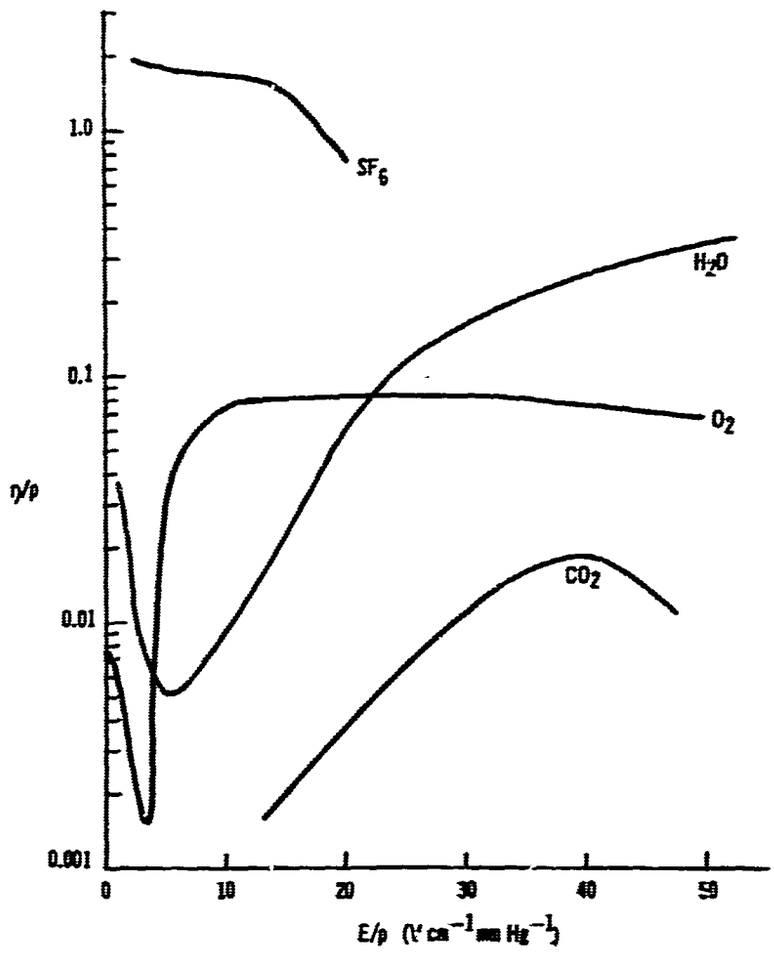


Figure 2.

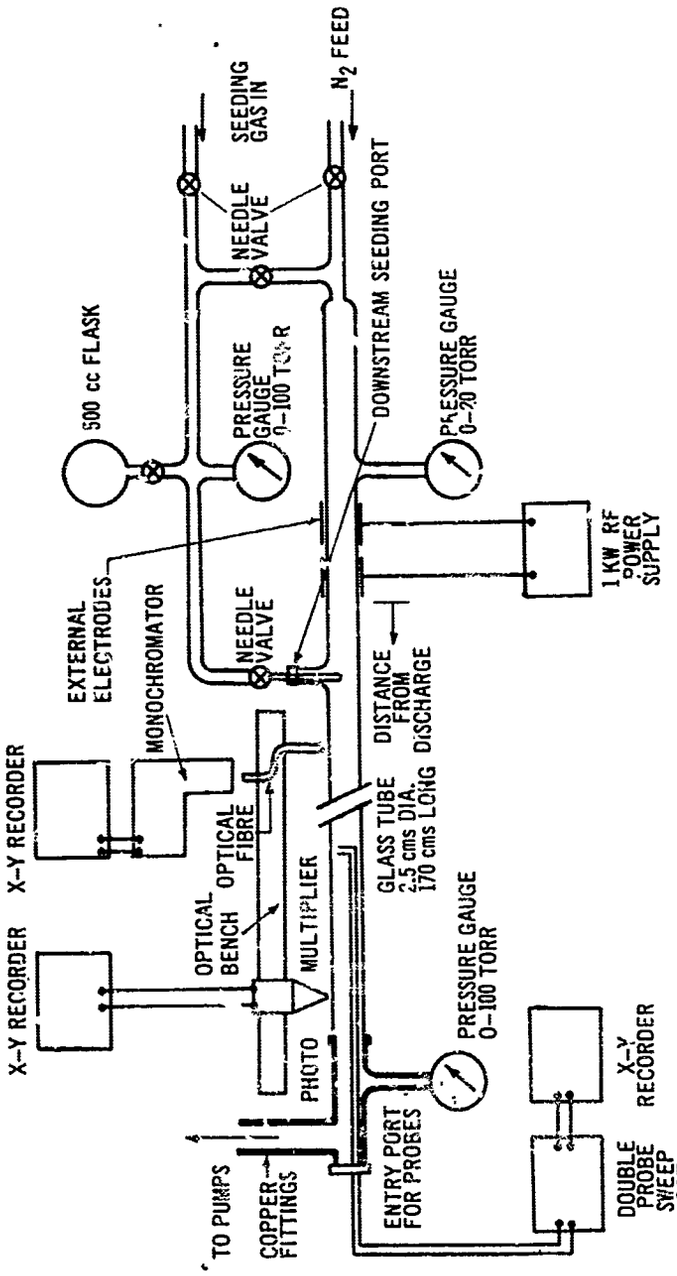

500 cc FLASK
PRESSURE GAUGE 0–100 TORR
NEEDLE VALVE
SEEDING GAS IN
N_2 FEED
DOWNSTREAM SEEDING PORT
PRESSURE GAUGE 0–20 TORR
1KW RF POWER SUPPLY
EXTERNAL ELECTRODES
NEEDLE VALVE
MONOCHROMATOR
X–Y RECORDER
X–Y RECORDER
OPTICAL BENCH
OPTICAL FIBRE
MULTIPLIER
DISTANCE FROM DISCHARGE
GLASS TUBE 2.5 cms DIA. 170 cms LONG
PRESSURE GAUGE 0–100 TORR
PHOTO
TO PUMPS
COPPER FITTINGS
ENTRY PORT FOR PROBES
X–Y RECORDER
DOUBLE PROBE SWEEP CCT

Figure 3.

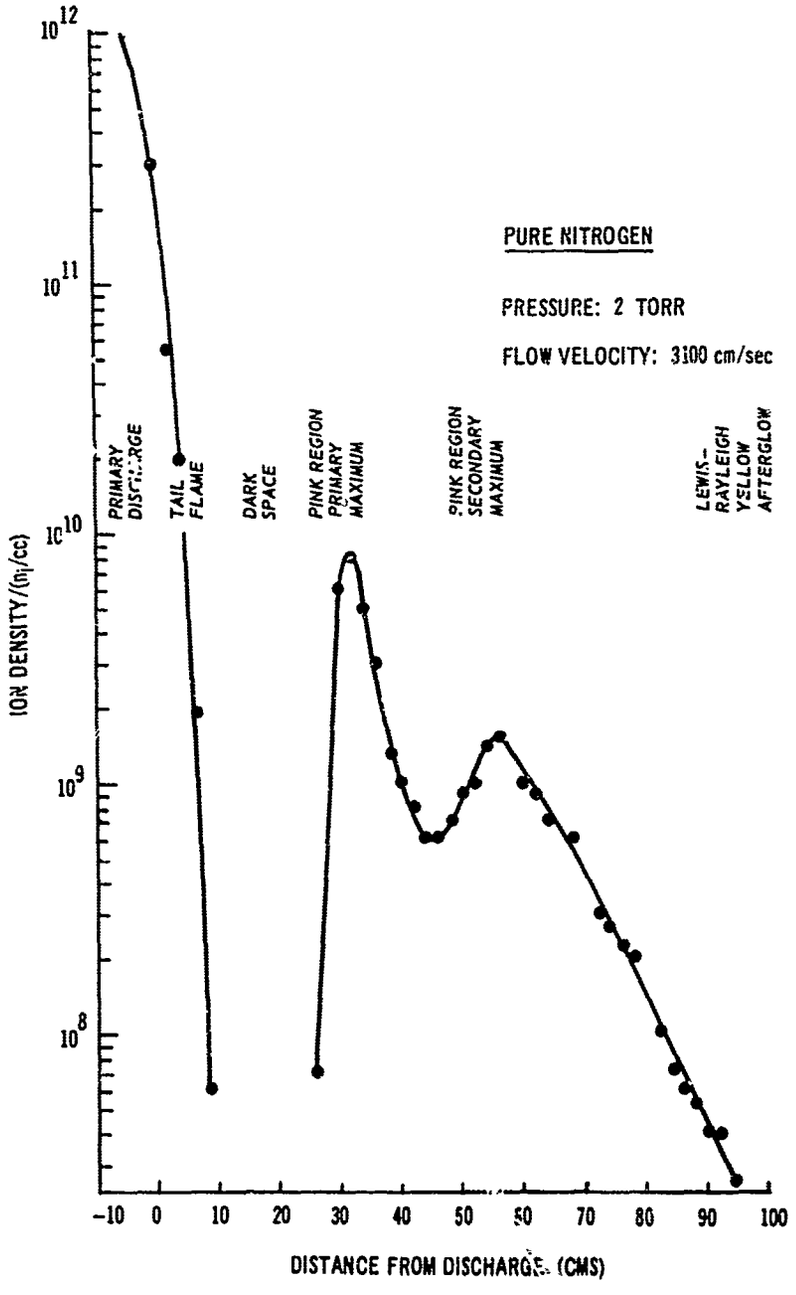

PURE NITROGEN
PRESSURE: 2 TORR
FLOW VELOCITY: 3100 cm/sec
PRIMARY DISCHARGE
TAIL FLAME
DARK SPACE
PINK REGION PRIMARY MAXIMUM
PINK REGION SECONDARY MAXIMUM
LEWIS-RAYLEIGH YELLOW AFTERGLOW
ION DENSITY/(n_i/cc)
10^{12}
10^{11}
10^{10}
10^{9}
10^{8}
−10 0 10 20 30 40 50 50 70 80 90 100
DISTANCE FROM DISCHARGE (CMS)

Figure 4.

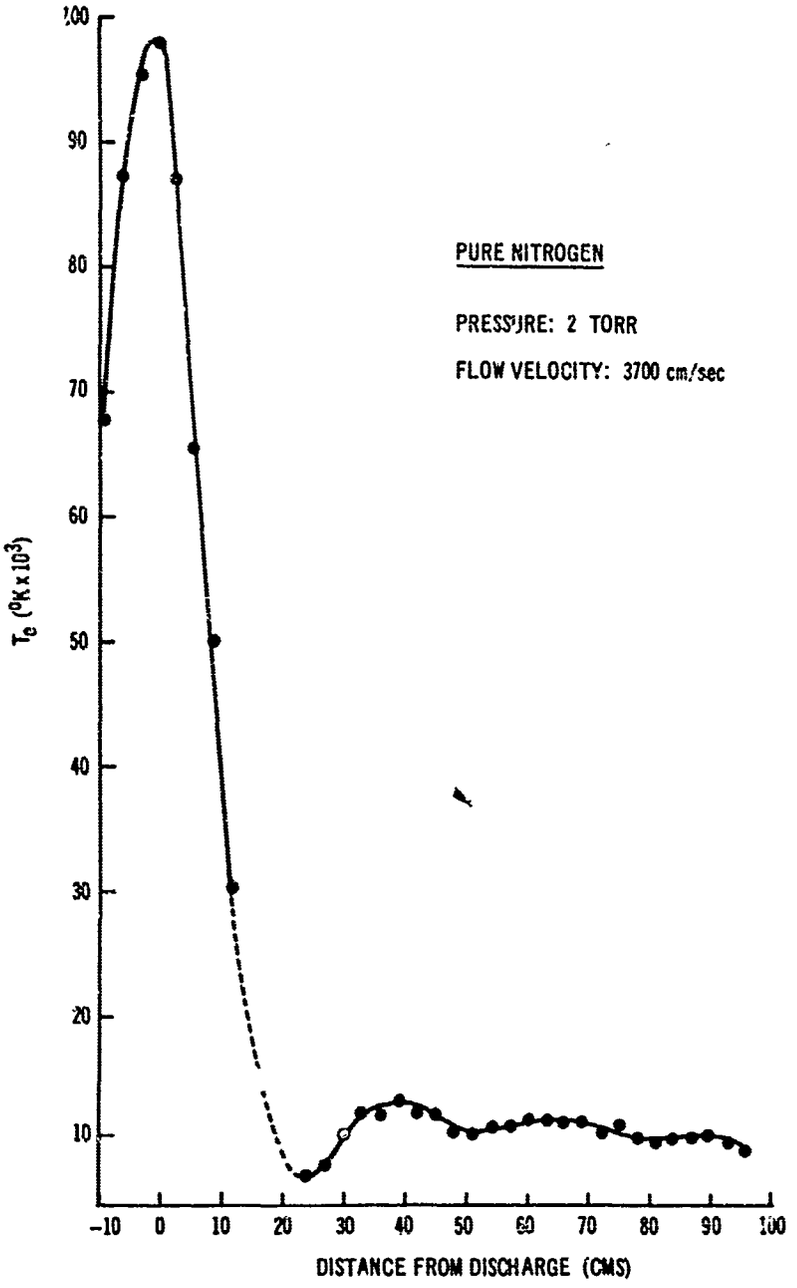

PURE NITROGEN
PRESSURE: 2 TORR
FLOW VELOCITY: 3700 cm/sec
T_e ($^0K \times 10^3$)
100
90
80
70
60
50
40
30
20
10
-10
0
10
20
30
40
50
60
70
80
90
100
DISTANCE FROM DISCHARGE (CMS)

Figure 5.

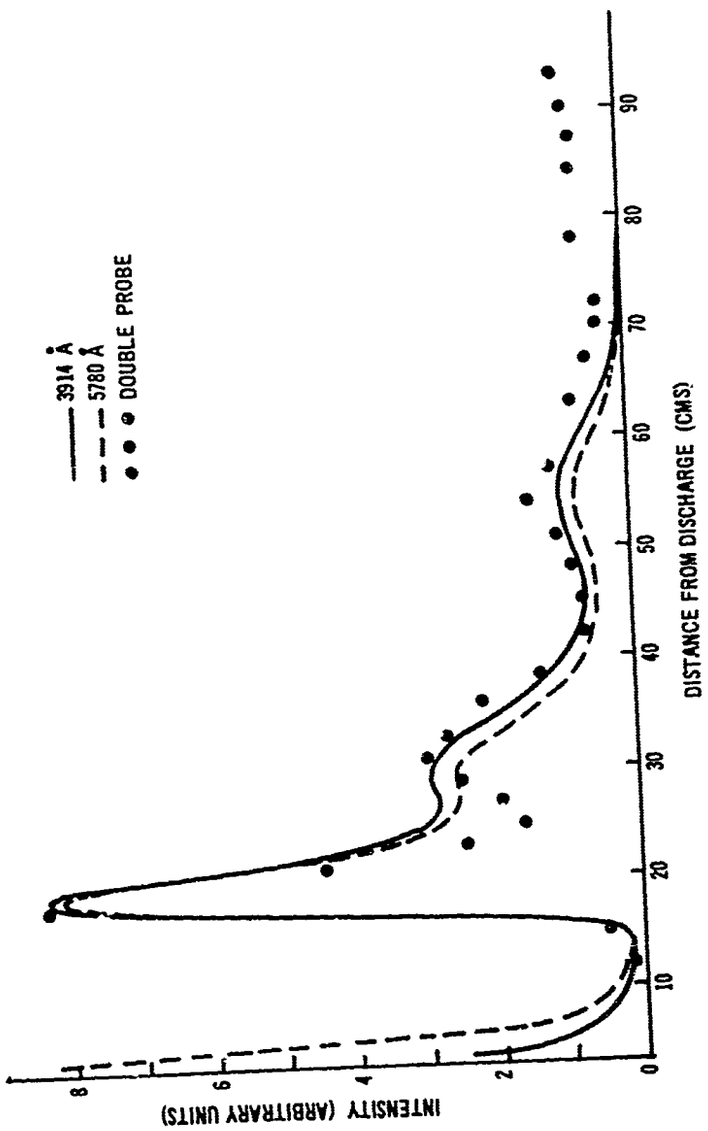

3914 Å
5780 Å
DOUBLE PROBE
INTENSITY (ARBITRARY UNITS)
DISTANCE FROM DISCHARGE (CMS)
0
2
4
6
8
10
20
30
40
50
60
70
80
90

Figure 6.

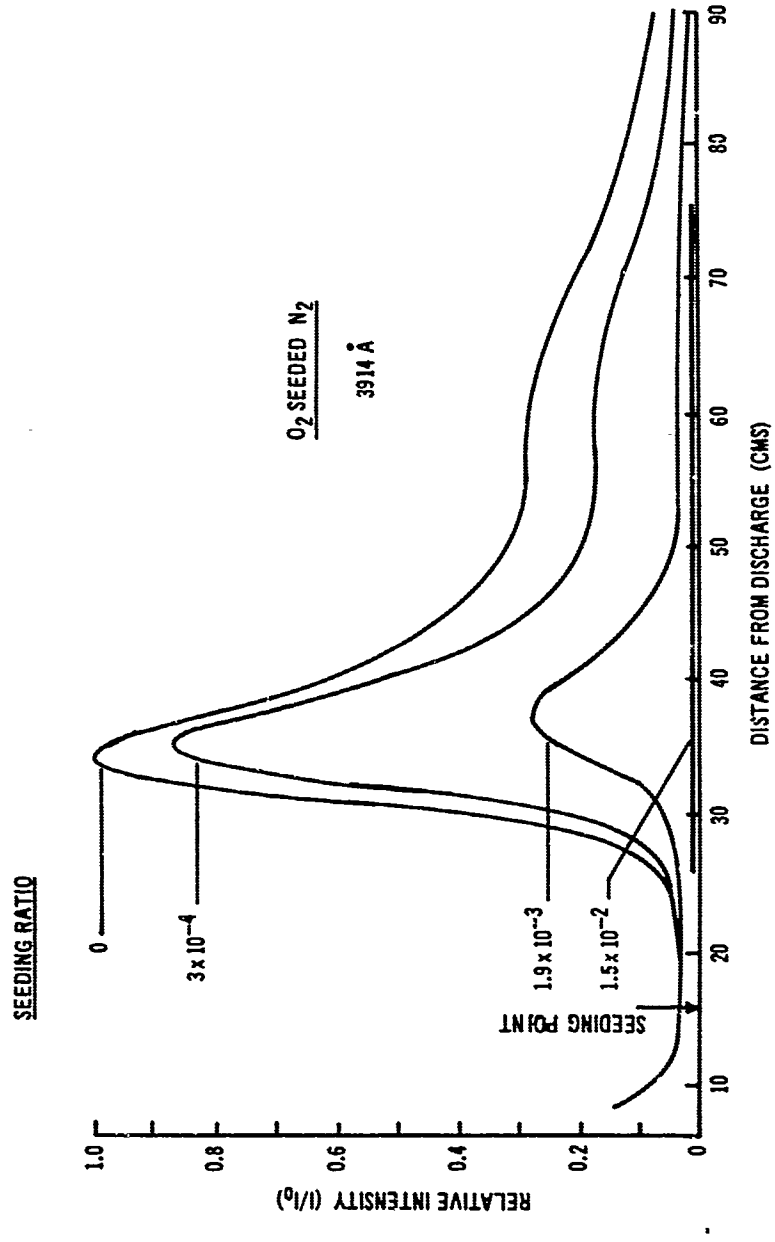

O_2 SEEDED N_2
3914 Å
SEEDING RATIO
0
3×10^{-4}
1.9×10^{-3}
1.5×10^{-2}
SEEDING POINT
RELATIVE INTENSITY (I/I_0)
1.0
0.8
0.6
0.4
0.2
0
10
20
30
40
50
60
70
80
90
DISTANCE FROM DISCHARGE (CMS)

Figure 7.

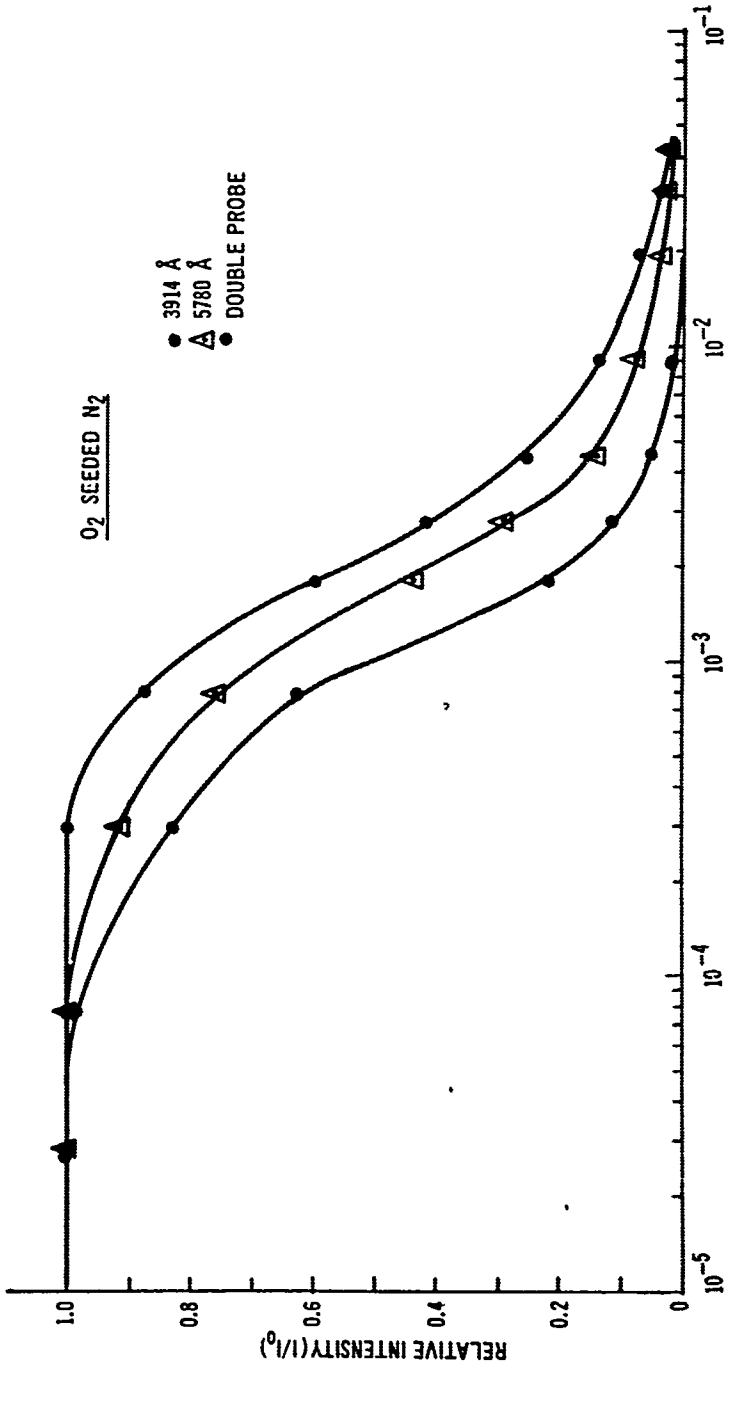

O_2 SEEDED N_2
3914 Å
5780 Å
DOUBLE PROBE
RELATIVE INTENSITY (I/I_0)
1.0
0.8
0.6
0.4
0.2
0
10^{-5}
10^{-4}
10^{-3}
10^{-2}
10^{-1}
SEEDING RATIO (O_2/N_2)

Figure 8.

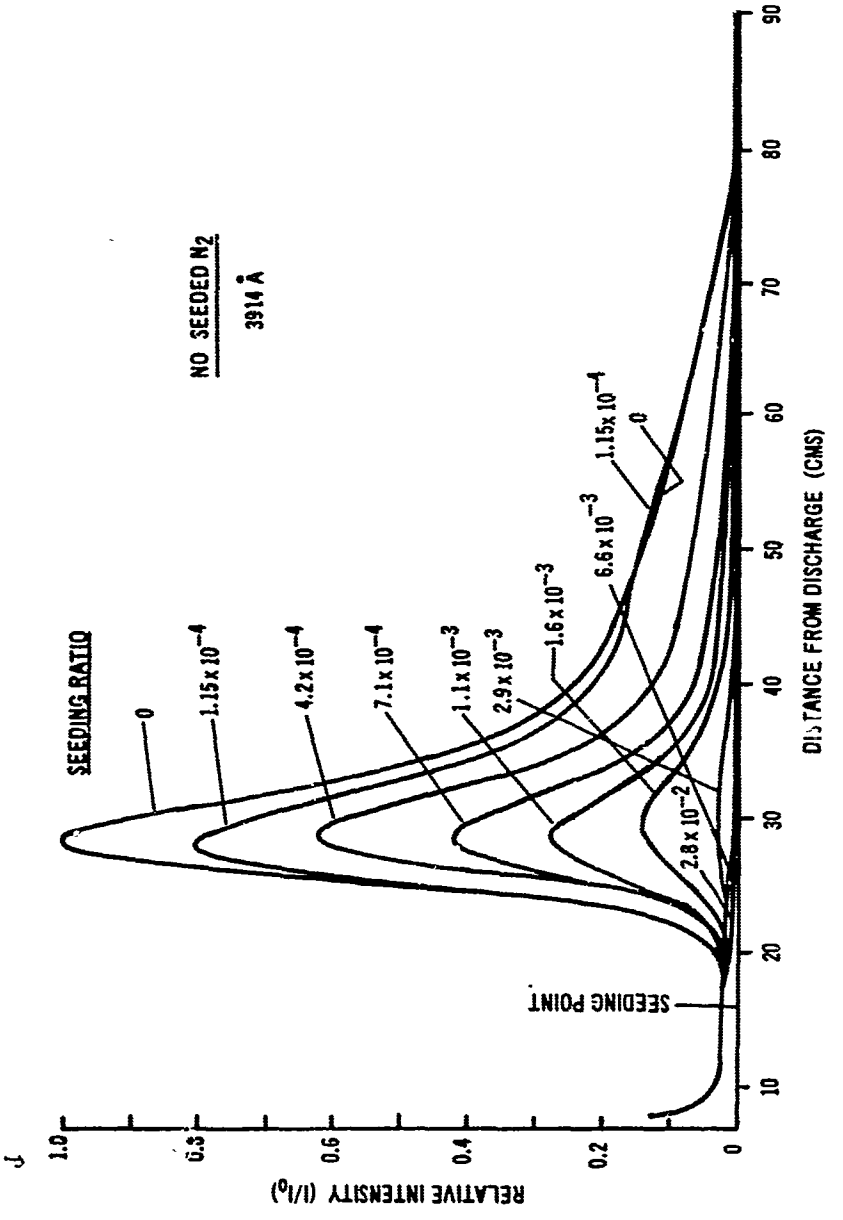

NO SEEDED N_2
3914 Å
SEEDING RATIO
0
1.15×10^{-4}
4.2×10^{-4}
7.1×10^{-4}
1.1×10^{-3}
2.9×10^{-3}
1.6×10^{-3}
6.6×10^{-3}
1.15×10^{-4}
0
2.8×10^{-2}
SEEDING POINT
RELATIVE INTENSITY (I/I_0)
DISTANCE FROM DISCHARGE (CMS)

Figure 9.

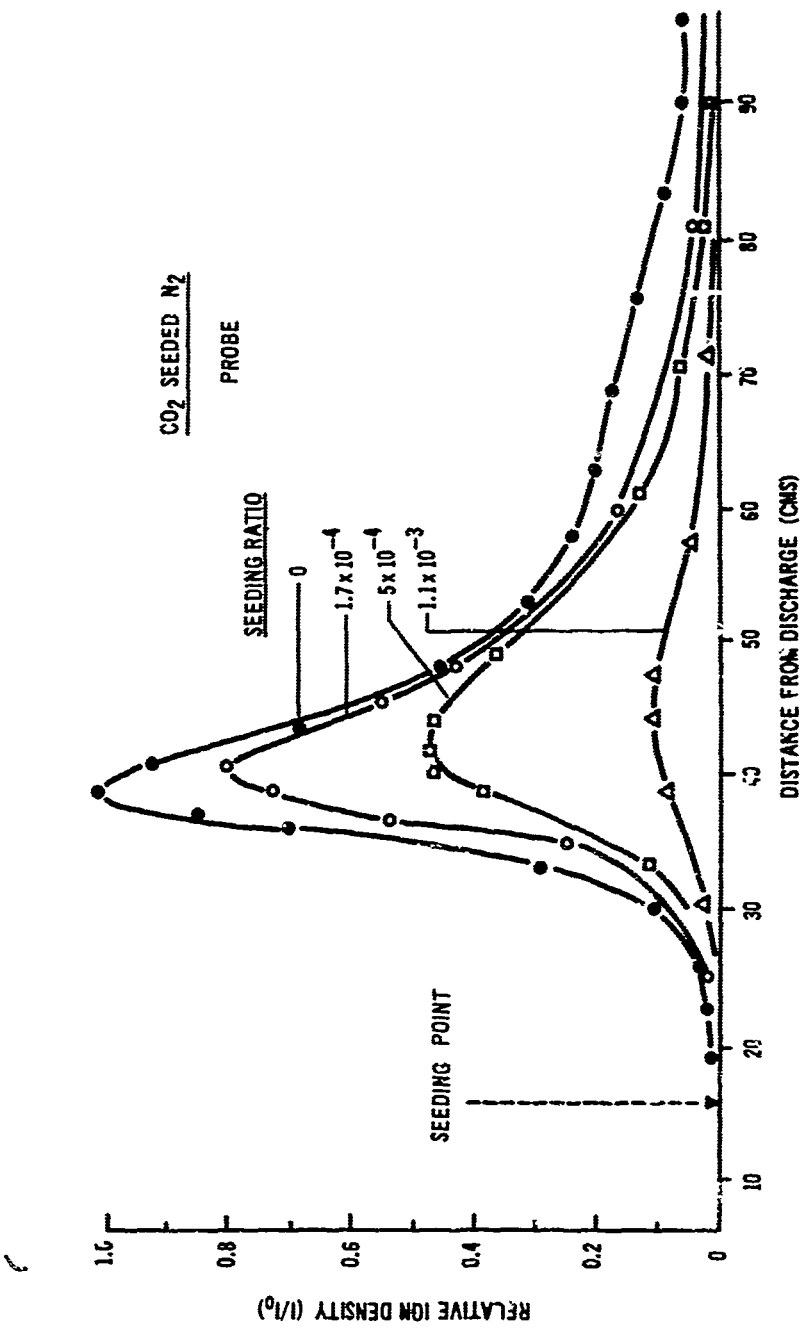

CO_2 SEEDED N_2
PROBE
SEEDING RATIO
0
1.7×10^{-4}
5×10^{-4}
1.1×10^{-3}
SEEDING POINT
RELATIVE ION DENSITY (I/I_0)
DISTANCE FROM DISCHARGE (CMS)
0
0.2
0.4
0.6
0.8
1.0
10
20
30
50
60
70
80
90

Figure 10.

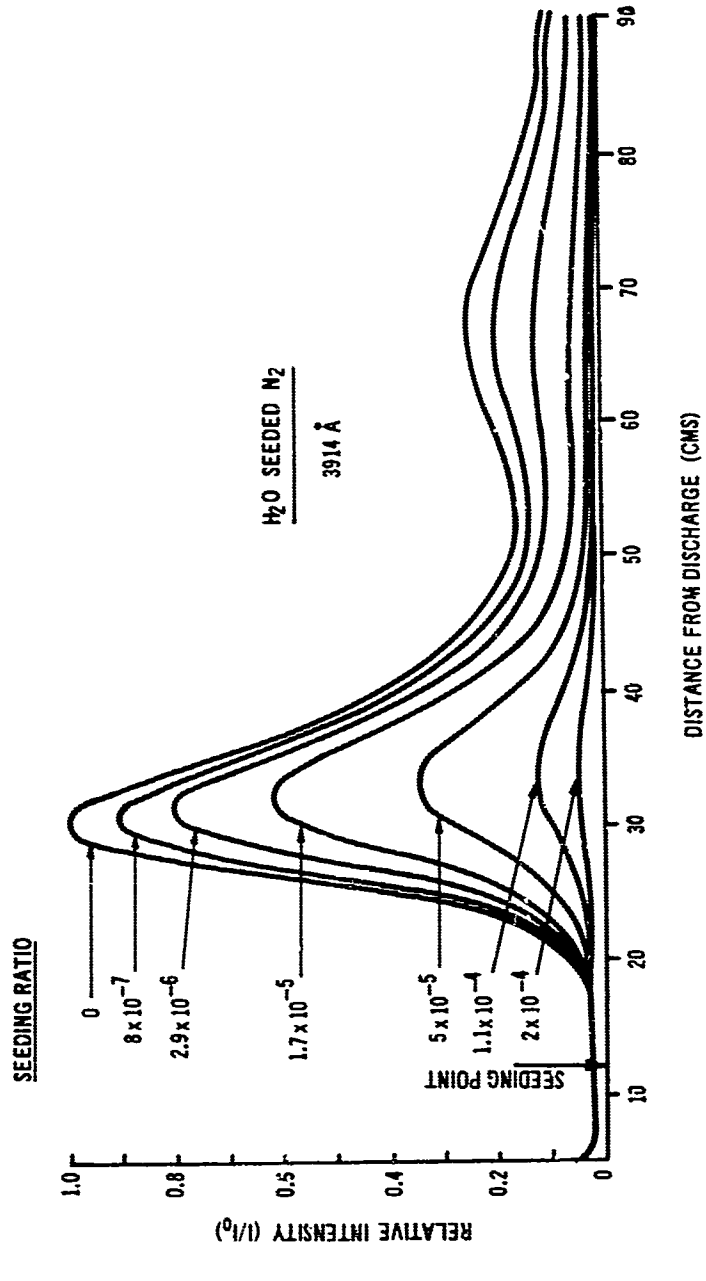

H_2O SEEDED N_2
3914 Å
SEEDING RATIO
0
8×10^{-7}
2.9×10^{-6}
1.7×10^{-5}
5×10^{-5}
1.1×10^{-4}
2×10^{-4}
SEEDING POINT
RELATIVE INTENSITY (I/I_0)
1.0
0.8
0.5
0.4
0.2
0
10
20
30
40
50
60
70
80
90
DISTANCE FROM DISCHARGE (CMS)

Figure 11.

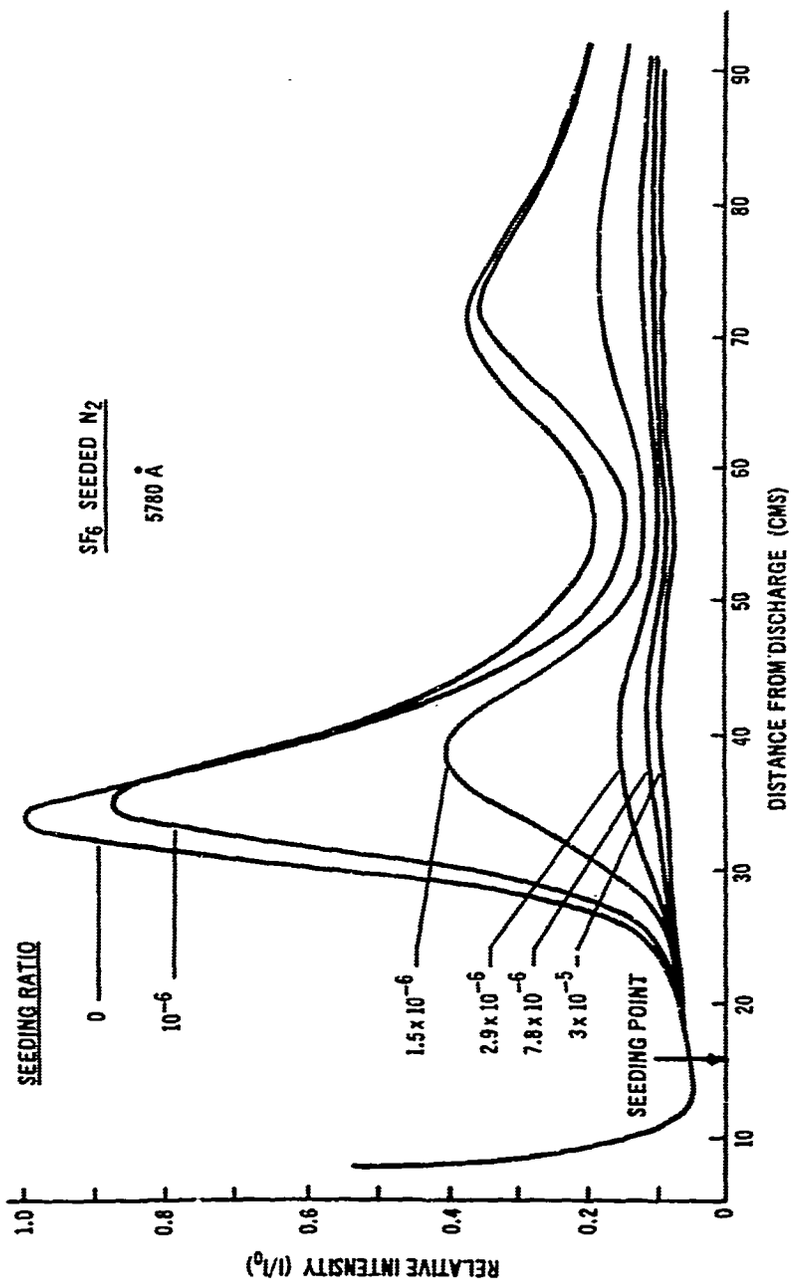

SF_6 SEEDED N_2
5780 Å
SEEDING RATIO
0
10^{-6}
1.5×10^{-6}
2.9×10^{-6}
7.8×10^{-6}
3×10^{-5}
SEEDING POINT
RELATIVE INTENSITY (I/I_0)
DISTANCE FROM DISCHARGE (CMS)
0
0.2
0.4
0.6
0.8
1.0
10
20
30
40
50
60
70
80
90

Figure 12.

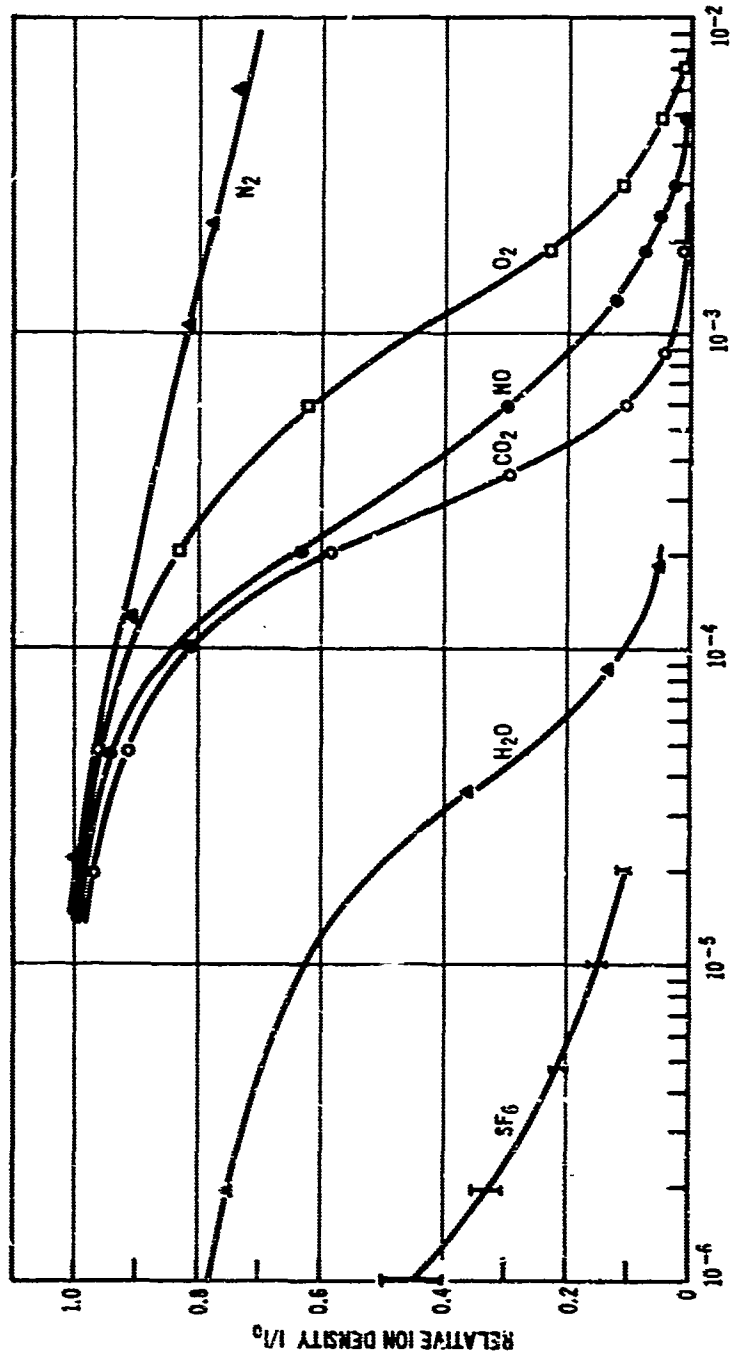

RELATIVE ION DENSITY I/I_0
1.0
0.8
0.6
0.4
0.2
0
10^{-2}
10^{-3}
10^{-4}
10^{-5}
10^{-6}
SEEDING RATIO
N_2
O_2
NO
CO_2
H_2O
SF_6

Figure 13.

XI. THE EFFECT OF CHEMICAL ADDITIVES ON MICROWAVE TRANSMISSION IN AN AIR PLASMA

Sami Atallah
Associate Professor

Wayne A. Sanborn
Research Engineer

Department of Chemical Engineering
Tufts University
Medford, Massachusetts

Third Symposium on the Plasma Sheath-
Plasma Electromagnetics of Hypersonic Flight
Sponsored by the Microwave Physics Laboratory
Air Force Cambridge Research Laboratories

Held in Boston, Massachusetts
21-22 September 1965

THE EFFECT OF CHEMICAL ADDITIVES ON MICROWAVE TRANSMISSION IN AN AIR PLASMA

ABSTRACT

The effect of several chemical additives on microwave transmission through a high temperature air plasma was found. Two types of plasma generators were used in this study; one employed an rf inductive heating coil and the other an industrial discharge plasma unit. Gaseous sulfur hexafluoride, propane and other hydrocarbons, sprays of water and a colloidal suspension of silica in water and micron size solid particles were injected separately into the air plasma operating at pressures ranging between atmospheric and 2.5 inches Hg.. The change in X-band microwave transmission across the plasma was noted. Sulfur hexafluoride was found most effective in improving transmission and this was attributed to the presence of highly electrophilic fluorine atoms which reduce the electron density of the plasma.

INTRODUCTION

One way of preventing the detection of reentering ballistic missiles and of improving radio communications with manned space vehicles during reentry is to reduce the free electron density of the plasma sheath which surrounds the reentering vehicle. This can be achieved by one of the following chemical means:

1. The injection of electrophilic atoms and radicals in the plasma: This method involves the injection of a chemical which produces, upon dissociation, a large number of free radicals or atoms having a high electron affinity. Electron attachment takes place according to the following reaction:

$$A + e^- + \text{kinetic energy} \rightarrow A^- + \text{kinetic energy} + \text{electron affinity}$$

The electron affinity is defined as the energy required to dissociate a negative molecular ion into the neutral molecule and a free electron. The halogen atoms are known to have high electron affinities, because an additional electron produces a relatively stable outside orbital shell. The cyanogen radical (CN) has also been found to have high electron affinity[1,2].

2. Quenching of the plasma with a highly endothermic reaction: This method depends on lowering the temperature of the plasma which in turn lowers the electron density in order to maintain equilibrium as described by the Saha equation. The dissociation reactions of all molecules are endothermic (heat absorbing). For instance, the heat required to dissociate propane according to the reaction

$$C_3H_8 \text{ (gas)} \rightarrow 3C \text{ (gas)} + 8H \text{ (gas)}$$

is 946 Kcal/mole at 25°C and is called the heat of atomization. The final temperature of the plasma can be calculated from values of the specific heats of the components of the system, the heat of atomization, amount of additive in the plasma, and the initial temperature of the plasma. For instance, the addition of .01 mole fraction of propane to an air plasma at 3230°K and atmospheric pressure lowers the temperature to 2060°K assuming complete gaseous dissociation. Typical values of standard heats of atomization at 25°C are listed in Table 2.

Table 1.

Standard Heats of Atomization at 25°C.

Compound	Formula	Heat of Atomization, Kcal/mole
Propane	C_3H_8	946
Propylene	C_3H_6	815
Allene	C_3H_4	683
Ethane	C_2H_6	670
Sulfur Hexafluoride	SF_6	508
Methane	CH_4	393
Water	H_2O	221

At low initial plasma temperatures, the quenching effect is probably the predominant cause for reducing the electron density of the plasma. At higher temperatures, the atoms and radicals become sufficiently excited so that electrons may be effectively absorbed by attachment. It should be kept in mind that quenching by a dissociation reaction is usually complicated by side reactions (which could be exothermic or endothermic) among the free radicals and atoms present in the plasma.

3. The introduction of micron size refractory dust particles in the plasma: This method was suggested theoretically by Rosen[3] and it utilizes the large collision cross section of a micron size refractory dust particle with respect to an electron. In the absence of thermal emission, when an electron collides with a dust particle, it is effectively absorbed, thus reducing the free electron concentration. Table 3 shows the calculated effect of particle addition to different plasmas according to Rosen's theory. The refractory particles were assumed to have a specific gravity of five.

Table 3

Effect of Particles Size and Distribution on Electron Absorption

Particle size, cm.	Plasma temp., °K	Electron density, cc^{-1}	Particle distribution, mg/l	Electrons absorbed, %
10^{-4}	3000	10^{8}	10	96.5
10^{-4}	3000	10^{11}	10	.003
10^{-4}	4000	10^{12}	10	.02
10^{-4}	4000	10^{12}	10^{5}	97.7
10^{-5}	4000	10^{12}	10	1.9
10^{-6}	4000	10^{12}	10	97.7

OBJECTIVE

The objective of this study was to investigate the effect of chemical additives on microwave transmission through an air plasma.

Since microwave transmission is governed by the number of free electrons in the plasma, reducing the number of electrons by means of one or more of the methods described above should lead to improved transmission.

APPARATUS

Two plasma generators were used in this investigation. One was a tuned plate, tuned grid, 40 megacycle oscillator powered by a 3000 volt DC power supply. The oscillator was capable of drawing 500 watts continuously and could be driven to 1000 watts for short runs. A water cooled rf coil inductively heated a stream of air flowing in a central glass tube. This type of plasma generator had been originally suggested by the Amperex Company[4] and used by other investigators[5]. A photograph of the apparatus is shown in Fig. 1. The injection of chemical additives was achieved either by premixing the additive with the air or by injecting the additive in a central tube as shown in Figs. 2 and 3. Gaseous additives were metered through rotameters. Liquids were atomized in the air stream and their flow rate calibrated against atomizing air pressure. Solid particles were fluidized in air. Their flow rate was calibrated by collecting and weighing all the particles leaving the fluidizer over a given time interval for a given air flow rate. The temperature of the rf plasma was slightly over 3200°K as indicated by melting point measurements. This temperature corresponds to an equilibrium electron density of about 3×10^{11} electrons/cc[6].

The second plasma generator was an industrial unit manufactured by Thermal Dynamics Corporation, Lebanon, N.H., model U-50N. It consisted of two power supplies which could be connected in series or parallel, each capable of supplying a maximum of 14 Kw of power.

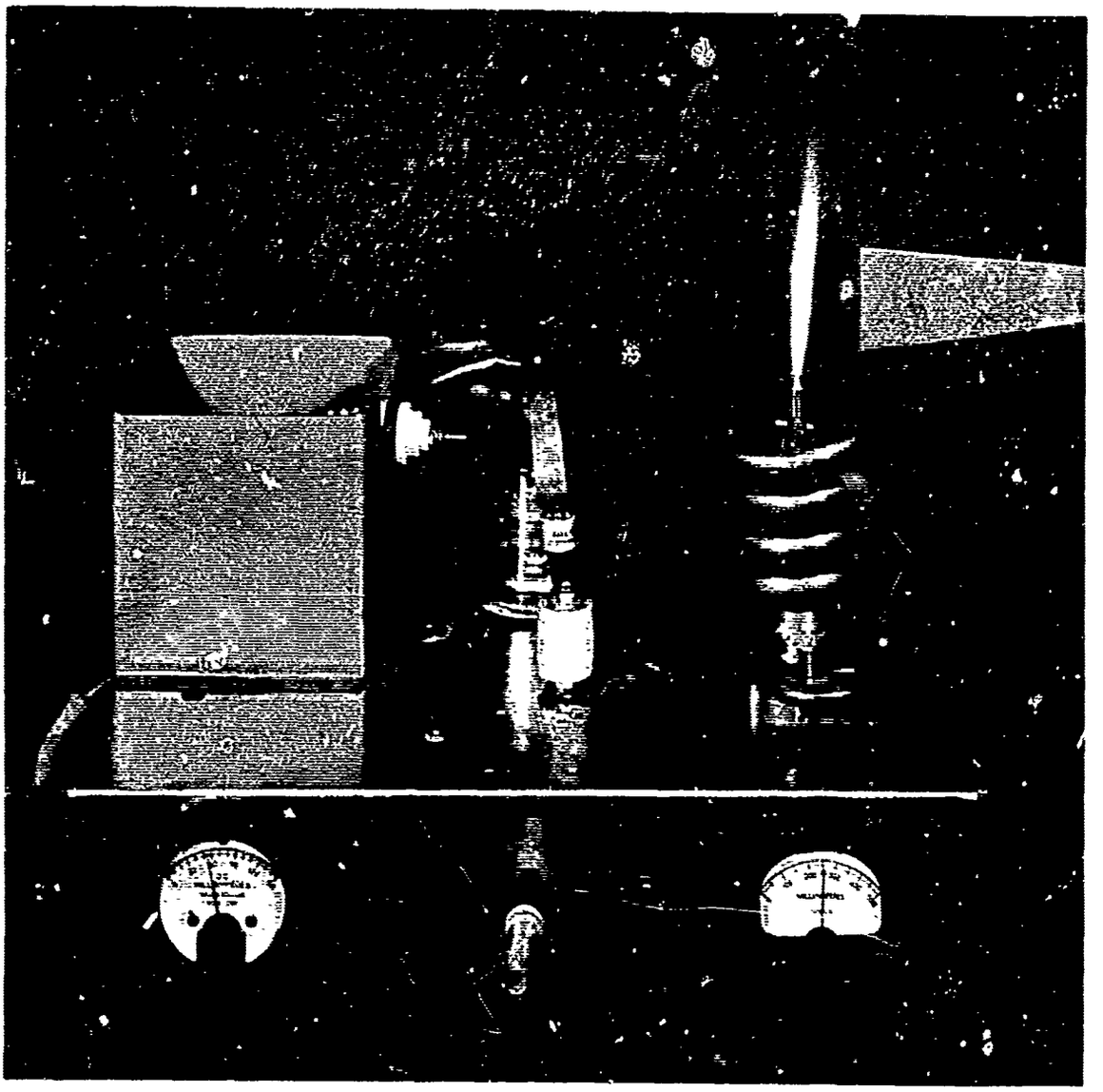


Figure 1 . RF Plasma Generator

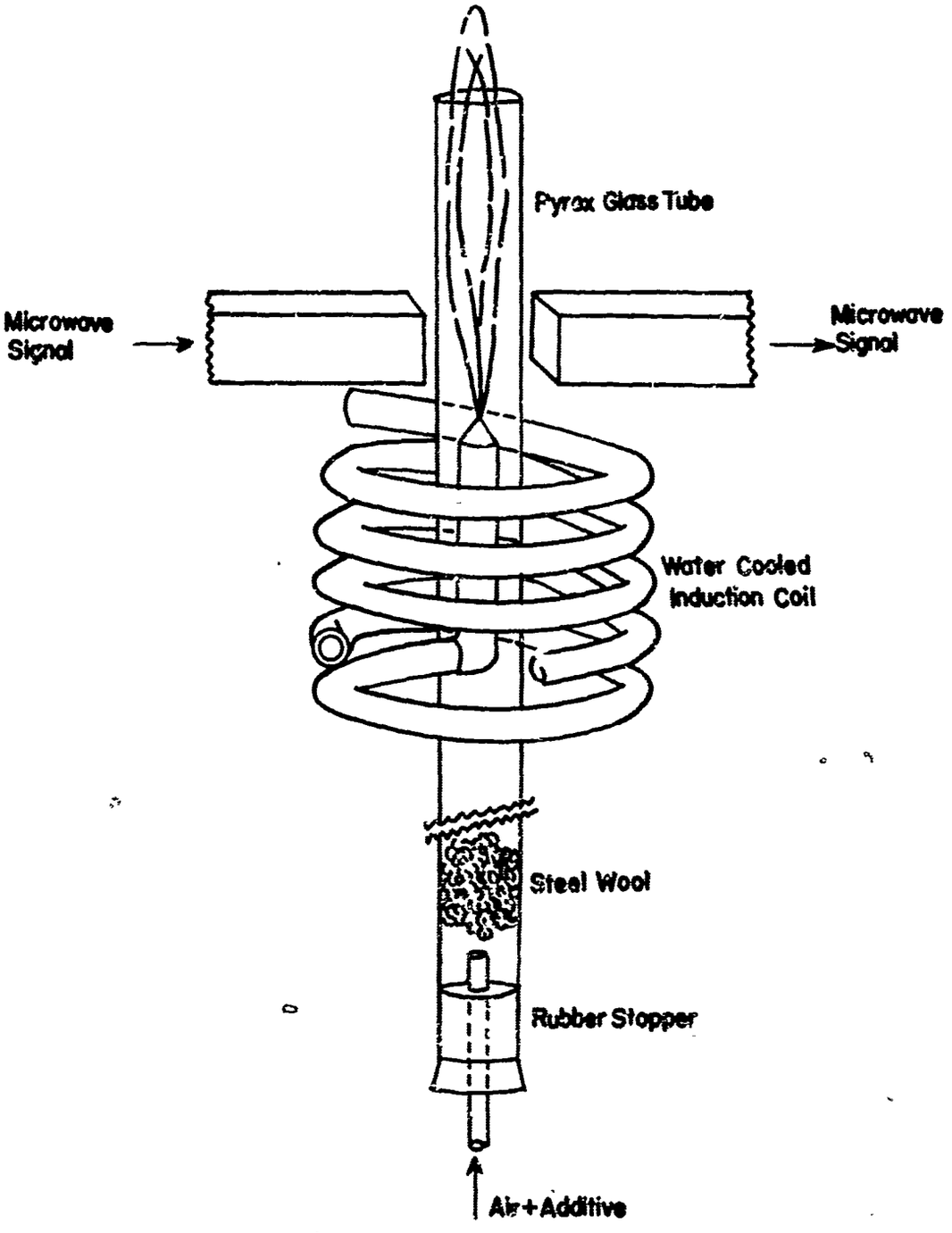


Figure 2. RF Plasma with Premixed Additive

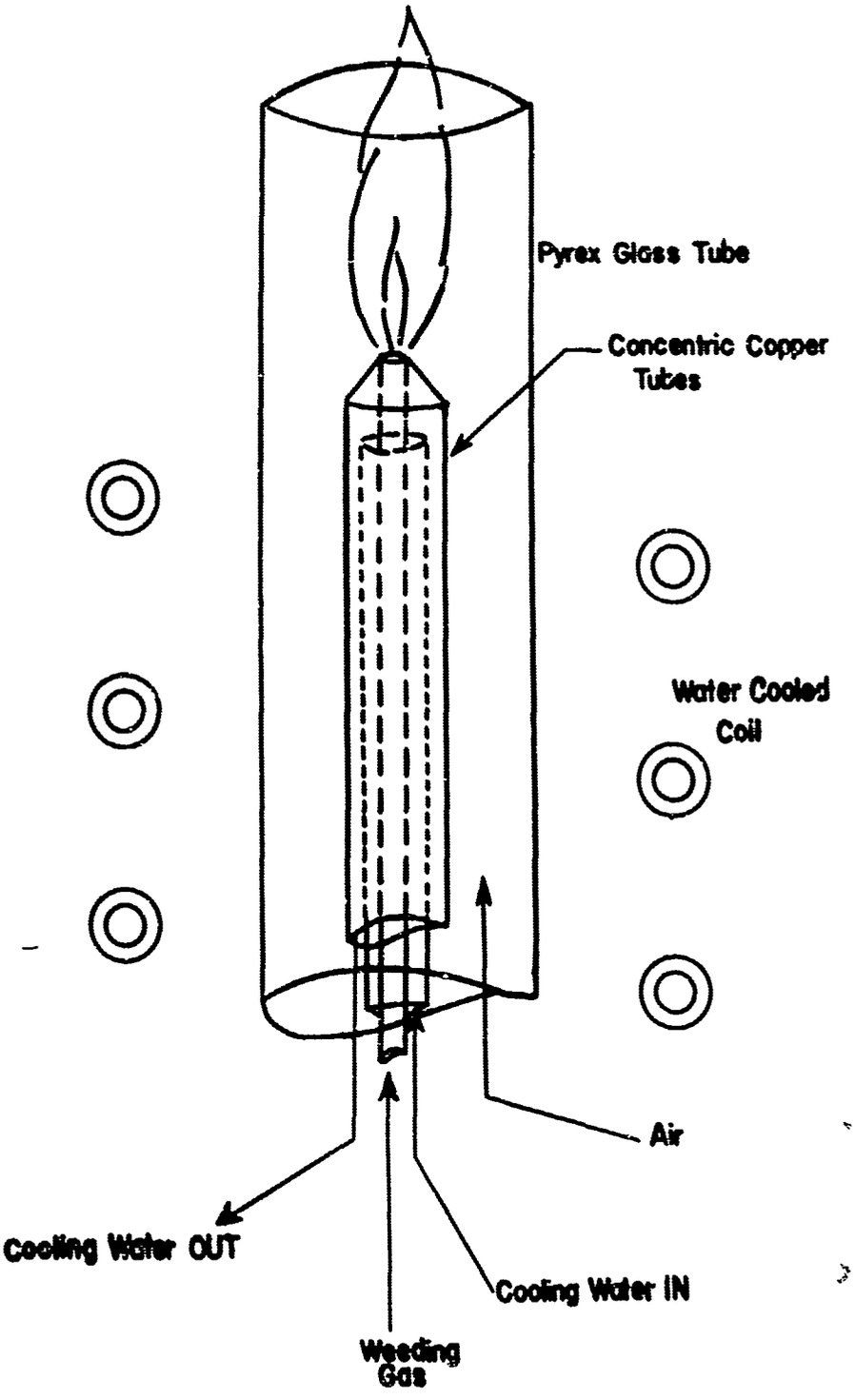


Figure 3 . RF Plasma with Central Tube for Additive

A control console with plasma gas flowmeters, switches, rheostat, voltmeter, and ammeter was used to run the plasma torch. The torch itself could be fitted with different types of nozzles depending on the plasma gas and flow rate to be used. A mixing nozzle was attached to the front of the torch where gaseous, liquid, or solid additives could be injected into the plasma stream. An air plasma was produced by generating a nitrogen plasma first, then adding the necessary amount of oxygen downstream in the mixing nozzle. The equilibrium temperature produced by this plasma generator when operated with synthetic air at atmospheric pressure were estimated at about 2800°K at 8 Kw and 4680°K at 20 Kw.

In order to operate under vacuum, the torch was inserted into the bottom of a six inch Pyrex glass cross. The upper arm was connected to a heat exchanger and a vacuum pump while the side arms were used for the introduction of microwave guides and cooling water tubes. Figure 4 is a sketch of this apparatus.

Most microwave transmission studies were made using the apparatus shown in Fig. 5. Earlier work was performed with a microwave transmission bridge. Most of the measurements were made in the x-band region (8.2-12.4Kmc). Ku-band (12.4-18Kmc) was used occasionally. The microwave signal was transmitted across the plasma and the attenuation noted. The change in transmission was recorded as the chemical additive was allowed to enter the mixing nozzle.

DISCUSSION OF RESULTS

Earlier work performed by the authors[7] was concerned with the effect of endothermic reactions on the electron density of an air plasma.

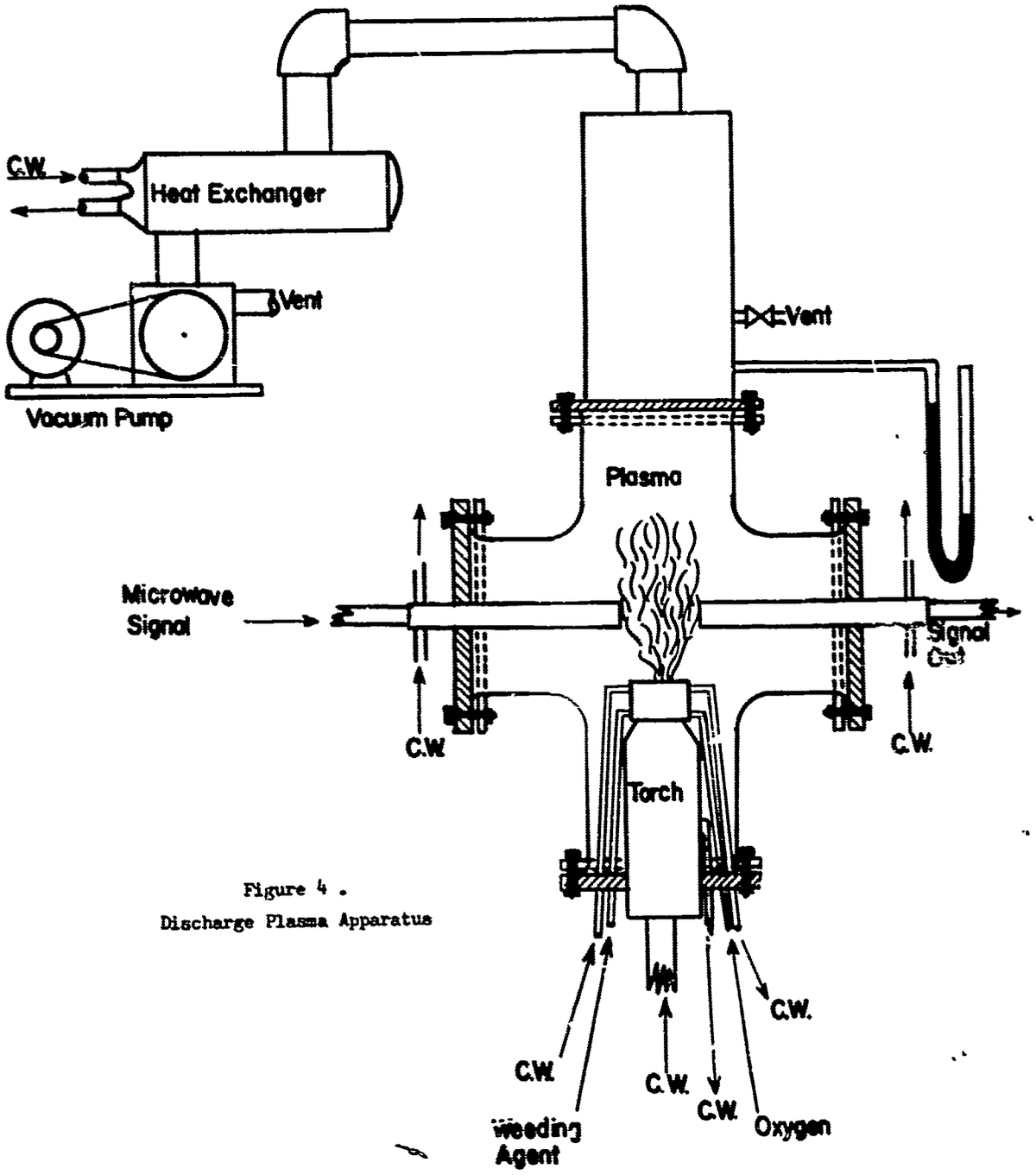


Figure 4 .
Discharge Plasma Apparatus

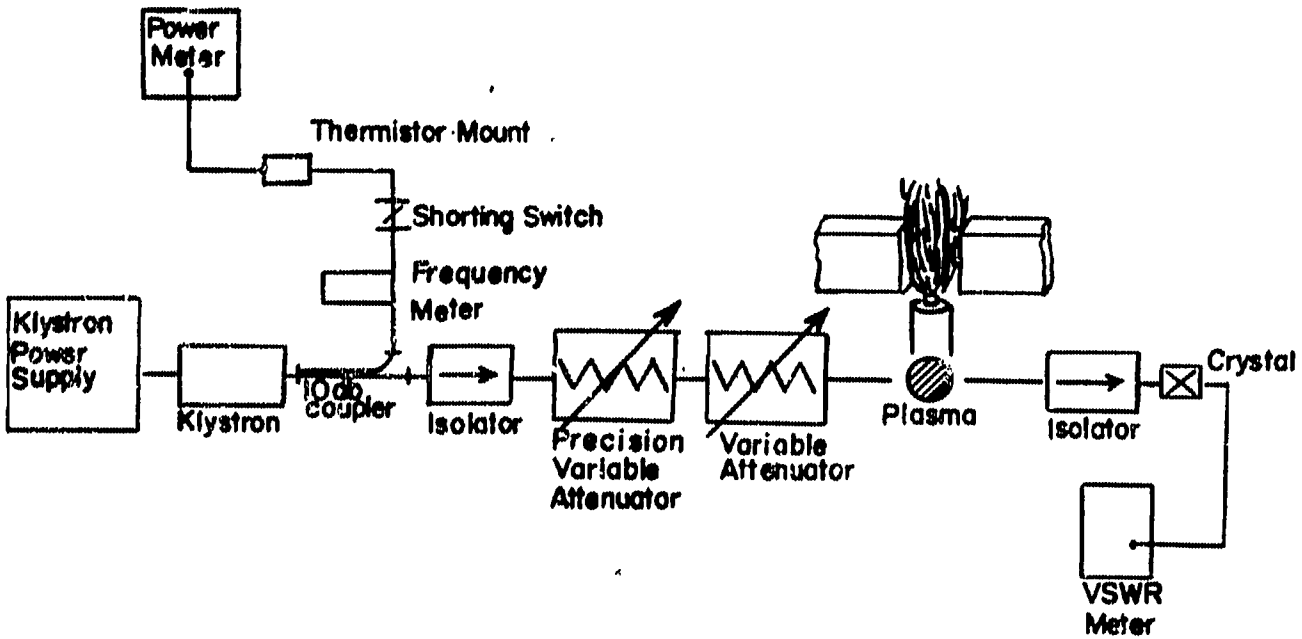


Figure 5 . Microwave Transmission Arrangement

The rf plasma having a temperature of about 3200°K was operated at atmospheric pressure. Several gaseous hydrocarbons and sulfur hexafluoride were premixed with air and the change in transmitted power noted. A plot of transmitted power ratio versus mole fraction of the weeding agent is shown in Fig. 6. The effectiveness of hydrocarbons in increasing microwave transmission was hastily attributed to the high energy required to dissociate them into their gaseous atomic products of hydrogen and carbon. It is doubtful, however, that gaseous carbon was present to any large extent because carbon sublimes at about 4000°K. Later observations showed that solid carbon was actually present in the flame, particularly when the hydrocarbon was fed centrally and not premixed with air. Assuming that the solid carbon particles have an average diameter of .3 microns (which corresponds to that of soot), a calculation can be made of the expected reduction in electron density according to Rosen's method[3]. The plasma was assumed to have an initial electron density of 3×10^{11} electrons/cc and that complete dissociation of the hydrocarbon additive into solid carbon and hydrogen took place. It was found that the addition of .01 mole fraction propane should result in a 99.41% reduction in the electron density while the addition of .001 mole fraction should weed out 98.72% of the electrons. Experimentally, using x-band microwaves, it was found that the central addition of .00636 mole fraction propane caused a reduction of 1.1 db on a plasma with 1.9 db attenuation while the addition of .00113 mole fraction caused a reduction of .37 db. If, as a first approximation, the electron density is assumed to be directly proportional to attenuation[8], the reduction in electron density is 58% and 19.5% respectively. The difference between the theoretical predictions and these values could

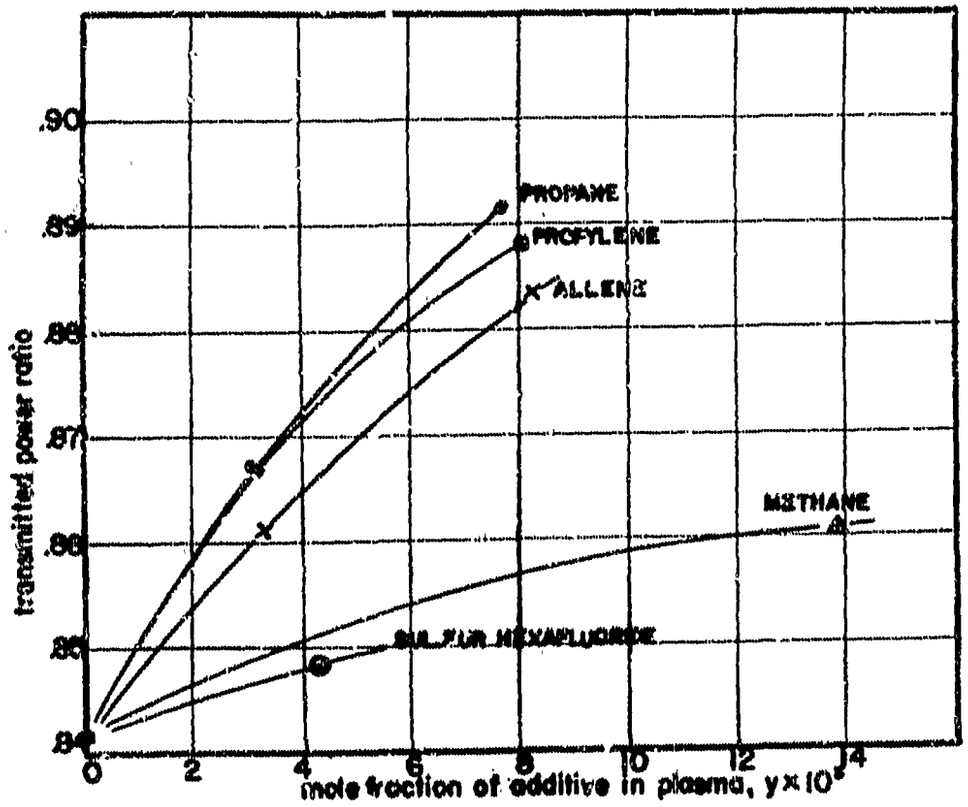


Figure 6 . Effect of Hydrocarbons and SF_6 on MW Transmission through RF Plasma

be attributed to the inevitable side reactions between the carbon and the other atomic species present. Spectrographic analysis revealed all possible diatomic combinations of C, H, O, and N atoms in the plasma. Furthermore, as soon as the solid carbon migrated to the lower temperature regions of the plasma, it immediately reacted with oxygen rendering it ineffective. It was also noted that feeding the additive centrally was much more effective than premixing it with air. This is due to the fact that central feeding introduced the additive at the hottest region of the plasma where the electron density is highest.

The rf air plasma was also used to study the effect of water sprays and a spray of a colloidal suspension of silica submicron particles in water on microwave transmission. In this experiment, a very small portion of the air entering the Pyrex glass tube was used to atomize water in a cosmetic atomizer before entering the plasma generator. It was found that the addition of silica particles to the water spray did make the plasma more transparent to Ku-band microwaves than by using pure water. Figure 7 shows a plot of the change in attenuation (which was obtained by subtracting the attenuation due to the plasma with additive from the attenuation of the plasma without additive) versus the rate of water or suspension injection in the plasma.

Micron and submicron particles of carbon black, silica and metallic aluminum were injected into the rf plasma at atmospheric pressure with no detectable effects on microwave transmission. Aluminum oxide particles increased microwave attenuation indicating an increase in electron density probably due to thermionic emission. Tests were performed on the discharge plasma at low pressures with the same solid particles and gave similar results.

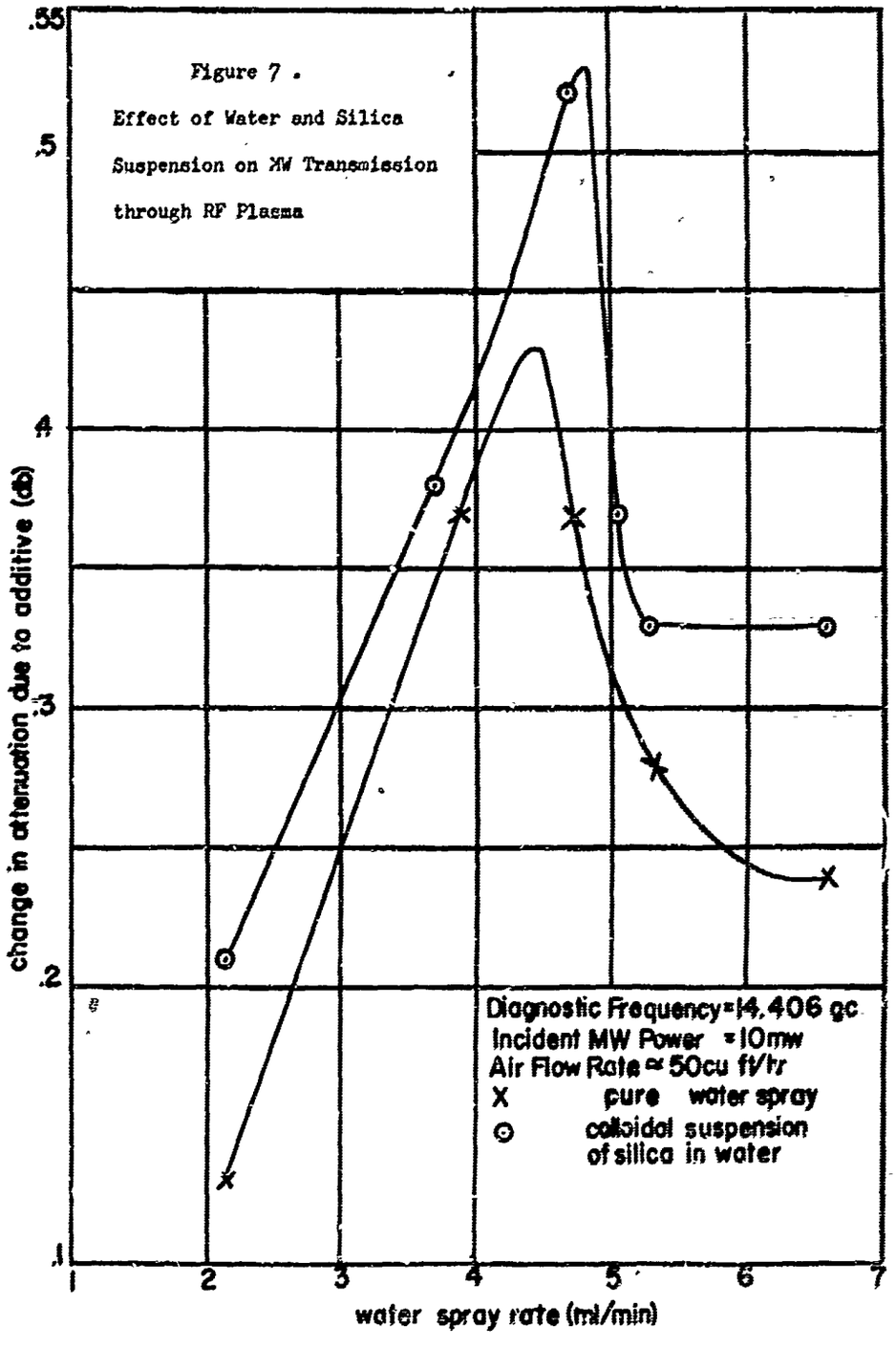


Figure 7 .

Effect of Water and Silica Suspension on MW Transmission through RF Plasma

The discharge plasma, operating at generator inputs of 8 Kw and 20 Kw and a total gas flow of 125 scfh, was used to investigate the effect of adding SF_6, C_3H_8 and other hydrocarbons on x-band microwave transmission at pressures ranging from atmospheric ($\simeq$30 inches Hg) to 2.5 inches Hg. A probing frequency of 9.525 Kmc and an incident microwave power of 10 mw were used. In each case, the additive was injected into the plasma at different rates and the change in transmitted power recorded. A square wave modulated signal was transmitted across the plasma. Figure 8 shows what happened to the square wave when the 8 Kw plasma was turned on and when various amounts of SF_6 were inject into the plasma. The ratio of the power transmitted while the plasma was turned on to that transmitted through the gap with the plasma off seemed to be a good measure of the disturbance and scattering of the signal. A maximum ratio of one is reached when enough additive is injected into the plasma in order to make it completely transparent to microwaves. It can be seen in Fig. 9 that the effectiveness of sulfur hexafluoride as an electron weeding agent improved at lower pressures while that of propane was reduced. The reason for this is that low pressures promote the dissociation of SF_6 into fluorine and sulfur, at least the first of which is known to have high electron affinity

On the other hand, at these high temperatures the heat of atomization is relatively small compared with the total enthalpy of the plasma and the small temperature drop due to dissociation alters the electron density very little. The gaseous products of dissociation of propane do not have the high affinity of fluorine for electrons and solid carbon is no longer available to behave as refractory dust particles. The other hydrocarbons, methane, ethane and propylene behaved very much

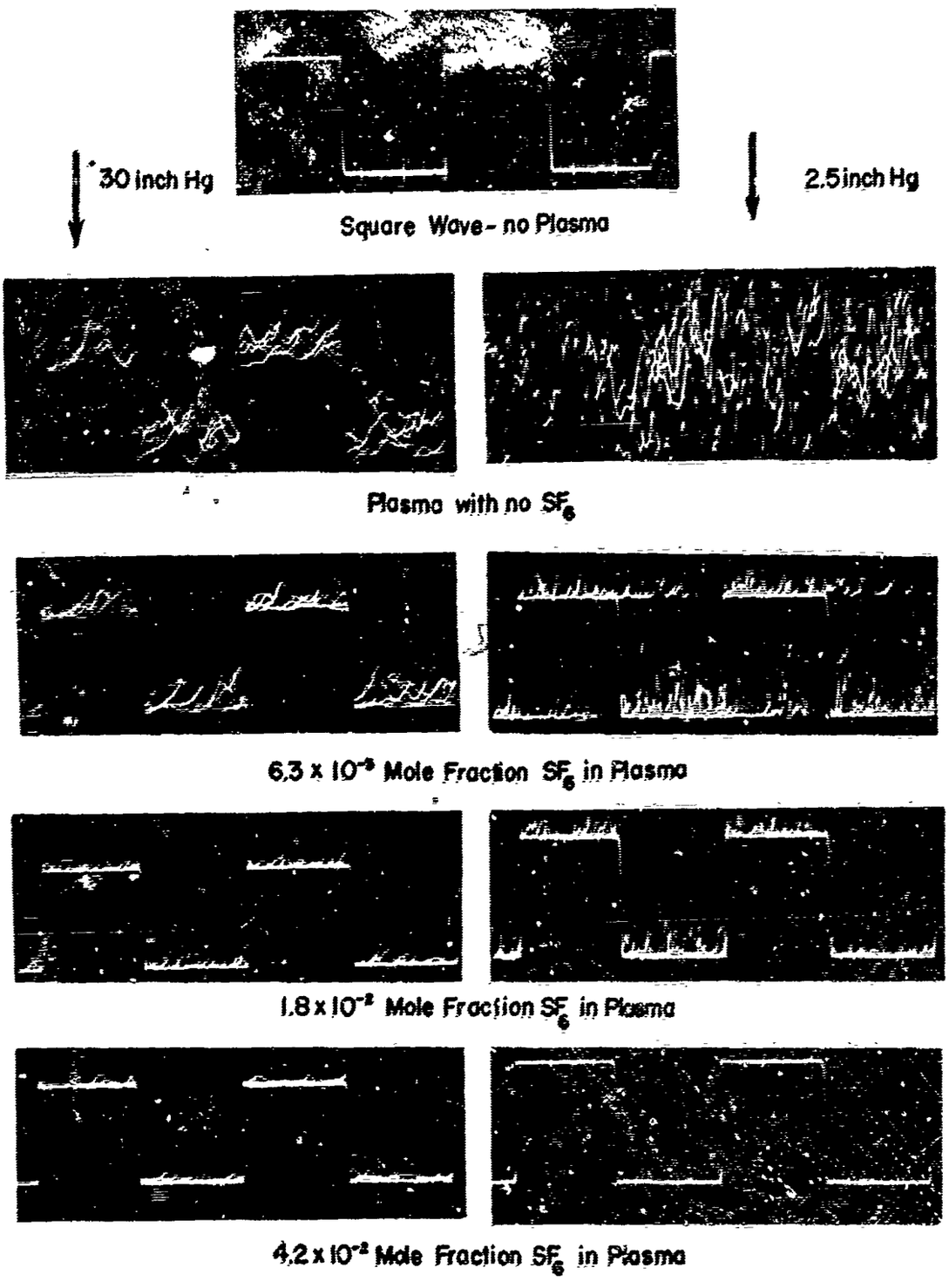


Figure I Effect of SF_6 addition on square wave modulated MW signal with plasma generator at 8 kw.

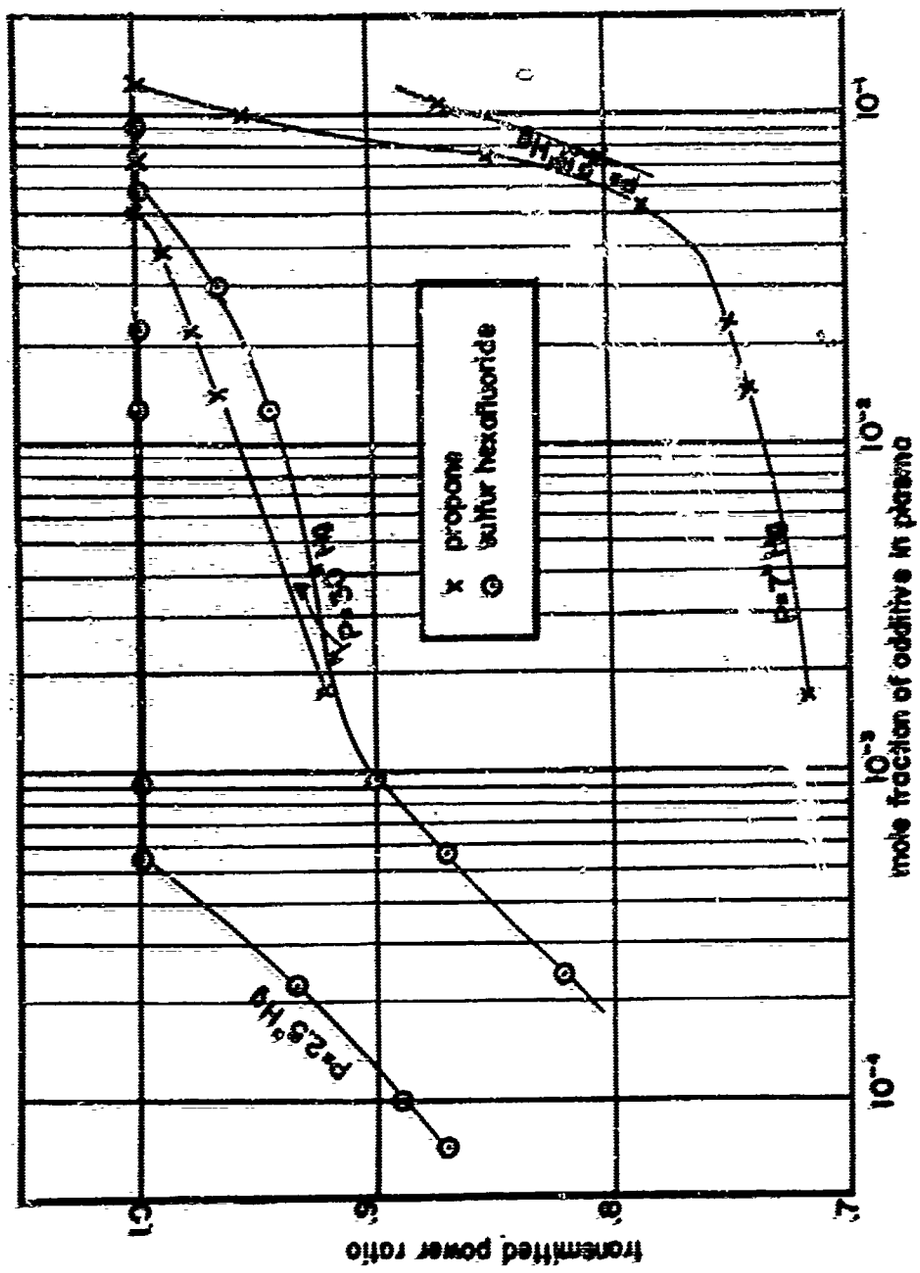


Figure 9. Seeding Effectiveness of SF_6 and Propane on Discharge Plasma Operated at 8kw

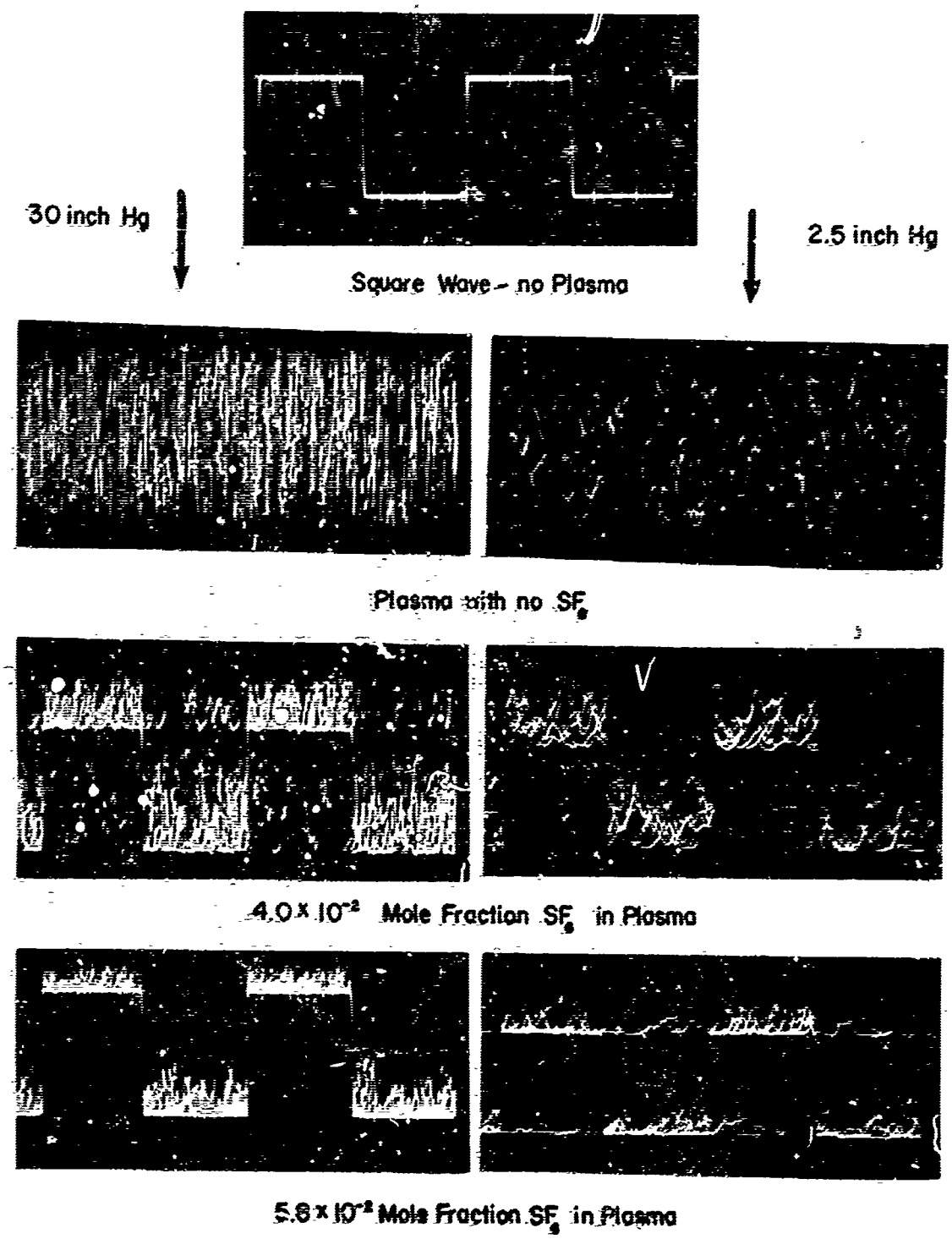


Figure 18. Effect of SF_6 addition on square wave modulated MW signal with plasma generator at 20 kw.

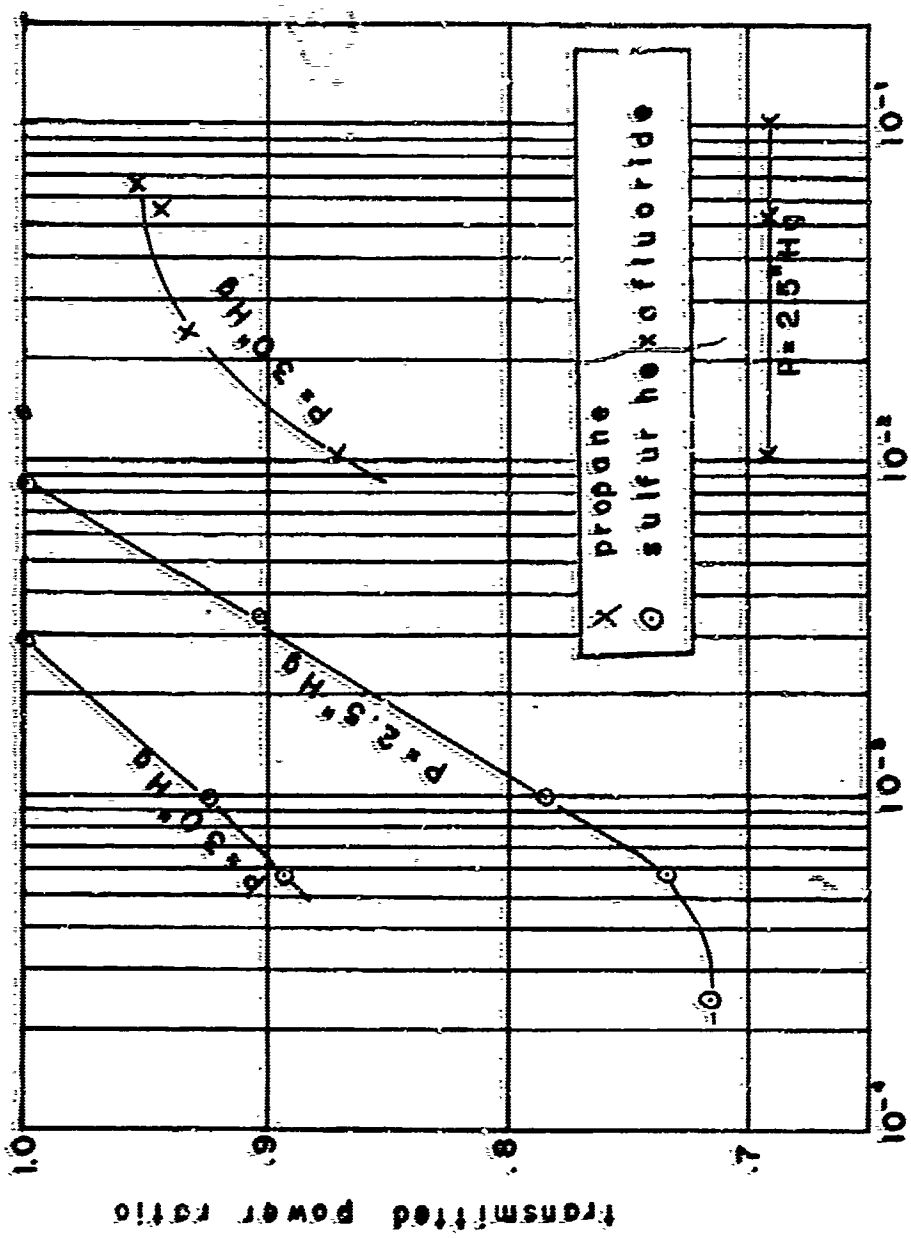


Figure 11 . Wedding Effectiveness of SF_6 and Propane on Discharge Plasma Operated at 20Kw

the same as propane. Figure 10 is similar to Fig. 8 except that the plasma was operated at 20 Kw. Figure 11 shows the transmitted power ratio versus mole fraction for this case. It can be seen that propane is still more effective at atmospheric pressure and less effective at low pressure. However, SF_6 is now more effective at atmospheric pressure and somewhat less effective at the low pressure.

The change in the behavior of SF_6 cannot be explained immediately. It was noted, however, that at high generator power levels, the Pyrex glass cross was etched considerably and a small amount of a flaky white powder was accumulated in the bottom of the chamber. X-ray diffraction analysis of this powder showed that it is most likely sodium fluoride, with the sodium coming from the glass wall. It is possible that at high power and low pressure, the reaction between fluorine and the glass wall depletes the plasma of its supply of fluorine atoms needed to reduce the electron density.

CONCLUSIONS

The results of this study show that it should be possible to alleviate the radio blackout problem by injecting certain chemical additives into the shock front surrounding reentering space vehicles. Sulfur hexafluoride seems to be most promising. Tests are being continued on water vapor and other halogen containing compounds. It is hoped that actual in-flight tests on these compounds will be performed in the near future.

REFERENCES

1. Herron, J. T., and Dibeler, V. H., "Electron Impact Study of the Cyanogen Halides", J. Am. Chem. Soc., 82, 1555-1559 (1960).

2. Morris, D. F. C., "Crystal Radius of the Cyanide Ion", Acta Crystallographica, 14, 547-548 (1961).

3. Rosen, G., "Method for the Removal of Free Electrons in a Plasma", Phys. of Fluids 5, No. 6, 737 (1962).

4. Amperex Electronics Company, Applications Laboratory, Report No. ALR-223, Hicksville, L. I., New York.

5. Bushman, R. S., "Study of a Seeded Plasma", ARL 62-310, March 1962. Contract AF 37(616)-8126.

6. Gilmore, F. R., "Equilibrium Composition and Thermodynamic Properties of Air to 24000°K", USAF Project RAND, RM-1543, The Rand Corporation, Santa Monica, California (1955).

7. Atallah, S. and Sanborn, W. A., "The Reduction of the Electron Density of a Plasma by Endothermic Reactions", Proceedings of the XVth International Astronautic Federation Congress, M. Lunc-editor, P. W. N. Warsaw and Gauthier-Villars, Paris, Vol. III, pp. 45-53 (1964).

8. Belcher, H., and Sugden, T. M., "Studies on the Ionization Produced by Metallic Salts in Flames. I. The Determination of the Collision Frequency of Electrons in Coal-Gas/Air Mixtures", Proc. Roy. Soc. London, 201, 480(1950), "II. Reactions Governed by Ionic Equilibria in Coal-Gas/Air Flames Containing Alkali Metal Salts", Proc. Roy. Soc. London, 202, 17 (1950).

ACKNOWLEDGEMENTS

This study was performed at Tufts University under Contract AF 19(628)-2377 with the Air Force Cambridge Research Laboratories, Office of Aerospace Research, United States Air Force, Bedford, Massachusetts.

The rf plasma generator was constructed with a grant from the Tufts University Faculty Research Fund.

The authors wish to express their gratitude to Mr. Walter Rotman, Plasma Electromagnetics Branch Chief at AFCRL and Mr. John F. Lennon, contract monitor, for their helpful suggestions and support.

XII. REDUCTION OF FREE ELECTRON CONCENTRATION IN A REENTRY PLASMA BY INJECTION OF LIQUIDS

By John S. Evans

NASA Langley Research Center
Langley Station, Hampton, Va.

ABSTRACT

Liquid droplets injected into an over-ionized plasma (such as the plasma sheath over an antenna on a reentry vehicle) are treated as sites for recombination of electrons and ions. Each droplet is considered to be a small spherical probe at floating potential. Thus, the rate at which it removes electrons from the plasma is equal to the rate at which ions reach its surface. Thermionic emission and secondary emission are neglected and all electrons and ions which strike a drop are assumed to be recombined.

Theoretical calculations are described for the reduction in electron concentration as a function of three parameters of interest for practical applications. These are the drop size, the mass injection rate, and the time required for the drops to flow from the injection point to the antenna.

The results of the calculations indicate that the addition of liquid droplets to a flowing plasma is capable of producing large reductions in electron concentration. However, it should be noted that the details of drop formation, mixing, acceleration, and evaporation were greatly simplified in the analysis. Since these processes can have important effects on the results and since the theoretical treatment of such complex phenomena is both difficult and uncertain, it appears that experimental validation of the theory is needed before conclusions can be reached about the applicability of the results.

INTRODUCTION

It is common knowledge in radio propagation studies that the presence of large numbers of free electrons can cause severe signal attenuation or radio blackout. Evidence now exists that electron concentration in the atmospheric entry plasma sheath can be reduced by injecting materials into the flow field over the entering body.[1,2,3,4]

Gas injection appears to be impractical because no way has been found to make a gas penetrate the ionized layer much beyond the boundary layer. Solid particle injection is also difficult, but, even if particles can be injected in a satisfactory way, they rapidly reach high temperature and thermionic emission limits their usefulness. Liquid injection holds the most promise, since adequate penetration can be achieved and since heat-transfer rates to small evaporating drops are such that both long lifetime and low drop temperature can be obtained.

The literature contains quite a bit of information on topics relating to material injection,[5,6,7,8] and some experiments have been performed to show the effects of material addition on free electron concentration. Carswell and Cloutier at RCA have seeded supersonic streams with electronegative gases,[9] Soo and Dimick at the University of Illinois have injected solid particles into flowing plasmas,[10] and Kurzius at Aerochem has been experimenting with water injection in seeded hydrocarbon flames.[11]

The NASA experiments[1,4,12,13] have proved that injection of liquid water can restore radio communication during actual atmospheric entry. This paper is concerned with a discussion of what is believed to be the way in which liquid injection is able to reduce the concentration of free electrons in the reentry plasma sheath. More information about the experiments and

more detailed discussions of the theoretical basis are given in NASA reports.[14,15]

THEORY

It should be made clear at the start that we are discussing injection of a liquid into an over-ionized* and relatively cool plasma flowing over the afterbody of a vehicle. The electrons present were produced in the high-temperature region near the stagnation point at the nose and persist in the expanded and cooled gas on the afterbody only because the rate of electron-ion recombination is too slow to cause them to disappear in the flow time over the body.† As is shown in figure 1, typical conditions for the plasma under discussion are: electron concentration (N_e) of the order of 10^{12} e/cm^3; flow velocity (u_g) about 3000 m/sec; temperature (T) about 2500° K; density (ρ_g) about 10^{-3} of sea level atmospheric density. There is an antenna at some point downstream, and it is desired to transmit signals from this antenna to a ground station.

A reasonable criterion for relief of radio blackout is to require that the electron concentration at the antenna station be less than $(N_e)_{critical} = \frac{f^2}{8.06 \times 10^7}$, where f is the transmitting frequency. For VHF transmission, this requires that N_e be less than 10^9 e/cm^3. Thus, if $N_{e0} = 10^{12}$ e/cm^3, a reduction of about three decades in electron concentration

*The term "over-ionized" here means that the concentration of free electrons is larger than it would be if the plasma were in thermal equilibrium at the local temperature.

†The plasma will become even colder when water is added but the effect of additional cooling on the dissociative recombination process ($NO^+ + e \rightarrow N + O$) is small.

is required for VHF transmission. This much reduction is not always necessary, since, if the thickness of the overdense plasma region is small enough, part of the signal energy penetrates the sheath and is radiated into space. For such thin plasma layers, a more moderate reduction of free electron density will increase the amount of energy which can penetrate and be radiated, and the signal strength at the ground station will be increased.

The determination of the dispersal and mixing of the liquid jet into the supersonic airstream and of the effects that momentum exchange and evaporation have on the resulting mixture is too involved and too little understood to discuss in this paper. These things are important parts of the overall problem, and the brief mention made of them here is not intended to imply otherwise.

The way in which water drops are able to cause free electrons to disappear is illustrated in figure 2, where a single drop is shown being bombarded by electrons and ions in a plasma. The electrons move faster and strike the drop more often than the ions. Thus the drop becomes negatively charged and deflects electrons, while it attracts ions. A steady-state condition is quickly attained in which the net current to the drop is zero. The drops are, in fact, small spherical Langmuir probes at floating potential, and the rate of removal of electrons from the plasma is the product of drop concentration (N_d) and the ion collection rate for a single drop. This rate of removal is given by the equation

$$\frac{dN_e}{dt} = -(\pi r^2 \bar{u}_e F_e N_e) N_d = -(\pi r^2 \bar{u}_i F_i N_i) N_d \qquad (1)$$

where r is the drop radius and $\bar{u}_e$ and $\bar{u}_i$ are mean thermal speeds of electrons and ions, respectively.

The collection efficiency of a drop for electrons (F_e) always has the form $F_e = \exp(-n\sigma)$, where n is the number of electron charges on the

drop and $\sigma = e^2/4\pi\epsilon_0 rkT$. The quantity $n\sigma$ is related to the floating potential by the equation

$$n\sigma = -\frac{eV_f}{kT} \tag{2}$$

As is indicated in figure 1, the electron and ion collection efficiencies are related in the steady state by the equation

$$\bar{u}_e F_e = \bar{u}_i F_i \tag{3}$$

where $\bar{u}_e$ and $\bar{u}_i$ are the mean thermal speeds of electrons and ions in the plasma. The following expression for F_i has been derived by integrating over the Boltzmann velocity distribution in a moving plasma:

$$F_i = \left(\frac{1}{2}\right)\exp\left(\frac{-4U_i^2}{\pi}\right) + \frac{\pi}{8U_i}\left(1 + 2n\sigma + \frac{8U_i^2}{\pi}\right)\operatorname{erf}\left(\frac{2U_i}{\pi^{1/2}}\right) \tag{4}$$

where U_i is the ratio of drop speed through the gas to the mean thermal ion speed. These expressions were derived on the basis of free molecule collisions with the drops and on the basis of $\frac{\lambda_D}{r} \gg 1$, where λ_D is the Debye length. It has also been assumed that thermionic and secondary emission of electrons by the drops is negligible and that all ions which reach a drop recombine with electrons.

We will assume that the stream of water is instantly converted into a fine spray of droplets upon entering the supersonic airstream. We will also assume that all drops have the same radius and that they are deposited in equal numbers per unit volume throughout a known fraction of the total cross section of the flow field. Reduction of drop radius with time by evaporation will be neglected.

To keep the problem simple, analysis of the effect of drops on electron concentration has been confined to changes along a typical stream

tube. Figure 3 illustrates how charge is conserved along such a stream tube, where diffusion of charge through the stream tube walls has been neglected. Charge conservation is expressed by

$$u_g N_e A + \Lambda n^* = \text{Constant} \tag{5}$$

where n^* is defined to be the total number of electrons removed from the plasma by a drop during its history in the flow, and Λ is defined by the equation for conservation of the number of drops present

$$\Lambda = u_d N_d A = \text{Constant} \tag{6}$$

In the steady state,

$$\frac{d}{dx}\left(u_g N_e A\right) = -\Lambda \frac{dn^*}{dx} \tag{7}$$

By following the drop motion, $\frac{dn^*}{dx}$ can be related to $\frac{dN_e}{dt}$, and

$$u_d\left[\frac{d}{dx}\left(u_g N_e A\right)\right] = \frac{d}{dt}\left(u_g N_e A\right) = -\Lambda \frac{dn^*}{dt} = -\left(\frac{\Lambda}{N_d}\right)\frac{dN_e}{dt} \tag{8}$$

By integration of this equation

$$N_e = N_{e0}\left(\frac{u_{g0}A_0}{u_g A}\right)\exp\left[-\Lambda \int_0^x \frac{\pi r^2 F_e \bar{u}_e dx}{u_g u_d A}\right] \tag{9}$$

This is an integral equation for the variation of electron concentration as a function of distance from the point where water is injected. Beckwith and Bushnell have integrated it using an electronic data processing machine which also calculates the acceleration of the drops and their gradual reduction in size due to evaporation. This is the more accurate way to solve the

ment

problem, and they are presenting their solutions and comparing them to experimental results in another paper at this meeting.[12]

To gain insight into the general nature of the problem and to assist in the recognition of the principal parameters, certain approximations can be made which allow equation (9) to be integrated directly. These approximations are:

1. $F_e\bar{u}_e = F_i\bar{u}_i \approx \bar{u}_i\left[F_{i0} - (F_{i0} - F_{i1})\frac{u_d}{u_{d1}}\right]$. (Linear variation of F_i between initial and final values.)

2. $u_g A = u_{g0}A_0$. (Constant density plasma.)

3. $\bar{u}_i$ = Constant. (The mean thermal ion speed actually varies as $T^{1/2}$.)

4. $u_d = at$ until $u_d = u_g$. (Drop undergoes constant acceleration until drop and gas speeds are equal.)

The integration of equation (9) then yields

$$N_e = N_{e0}\exp\left[-h\left(\frac{x}{r}\right) - g\left(\frac{x}{r}\right)^{1/2}\right] \tag{10}$$

where

$$h = \frac{3\rho_{g0}}{4\rho_w}\left[\frac{\bar{u}_i(F_{i1} - F_{i0})}{u_{g0}}\right]M^*(1 + M^*)$$

$$g = \left(\frac{3\rho_{g0}}{2\rho_w}\right)^{1/2}\left[\frac{\bar{u}_i F_{i0}}{u_{g0}}\right]M^*$$

In these equations, r is drop radius, ρ_{g0} is gas density at the injection point, ρ_w is the density of water, and M^* is the ratio of the mass flow of water in the stream tube to the mass flow of gas in the stream tube.

The approximate solution given in equation (10) is essentially an exponential decay of electron concentration with distance from the injection point. Since the drop radius appears only in the ratio x/r, universal solution curves can be prepared which are independent of drop radius. Experience with the solutions has shown that the parameters h and g are, for the most part, functions of the mass flow ratio M^*. From equation (10), one concludes that the principal parameters of the problem are: (1) the drop radius r; (2) the mass flow ratio M^*; and (3) the distance downstream of the injection point x.

Comparison with machine computed results as in figure 4, indicates that the approximate solutions give nearly the same results as the machine solutions. However, it should be noted that N_e/N_{e0} is plotted against time in figure 4. Because of the assumed constant acceleration of drops in the analytical method, the calculated distance from the injection point as a function of elapsed time since injection becomes progressively worse as time goes on, and plots of N_e/N_{e0} against x/r (not shown) do not agree as well as the curves of figure 4. Thus, one is reminded that time of exposure of the drops to the plasma is the fundamental variable, rather than the distance they have traveled. For practical use, curves of N_e/N_{e0} against x/r are more convenient, and can still be used, if careful attention is paid to determination of the proper time-distance relationship.

Another point of disagreement between the analytical and machine solutions is illustrated in figure 4 by the curves for $M^* = 1$. If enough time elapses before electron concentration comes down to the desired level, evaporation reduces the radii of the drops enough to noticeably decrease their

effectiveness. Since the analytical solutions do not account for any reduction in drop radius, they do not show this effect.

Since the more accurate machine solutions are available, they are used for design work and analysis of experimental results. The analytical solutions are useful for studies of the general nature of the effects of water injection, for making rough estimates, and as an aid in interpreting the machine solutions.

APPLICATION

We can now examine some of the effects predicted by theory, as illustrated in figures 5 and 6. Figure 5 shows values of the mass flow ratio M^* required to achieve given reduction factors N_e/N_{e0} at a fixed distance downstream from the injection point. This type of plot would be useful for determining the rate of water injection to achieve signal recovery for an antenna located at a given distance from the injection orifice.

Two points can be made about this figure. One, if the water injection rate is such that the value of M^* lies about halfway up the ordinate scale shown, then $N_e/N_{e0} = 10^{-3}$ will not be obtained with drops 10^{-5} meters in radius, but will easily be obtained with drops 10^{-6} meters in radius. This illustrates the importance of breaking up the water jet into a fine spray. The other point to be made is that, for given drop radius, the electron concentration at the antenna goes down as the mass flow ratio becomes larger. One would expect, of course, that if a little water reduced the electron concentration at the antenna a certain amount, then more water would have a larger effect.

Figure 6 shows that the injection rate of water required to achieve a transparent plasma typically grows smaller as altitude increases. The reason

for this is the rapid decrease in air density with altitude. The drops do not accelerate to gas speed as rapidly when the air density is low and therefore a larger number of drops per unit volume is obtained from a given mass of water injected per second.

For the design of water injection systems, one needs in addition to plots of N_e/N_{e0} against x/r and curves like those in figures 5 and 6, information on the drop size distribution produced by aerodynamic breakup in low-density supersonic flow and on the distribution of drops over the cross section of the flow field. Much remains to be learned about these matters. However, Beckwith and Huffman[6] have correlated experimental measurements of penetration and distribution of liquids injected into supersonic streams in such a way that the results can be used for the design of practical injection systems.[1,4]

SUMMARY

The principal parameters of the problem are:

1. The drop radius, r
2. The mass flow ratio, M^*
3. The flow time of drops after their injection into the flow.

The basic process is recombination of electrons and ions on volume-dispersed surface area.

The recombination rate is controlled by:

1. Collision rate of ions with drops
2. Surface area of drops per unit volume

The collision rate of ions with drops is a function of:

1. Relative speed between gas and drops $(u_g - u_d)$
2. Drop potential $\left(\frac{kTn\sigma}{e}\right)$

The drop potential is the floating potential of a spherical probe. It is a function of:

1. Relative speed $(u_g - u_d)$

2. Ratio of drop radius to Debye length $\left(\frac{r}{\lambda_D}\right)$

The important physical processes are:

1. Breakup of liquid jet (determines drop radius and distribution of liquid in the flow field).

2. Evaporation of drops (determines rate of reduction of drop radius, affects surface conditions of drops, and affects flow properties of gas).

3. Two-phase flow interactions (determines speed of drops relative to gas and the flow properties of the drop-gas mixture).

4. Ion collection rate of drops (electron removal rate is controlled by the ion collection rate).

The complexity of the problem is such that reliance on purely theoretical predictions of the results of injecting water into a reentry plasma is precluded. The best that one can hope for is to obtain meaningful correlations between observed effects and theoretical results. Even the achievement of this limited objective will be of great value in the application of water injection as a practical means for restoring radio communication with reentry vehicles.

REFERENCES

1. W. F. Cuddihy, Ivan E. Beckwith, and Lyle C. Schroeder, "RAM B2 Flight Test of a Method for Reducing Radio Attenuation During Hypersonic Reentry," NASA TM X-902 (1963) CONFIDENTIAL.

2. J. Kendrick Hughes, "Investigation of the Radio Blackout Problem in a Plasma-Sheath Simulation Facility," Paper No. 12 in Proc. of NASA Conf. on Communicating Through Plasmas of Atmospheric Entry and Exhaust, NASA SP-52 (1964) CONFIDENTIAL.

3. Dwain F. Spencer, "An Evaluation of the Communication Blackout Problem for a Blunt Mars-Entry Capsule and a Potential Method for the Elimination of Blackout," JPL TR 32-594 (1964).

4. Lyle C. Schroeder, "Flight Results of Gemini Reentry Communications Experiment," Paper No. 22 in Conf. on Langley Research Related to Apollo Mission, NASA SP-101 (1965) CONFIDENTIAL.

5. Bruce J. Clark, "Breakup of a Liquid Jet in a Transverse Flow of Gas," NASA TN D-2424 (August 1964).

6. Ivan E. Beckwith and Jarrett K. Huffman, "Injection and Distribution of Liquids in the Flow Fields of Blunt Shapes at Hypersonic Speeds," NASA TM X-989 (August 1964) CONFIDENTIAL.

7. H. L. Green and W. R. Lane, Particulate Clouds: Dusts, Smokes and Mists, Second Ed., E. and F. N. Spon, Ltd., London, 1964.

8. A. A. Putnam, et al., "Injection and Combustion of Liquid Fuels," WADC TR 56-344 (March 1957).

9. Allan I. Carswell and Giles G. Cloutier, "Supersonic Plasma Streams Seeded with Electronegative Gases," Physics of Fluids, vol. 7, no. 4, p. 602 (1964).

10. S. L. Soo and R. C. Dimick, "Experimental Study of Thermal Electrification of a Gas-Solid System," Proc. of the Winter Annual Meeting of the ASME, Philadelphia, Pa. (Nov. 17-22, 1963), p. 43.

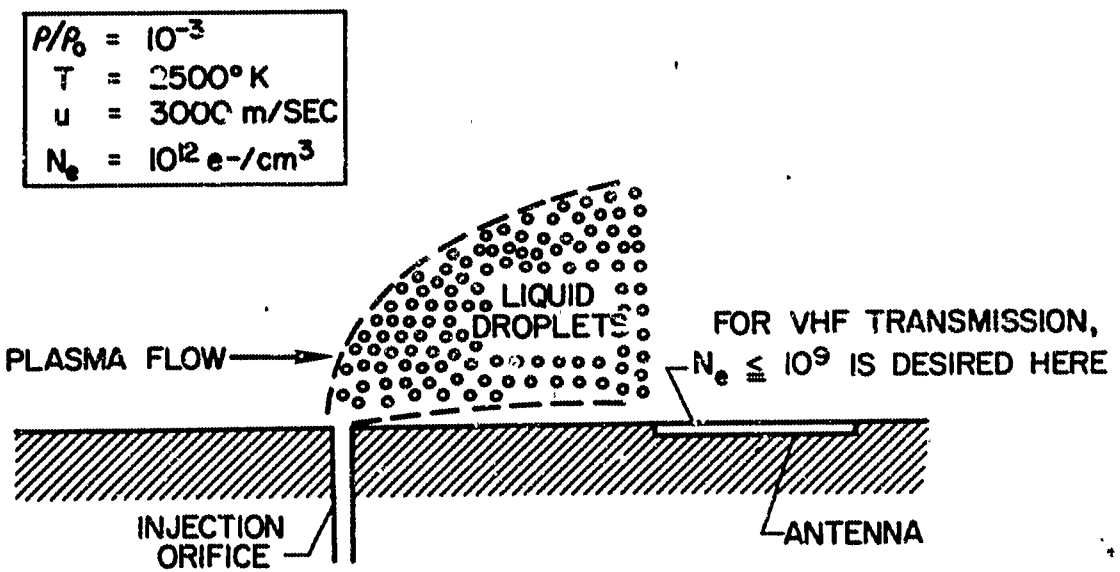
11. Shelby C. Kurzius, R. Ellison, and R. H. Raab, "Effects of Water Droplets on Re-entry Plasma Sheaths," Proc. of the Classified Session of the Third Symposium on the Plasma Sheath, Boston, Mass. (Sept. 21-23, 1965), AFCRL-66-608, Aug. 1966.

12. I. E. Beckwith and D. M. Bushnell, "Depletion of Free Electrons By Water Injection into the Flow Fields of Hypersonic Vehicles," Proc. of the Classified Session of the Third Symposium on the Plasma Sheath, Boston, Mass. (Sept. 21-23, 1965), AFCRL-66-608, Aug. 1966.

13. L. C. Schroeder, "Gemini Reentry Communications Experiment," Proc. of the Classified Session of the Third Symposium on the Plasma Sheath, Boston, Mass. (Sept. 21-23, 1965), AFCRL-66-608, Aug. 1966.

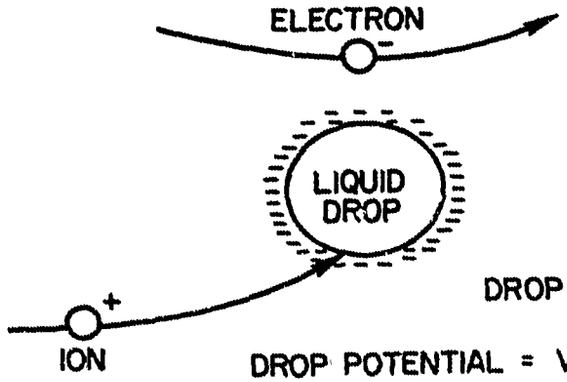
14. John S. Evans, "Charge Recombination on Water Droplets in a Plasma," NASA TM X-1186 . CONFIDENTIAL.

15. William F. Cuddihy, Ivan E. Beckwith, and Lyle C. Schroeder, "Flight Test and Analysis of a Method for Reducing Radio Attenuation During Hypersonic Flight," NASA TM X- . CONFIDENTIAL.



NASA

Figure 1.- Typical initial conditions for liquid injection.



DROP CHARGE = $-ne$

DROP POTENTIAL = $V_f = -\left(\frac{kT}{e}\right)n\sigma$, WHERE

$$\sigma = \frac{e^2}{4\pi\epsilon_0 r kT}$$

$$\frac{dN_e}{dt} = -\left(\pi r^2 \bar{u}_e F_e N_e\right)N_d \quad -\left(\pi r^2 \bar{u}_i F_i N_i\right)N_d$$

WHERE $F_e = \exp(-n\sigma) = \exp\left(\frac{eV_f}{kT}\right)$ and F_i IS A FUNCTION OF BOTH $n\sigma$ AND THE SPEED OF THE DROP RELATIVE TO THE PLASMA

NASA

Figure 2.- Liquid drop as a spherical probe at floating potential.



CHARGE CONSERVATION:

$$u_g N_e A + \Lambda n^* = \text{CONSTANT}$$

VIRTUAL CHARGE ON A DROP

$n^* \equiv$ TOTAL NUMBER OF ELECTRONS REMOVED FROM PLASMA BY A DROP DURING ITS HISTORY IN THE FLOW

CONSERVATION OF NUMBER OF DROPS:

$$\Lambda = u_d N_d A = \text{CONSTANT}$$

IN THE STEADY STATE:

$$d/dx\,(u_g N_e A) = -\Lambda \frac{dn^*}{dx}$$

FOLLOWING THE MOTION OF THE DROPS:

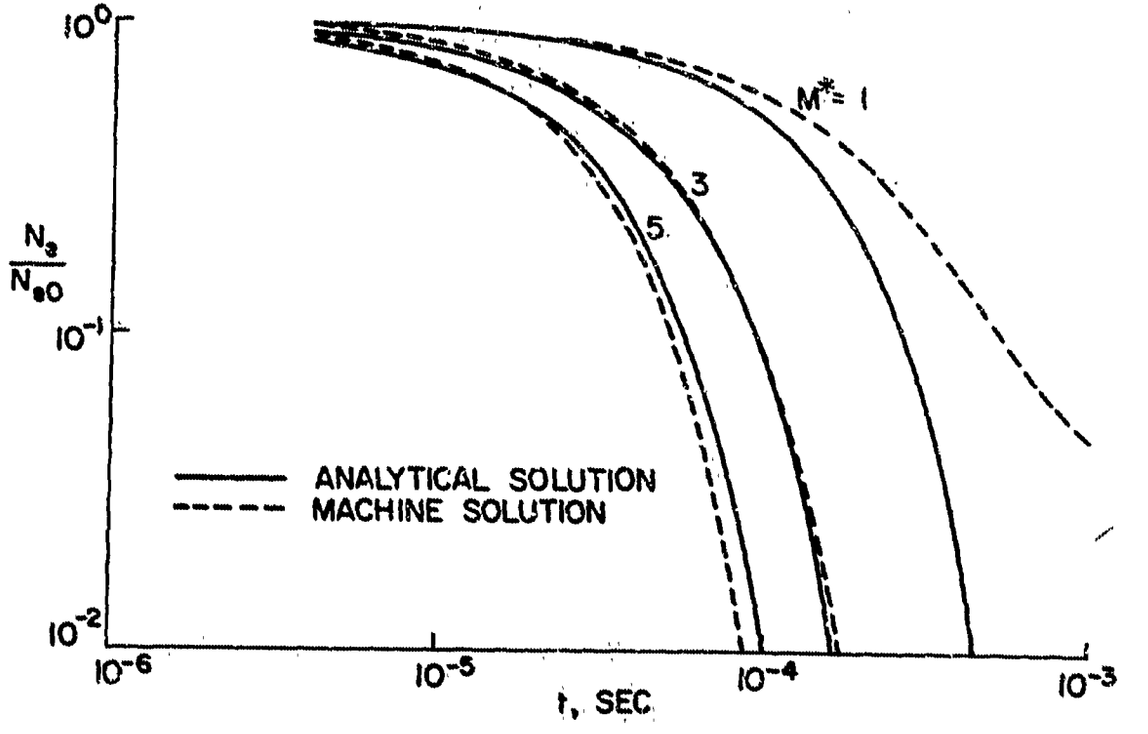
$$u_d \left[d/dx\,(u_g N_e A)\right] = d/dt\,(u_g N_e A) = -\Lambda\left(\frac{dn^*}{dt}\right) = -\frac{\Lambda}{N_d}\left(\frac{dN_e}{dt}\right)$$

INTEGRATING:

$$N_e = N_{eo}\left(\frac{u_{go} A_o}{u_g A}\right) \exp\left[-\Lambda \int_o^x \frac{\pi r^2 F_e \bar{u}_e\, dx}{u_g u_d A}\right]$$

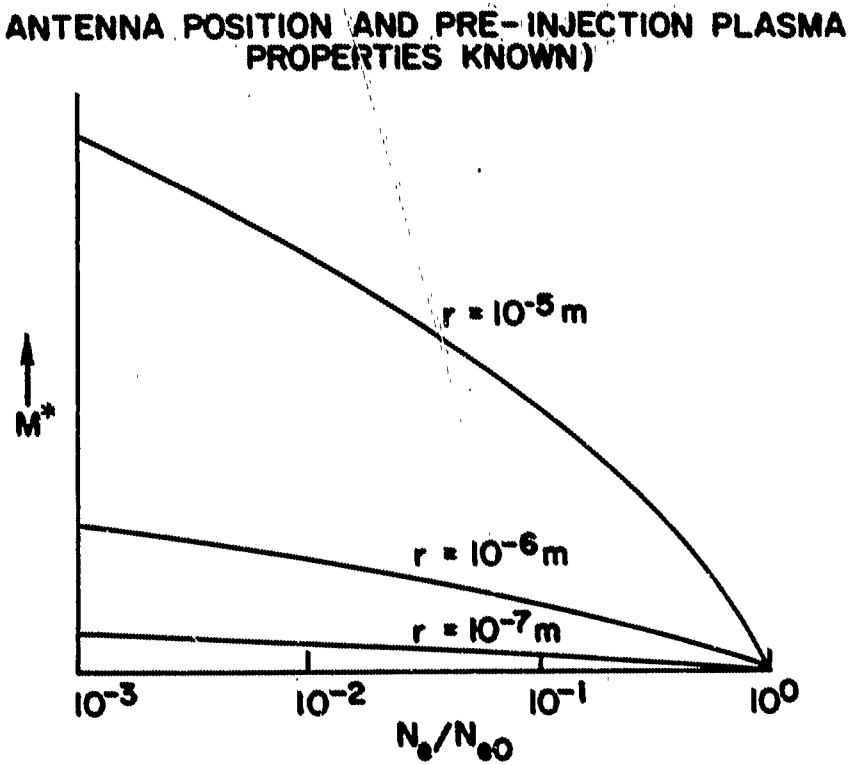
NASA

Figure 3.- Conservation of charge along a stream tube.



NASA

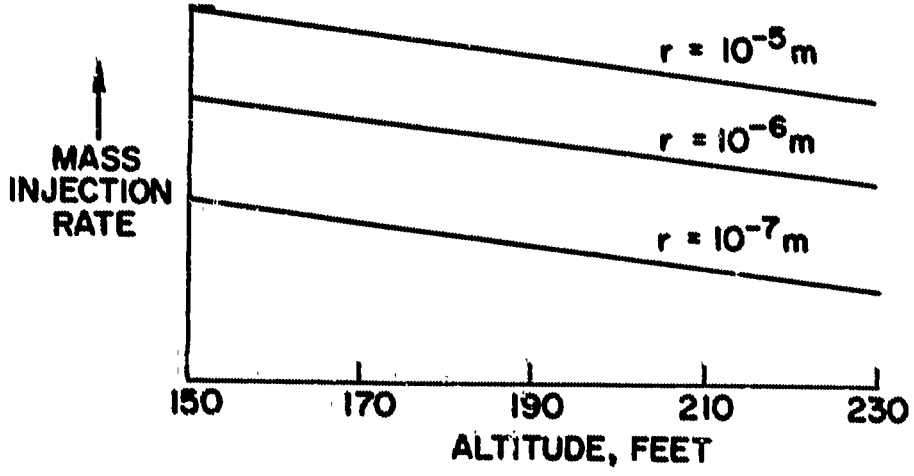
Figure 4.- Comparison of analytical and machine solutions for electron decay.



NASA

Figure 5.- Mass flow to achieve given reduction in electron concentration.

(ANTENNA POSITION FIXED; PRE-INJECTION PLASMA PROPERTIES ARE FUNCTIONS OF VEHICLE SPEED AND ALTITUDE)



NASA

Figure 6.- Mass flow to achieve $N_e/N_{e0} = 10^{-3}$.

Unclassified
Security Classification

DOCUMENT CONTROL DATA - R&D

(Security classification of title, body of abstract and indexing annotation must be entered when the overall report is classified)

1. ORIGINATING ACTIVITY *(Corporate author)* Hq AFCRL, OAR (CRD) United States Air Force Bedford, Massachusetts 01730	2a. REPORT SECURITY CLASSIFICATION Unclassified 2b. GROUP -

3. REPORT TITLE Proceedings of the Third Symposium on the Plasma Sheath–Plasma Electromagnetics of Hypersonic Flight: Volume III. Reentry Plasmas: Simulation, Diagnostics, and Alleviation Techniques

4. DESCRIPTIVE NOTES *(Type of report and inclusive dates)*
Proceedings of Symposium

5. AUTHOR(S) *(Last name, first name, initial)*
Rotman, W., Moore, H., Papa, R., Lennon, J.

6. REPORT DATE May 1967	7a. TOTAL NO. OF PAGES 360	7b. NO. OF REFS 206
8a. CONTRACT OR GRANT NO. b. PROJECT AND TASK NO. 4642, all tasks c. DOD ELEMENT 62405394 d. DOD SUBELEMENT 681000	9a. ORIGINATOR'S REPORT NUMBER(S) AFCRL-67-0280 (Volume III) Special Reports No. 64 (III) 9b. OTHER REPORT NO(S) *(Any other numbers that may be assigned this report)* AFCRL-67-0280 (Volume III)	

10. AVAILABILITY/LIMITATION NOTICES
[redacted]

11. SUPPLEMENTARY NOTES -	12. SPONSORING MILITARY ACTIVITY Hq AFCRL, OAR (CRD) United States Air Force Bedford, Massachusetts 01730

13. ABSTRACT

This volume is a collection of the unclassified papers presented at the Third Symposium on the Plasma Sheath—Plasma Electromagnetics of Hypersonic Flight. This symposium consisted of the review of progress in reentry communication studies during the three year period since the prior meeting. The program of this symposium on plasma electromagnetics of hypersonic flight involves a wide range of scientific disciplines, including electromagnetics, aerodynamics, aerothermochemistry, plasma dynamics, electronics, and high-temperature phenomena. The papers were selected to explore as many of these facets of research, including the results of laboratory, flight, and system tests, as time permitted.

DD FORM 1 JAN 64 1473

Unclassified
Security Classification

Unclassified
Security Classification

14. KEY WORDS	LINK A		LINK B		LINK C	
	ROLE	WT	ROLE	WT	ROLE	WT
Plasma Electromagnetics Hypersonic-Flight Reentry Communications						

INSTRUCTIONS

1. ORIGINATING ACTIVITY: Enter the name and address of the contractor, subcontractor, grantee, Department of Defense activity or other organization *(corporate author)* issuing the report.

2a. REPORT SECURITY CLASSIFICATION: Enter the overall security classification of the report. Indicate whether "Restricted Data" is included. Marking is to be in accordance with appropriate security regulations.

2b. GROUP: Automatic downgrading is specified in DoD Directive 5200.10 and Armed Forces Industrial Manual. Enter the group number. Also, when applicable, show that optional markings have been used for Group 3 and Group 4 as authorized.

3. REPORT TITLE: Enter the complete report title in all capital letters. Titles in all cases should be unclassified. If a meaningful title cannot be selected without classification, show title classification in all capitals in parenthesis immediately following the title.

4. DESCRIPTIVE NOTES: If appropriate, enter the type of report, e.g., interim, progress, summary, annual, or final. Give the inclusive dates when a specific reporting period is covered.

5. AUTHOR(S): Enter the name(s) of author(s) as shown on or in the report. Enter last name, first name, middle initial. If military, show rank and branch of service. The name of the principal author is an absolute minimum requirement.

6. REPORT DATE: Enter the date of the report as day, month, year, or month, year. If more than one date appears on the report, use date of publication.

7a. TOTAL NUMBER OF PAGES: The total page count should follow normal pagination procedures, i.e., enter the number of pages containing information.

7b. NUMBER OF REFERENCES: Enter the total number of references cited in the report.

8a. CONTRACT OR GRANT NUMBER: If appropriate, enter the applicable number of the contract or grant under which the report was written.

8b, 8c, & 8d. PROJECT NUMBER: Enter the appropriate military department identification, such as project number, subproject number, system numbers, task number, etc.

9a. ORIGINATOR'S REPORT NUMBER(S): Enter the official report number by which the document will be identified and controlled by the originating activity. This number must be unique to this report.

9b. OTHER REPORT NUMBER(S): If the report has been assigned any other report numbers *(either by the originator or by the sponsor)*, also enter this number(s).

10. AVAILABILITY/LIMITATION NOTICES: Enter any limitations on further dissemination of the report, other than those imposed by security classification, using standard statements such as:

(1) "Qualified requesters may obtain copies of this report from DDC."

(2) "Foreign announcement and dissemination of this report by DDC is not authorized."

(3) "U. S. Government agencies may obtain copies of this report directly from DDC. Other qualified DDC users shall request through _____."

(4) "U. S. military agencies may obtain copies of this report directly from DDC. Other qualified users shall request through _____."

(5) "All distribution of this report is controlled. Qualified DDC users shall request through _____."

If the report has been furnished to the Office of Technical Services, Department of Commerce, for sale to the public, indicate this fact and enter the price, if known.

11. SUPPLEMENTARY NOTES: Use for additional explanatory notes.

12. SPONSORING MILITARY ACTIVITY: Enter the name of the departmental project office or laboratory sponsoring *(paying for)* the research and development. Include address.

13. ABSTRACT: Enter an abstract giving a brief and factual summary of the document indicative of the report, even though it may also appear elsewhere in the body of the technical report. If additional space is required, a continuation sheet shall be attached.

It is highly desirable that the abstract of classified reports be unclassified. Each paragraph of the abstract shall end with an indication of the military security classification of the information in the paragraph, represented as *(TS), (S), (C), or (U).*

There is no limitation on the length of the abstract. However, the suggested length is from 150 to 225 words.

14. KEY WORDS: Key words are technically meaningful terms or short phrases that characterize a report and may be used as index entries for cataloging the report. Key words must be selected so that no security classification is required. Identifiers, such as equipment model designation, trade name, military project code name, geographic location, may be used as key words but will be followed by an indication of technical context. The assignment of links, rules, and weights is optional.

Unclassified
Security Classification